

THÈSE DE DOCTORAT

Soutenue à Aix-Marseille Université

le 04/02/2022 par

Gabriel FARAG

Modélisation des écoulements compressibles via les méthodes Lattice-Boltzmann

Discipline

Sciences pour l'Ingénieur

Spécialité

Mécanique et physique des fluides

École doctorale

ED 353 Sciences pour l'Ingénieur :
mécanique, physique, micro et
nanoélectrique

Laboratoire

UMR7340 - Laboratoire de Mécanique,
Modélisation et Procédés Propres (M2P2)

Composition du jury

• Rémi ABGRALL	Rapporteur
• Univertität Zürich	
• Jonas LATT	Rapporteur
• Université de Genève	
• Paola CINNELLA	Examinatrice
• Sorbonne Université	
• Manfred KRAFCZYK	Examineur
• Technische Universität Braunschweig	
• Pierre SAGAUT	Examineur
• Aix-Marseille Université	
• Pierre BOIVIN	Directeur de thèse
• Aix-Marseille Université	
• Guillaume CHIAVASSA	Co-Directeur de thèse
• Centrale Marseille	



Je soussigné, Gabriel Farag, déclare par la présente que le travail présenté dans ce manuscrit est mon propre travail, réalisé sous la direction scientifique de Pierre Boivin et Guillaume Chiavassa, dans le respect des principes d'honnêteté, d'intégrité et de responsabilité inhérents à la mission de recherche. Les travaux de recherche et la rédaction de ce manuscrit ont été réalisés dans le respect à la fois de la charte nationale de déontologie des métiers de la recherche et de la charte d'Aix-Marseille Université relative à la lutte contre le plagiat.

Ce travail n'a pas été précédemment soumis en France ou à l'étranger dans une version identique ou similaire à un organisme examinateur.

Fait à Marseille le 22 février 2022



Gabriel FARAG



Cette œuvre est mise à disposition selon les termes de la [Licence Creative Commons Attribution - Pas d'Utilisation Commerciale - Pas de Modification 4.0 International](https://creativecommons.org/licenses/by-nc-nd/4.0/).

« *Impose ta chance, serre ton bonheur et va vers ton risque.* »

— René Char, *Les Matinaux*

Résumé

Depuis la fin des années 1970, les codes de mécanique des fluides numériques sont devenus essentiels du fait de la montée en complexité de leurs applications. Les petites échelles nécessaires pour les applications industrielles demandent souvent des maillages fins ou de petits pas de temps. Ce qui augmente considérablement le coût de calcul des simulations.

Pour obtenir un code de calcul plus rapide, une approche possible consiste à utiliser la méthode Lattice-Boltzmann. Provenant de la théorie cinétique des gaz, cette méthode a largement gagnée en popularité parmi les mécaniciens des fluides du fait de son faible coût et de la facilité d'implémentation de son algorithme collision & transport. Cependant, les approximations utilisées par la méthode Lattice-Boltzmann classique limitent son utilisation aux écoulements faiblement compressibles. Pourtant, quelques modèles compressibles ont été proposés. L'objectif de ce manuscrit est d'améliorer la robustesse et la précision des méthodes Lattice-Boltzmann pour le compressible.

Dans ce but, la méthode Lattice-Boltzmann est complètement réinterprétée comme un schéma numérique. Ce qui permet une démonstration simple et parcimonieuse des équations de Navier-Stokes-Fourier équivalentes en utilisant la seule hypothèse que le pas de temps est suffisamment petit. En utilisant ce formalisme, nous montrons que l'ordre de précision ainsi que la loi de comportement mécanique du modèle dépendent du noyau de collision utilisé. Plusieurs modèles sont étudiés et nous montrons que le nombre de Knudsen n'est pas le seul paramètre à contrôler la consistance avec le modèle de Navier-Stokes-Fourier. De plus, la capacité de l'équation d'entropie à modéliser les écoulements faiblement supersoniques est expliquée avec des arguments de la théorie des chocs classiques. Un schéma MUSCL-Hancock est ensuite utilisé pour discrétiser l'équation d'entropie et augmenter la stabilité et la précision par rapport aux schémas précédents.

Avec ce nouveau formalisme, un modèle basé sur la pression est proposé et validé sur plusieurs cas tests. Ensuite, nous unifions tous les modèles compressibles précédemment proposés par notre groupe sous une seule formulation générale et nous étudions les différences et choix optimaux pour les différents degrés de liberté de nos modèles. Finalement, ce modèle unifié est validé sur des écoulements hautement supersoniques sans chocs et faiblement supersoniques avec chocs.

Mots clés : Lattice-Boltzmann, Mécanique des Fluides Numérique, Écoulements compressibles, Ondes de Chocs, Nombre de Mach, Analyse d'Équations modifiées, Série de Taylor, Différences Finies, Équation d'entropie, Lois de comportement

Abstract

Since the late 1970's, computational fluid dynamics solvers became essentials due to increasingly complex applications requiring fluid solutions. The small scales necessary for industrial applications often need a very fine grid or very small timestep. This dramatically increases the computational cost of nowadays simulations.

To design more computationally efficient solvers, a popular approach is to use Lattice-Boltzmann methods. Originating from the kinetic theory of gases, this method have gained a tremendous popularity among fluid dynamicists due to its cheap and easily implemented collide & stream algorithm. However, its intrinsic assumptions confines classical Lattice-Boltzmann solvers to weakly compressible flows. Yet, some compressible models have been proposed. The purpose of this manuscript is to improve the robustness as well as accuracy of compressible Lattice-Boltzmann models.

To this end, the Lattice-Boltzmann method is fully reinterpreted as a numerical scheme. This allows a straightforward and parsimonious derivation of the equivalent Navier-Stokes-Fourier system using the sole assumption of a negligible timestep. Using this formalism, the order of accuracy is shown to depend on the collision kernel, as well as the mechanical constitutive model. Various models are investigated and we show that the Knudsen number is not the sole parameter controlling the consistency with the Navier-Stokes-Fourier model. Additionally, capabilities of the entropy equation to model low supersonic flows is explained through standard shock wave theory arguments. A MUSCL-Hancock scheme is employed to discretize the entropy equation and improve both stability and accuracy compared to previous schemes.

Equipped with this new formalism, a compressible pressure-based model is proposed and validated on various supersonic test cases. Then, we unify all compressible models proposed by our group under a single formalism and investigate the differences and optimal choices for the various degrees of freedom of our family of models. Finally, this unified model is validated on high supersonic smooth flows and low supersonic shocked flows.

Mots clés: Lattice-Boltzmann, Computational Fluid Dynamics, Compressible Flows, Shock waves, Mach Number, Modified Equation Analysis, Taylor Series Expansion, Finite Differences, Entropy Equation, Constitutive Equations

Remerciements

Mes remerciements vont en premier lieu à ma prof de Physique-Chimie de terminale, Nathalie Barde. Elle a cultivé ma curiosité pour la Physique et m'a incité à lire du Feynman et de la vulgarisation scientifique. Je pense avec le recul que c'est un point crucial de mon éducation parce que ce sont ces lectures qui m'ont donné goût au fait d'apprendre et comprendre.

Je remercie aussi Pierre Boivin, Guillaume Chiavassa et Pierre Sagaut pour leur soutien, la liberté et la confiance qui m'ont été offertes et qui ont fait que j'ai réussi à bien m'amuser pendant ces quelques années de thèse.

De manière générale, je remercie tout le personnel et tous les doctorants du labo, mais plus particulièrement les personnes m'ayant le plus tiré vers le haut : Song, Thomas, Gauthier et Said.

Enfin, je remercie mes parents ainsi que Sarah de m'avoir supporté, écouté et conseillé lorsque j'en avais besoin.

Parce que je sais que ce manuscrit sera principalement lu par des doctorants, je profite de la tribune qui m'est offerte pour rappeler qu'il y a un soleil au bout du tunnel et que son éclat est d'avantage conditionné par votre combativité et votre esprit critique durant votre thèse que par votre intelligence ou votre parcours.

- De plus, il y a des priorités dans la vie, voici un peu de propagande littéraire,
- *"Nous autres"*, Evgueni Ziamatine
 - *"Système 1 / Système 2 : Les deux vitesses de la pensée"*, Daniel Kahneman
 - Tout le cycle *"Hyperion-Endymion"*, Dan Simmons
 - *"La guerre des salamandres"*, Karel Čapek
 - *"L'été"*, Albert Camus
 - *"Nous les robots"*, *"Les cavernes d'acier"*, *"Face aux feux du soleil"*, Isaac Asimov
 - *"Le principe"*, Jérôme Ferrari

Contents

	3
Résumé	4
Abstract	5
Remerciements	6
Contents	7
List of Figures	11
Nomenclature	13
Introduction	15
1 Navier-Stokes-Fourier model	22
1.1 Continuum mechanics for fluid dynamics	22
1.1.1 Thermodynamics principles	23
1.1.2 Closure models	23
1.1.3 Closed Navier-Stokes-Fourier System	26
1.2 Vaschy Buckingham Theorem, or Π Theorem	27
1.3 Recap	28
2 From the kinetic theory of gases to the lattice-Boltzmann scheme	29
2.1 Kinetic theory of gases and continuous Boltzmann equation	30
2.1.1 Hilbert and Chapman-Enskog expansions	33
2.1.2 Grad moment system	35
2.2 Gauss-Hermite quadrature and velocity space discretization	37
2.3 About the traditional interpretation of lattice-Boltzmann schemes	41
2.4 Recap	44
3 Lattice-Boltzmann scheme	45
3.1 Relaxation equation	46
3.2 Space and time discretization	49
3.3 Lattice-Boltzmann collision kernels	53
3.3.1 Multiple Relaxation Time kernels	53
3.3.2 Regularized kernels	55
3.3.3 Other kernels	56

3.4	Boundary conditions in the lattice-Boltzmann method	56
3.5	The Lattice-Boltzmann Scheme, from time t to $t + \Delta t$	57
3.5.1	Lattice-Boltzmann definitions	58
3.5.2	Structure of a generic lattice-Boltzmann scheme	60
3.6	Recap	63
4	Taylor expansion based description of the lattice-Boltzmann scheme	64
4.1	Taylor expansion	65
4.2	Taylor expansion for filtered kernels	68
4.3	Application : Athermal Lattice-Boltzmann Method	71
4.3.1	Numerical scheme	71
4.3.2	Continuous equivalent equations	73
4.3.3	Domain of validity in term of dimensionless numbers	74
4.4	Application : Interpretation of collision models	76
4.4.1	Modeling of lag effects in constitutive equations	77
4.4.2	BGK kernel	79
4.4.3	Regularized kernels	79
4.4.4	Recursive Regularized kernels	80
4.4.5	Hybrid Recursive Regularization kernels	80
4.4.6	Traceless Recursive Regularized kernels	81
4.5	Application : Thermal Lattice-Boltzmann Method, ρ -based model	82
4.5.1	Recursive Regularized- ρ numerical scheme	83
4.5.2	Continuous equivalent equations	84
4.6	Comparison with other Taylor expansions	86
4.6.1	Previous Taylor expansions for lattice-Boltzmann	86
4.6.2	Taylor expansion proposed by <i>Wissocq and Sagaut, 2021</i>	89
4.7	Limits of the proposed Taylor expansion	91
4.8	Recap	94
5	Thermal coupling with finite difference	96
5.1	Is the entropy equation viable for compressible flows ?	97
5.1.1	Shocks with non-conservative entropy equation	98
5.1.2	Contact surfaces with non-conservative entropy equation	100
5.2	Discretization of the entropy equation	100
5.2.1	Passive scalar advection	100
5.2.2	Finite difference schemes	106
5.2.3	MUSCL-Hancock method	107
5.3	Recap	108
6	Pressure-based lattice-Boltzmann model	109
6.1	Hybrid Recursive Regularized pressure based model	110
6.2	Continuous equivalent equations	113
6.3	Results	115
6.3.1	Isentropic vortex advection	115

6.3.2	Entropy spot advection	117
6.3.3	Acoustic wave propagation	118
6.3.4	Thermal Couette Flow	118
6.3.5	Shock wave inner structure	120
6.3.6	One-dimensional shock tube	124
6.3.7	Shock-Vortex interaction	124
6.4	Recap	125
7	Unified model, bridging between pressure-based and density-based methods	128
7.1	Hybrid recursive regularized lattice Boltzmann models	129
7.1.1	Forceless p -based model	129
7.1.2	Forceless improved- ρ -based model	130
7.1.3	Forceless model comparison	131
7.1.4	Non-equilibrium definition in p -based	133
7.1.5	Consistent BGK p -based	135
7.1.6	Comparison accounting for force terms	135
7.2	Unified model on standard lattice	137
7.2.1	Unified LB scheme	138
7.2.2	Interpretation of δ_{0i}	140
7.2.3	Coupled models	141
7.2.4	Step-by-step unified scheme	144
7.3	Numerical validations	145
7.3.1	Isentropic vortex	145
7.3.2	Entropy spot	147
7.3.3	Thermal Couette flow	149
7.3.4	2D Riemann problems	149
7.3.5	Compressible double shear layer	151
7.3.6	Shock-vortex interaction	151
7.3.7	Shock-entropy spot interaction	153
7.4	Recap	156
	Conclusion and perspectives	157
7.5	Conclusion	157
7.6	Perspectives	159
7.7	Scientific communications	161
	Appendices	163
A	The D3Q19 complete basis	163
B	Toward a conservative scheme	166
B.1	U -scheme	166
B.2	C -scheme	167
B.3	UC -scheme	167
B.4	Correction to the U -scheme	168

C	2D Riemann initial states	169
D	Linear Interaction Approximation	170
	D.1 Description of the mean flow solution	170
	D.2 The Kovasznay modal decomposition for fluctuations	172
	D.3 The normal-mode-based LIA	173
Bibliography		175

List of Figures

2.1	Maxwellian distributions	32
2.2	D1Q3 discretized equilibrium	38
3.1	Effect of $\Delta t/\tau$ on a relaxation model.	48
3.2	Order of relaxation schemes.	49
4.1	Over-relaxation du Crank-Nicolson	93
4.2	Over-relaxation du Crank-Nicolson, $\sigma = 0.9$	94
5.1	Consistency of the entropy equation for shocks.	99
5.2	Comparison of advection schemes.	105
6.1	p -based model, vortex advection.	116
6.2	p -based model, entropy spot advection.	117
6.3	p -based model, 1D $u + c$ pressure wave.	118
6.4	p -based model, thermal Couette flow result.	120
6.5	p -based model, thermal Couette flow, convergence.	121
6.6	p -based model, shock inner structure as a function of Mach.	122
6.7	p -based model, shock inner structure as a function of γ .	123
6.8	p -based model, Sod-like results.	124
6.9	p -based model, shock-vortex interaction over time.	125
6.10	p -based model, shock-vortex interaction, radial cuts.	126
6.11	p -based model, shock-vortex interaction, circumferential cuts.	127
7.1	Unified model, vortex advection, colormaps.	146
7.2	Unified model, vortex advection, cuts.	146
7.3	Unified model, entropy spot advection, colormaps.	147
7.4	Unified model, entropy spot advection, cuts.	148
7.5	Unified model, entropy spot advection, scheme comparison.	148
7.6	Unified model, thermal Couette flow.	149
7.7	Unified model, 2D Riemann problems.	150
7.8	Unified model, compressible double shear layer, colormaps.	152
7.9	Unified model, compressible double shear layer, cuts.	153
7.10	Unified model, shock-vortex interaction.	154
7.11	Unified model, shock entropy spot interaction, entropy fields.	154
7.12	Unified model, shock entropy spot interaction, vorticity fields.	155
7.13	Unified model, shock entropy spot interaction, pressure fields.	155
7.14	Pressure coefficient on the top surface of the ONERA M6 wing	159

7.15 Iso-surface of the progress variable at 0.5 for two configurations of the VOLVO burner	160
D1 Sketch of the LIA configuration.	173
D2 Analytical entropy spot from Linear-Interaction-Approximation.	174

Nomenclature

Classical fluid mechanics and CFD :

t	Time coordinate
x_α, \mathbf{x}	Space coordinate
ρ	Density
u_α, \mathbf{u}	Fluid velocity
E	Total energy
p	Pressure
T	Temperature
r	Gas constant
$\mathcal{T}_{\alpha\beta}$	Navier-Stokes-Fourier stress-tensor
q_α	Heat flux
\dot{m}	Arbitrary mass source
$\rho\mathcal{F}_\alpha$	Arbitrary momentum source
$\rho\dot{q}$	Arbitrary energy source
e	Internal energy
s	Entropy
h	Enthalpy
C_v, C_p	Specific heats
γ	Adiabatic exponent
c_s	Constant sound speed (for isothermal fluids)
c	Sound speed
μ	Dynamic viscosity
μ_b	Bulk viscosity
λ	Heat conductivity
Ma	Mach number
Re	Reynolds number
Pr	Prandtl number
Kn	Knudsen number
CFL	Courant-Friedrichs-Lewy number

Δt Timestep

Δx Spacestep

Continuous kinetic theory of gases :

c_α, \mathbf{c} Velocity coordinate

f Distribution, population

Ω Collision kernel

f^{eq} Equilibrium distribution or Maxwellian distribution

f^{neq} Non-equilibrium distribution

τ Relaxation time

ω Weight for Hermite polynomials

$\mathcal{H}^{(n)}$ n^{th} order Hermite polynomials

$\mathbf{a}^{(n)}$ n^{th} order Hermite moment

$\mathbf{\Pi}^{(n)}$ n^{th} order raw moment

Dummy variables :

ϕ Arbitrary variable

ϕ_0 Initial ϕ

ϕ_a Analytical value of ϕ

ϕ^* Nondimensionalized ϕ

$\nabla^n \phi$ n^{th} order tensor gradient of ϕ

$\mathcal{O}(\phi^n)$ Of order $\phi^n, \propto \phi^n$

Lattice-Boltzmann variables

$c_{i\alpha}$ α^{th} component of the i^{th} discrete velocity

ω_i Discrete weights

f_i Discrete distributions

f_i^{eq} Discrete equilibrium distributions

f_i^{neq} Discrete non-equilibrium distributions

Ω_i Discrete collision kernels

F_i Force distributions

$\bar{f}_i, \bar{f}_i^{neq}$ Offset discrete distributions

f_i^{col} Discrete post-collision distributions

$a_{\alpha_1 \dots \alpha_n}^{f, (n)}$ n^{th} order Hermite moment of distributions f_i

$\Pi_{\alpha_1 \dots \alpha_n}^{f, (n)}$ n^{th} order raw moment of distributions f_i

$D_{\alpha_1 \dots \alpha_n}^{f, (n)}$ n^{th} order isotropy defect of distributions f_i

θ Normalized temperature, $\rho\theta = p/c_s^2$

Introduction

Computational Fluid Dynamics

In the history of the study and development of the discipline of fluid dynamics [1–3], the two oldest approaches are the experimental and theoretical methods. The third one, the computational method, is more recent. Due to increasingly fast and cheap computations, it is nowadays possible to do *numerical experiments*. They consist in reproducing fluid flows on computers using models. By doing so, it is possible to *measure* and *predicts* the behavior of flows that are simply out of the scope of theoretical developments, experimental measurements, or simply financially not feasible.

This is the bright side of computational fluid dynamics (CFD). Of course, CFD comes with a cost, *modeling*. Both experimental and theoretical approaches use models, but CFD has the unique capability to provide predictions and accurate results for practical and very complex applications *based* on a given set of models that were implemented in the numerical solver. This means that one often does not have to understand the underlying models and assumptions of a numerical code when using it. Hence, the careful user of a numerical solver needs to keep in mind that the solution it provides does not only comes with inevitable numerical errors, but also possibly with modeling uncertainties. This means that CFD should remain in constant interaction with theoretical and experimental fluid dynamics in order to check that the assumptions and models are consistent and that they approximate with a decent accuracy the desired Physics.

Sometimes, multiple alternative models exist, with slightly different targeted validity. It turns out to be the case in this manuscript, where compressible fluid dynamics is modeled by the LBM [4] instead of the more classical Navier-Stokes-Fourier model (NSF) [5, 6]. Indeed, the main objective of this manuscript is to explain and design LB schemes that are able to produce robust and accurate solutions approaching the traditional NSF fluid flow solutions. In this sense, our approach will be to *bend* the LB solver in order to mimic NSF approach.

The lattice-Boltzmann Method

The LBM originates from the kinetic theory of gases. More specifically, it corresponds to the space-time discretization of the Boltzmann equation [7] with discretized

velocity space [4]. As a result, it inherited most of its theoretical background. Fortunately, the kinetic theory of gases is a mesoscopic description of particles whose averaging provides a macroscopic description somehow equivalent to the NSF system. In this sense, the Boltzmann approach seems to encompass and even generalize the NSF model to rarefied gases. In fact, the theoretical framework of the Boltzmann equation is often used to bridge LB and NSF models. However, along the path of doing so, we will show in this manuscript that some interpretations, assumptions and models of the classical LB literature are not parsimonious enough and lead to black-box models.

Yet, the LBM proved to be an efficient numerical solver for a wide variety of applications, even including non-fluid models such as the advection-diffusion equation [8, 9] which is neither a rarefied flow model nor a classical NSF model. Therefore, the LBM originated from Boltzmann, but is now able to approximate other mathematical models. To name just a few among surprising applications,

- Wave propagation in elastic solids [10],
- Schrödinger equation [11],
- Epidemics propagation [12],
- Finance [13],

This shows that the LB scheme have now emerged as a fully fledged numerical method and that a gas kinetic theory interpretation of LB solver is not sufficiently inclusive.

However, one could legitimately ask : *But, why is LB a research field ?* Computational Science has at its disposal a vast panoply of numerical methods to solve a given problem. However, LB, due to its algorithmic structure – linear transport with non-linear terms evaluated locally – makes it an attractive candidate for complex problems requiring high performance computing. In this manuscript, we only seek to extend stability and accuracy of compressible LB solver with constraints of a relatively compact stencil and $\mathcal{O}(1)$ CFL number [14]. Therefore, the actual computational cost and other performance/efficiency considerations are completely ignored in what follows. The interested reader about LB performances is referred to [15–20] and more specifically to [21], where a model developed during this Ph.D was benchmarked in the context of low Mach compressible combustion.

The lattice-Boltzmann scheme as a numerical scheme

Our solution to the traditional black-box description of LB schemes is therefore to ignore the kinetic description of LBM and to fully describe it as a numerical method. We will show that this approach leads to a *deductive* description, saves a lot of necessary *a priori* assumptions and allows to deduce *a posteriori* the range of consistency

of a given LB scheme towards a given system of partial differential equations. To get a new description of LB solvers, we use some classical concepts such as consistency of numerical schemes [14, 22–24] and dimensional analysis [25–28]. In light of this deductive interpretation of the LB scheme, different topics will be discussed : the choice of discretization, the over/under-relaxation phenomenon, the mandatory conditions for explicitness of LB schemes, Multiple Relaxation Time (MRT) kernels, their ties with filtered/regularized kernels, boundary conditions, order of accuracy of complex LB kernels, continuous limits, LB modeling of constitutive equations and consistency of some nowadays LB compressible models are deduced then discussed. This represents – to the best of the author’s knowledge – the first systematic deduction of what is actually solved by complex LB schemes, what are the achievable NSF solutions in term of nondimensional numbers and how higher "non-hydrodynamic" terms could be directly tied to alternative fluid models. Note that all those deductions are based on the sole assumption that Δt is sufficiently small to neglect numerical errors. In this sense, this manuscript only discusses the consistency of LB schemes, stability being measured by numerical experiments later in the manuscript. Note that fully numerical descriptions of LB schemes could be found in the literature prior to the present work. However, we will show that all contributions we were able to find in the literature fell – consciously or not – into the pitfall of a low Mach assumption and/or into the pitfall of grid dependent nondimensional numbers.

Compressible simulations with ProLB : "Pressure-based" and "Unified" models

Additionally to the critical review of the classical framework of LB schemes and the proposal of its replacement by a more deductive description based on consistency study and dimensional analysis, compressible simulations were performed on ProLB [29]. This code is a LB code developed by a consortium of companies and laboratories : CS Group [30], Airbus [31], Renault [32], Ecole Centrale Lyon (LMFA laboratory [33]) and Aix-Marseille University (M2P2 laboratory [34]), where the numerical scheme design and modeling are carried out.

In order to create a fully compressible LB solver, thermal effects need to be described. Which means that the acoustic scaling $\Delta x / \Delta t = \text{cste}$ is retained throughout this manuscript instead of the diffusive scaling $\Delta t \propto \Delta x^2$ [4]. The thermal effects are not naturally encompassed in classical athermal¹ LB models [4, 35–37]. To circumvent this problem, 3 different strategies could be employed :

- **Multi-speed.** The first and straightforward strategy is to increase the size of the stencil, which is also called *lattice* in LBM. By doing so, more points – and equivalently more discrete velocities – are involved in the LB scheme. This allows to encompass necessary higher order moments (energy fluxes and fluxes of the energy fluxes) and to get an accurate total energy conservation. However, the

1. For what concerns us in this manuscript, athermal = isothermal.

size of necessary lattices [4, 38] are of the order of more than 100 neighbors in 3D, which leads to an expensive solver.

- **Double Distribution Function.** The mass/momentum on one side and energy on the other side are solved by two different sets of populations, f_i and g_i for example, usually with the same lattice. This allows to keep a compact lattice but lead to a very high number of locally defined fields, twice the number of discrete velocities plus all macroscopic moments and transport coefficients.
- **Hybrid lattice-Boltzmann.** In this method, the mass/momentum on one side are solved by a lattice-Boltzmann scheme while the energy – or any other thermodynamic variable – is solved as a single scalar by finite differences. This allows to retain the low computational time of the low Mach lattice-Boltzmann method with only one additional scalar energy solved by finite differences.

Our main target being a low computational time, the third option was retained. Therefore throughout this manuscript, mass and momentum are solved by the set of populations f_i , and an additional thermodynamic variable – entropy or total energy – is discretized by classical finite differences, leading to a 2 way coupled LB-FD hybrid algorithm.

In this context, and using a numerical description of LBM, we designed a new "pressure-based" lattice-Boltzmann scheme² which is able to solve mass and momentum equations coupled to an entropy equation in order to model thermal effects. This new model is then validated on academical simulations and it is shown to be able to mimic NSF supersonic flows. A second model, named unified model, is also designed in order to bridge between preexisting thermal LB models and the present pressure-based model. We will see that the difference between preexisting and pressure-based model only lie in the fourth order equilibrium moments. This unified model is also validated on compressible test cases.

Outline of the manuscript

The detailed structure of this manuscript is as follows.

Chapter 1 : Navier-Stokes-Fourier model This Chapter is devoted to recalling the classical NSF model used to describe the viscous compressible fluid dynamics. The conservation of mass, momentum and energy are recalled in Sec. 1.1. The first and second principles of Thermodynamics are provided in Sec. 1.1.1, they are used as guidelines to derive the additional necessary closures for the mass/momentum/energy system. Then equations of state are discussed in Sec. 1.1.2.1 and mechanical/thermal constitutive equations in Sec. 1.1.2.2. Using all these models leads to the closed NSF system describing the dynamics of viscous compressible flows.

2. Pressure-based only refers to the 0th order term of the distribution. Not to be confused with the traditional "pressure-based" naming in CFD, corresponding to some low-Mach solvers.

Chapter 2 : From the kinetic theory of gases to the Lattice-Boltzmann scheme This Chapter presents the usual tools to link the NSF system to the more general Boltzmann equation. The Hilbert and Chapman-Enskog expansions are recalled in Sec. 2.1.1, along with the less popular but equally important Grad moment system in 2.1.2. The Gauss-Hermite quadrature is also explained in Sec. 2.2. Those are the most important tools that allow to link the LB model to the NSF model. In Sec. 2.3, we question and raise some concerns on the validity of the traditional LB framework.

Chapter 3 : Lattice-Boltzmann scheme In this Chapter, we discuss the LB discretization, collision kernels, boundary conditions and we also recall the necessary step-by-step algorithm that we should follow when implementing a LB solver. First, some properties of discretized relaxation equations are discussed in Sec. 3.1 using a simplified 0 dimensional model. Then, the Discrete Velocity Boltzmann Equation (DVBE) is discretized using the Crank-Nicolson (trapezoidal rule) in Sec. 3.2. The discretization of more advanced collision kernels is discussed in Sec. 3.3. Most important kernels for this manuscript are the MRT 3.3.1 and regularized models 3.3.2. The classical and regularized boundary conditions for LB are explained in 3.4. The last Sec. 3.5 is devoted to a reminder of the actual structure of a LB solver between time t and $t + \Delta t$. Usual definitions are recalled in Sec. 3.5.1 and the step-by-step structure in given in Sec. 3.5.2.

Chapter 4 : Taylor expansion based description of the Lattice-Boltzmann scheme This Chapter contains the main novelty of this manuscript. In Sec. 4.1, the Taylor expansion for a classical LB model is presented, proving the expected 2^{nd} order accuracy. In Sec. 4.2, the Taylor expansion procedure is applied to a generic regularized model. The newly proposed Taylor expansion is applied to the classical athermal LB model in Sec. 4.3, where we show that the low Knudsen assumption is not the only necessary criterion to conclude that a given LB model is consistent to NSF. In Sec. 4.4, the consistency of different collision kernels is discussed : BGK, regularized, recursive regularized, hybrid recursive regularized, and traceless recursive regularized kernels are discussed and compared to alternative constitutive models with time lag effects mentioned in Sec. 4.4.1. The consistency of the classical thermal density-based model is also analyzed in Sec. 4.5. Other Taylor expansions descriptions of the LB scheme are compiled from the literature and compared to the present one in Sec. 4.6. Lastly, some perspectives on the Taylor expansion view of LB schemes are presented in Sec. 4.7, along with a discussion on the validity of the Taylor series truncation.

Chapter 5 : Thermal coupling with finite difference In this Chapter, we discuss how the mass/momentum LB solver is coupled to a finite difference solver in order to restore thermal effects. Due to stability reasons, the entropy equation is adopted, the validity of this choice is discussed in Sec. 5.1. Then the entropy scheme is thoroughly discussed and explained in Sec. 5.2.

Chapter 6 : Pressure-based lattice-Boltzmann model This Chapter is devoted to the first of the 2 models developed during this Ph.D. Its numerical scheme is detailed in Sec. 6.1. Then, using our Taylor expansion, the formalism previously proposed is used in Sec. 6.2 to get the continuous limit of the proposed numerical scheme. Then, the scheme is validated in Sec. 6.3 on different test cases :

- Isentropic vortex advection in Sec. 6.3.1.
- Entropy spot advection 6.3.2.
- 1D acoustic wave propagation in Sec. 6.3.3.
- Thermal Couette flow in Sec. 6.3.4.
- Shock-wave inner structure in Sec. 6.3.5.
- One dimensional shock tube in Sec. 6.3.6.
- Shock-vortex interaction in Sec. 6.3.7.

Chapter 7 : Unified model, bridging between pressure-based and density-based methods In this chapter, the previous density-based, pressure-based and improved-density-based models are merged into a single formalism. In Sec. 7.1, these previous models are extensively discussed and compared. In Secs.7.1.1-7.1.5 the pressure-based and improved-density-based are recalled and then compared without any force correction term. In Sec. 7.1.6, the two different yet very close strategies employed in the density-based, p-based and improved-density-based for the force term are explained. The unified model is proposed in Sec. 7.2, its numerical scheme is detailed in Sec. 7.2.1, a link with fourth order Hermite polynomials is made in Sec. 7.2.2 and the thermal coupling, shock sensor, collision kernel, and other details of the solver are listed in Sec. 7.2.3. Lastly, this unified model is benchmarked in Sec. 7.3 on different compressible test cases :

- Isentropic vortex advection in Sec. 7.3.1.
- Entropy spot advection in Sec. 7.3.2.
- Thermal Couette flow in Sec. 7.3.3.
- 2D Riemann problems in Sec. 7.3.4.
- Double shear layer in Sec. 7.3.5.
- Shock-vortex interaction in Sec. 7.3.6.
- Shock-entropy spot interaction in Sec. 7.3.7.

Conclusion Conclusion and perspectives of what we believe should be done in order to improve LB schemes for compressible flows.

Appendices Some additional content can be found in the appendices. The D3Q19 lattice used in this manuscript can be found in Appendix A, some details about an attempt to discretize the total energy in conservative form are reported in Appendix

B, initial conditions of the 2D Riemann problems can be found in Appendix **C** and some details about the Linear Interaction Analysis can be found in Appendix **D**, a side project carried out during this Ph.D alongside the main LB activity.

1. Navier-Stokes-Fourier model

Sommaire

1.1	Continuum mechanics for fluid dynamics	22
1.1.1	Thermodynamics principles	23
1.1.2	Closure models	23
1.1.2.1	Equations of state	24
1.1.2.2	Constitutive equations	25
1.1.3	Closed Navier-Stokes-Fourier System	26
1.2	Vaschy Buckingham Theorem, or Π Theorem	27
1.3	Recap	28

In this chapter, we provide the basic equations, vocabulary and models that we will try to discretize and approximate throughout this manuscript using the lattice-Boltzmann method (LBM).

In Sec. 1.1, the continuous system of Navier-Stokes-Fourier (NSF) is recalled along with related notions of Thermodynamics, equations of state and constitutive equations. This merely serves as a reminder, for more extensive and thorough discussions, the reader is referred to classical textbooks on fluid dynamics [5, 6, 39–41].

In Sec. 1.2, the important theorem of Vaschy Buckingham – Π theorem – is recalled. It is a cornerstone of fluid mechanics as it formalizes the use of nondimensional numbers. Since a lot of LB concepts and test cases are presented in nondimensional units in this manuscript, recalling this theorem will be found to be useful.

1.1. Continuum mechanics for fluid dynamics

Mechanical engineering traditionally models the fluid by a set of partial differential equations in conservative form, the NSF system. They correspond to physical principles of conservation of mass ρ , momentum ρu_α and density total energy ρE , where the total energy $E = e + 0.5u_\alpha^2$ is the sum of internal e and kinetic $0.5u_\alpha^2$ energies. In D

1. Navier-Stokes-Fourier model – 1.1. Continuum mechanics for fluid dynamics

dimensions, the NSF system consists of $D + 2$ equations,

$$\frac{\partial \rho}{\partial t} + \frac{\partial \rho u_\beta}{\partial x_\beta} = \dot{m}, \quad (1.1)$$

$$\frac{\partial \rho u_\alpha}{\partial t} + \frac{\partial [\rho u_\alpha u_\beta + p \delta_{\alpha\beta} - \mathcal{T}_{\alpha\beta}]}{\partial x_\beta} = \rho \mathcal{F}_\alpha, \quad (1.2)$$

$$\frac{\partial \rho E}{\partial t} + \frac{\partial [(\rho E + p) u_\beta + q_\beta - u_\alpha \mathcal{T}_{\alpha\beta}]}{\partial x_\beta} = \rho \mathcal{F}_\gamma u_\gamma + \rho \dot{q}, \quad (1.3)$$

where p is the thermodynamic pressure, $\mathcal{T}_{\alpha\beta}$ is the stress tensor and q_β is the heat flux. Additionally, arbitrary source terms \dot{m} , $\rho \mathcal{F}_\alpha$ and $\rho \dot{q}$ have been introduced in order to account for coupled arbitrary models. This system of $D + 2$ equations is *open* in the sense that there are more than 3 variables : $\rho, u_\alpha, E, p, \mathcal{T}_{\alpha\beta}, q_\alpha$. Therefore, additional constraints should be provided in order to close the system [42].

1.1.1. Thermodynamics principles

The *first principle* of thermodynamics [6, 43] states that internal energy e , entropy s and volume v variations follow

$$de = T ds - p dv. \quad (1.4)$$

Noting that the specific volume v is related to the density ρ by $v = 1/\rho$ one can write that

$$de = T ds + \frac{p}{\rho^2} d\rho. \quad (1.5)$$

Considering Eq. (1.5) as the definition of entropy s and using Eqs. (1.1-1.3) one can prove that

$$\rho T \left(\frac{\partial s}{\partial t} + u_\beta \frac{\partial s}{\partial x_\beta} \right) + \frac{\partial q_\gamma}{\partial x_\gamma} - \mathcal{T}_{\alpha\beta} \frac{\partial u_\beta}{\partial x_\alpha} = \rho \dot{q} + \dot{m} \left(\frac{u_\gamma^2}{2} - e - \frac{p}{\rho} \right). \quad (1.6)$$

Using Eq. (1.6), the *second principle* could be replaced [5, 44] by the local inequality

$$\mathcal{T}_{\alpha\beta} \frac{\partial u_\beta}{\partial x_\alpha} - \frac{q_\alpha}{T} \frac{\partial T}{\partial x_\alpha} \geq 0, \quad (1.7)$$

Because either the first or second term of Eq. (1.7) could locally vanish, both should be independently positive, which leads to some constraints on $\mathcal{T}_{\alpha\beta}$ and q_α .

1.1.2. Closure models

Thanks to the first and second thermodynamic laws Eqs. (1.5,1.7), we can close the system of equations (1.1-1.3). These closures are known as *equations of state* and *constitutive equations*.

1.1.2.1. Equations of state

Let us first notice that Eq. (1.5) provides a link between 3 thermodynamic variables e , s and ρ , however, links with variables T and p are still missing. This gap is bridged by employing the empirical *caloric* and *thermal* equations of state [43] that ties density ρ and temperature T on one side and internal energy e and pressure p on the other side. They are expressed by

$$e = e(\rho, T), \quad (1.8)$$

$$p = p(\rho, T). \quad (1.9)$$

Providing that those two functions $p(\rho, T)$ and $e(\rho, T)$ are known, using Eqs. (1.5,1.8,1.9) one can compute e , s , ρ , T and p by only knowing 2 variables among them. Because density ρ and internal energy e are already implicitly embedded in Eqs. (1.1-1.3), we must only add Eqs. (1.5,1.8,1.9) to fully describe all links between thermodynamic variables. Additionally, equations of state usually employ *specific heats* at constant volume and pressure, C_v and C_p ,

$$C_v = \frac{\partial e}{\partial T}, \quad C_p = \frac{\partial h}{\partial T}, \quad (1.10)$$

where $h = e + \frac{p}{\rho}$ is the enthalpy [6]. The ratio of specific heats is known as the *adiabatic exponent* γ and is defined by

$$\gamma = \frac{C_p}{C_v}. \quad (1.11)$$

Throughout this manuscript, 2 different equations of state will be mentioned.

Athermal/isothermal gas law. Because this model assumes a constant temperature T , the caloric equation of state is unnecessary, only pressure p is linked to density ρ throughout

$$p = \rho c_s^2, \quad (1.12)$$

where c_s is the constant sound speed. This describes a barotropic fluid [44] and no energy equation is necessary, the mass conservation Eq. (1.1) is sufficient to describe the whole thermodynamic behavior. Note that the word *athermal* is extensively used in the LB literature. In a context of CFD, it should be considered as equivalent to *isothermal*.

Ideal gas law. This is the most widely known equation of state for compressible flows. Pressure p is linked to the density ρ and temperature T throughout the ideal gas law

$$p = \rho r T, \quad (1.13)$$

1. Navier-Stokes-Fourier model – 1.1. Continuum mechanics for fluid dynamics

where $r = R/W$ is a gas dependent constant [5, 6, 39], R is the universal gas constant and W the molecular weight. Internal energy e is computed as

$$e = \int C_v(T) dT + e_0, \quad (1.14)$$

while the specific heats verifies

$$r = C_p(T) - C_v(T). \quad (1.15)$$

This EOS is said to describe a perfect gas when $C_p = \text{const}$ and an ideal gas when $C_p = C_p(T)$. In this sense, all perfect gas are ideal ones.

1.1.2.2. Constitutive equations

With a complete description of the links between thermodynamic variables, we can now address the last few variables we need to describe. These are the stress tensor $\mathcal{T}_{\alpha\beta}$ and heat flux q_α . Functions $\mathcal{T}_{\alpha\beta} = \mathcal{T}_{\alpha\beta}(p, T, u_\alpha)$ and $q_\alpha = q_\alpha(p, T, u_\alpha)$ are known as mechanical and thermal constitutive equations. When those functions are set to 0,

$$\mathcal{T}_{\alpha\beta} = 0, \quad (1.16)$$

$$q_\alpha = 0, \quad (1.17)$$

the system is closed and corresponds to the Euler system. Except for the Euler very simple case, let us now restrict ourselves to isotropic fluids, i.e. fluids without any preferred direction.

Stress tensor $\mathcal{T}_{\alpha\beta}$. The internal frictions of a fluid is modeled by $\mathcal{T}_{\alpha\beta}$. This phenomenon only happens when velocity gradients are non-zero. Therefore, $\mathcal{T}_{\alpha\beta}$ could be searched as a power series of velocity gradients. When those gradients are sufficiently low, we can assume that higher order derivatives than first order ones are negligible and that stress tensor $\mathcal{T}_{\alpha\beta}$ only depends linearly on those first order gradients.

One could argue that velocity gradients are not negligible in compressible flows and especially in shocks. But one also have to remember that shocks are extremely thin regions in which continuum mechanics assumptions underlied by Eqs. (1.1-1.3) are no longer valid [45]. Moreover, the internal structure of a shock – its thickness being of the order of the mean free path [46, 47] – is never numerically resolved. Therefore, additional modeling of $\mathcal{T}_{\alpha\beta}$ for very high gradients seems unnecessary because it will never be properly resolved in regions where it could make a difference.

Additionally, $\mathcal{T}_{\alpha\beta}$ should vanish while performing a solid rotation of the fluid with constant angular speed $\mathbf{\Omega}_r$ such that $\mathbf{u} = \mathbf{\Omega}_r \times \mathbf{r}$. Which means that only some specific combinations of velocity gradients are allowed [5, 6]. For a newtonian [40] fluid, the

1. Navier-Stokes-Fourier model – 1.1. Continuum mechanics for fluid dynamics

most general form that verifies all those assumptions is

$$\mathcal{T}_{\alpha\beta} = \mu \left[\frac{\partial u_\alpha}{\partial x_\beta} + \frac{\partial u_\beta}{\partial x_\alpha} - \delta_{\alpha\beta} \frac{2}{3} \frac{\partial u_\gamma}{\partial x_\gamma} \right] + \mu_b \delta_{\alpha\beta} \frac{\partial u_\gamma}{\partial x_\gamma}, \quad (1.18)$$

where the shear viscosity μ and bulk viscosity μ_b (sometimes called volume viscosity [5, 41]) have been introduced. These coefficients respectively accounts for stresses due to deformations without change of volume and isotropic expansions/compressions [40]. In order to verify the second principle Eq. (1.7), both viscosities should be positive, $\mu \geq 0$ and $\mu_b \geq 0$. Generally speaking, viscosities are instantaneous functions of p and T [5, 6]. Note that while μ was extensively studied and modeled [6], physical models and measures of μ_b are often difficult to obtain [48]. Therefore, while the Stokes hypothesis $\mu_b = 0$ is known to be physically inaccurate for most non-monatomic gases, it is practically used in numerical simulations and implicitly corresponds to the *ansatz* of the coincidence between thermodynamic and mechanical pressures [41, 48].

Heat flux q_α . Similarly to the stress tensor, because heat flux should be a function of temperature gradients, we model q_α by a power series of gradients of temperature. For sufficiently low gradients, this sum can be truncated to its first term $\propto \partial T / \partial x_\alpha$. Additionally, for an isotropic fluid, no preferred direction can be distinguished, which means that the only possible heat flux q_α verifying all our assumptions is

$$q_\alpha = -\lambda \frac{\partial T}{\partial x_\alpha}. \quad (1.19)$$

In order to satisfy the second principle Eq. (1.7), the heat conductivity should verifies $\lambda \geq 0$.

1.1.3. Closed Navier-Stokes-Fourier System

Collecting Eqs. (1.1-1.3) and Eqs. (1.8-1.19) we end up with a fully closed system of evolution equations,

$$\frac{\partial \rho}{\partial t} + \frac{\partial \rho u_\beta}{\partial x_\beta} = \dot{m}, \quad (1.20)$$

$$\frac{\partial \rho u_\alpha}{\partial t} + \frac{\partial [\rho u_\alpha u_\beta + p \delta_{\alpha\beta} - \mathcal{T}_{\alpha\beta}]}{\partial x_\beta} = \rho \mathcal{F}_\alpha. \quad (1.21)$$

$$\frac{\partial \rho E}{\partial t} + \frac{\partial [(\rho E + p) u_\beta + q_\beta - u_\alpha \mathcal{T}_{\alpha\beta}]}{\partial x_\beta} = \rho \mathcal{F}_\gamma u_\gamma + \rho \dot{q}, \quad (1.22)$$

1. Navier-Stokes-Fourier model – 1.2. Vaschy Buckingham Theorem, or Π Theorem

with additional instantaneous equations

$$\mathcal{T}_{\alpha\beta} = \mu \left[\frac{\partial u_\alpha}{\partial x_\beta} + \frac{\partial u_\beta}{\partial x_\alpha} - \delta_{\alpha\beta} \frac{2}{3} \frac{\partial u_\gamma}{\partial x_\gamma} \right] + \mu_b \delta_{\alpha\beta} \frac{\partial u_\gamma}{\partial x_\gamma}, \quad (1.23)$$

$$q_\alpha = -\lambda \frac{\partial T}{\partial x_\alpha}, \quad (1.24)$$

$$e = e(\rho, T), \quad (1.25)$$

$$p = p(\rho, T). \quad (1.26)$$

This system describes the evolution of density ρ , momentum ρu_α and density total energy ρE over time, all other variables (e.g. e , p , T , $\mathcal{T}_{\alpha\beta}$ and q_α) are known functions of the conservative variables ρ , ρu_α and ρE . This system is our target, and we would like to design LB schemes being able to discretize Eqs. (1.20-1.26).

1.2. Vaschy Buckingham Theorem, or Π Theorem

This section is devoted to a fundamental tool of both Physics and Mechanics, the Buckingham Π Theorem [25–28, 49]. This tool allows to reduce the number of parameters to its bare minimum and to identify which parameters are really important in a given situation. Due to its fundamental nature, this theorem and its consequences will be used all along this manuscript without even mentioning it.

Assume a given problem, with an initial condition, its geometrical bodies, its boundary conditions, its external forces, etc... This problem involves k fundamental units (m, kg, s, ...) and is fully described by n dimensional parameters a_1, \dots, a_n (inlet velocity, length of a body, wall temperature, ...) such that the system of equations that describes the physical problem can be written as

$$f(a_1, \dots, a_n) = 0, \quad (1.27)$$

Then, it is possible to define $n - k$ non-dimensional parameters π_1, \dots, π_{n-k} by combining the n dimensional parameters a_1, \dots, a_n and Eq. (1.27) can be equivalently replaced by a more simple system

$$g(\pi_1, \dots, \pi_{n-k}) = 0, \quad (1.28)$$

whose solution now only depends on $n - k$ parameters. Assuming two given problems described by $f(a_1, \dots, a_n)$ and $f(a'_1, \dots, a'_n)$, their solutions are said to be similar if their non-dimensional numbers are identical, $\pi_1 = \pi'_1, \dots, \pi_{n-k} = \pi'_{n-k}$. The Physics of a problem should not depend on the employed system of units and is more easily described by $n - k$ parameters than by n . The non-dimensional system is the one that allows to manipulate only $n - k$ parameters. We will use it almost systematically in this manuscript. Non-dimensional parameters being traditionally used in Mechanics, most – if not all – of the test cases are preferably presented with classical adimensional numbers – Mach, Reynolds, Prandtl or Knudsen – as primary parameters rather than $\text{m}\cdot\text{s}^{-1}$ velocities or K temperatures.

Another point that should be mentioned about the Π theorem is its implicit and traditional use in a lot of the LB literature throughout the so-called lattice units $\Delta x = 1$ and $\Delta t = 1$. While the Π theorem ensures that all systems of units are equivalent, some of them are clearly preferable than others. Being humans, we are unfortunately subject to making a lot of mistakes, while setting $\Delta x = 1$ and $\Delta t = 1$ may be convenient in numerical codes, it may create misunderstandings about the fundamental equations describing the LBM. By getting used to see a 1 instead of a Δt , one can easily forget that an implicit Δt is actually here, instead of a 1, which could lead to basic misconceptions about the method. In order to avoid those misconceptions, lattice units are not used in this manuscript. Instead, an arbitrary system of units is selected where Δx and Δt can have any desired values.

Note that in this manuscript, 4 nondimensional numbers will be regularly encountered ;

- The **Mach** number $\text{Ma} = u/c$, which corresponds to the ratio between the velocity and the sound speed [5, 6].
- The **Reynolds** number $\text{Re} = \rho u L / \mu$, which corresponds to the ratio of the viscous and convective characteristic times [6, 40].
- The **Prandtl** number $\text{Pr} = C_p \mu / \lambda$, which is the ratio between viscous and heat diffusion effects [5, 6].
- The **Knudsen** number $\text{Kn} = L_{mfp} / L$, corresponding to the ratio between particles mean free path and macroscopic length [6, 7, 46, 50]. Knudsen, Mach and Reynolds are also linked by the von Kármán relation $\text{Kn} \propto \text{Ma} / \text{Re}$.

1.3. Recap

In this Chapter, the classical NSF system along with its usual closures were recalled. In this manuscript, this system is considered as the target system we are trying to approximate. Therefore, it was of utmost importance to detail and explain those closures, in order to be able to compare it with LB models. In this sense, the NSF system is considered as the reference and we try to design LB models approaching this system of equations. Additionally, important notions of dimensional analysis were recalled.

2. From the kinetic theory of gases to the lattice-Boltzmann scheme

Sommaire

2.1 Kinetic theory of gases and continuous Boltzmann equation	30
2.1.1 Hilbert and Chapman-Enskog expansions	33
2.1.2 Grad moment system	35
2.2 Gauss-Hermite quadrature and velocity space discretization	37
2.3 About the traditional interpretation of lattice-Boltzmann schemes	41
2.4 Recap	44

The first ever reported LB model is due to [51]. It was interpreted by the authors as “*an alternative technique to the lattice-gas automata for the study of hydrodynamic properties*” and was simultaneously corresponding to a finite difference discretization of a simplified Boltzmann equation [7, 45].

More than its similarities with lattice-gas automata it is its link with the Boltzmann equation that was retained by the scientific community. Nowadays, the LBM emerged as an independent CFD technique. Being intrinsically related to the Boltzmann equation, this research field inherited from viewpoints and interpretations stemming from the kinetic theory of gases. This chapter is devoted to recalling the conventional viewpoint presented in textbooks and meant to describe and understand the LBM.

To this end, the chapter is organized as follows: in Sec. 2.1, some concepts of the kinetic theory of gases are recalled. The Hilbert and Chapman-Enskog expansions along with the Grad moment system and the importance of Hermite polynomials are also discussed. Secondly, velocity space is discretized in Sec. 2.2 leading to the discrete velocity Boltzmann equation (DVBE). In the last part of this chapter, Sec. 2.3, are emphasized some vulnerabilities of the classical LB framework presented here.

2.1. Kinetic theory of gases and continuous Boltzmann equation

A flow is usually modeled on a macroscopic scale using continuum mechanics and more specifically the NSF system [5, 6, 40], Eqs. (1.20-1.26). This viewpoint was recalled in Chapter 1. Another choice is to model on the molecular level by describing particles trajectories, which is not affordable for simulations on contemporary computers since the Avogadro constant [43] is of order 6.022×10^{23} , which means that too many particles and therefore trajectories should be simultaneously described. An affordable choice is therefore to use a mesoscopic description in which is described the number of particles rather than particles itself.

Defining the density $\rho(t, \mathbf{x})$ as the mass per unit volume of particles at time t and position \mathbf{x} , a generalized mesoscopic density can be written as $f(\mathbf{c}, t, \mathbf{x})$. Traditionally called distribution or population, it corresponds to the mass per unit volume at time t and position \mathbf{x} of particles moving with velocity \mathbf{c} . Therefore, the total mass per unit volume of particles at time t and position \mathbf{x} is

$$\rho(t, \mathbf{x}) = \int f(\mathbf{c}, t, \mathbf{x}) d\mathbf{c}. \quad (2.1)$$

Considering contributions $\mathbf{c}f$ from all velocities \mathbf{c} to the momentum lead to

$$\rho(t, \mathbf{x})\mathbf{u}(t, \mathbf{x}) = \int \mathbf{c}f(\mathbf{c}, t, \mathbf{x}) d\mathbf{c}, \quad (2.2)$$

where $\mathbf{u}(t, \mathbf{x})$ is the macroscopic velocity of the fluid, corresponding to the classical velocity variable described by continuum mechanics in Chapter 1. Similarly, the total density energy $\rho(t, \mathbf{x})E(t, \mathbf{x})$ of the fluid can be recovered from distribution $f(\mathbf{c}, t, \mathbf{x})$,

$$\rho(t, \mathbf{x})E(t, \mathbf{x}) = \int |\mathbf{c}|^2 f(\mathbf{c}, t, \mathbf{x}) d\mathbf{c}. \quad (2.3)$$

Total energy contains two contributions $\frac{1}{2}\rho|\mathbf{u}|^2 f$ and $\frac{1}{2}\rho|\mathbf{c} - \mathbf{u}|^2 f$ that respectively correspond to the kinetic energy (bulk motion of particles) and the internal energy e (thermal random motion of particles).

Equations. (2.1-2.3) are called *moments* of the distribution f . Thanks to those moments, physical properties of the fluid are known at (t, \mathbf{x}) as long as $f(\mathbf{c}, t, \mathbf{x})$ is also known. Therefore, the evolution over time of moments ρ , $\rho\mathbf{u}$ and ρE is entirely contained in the evolution of f . The question is now to model properly the evolution equation driving f . Particles and hence distributions f are subject to changes from only two different physical phenomena,

- The first one is the free streaming of particles, describing the motion of particles with velocity \mathbf{c} , modeled by a linear advection operator $\frac{\partial f}{\partial t} + c_\alpha \frac{\partial f}{\partial x_\alpha}$.
- The second one is the collision of particles $\Omega(f)$, which encompasses non-linear phenomena such as collisions, hardness of particles and intermolecular forces

2. From the kinetic theory of gases to the lattice-Boltzmann scheme – 2.1. Kinetic theory of gases and continuous Boltzmann equation

acting remotely as a function of intermolecular distance [7, 45].

Equating these two terms into a single equation yields the Boltzmann equation,

$$\frac{\partial f}{\partial t} + c_\alpha \frac{\partial f}{\partial x_\alpha} = \Omega(f), \quad (2.4)$$

which is the equation describing the distribution evolution for a given type of particles (hard spheres, soft spheres, Maxwell molecules, etc [45]) associated to a collision kernel $\Omega(f)$. It is important to note that all thermodynamic and hydrodynamic models serving to close the system of conservation equations in continuum mechanics, namely the thermal $p = p(\rho, T)$ and caloric $e = e(\rho, T)$ equations of state, mechanical $\mathcal{T} = \mathcal{T}(\nabla \mathbf{u})$ and caloric $\mathbf{q} = \mathbf{q}(\nabla T)$ constitutive laws are emerging phenomena of the choice of molecules and intermolecular potential, which are entirely modeled in $\Omega(f)$. For this reason, it is often said that all physical models (equations of state, constitutive equations, see Sec. 1.1.2) are encompassed in the collision kernel $\Omega(f)$. A crucial specificity of the collision model $\Omega(f)$ is that it should conserve mass, momentum and energy, which is equivalent [45] to

$$\int \Omega d\mathbf{c} = 0, \quad \int \mathbf{c} \Omega d\mathbf{c} = 0, \quad \int |\mathbf{c}|^2 \Omega d\mathbf{c} = 0. \quad (2.5)$$

In the literature, 1, \mathbf{c} and $|\mathbf{c}|^2$ play an important role and are referred to as collision invariants. From those collision invariants, one can analytically [4, 7, 45] show that a particular solution of the Boltzmann equation Eq. (2.4) is the equilibrium distribution f^{eq} , also known as Maxwellian, which is solution of $\Omega(f^{eq}) = 0$ and can be expressed in 3D by

$$f^{eq} = \frac{\rho}{(2\pi r T)^{3/2}} e^{-(|\mathbf{c}-\mathbf{u}|^2)/2rT}. \quad (2.6)$$

When $f = f^{eq}$, the fluid is said to be at equilibrium. Fig. 2.1 shows the Maxwellian distributions for different Ma and sound speed $\sqrt{\gamma r T}$, with $\rho = 1$ and $\gamma = 1.4$.

2. From the kinetic theory of gases to the lattice-Boltzmann scheme – 2.1. Kinetic theory of gases and continuous Boltzmann equation

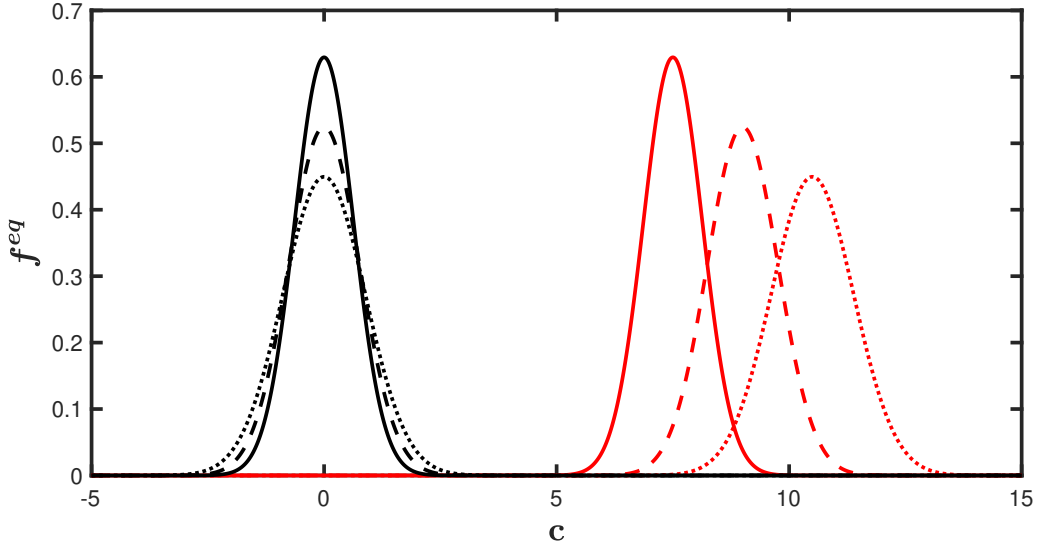


Figure 2.1. – Maxwellian distributions for different sound speeds and Mach numbers.
 Ma = 0 : $\sqrt{\gamma r T} = 0.75$ —; $\sqrt{\gamma r T} = 0.9$ - - -; $\sqrt{\gamma r T} = 1.05$
 Ma = 10 : $\sqrt{\gamma r T} = 0.75$ —; $\sqrt{\gamma r T} = 0.9$, - - -; $\sqrt{\gamma r T} = 1.05$,

Therefore, the non-equilibrium distribution f^{neq} is defined as

$$f^{neq} = f - f^{eq}. \quad (2.7)$$

Additionally, because of Eqs. (2.5), equilibrium distribution also verifies that

$$\rho = \int f^{eq} d\mathbf{c}, \quad \rho \mathbf{u} = \int \mathbf{c} f^{eq} d\mathbf{c}, \quad \rho E = \int |\mathbf{c}|^2 f^{eq} d\mathbf{c}. \quad (2.8)$$

The first and historical collision model Ω was obtained by Boltzmann himself [52] and corresponds to a hard spheres gas with vanishing intermolecular potential. However, a simpler yet satisfactory model is often used, the Bhatnagar-Gross-Krook (BGK) [53] model,

$$\Omega_{\text{BGK}} = \frac{-1}{\tau} f^{neq}. \quad (2.9)$$

In which f relaxes towards f^{eq} with a characteristic relaxation time τ . This approximation reasonably holds when f does not depart too much from f^{eq} [50], regardless of the value of the Knudsen number Kn .

Being theoretically able to describe rarefied [45] to continuum [6] gas flows, one would expect the Boltzmann Eq. (2.4) to reproduce NSF solutions in the asymptotic $\text{Kn} \ll 1$ limit. This link between continuous NSF equations and continuous Boltzmann equation is not straightforward and usually needs a perturbation analysis which is by construction only valid for some specific cases [54–56]. We shall recall hereafter some historical methods allowing to link the kinetic Boltzmann equation to the continuum NSF system.

2. From the kinetic theory of gases to the lattice-Boltzmann scheme – 2.1. Kinetic theory of gases and continuous Boltzmann equation

2.1.1. Hilbert and Chapman-Enskog expansions

The question of a systematic derivation of the NSF system from kinetic theory is owed to Hilbert [57, 58]. Its first attempt is based on the assumption that $\text{Kn} \ll 1$ and that the collision characteristic time can be expressed as $\tau = \text{Kn} \tilde{\tau}$ with $\tilde{\tau} = \mathcal{O}(1)$. The rescaled Boltzmann-BGK equation then reads

$$\text{Kn} \left(\frac{\partial f}{\partial t} + c_\alpha \frac{\partial f}{\partial x_\alpha} \right) = -\frac{1}{\tilde{\tau}} (f - f^{eq}). \quad (2.10)$$

A singular perturbation procedure [59] is then performed by taking the limiting case $\text{Kn} \rightarrow 0$. Then, we can search for the solution f as an infinite expansion,

$$f = \sum_{n=0}^{\infty} \text{Kn}^n f^{(n)} = f^{(0)} + \text{Kn} f^{(1)} + \text{Kn}^2 f^{(2)} + \dots, \quad (2.11)$$

where all $f^{(n)}$ are $\mathcal{O}(1)$. Making the hypothesis that Eq. (2.11) is convergent we insert it inside Eq. (2.10). Then by assuming a scale separation between orders in Kn and collecting terms by orders we end up with an infinite hierarchy of equations

$$f^{(0)} - f^{eq} = 0, \quad (2.12)$$

$$-\frac{1}{\tilde{\tau}} f^{(n)} = \frac{\partial f^{(n-1)}}{\partial t} + c_\alpha \frac{\partial f^{(n-1)}}{\partial x_\alpha}, \quad (2.13)$$

with $n > 0$. This hierarchy of equations, called Hilbert expansion, exhibits some remarkable properties. The first equation confirms that the zeroth order distribution $f^{(0)}$ should match the equilibrium distribution f^{eq} . The second equation shows that the n^{th} equation depends on the $(n-1)^{\text{th}}$ distribution only in a sequential manner. Then, by truncating at any order n in the infinite expansion it is possible to get an approximate solution of Eq. (2.10). It is reported by literature [7, 60] that the problem of this procedure is that it fails to capture very steep gradients because a n^{th} order truncated Hilbert expansion would exhibit a $(n+1)^{\text{th}}$ order space derivative in its leading error, indicating that a high degree of smoothness is necessary for Hilbert expansion to converge. In other words, regions with high gradients such as boundary layers or shocks [7, 37, 60] may not be properly described by Hilbert procedure, which is ill-equipped to deal with such applications. A way to circumvent this problem is to use the Chapman-Enskog expansion [7, 60] instead of the Hilbert expansion. The only difference with the Hilbert expansion lies in the fact that the time derivative is now also expanded,

$$\frac{\partial f}{\partial t} = \sum_{n=0}^{\infty} \text{Kn}^n \frac{\partial f}{\partial t_n} = \frac{\partial f}{\partial t_0} + \text{Kn}^1 \frac{\partial f}{\partial t_1} + \text{Kn}^2 \frac{\partial f}{\partial t_2} + \dots, \quad (2.14)$$

where $\partial/\partial t_n$ denotes the contribution from the n^{th} order to the physical time deriva-

2. From the kinetic theory of gases to the lattice-Boltzmann scheme – 2.1. Kinetic theory of gases and continuous Boltzmann equation

tive $\partial/\partial t$. Plugging Eqs. (2.11, 2.14) inside Eq. (2.10) leads to

$$\text{Kn} \left(\sum_{n=0}^{\infty} \text{Kn}^n \frac{\partial}{\partial t_n} + c_\alpha \frac{\partial}{\partial x_\alpha} \right) \left[\sum_{m=0}^{\infty} \text{Kn}^m f^{(m)} \right] = -\frac{1}{\tilde{\tau}} \left(\left[\sum_{m=0}^{\infty} \text{Kn}^m f^{(m)} \right] - f^{eq} \right). \quad (2.15)$$

Assuming a scale separation between orders in Kn and collecting terms by orders we end up with a new infinite hierarchy of equations. The 3 leading orders in Kn now read

$$f^{(0)} - f^{eq} = 0, \quad (2.16)$$

$$-\frac{1}{\tilde{\tau}} f^{(1)} = \frac{\partial f^{(0)}}{\partial t_0} + c_\alpha \frac{\partial f^{(0)}}{\partial x_\alpha}, \quad (2.17)$$

$$-\frac{1}{\tilde{\tau}} f^{(2)} = \frac{\partial f^{(1)}}{\partial t_0} + \frac{\partial f^{(0)}}{\partial t_1} + c_\alpha \frac{\partial f^{(1)}}{\partial x_\alpha}. \quad (2.18)$$

Again, the zeroth order distribution satisfies $f^{(0)} = f^{eq}$, but a slight difference appears in higher orders, the n^{th} equation now depending not only on the $(n-1)^{\text{th}}$ but also on any $(n-m)^{\text{th}}$ order with $m < n$. Similarly to the Hilbert expansion, this recursive behavior means that Chapman-Enskog expansion only addresses low-Knudsen solutions with f depending only implicitly on time via the macroscopic variables appearing inside the Maxwellian Eq. (2.6). In other words, the Chapman-Enskog expansion only describes solutions $f(t)$ with autonomous time dependencies $f(\rho(t), u(t), T(t), \nabla^n \rho(t), \nabla^n u(t), \nabla^n T(t))$ with ∇^n the 0^{th} to n^{th} order rank space derivatives. More general solutions f are simply out of the scope of the Chapman-Enskog expansion [61]. The next step is to take successive moments of this infinite hierarchy. Integrating the first three order moments of Eq. (2.17) leads to the Euler equations

$$\frac{\partial \rho}{\partial t_0} + \frac{\partial \rho u_\alpha}{\partial x_\alpha} = -\frac{1}{\tilde{\tau}} \int f^{(1)} d\mathbf{c}, \quad (2.19)$$

$$\frac{\partial \rho u_\alpha}{\partial t_0} + \frac{\partial [\rho u_\alpha u_\beta + \delta_{\alpha\beta} p]}{\partial x_\beta} = -\frac{1}{\tilde{\tau}} \int c_\alpha f^{(1)} d\mathbf{c}, \quad (2.20)$$

$$\frac{\partial \rho E}{\partial t_0} + \frac{\partial [\rho u_\beta (E + RT)]}{\partial x_\beta} = -\frac{1}{\tilde{\tau}} \int c_\beta c_\beta f^{(1)} d\mathbf{c}. \quad (2.21)$$

Similarly, the first three order moments of Eq. (2.18) lead to

$$\frac{\partial \rho}{\partial t_1} + \int \left(\frac{\partial}{\partial t_0} + c_\beta \frac{\partial}{\partial x_\beta} \right) f^{(1)} d\mathbf{c} = -\frac{1}{\tilde{\tau}} \int f^{(2)} d\mathbf{c}, \quad (2.22)$$

$$\frac{\partial \rho u_\alpha}{\partial t_1} + \int \left(\frac{\partial}{\partial t_0} + c_\beta \frac{\partial}{\partial x_\beta} \right) c_\alpha f^{(1)} d\mathbf{c} = -\frac{1}{\tilde{\tau}} \int c_\alpha f^{(2)} d\mathbf{c}, \quad (2.23)$$

$$\frac{\partial \rho E}{\partial t_1} + \int \left(\frac{\partial}{\partial t_0} + c_\beta \frac{\partial}{\partial x_\beta} \right) c_\alpha c_\alpha f^{(1)} d\mathbf{c} = -\frac{1}{\tilde{\tau}} \int c_\beta c_\beta f^{(2)} d\mathbf{c}, \quad (2.24)$$

which can be interpreted as a correction to the Euler equations Eqs. (2.19–2.21),

2. From the kinetic theory of gases to the lattice-Boltzmann scheme – 2.1. Kinetic theory of gases and continuous Boltzmann equation

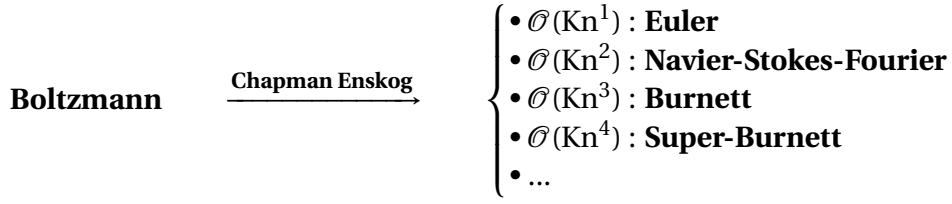


Table 2.1. – Schematic view of the hierarchy of models produced by different truncations of the Chapman-Enskog expansion. $\mathcal{O}(\text{Kn}^n)$ means that n^{th} and higher orders are neglected.

leading to the NSF system of equations. Note that this system is not closed yet because we do not know how to evaluate $\int \Psi f^{(n)} d\mathbf{c}$ with $n > 0$ and $\Psi = [1, c_\alpha, c_\alpha c_\alpha]$. The Chapman-Enskog expansion being a formal search of Boltzmann equation solution any constraint can be used to close the system. Thus, *solvability constraints* [4, 37] are applied,

$$\int \Psi f^{(n)} d\mathbf{c} = 0, \quad n > 0. \quad (2.25)$$

This is an essential step of the Chapman-Enskog expansion because it allows to close the system and prevents the infinite hierarchy to impact the orders of interest $n = 0, 1, 2$ corresponding to mass, momentum and energy. Using the solvability conditions, neglecting higher orders and collecting Eqs. (2.19–2.24) the NSF system can be deduced,

$$\frac{\partial \rho}{\partial t} + \frac{\partial \rho u_\beta}{\partial x_\beta} = \mathcal{O}(\text{Kn}^2), \quad (2.26)$$

$$\frac{\partial \rho u_\alpha}{\partial t} + \frac{\partial [\rho u_\alpha u_\beta + \delta_{\alpha\beta} p]}{\partial x_\beta} + \frac{\partial}{\partial x_\beta} \int c_\beta c_\alpha f^{(1)} d\mathbf{c} = \mathcal{O}(\text{Kn}^2), \quad (2.27)$$

$$\frac{\partial \rho E}{\partial t} + \frac{\partial [\rho u_\beta (E + RT)]}{\partial x_\beta} + \frac{\partial}{\partial x_\beta} \int c_\beta c_\alpha c_\alpha f^{(1)} d\mathbf{c} = \mathcal{O}(\text{Kn}^2), \quad (2.28)$$

this system being closed [4] by moments of Eq. (2.17) to obtain stress-tensor $\int c_\beta c_\alpha f^{(1)} d\mathbf{c}$ and heat flux $\int c_\beta c_\alpha c_\alpha f^{(1)} d\mathbf{c}$. To summarize, in order to perform this simple Chapman-Enskog expansion the convergent nature of the f expansion Eq. (2.11) and its truncation, the scale separation between orders in Kn, the BGK collision kernel and the solvability conditions Eq. (2.25) were assumed to be valid. Note that by truncating the Chapman-Enskog expansion, different macroscopic models can be obtained, as summarized in Table 2.1.

2.1.2. Grad moment system

Aside the well known Chapman-Enskog expansion, another attempt to link the Boltzmann equation to the continuum mechanics was performed by Grad [62]. It is

2. From the kinetic theory of gases to the lattice-Boltzmann scheme – 2.1. Kinetic theory of gases and continuous Boltzmann equation

of historical importance for LBMs as it introduced the use of Hermite polynomials $\mathcal{H}^{(n)}$ to analyze the Boltzmann equation. The main idea is to project the distribution f onto the Hermite polynomials [63] basis composed by n^{th} order rank symmetric tensors $\mathcal{H}^{(n)}$ of n^{th} degree polynomials in \mathbf{c} , leading to

$$f(\mathbf{c}) = \omega(\mathbf{c}) \sum_{n=0}^{\infty} \frac{1}{n!} \mathbf{a}^{(n)} : \mathcal{H}^{(n)}(\mathbf{c}), \quad (2.29)$$

where the weight $\omega(\mathbf{c})$, the n^{th} order Hermite moment $\mathbf{a}^{(n)}$ and Hermite polynomial $\mathcal{H}^{(n)}$ have been used,

$$\mathbf{a}^{(n)} = \int \mathcal{H}^{(n)} f d\mathbf{c}, \quad \omega(\mathbf{c}) = \frac{1}{(2\pi)^{3/2}} e^{-\mathbf{c} \cdot \mathbf{c}/2}, \quad \mathcal{H}^{(n)}(\mathbf{c}) = \frac{(-1)^n}{\omega(\mathbf{c})} \nabla^n \omega(\mathbf{c}). \quad (2.30)$$

Let us make the assumption that the relevant physical phenomena we are interested in are sufficiently well modeled by a N^{th} order truncation of f , Eq. (2.29),

$$f^{(N)}(\mathbf{c}) \approx \omega(\mathbf{c}) \sum_{n=0}^N \frac{1}{n!} \mathbf{a}^{(n)} : \mathcal{H}^{(n)}(\mathbf{c}). \quad (2.31)$$

Note that unlike the Hilbert and Chapman-Enskog methods, the Grad moment technique explores every possible Boltzmann equation solutions when $N \rightarrow \infty$ thanks to the completeness of the Hermite basis. Now, let us consider any finite value N . It means that $f^{(N)}$ can be equivalently described by a finite set of independent moments $\mathbf{a}^{(0)}, \dots, \mathbf{a}^{(N)}$. In other words, injecting Eq. (2.31) into the Boltzmann Eq. (2.4),

$$\frac{\partial f^{(N)}}{\partial t} + c_\alpha \frac{\partial f^{(N)}}{\partial x_\alpha} = \Omega(f_N), \quad (2.32)$$

and taking moments of this system leads to a finite set of moments equations which is completely equivalent to Eq. (2.32). This system describes the temporal evolution of variables $\mathbf{a}^{(0)}, \dots, \mathbf{a}^{(N)}$. Equivalently, different moments could be introduced, known as raw moments $\mathbf{\Pi}^{(n)}$,

$$\mathbf{\Pi}^{(n)} = \int (\mathbf{c})^n f d\mathbf{c}. \quad (2.33)$$

In which case, taking raw moments of Eq. (2.32) provides a system of evolution equations for variables $\mathbf{\Pi}^{(0)}, \dots, \mathbf{\Pi}^{(N)}$. This is exactly what has been done by Grad in 1949 to form the Grad-13 system of equations [37, 62]. This system is a set of 13 different moments corresponding to mass $\mathbf{\Pi}^{(0)}$, momentum $\mathbf{\Pi}_\alpha^{(1)}$, total energy/stress-tensor $\mathbf{\Pi}_{\alpha\beta}^{(2)}$ and energy flux $\mathbf{\Pi}_{\alpha\beta\gamma}^{(3)}$. Therefore, the Grad-13 system can be written in two equivalent formats, the first one is

$$\frac{\partial f_{G13}}{\partial t} + c_\alpha \frac{\partial f_{G13}}{\partial x_\alpha} = \Omega(f_{G13}), \quad (2.34)$$

2. From the kinetic theory of gases to the lattice-Boltzmann scheme – 2.2.
Gauss-Hermite quadrature and velocity space discretization

and the second one,

$$\frac{\partial \Pi^{f_{G13,(0)}}}{\partial t} + \frac{\partial \Pi_{\alpha}^{f_{G13,(1)}}}{\partial x_{\alpha}} = 0, \quad (2.35)$$

$$\frac{\partial \Pi_{\alpha}^{f_{G13,(1)}}}{\partial t} + \frac{\partial \Pi_{\alpha\beta}^{f_{G13,(2)}}}{\partial x_{\beta}} = 0, \quad (2.36)$$

$$\frac{\partial \Pi_{\alpha\beta}^{f_{G13,(2)}}}{\partial t} + \frac{\partial \Pi_{\alpha\beta\gamma}^{f_{G13,(3)}}}{\partial x_{\gamma}} = \int c_{\alpha} c_{\beta} \Omega(f_{G13}) d\mathbf{c}, \quad (2.37)$$

$$\frac{\partial \Pi_{\alpha\beta\beta}^{f_{G13,(3)}}}{\partial t} + \frac{\partial \Pi_{\alpha\beta\beta\gamma}^{f_{G13,(4)}}}{\partial x_{\gamma}} = \int c_{\alpha} c_{\beta} c_{\beta} \Omega(f_{G13}) d\mathbf{c}. \quad (2.38)$$

$$(2.39)$$

While a link between macroscopic equations and Boltzmann equation has already been produced throughout the Hilbert or the Chapman-Enskog expansions presented in Sec. 2.1.1, Grad's interpretation using Hermite polynomials presents an undeniable advantage : given a certain truncated expansion Eq. (2.29), it provides without any assumptions the equivalent set of macroscopic equations, which is of course not exactly the NSF system presented in Chapter 1.

2.2. Gauss-Hermite quadrature and velocity space discretization

Now that a bridge has been established between macroscopic equations and the Boltzmann equation, let us discuss discretization. Continuous solutions $f(\mathbf{c}, t, \mathbf{x})$ are evolving in a 7-dimensional space made of t, x, y, z, c_x, c_y and c_z . In order to implement an efficient LB solver, one should discretize all of these 7 different parameters. The first one we are interested in is the velocity space corresponding to $\mathbf{c} = (c_x, c_y, c_z)$. Physically, velocity \mathbf{c} appearing in Eq. (2.4) is the velocity of particles, or molecular velocity. For most particles, \mathbf{c} is expected to be of the order of \mathbf{u} , the mean velocity of the flow. Because of thermal random motion, some particles are going faster or slower than \mathbf{u} , nevertheless, the relevant physical information is physically expected to be mainly localized around $\mathbf{c} \approx \mathbf{u}$. An indication of the dispersion of particle velocities around $\mathbf{c} \approx \mathbf{u}$ is the sound speed $\sqrt{\gamma r T}$, as it can be seen on Fig. 2.1. The sound speed is related to the energy embedded by random thermal motions [6, 43, 45, 46]. Assuming that physical information carried by extremely low and high speeds \mathbf{c} compared to \mathbf{u} is negligible means that f can be assumed to be non-zero only on a finite interval of velocities \mathbf{c} whose the characteristic value is controlled by \mathbf{u} and characteristic width by $\sqrt{\gamma r T}$.

However in order to keep the physical kinetic interpretation, the velocity space discretization would be expected to map with a sufficient amount of points at least the

2. From the kinetic theory of gases to the lattice-Boltzmann scheme – 2.2.
Gauss-Hermite quadrature and velocity space discretization

finite portion of the velocity space \mathbf{c} "around" the particular value \mathbf{u} . In practice, this is not the kind of arguments that was retained to serve as guideline during the discretization process of \mathbf{c} . Instead, to mimic a lattice gas automaton [64], discretized velocities $c_{i\alpha}$ are taken as integer values of the characteristic numerical velocity $\frac{\Delta x}{\Delta t}$. In LB, the velocity space is usually poorly discretized, typically only using a 3 points stencil in 1D. Indeed, the amount of discrete velocities $c_{i\alpha}$ is kept as low as possible in order to reduce computational costs. A comparison between the Maxwellian equilibrium distribution and the LB D1Q3 equilibrium can be seen on Fig. 2.2, where we clearly see that the discretized equilibrium is only captured by 3 points. In fact, these lattice points are always chosen such that mass, momentum and total energy are the same between the discretized and continuous equilibrium.

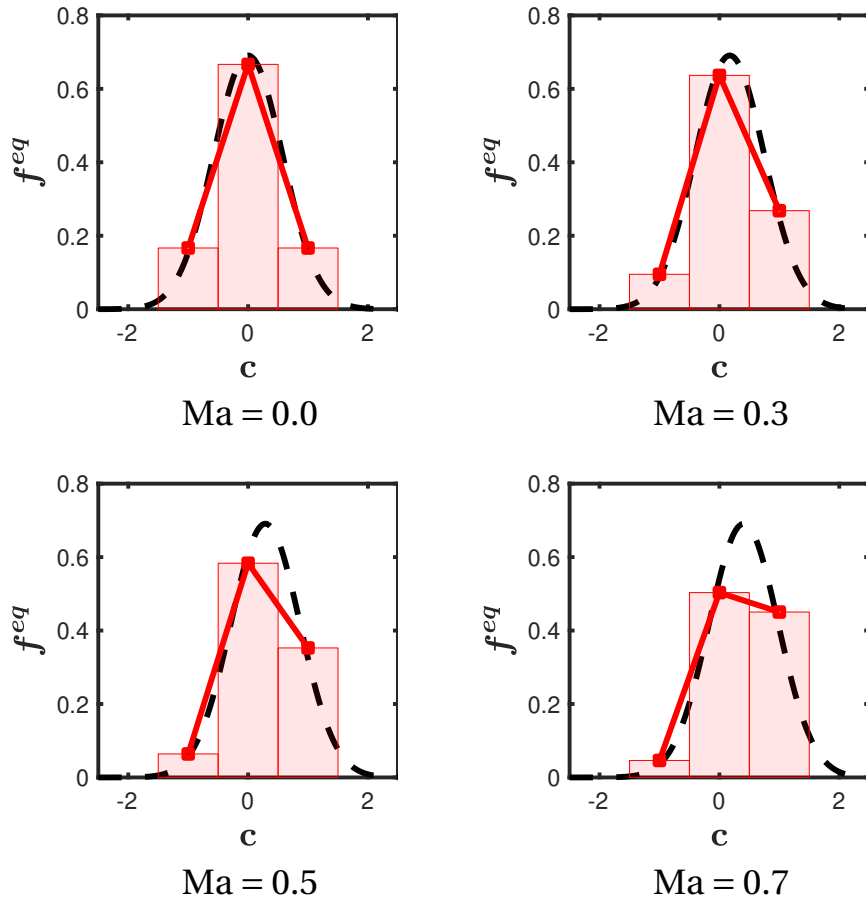


Figure 2.2. – D1Q3 discretized — versus continuous Maxwellian --- Eq. (2.6).
The discretized distribution is built such that its discrete 0^{th} , 1^{st} and 2^{nd} order moments exactly match the equivalent continuous moments of the continuous Maxwellian. For 0^{th} order it means that areas of red rectangles are identical to areas below the black curves.

Additionally, velocities are chosen such that the LB stencil made of q discrete veloc-

2. From the kinetic theory of gases to the lattice-Boltzmann scheme – 2.2.
Gauss-Hermite quadrature and velocity space discretization

ities verifies the following symmetry/isotropy properties [4, 63, 65],

$$\sum_{i=0}^{q-1} \omega_i = 1, \quad (2.40)$$

$$\sum_{i=0}^{q-1} \omega_i c_{i\alpha} = 0, \quad (2.41)$$

$$\sum_{i=0}^{q-1} \omega_i c_{i\alpha} c_{i\beta} = c_s^2 \delta_{\alpha\beta}, \quad (2.42)$$

$$\sum_{i=0}^{q-1} \omega_i c_{i\alpha} c_{i\beta} c_{i\gamma} = 0, \quad (2.43)$$

$$\sum_{i=0}^{q-1} \omega_i c_{i\alpha} c_{i\beta} c_{i\gamma} c_{i\delta} = c_s^4 (\delta_{\alpha\beta} \delta_{\gamma\delta} + \delta_{\alpha\gamma} \delta_{\beta\delta} + \delta_{\alpha\delta} \delta_{\beta\gamma}), \quad (2.44)$$

$$\sum_{i=0}^{q-1} \omega_i c_{i\alpha} c_{i\beta} c_{i\gamma} c_{i\delta} c_{i\epsilon} = 0, \quad (2.45)$$

where $c_s = \Delta x / (\sqrt{3} \Delta t)$ is the lattice sound speed, corresponding to the actual sound speed for athermal models, $c_{i\alpha}$ is the discretized velocity and ω_i is the discretized lattice weight that ensures that any N^{th} order polynomial $P^{(N)}(c_{i\alpha})$ exactly verifies

$$\int \omega(\mathbf{c}) P^{(N)}(\mathbf{c}) d\mathbf{c} = \sum_{i=0}^{q-1} \omega_i P^{(N)}(c_i). \quad (2.46)$$

The highest order $N = M$ verifying Eq. (2.46) is said to be the quadrature order of the lattice. Noting that computing the K^{th} order moment of the L^{th} order distribution function means that a $(K + L)^{th}$ order polynomial is involved, we see that $K + L$ should necessarily be smaller or equal to M – the quadrature order of the lattice – in order to verify exactly

$$\alpha_{\alpha_1 \dots \alpha_n}^{f, (n)} = \sum_{i=0}^{q-1} \mathcal{H}_{i\alpha_1 \dots \alpha_n}^{(n)} f_i = \int \mathcal{H}_{i\alpha_1 \dots \alpha_n}^{(n)} f_i d\mathbf{c}, \quad (2.47)$$

$$\Pi_{\alpha_1 \dots \alpha_n}^{f, (n)} = \sum_{i=0}^{q-1} c_{i\alpha_1} \dots c_{i\alpha_n} f_i = \int c_{i\alpha_1} \dots c_{i\alpha_n} f_i d\mathbf{c}. \quad (2.48)$$

Which are consequences of Eq. (2.46) for the 2 particular cases $\omega_i P^{(N)}(c_i) = \mathcal{H}_{i\alpha_1 \dots \alpha_n}^{(n)} f_i$ and $\omega_i P^{(N)}(c_i) = c_{i\alpha_1} \dots c_{i\alpha_n} f_i(c_i)$. Note that the perfect matching between discrete sums and continuous integrals in Eqs. (2.47, 2.48) is mandatory for at least $n = 0, 1, 2$ in order for f_i to still match mass/momentum/energy definitions Eqs. (2.1, 2.3) on a poorly discretized velocity space.

In lattice Boltzmann, a d dimensional lattice with q velocities is referred to as $DdQq$. Most notorious lattices are D1Q3, D2Q9, D3Q19 and D3Q27. They are called standard

2. From the kinetic theory of gases to the lattice-Boltzmann scheme – 2.2.
Gauss-Hermite quadrature and velocity space discretization

lattices and only involve the first layer of neighboring points, which makes them computationally cheap, which is why they are often used in LB simulations. However, these lattices exhibit a low quadrature order of 5. This means that using a 3^{rd} order equilibrium distribution, only moments up to 2^{nd} order are properly captured by the lattice. Higher order moments, such as some 3^{rd} order ones would not be accurately computed. This is due to the fact that because a DdQq lattice only exhibits q degrees of freedom, it also corresponds to only q Hermite polynomials and therefore only q independent moments can be described by DdQq. Other moments are linear functions of the q independent moments. A very simple example can be found in [4]. Let us consider a D2Q9 lattice, then $c_{i\alpha} \in \{-1, 0, +1\} \frac{\Delta x}{\Delta t}$ such that $c_{i\alpha}^3 = \left(\frac{\Delta x}{\Delta t}\right)^2 c_{i\alpha}$, leading to

$$\Pi_{\alpha\alpha\alpha}^{eq} = \sum_{i=0}^8 c_{i\alpha}^3 f_i^{3,eq} = \left(\frac{\Delta x}{\Delta t}\right)^2 \sum_{i=0}^8 c_{i\alpha} f_i^{3,eq} = \left(\frac{\Delta x}{\Delta t}\right)^2 \Pi_{\alpha}^{eq}. \quad (2.49)$$

This shows an example in which a 3^{rd} order moment is linearly dependent on one of the q independent lower order moments. This is not supposed to happen and it introduces errors. For standard lattices it directly introduces an error in both the energy equation and the stress tensor through $D_{\alpha\dots\alpha_n}^{f,(n)}$ which is traditionally called isotropy defect, see here the 3^{rd} order isotropy defect,

$$D_{\alpha\beta\gamma}^{f,(3)} = \int c_{\alpha} c_{\beta} c_{\gamma} f d\mathbf{c} - \sum_{i=0}^{q-1} c_{\alpha} c_{\beta} c_{\gamma} f \neq 0. \quad (2.50)$$

Through the discretization of the velocity space and the projection of distributions onto Hermite polynomials, the fully continuous variable $f(\mathbf{c}, t, \mathbf{x})$ is replaced by q discrete variables $f_i(\mathbf{c}_i, \mathbf{x}, t)$ whose system of equations is summarized by the Discrete Velocity Boltzmann Equation, or DVBE,

$$\frac{\partial f_i}{\partial t} + c_{i\alpha} \frac{\partial f_i}{\partial x_{\alpha}} = \Omega_i, \quad (2.51)$$

which is a *lattice dependent* system made of q evolution equations numbered $i = 0 \dots q-1$. An important conclusion which is usually not highlighted is that in LB solvers, a change of lattice/stencil is also a change of the DVBE physical model, and equivalently a change of the associated Grad-moment model (see Sec. 2.1.2) obtained from the projection of distributions onto the truncated Hermite polynomial basis associated to a given DdQq lattice.

In this chapter, we have seen that the velocity space discretization follows an unusual path. While a discretization process usually introduces errors proportional to a power of the "spacing" between 2 discrete points, here the velocity space discretization was chosen in order to perfectly match low order moments typically involved in a NSF model. In other words on Fig. 2.2, red points – the discretized f^{eq} – are chosen such that their discrete 0^{th} , 1^{st} and 2^{nd} order moments exactly match the continuous 0^{th} ,

2. From the kinetic theory of gases to the lattice-Boltzmann scheme – 2.3. About the traditional interpretation of lattice-Boltzmann schemes

1st and 2nd order moments of the Maxwellian distribution with a minimum amount of points. This leads to an extremely poorly discretized equilibrium, as can be seen in Fig. 2.2. For these reasons, we should recall that while the lattice Boltzmann method is historically inherited from the Boltzmann equation (2.4), it is certainly not a classical mesoscopic solver because the velocity space discretization was based on macroscopic and computational costs considerations rather than mesoscopic Physics. Additionally, we recall from Sec. 2.1 that macroscopic models – such as equations of state and constitutive equations – are entirely hidden inside Ω_i , then different collisions would lead to different macroscopic models, possibly different from the NSF one. Therefore, while it is sometimes presented as such, it seems too simple to conclude in good faith that LB describes more general Physics compared to NSF models by considering a mesoscopic approach, and we believe that any similar statement should be welcomed by skepticism. A more reasonable statement would be that when properly built, a LB scheme *could* approximate a NSF model depending on its equilibrium f^{eq} and its collision term Ω_i . Another reasonable statement would be that when the size of the lattice goes to infinity, the DVBE equation discretized by the LB scheme *could* approximate the solution of the fully continuous Boltzmann model Eq. (2.4), given that the collision model Ω_i is compatible with kinetic theory of gases. Indeed, LB corresponds to a lattice/equilibrium/collision dependent model and an efficient and robust space-time discretization [66].

2.3. About the traditional interpretation of lattice-Boltzmann schemes

Let us now summarize the main results of this chapter :

- First, a bridge was established between the Boltzmann equation (2.4) and the NSF system in Sec. 2.1 using various methods, including the most common one, the Chapman-Enskog method.
- Second, the discretization of velocity space was described in Sec. 2.2, allowing to bridge between the Boltzmann Eq. (2.4) and the discrete velocity Boltzmann equation (2.51).

However, while paving the path between NSF and LB scheme, some unusual premises were necessary :

- I/ By performing an Hilbert or Chapman-Enskog expansion we are trying to replace the kinetic Boltzmann Eq. (2.4) by an infinite expansion providing an infinite number of terms : Euler, NSF, Burnett, etc, see Table 2.1. Then, this expansion is arbitrarily truncated to the NSF level and higher order terms $\mathcal{O}(\text{Kn}^2)$ are simply ignored.

To the best of the authors' knowledge the range of validity of such truncated finite expansions is usually not questioned nor recalled in the LB literature. For instance, the Chapman-Enskog expansion first assumes that the time derivative

2. From the kinetic theory of gases to the lattice-Boltzmann scheme – 2.3. About the traditional interpretation of lattice-Boltzmann schemes

Eq. (2.14) and populations f Eq. (2.11) can be expanded, but none of these assumptions seems to be explicable, particularly when we also remark that this leads to a singular perturbation analysis, meaning that the smallness parameter Kn appears in front of the highest order derivative in the equation. Such singular perturbation expansion is known to exhibit unexpected behaviors when truncated [59], *i.e.* the Chapman-Enskog expansion is asymptotic rather than convergent [4, 37, 61, 67, 68]. Therefore, for a given physical application there is an optimal number of terms to keep in the infinite Chapman-Enskog expansion because higher-order terms may introduce unphysical behaviors. For example, higher order approximations than NSF, namely the Burnett and Super-Burnett equations – see Table 2.1 – can be derived from the Boltzmann equation using Chapman-Enskog. However, negative viscosity for high gradients and short wave instabilities of the Burnett and Super-Burnett equations [56] are reported in the literature. This phenomenon was first observed by Bobylev [69, 70]. This means that higher order approximations in the Chapman-Enskog expansion may lead to less stable and less physical results [56, 71], endorsing a case-dependent convergence of a clipped infinite expansion such as the Chapman-Enskog expansion. In standard LB theory, the expansion is truncated and higher order contributions are assumed negligible, but no argument is provided to support this simplification.

- II/ We have seen in Sec. 2.1.1 that a separation between orders in Kn and some solvability constraints Eq. (2.25) were necessary. The validity of these premises can be reasonably questioned by the absence of general arguments to support them for an arbitrary model. It can also be highlighted that the Chapman-Enskog expansion is often performed with a very simple BGK collision operator, which is now hardly used in practical applications for its behavior in shear flows [72] and porous flows [73]. Although the formal Chapman-Enskog expansion is possible with the quadratic Boltzmann collision operator [7, 60], or the MRT kernel [4], a *rigorous* extension to complex collision kernels such as Regularized [74–76] or Entropic [77–79] remains unknown, at least to the authors' knowledge. In those kernels at least a part of the non-equilibrium population is systematically filtered out and replaced by a reconstructed population, similarly to Eq. (4.17). This filtering is out of the scope of the formal Chapman-Enskog expansion because finding an explicit solution $f^{(n)}$ as a function of $f^{(n-1)}, f^{(n-2)}, \dots$ as simply as in Eqs. (2.16–2.18) would require to invert a complex collision kernel.
- III/ The velocity space was discretized in order to exactly enforce macroscopic constraints and reduce the computational cost of the algorithm. By doing so, nothing proves that the physical mesoscopic properties of the Boltzmann model were retained.
- IV/ The Chapman-Enskog expansion is not unified and often does not even corresponds to what is actually called Chapman-Enskog expansion in the Boltzmann equation literature [7, 60]. Chapman-Enskog expansions presented by 4 of the most classical LB textbooks [4, 35–37] are reported in Table 2.2, showing that

2. From the kinetic theory of gases to the lattice-Boltzmann scheme – 2.3. About the traditional interpretation of lattice-Boltzmann schemes



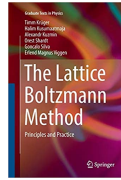
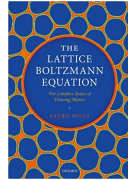
Textbooks :				
$f =$	$\sum_{n=0}^{\infty} \epsilon^n f^{(n)}$	$\sum_{n=0}^{\infty} \epsilon^n f^{(n)}$	$\sum_{n=0}^{\infty} \epsilon^n f^{(n)}$	$\sum_{n=0}^{\infty} \epsilon^n f^{(n)}$
$\frac{\partial}{\partial t} =$	$\epsilon \frac{\partial}{\partial t_1} + \epsilon^2 \frac{\partial}{\partial t_2}$	$\epsilon \frac{\partial}{\partial t_1} + \epsilon^2 \frac{\partial}{\partial t_2}$	$\sum_{n=1}^{\infty} \epsilon^n \frac{\partial}{\partial t_n}$	$\sum_{n=1}^{\infty} \epsilon^n \frac{\partial}{\partial t_n}$
$\frac{\partial}{\partial x} =$	$\epsilon \frac{\partial}{\partial x_1}$	$\epsilon \frac{\partial}{\partial x_1}$	$\epsilon \frac{\partial}{\partial x_1}$	$\sum_{n=1}^{\infty} \epsilon^n \frac{\partial}{\partial x_n}$

Table 2.2. – Comparison of different Chapman-Enskog expansions presented by classical LB textbooks [4, 35–37].

only [35, 36] agree with each other. They chose to expand the time derivative not as an infinite expansion but as a linear composition of a fast convective time t_1 and a slow diffusive time t_2 , in contrast to [4, 37] that merely considers – as the historical Chapman-Enskog – $\partial/\partial t_n$ as mathematical derivatives and insists that they should not be physically interpreted. Under the assumption that each physical scales are important, space derivative is almost never expanded, except by [37]. It is worth noting that only [4] is actually equivalent to the historical Chapman-Enskog expansion [7, 60] while [35, 36] presented a simplified version and [37] a different one. All these versions provided the exact same results up to $\mathcal{O}(\text{Kn}^1)$ terms, however, higher order differences in error terms $\mathcal{O}(\text{Kn}^2)$ arise from these different expansions [4, 35–37].

To summarize this chapter, a theoretical framework does exist in the LB literature. A consensus seems absent and differences between versions of this framework are usually not explained. These frameworks are not fully deductive, need costly premises and are known to produce unphysical models when more terms are kept in the infinite expansion. When carefully thinking about it, the Chapman-Enskog expansion itself seems superfluous because the equivalence between a continuous macroscopic system and the LB equation can be readily obtained throughout the Hermite polynomials, see Sec. 2.1.2. Therefore, while the classical LB theoretical framework has already been presented in this chapter, it does not seem parsimonious enough to us because it is a black-box description. This problem will be addressed in the next two chapters, where we will show that absolutely none of the aforementioned unexplained premises are actually necessary to understand, design and use the LBM. Now, let us present and explain the LB space-time discretization, its capabilities and its drawbacks.

2.4. Recap

In this Chapter, we recalled the traditional notions and tools that are commonly met in the LBM theoretical foundations. However, we believe that the amount of dark-corners and shortcuts used in this traditional approach is sufficient to shed some reasonable doubts on the predictive capacity of the usual interpretation of LBM. Our main two concerns are :

- We do not know how the *extremely* coarse velocity discretization allows to reasonably maintain the mesoscopic kinetic theory interpretation of LB models.
- The Chapman-Enskog expansion is not sufficiently well backed up by actual arguments. Indeed, except the comfortable link with NSF, most actual arguments pleads against its use, see Sec. 2.3.

The classical LB framework is a convenient tool to bridge between LBM and NSF. However, it is an inductive demonstration and its range of validity is not clear enough. In the next two Chapters, we will propose a deductive bridge between LBM and NSF.

3. Lattice-Boltzmann scheme

Sommaire

3.1	Relaxation equation	46
3.2	Space and time discretization	49
3.3	Lattice-Boltzmann collision kernels	53
3.3.1	Multiple Relaxation Time kernels	53
3.3.2	Regularized kernels	55
3.3.3	Other kernels	56
3.3.3.1	Entropic kernels	56
3.3.3.2	Cumulant kernels	56
3.4	Boundary conditions in the lattice-Boltzmann method	56
3.5	The Lattice-Boltzmann Scheme, from time t to $t + \Delta t$	57
3.5.1	Lattice-Boltzmann definitions	58
3.5.2	Structure of a generic lattice-Boltzmann scheme	60
3.6	Recap	63

In this Section, we provide a thorough discussion on the space-time discretization of the DVBE, which is the set of advection-relaxation equations actually solved by a LB solver. In Sec. 3.1, advection is discarded and we focus on a simple discretized relaxation equation for a scalar ϕ . Then we highlight some typical behaviors observed when such equation is discretized. In Sec. 3.2, we discretize the DVBE equipped with an arbitrary collision term Ω_i and an arbitrary forcing term F_i ,

$$\frac{\partial f_i}{\partial t} + c_{i\alpha} \frac{\partial f_i}{\partial x_\alpha} = \Omega_i + F_i. \quad (3.1)$$

The classical change of variables $f_i \rightarrow \bar{f}_i$ is discussed along with its meaning. In Sec. 3.3, different collision kernels are discussed, in particular BGK, MRT and regularized kernels. The LB boundary conditions are discussed in Sec. 3.4. In Sec. 3.5, the content of this chapter is summarized. We show – using a generic LBM – what are the 4 mandatory basic steps to get the updated $t + \Delta t$ solution from of the initial solution t . This Section also provides necessary notations that will be used throughout this manuscript.

3.1. Relaxation equation

The LBM involves a relaxation term. It can be stiff and it is not as widespread in CFD as advection and diffusion models, therefore we think it is better to discuss a simple relaxation model first in order to understand how those models are working and what are the typical numerical errors encountered when discretized. Therefore, we consider the relaxation equation

$$\frac{d\phi}{dt} = -\frac{1}{\tau} (\phi - \phi^{eq}). \quad (3.2)$$

with constant coefficients τ and ϕ^{eq} , the analytical solution is

$$\phi_a(t) = (\phi_0 - \phi^{eq}) e^{-t/\tau} + \phi^{eq}, \quad (3.3)$$

where ϕ_0 is the initial solution,

$$\phi_0 = \phi(t = 0). \quad (3.4)$$

Starting from the initialization ϕ_0 , the solution ϕ will *relax* towards ϕ^{eq} with a characteristic time τ . The relaxation term is therefore a stabilizing term, and tends to damp the initial solution ϕ_0 over time as long as τ is positive. Now, let us see what happens when we discretize Eq. (3.2),

$$\phi(t + \Delta t) - \phi(t) = - \int_0^{\Delta t} \left[\frac{1}{\tau} (\phi - \phi^{eq}) \right] (t + s) ds. \quad (3.5)$$

To evaluate the integral in the right-hand-side, let us use 3 different schemes,

$$\phi(t + \Delta t) - \phi(t) = \Delta t \left[-\frac{1}{\tau} (\phi - \phi^{eq}) \right] (t), \quad (3.6)$$

$$\phi(t + \Delta t) - \phi(t) = \Delta t \left[-\frac{1}{\tau} (\phi - \phi^{eq}) \right] (t + \Delta t), \quad (3.7)$$

$$\phi(t + \Delta t) - \phi(t) = \frac{\Delta t}{2} \left[-\frac{1}{\tau} (\phi - \phi^{eq}) \right] (t + \Delta t) + \frac{\Delta t}{2} \left[-\frac{1}{\tau} (\phi - \phi^{eq}) \right] (t), \quad (3.8)$$

namely the backward rectangle explicit Eq. (3.6), forward rectangle implicit Eq. (3.7) and trapezoidal semi-implicit Eq. (3.8) numerical schemes. Note that the semi-implicit scheme is also known as the Crank-Nicolson scheme. The explicit scheme Eq. (3.6) belongs to the family of explicit methods, while the Crank-Nicolson Eq. (3.8) and implicit Eq. (3.7) are apparently implicit methods because $t + \Delta t$ appears in both the left and right-hand-sides. Note that the Crank-Nicolson scheme is the scheme employed by most recent LB models. Because of this, it is of utmost importance [4] to understand and describe this scheme and its numerical properties. Using the traditional change of variable

$$\bar{\phi} = \phi + \frac{\Delta t}{2\tau} (\phi - \phi^{eq}), \quad (3.9)$$

3. Lattice-Boltzmann scheme – 3.1. Relaxation equation

and injecting it inside Eq. (3.8) leads to

$$\bar{\phi}(t + \Delta t) = \left[\bar{\phi} - \frac{\Delta t}{\tau} (\phi - \phi^{eq}) \right] (t), \quad (3.10)$$

which is not a satisfactory expression because both ϕ and $\bar{\phi}$ appears at the same time. Using Eq. (3.9) provides

$$\phi = \frac{2\tau}{2\tau + \Delta t} \bar{\phi} + \frac{\Delta t}{2\tau + \Delta t} \phi^{eq}, \quad (3.11)$$

which can be directly injected inside Eq. (3.10), finally leading to

$$\bar{\phi}(t + \Delta t) = \left[\bar{\phi} - \frac{\Delta t}{\tau + \frac{\Delta t}{2}} (\bar{\phi} - \phi^{eq}) \right] (t). \quad (3.12)$$

Note that while we assumed constant τ and ϕ^{eq} coefficients this demonstration still stands for variable coefficients. While the scheme Eq. (3.8) was identified as implicit, the algorithm is now explicit for the numerical variable $\bar{\phi}$, but remember that ϕ is the variable of interest. Using the inverse change of variable Eq. (3.11) leads to

$$\phi(t + \Delta t) = \left[\frac{2\tau}{2\tau + \Delta t} \right] (t + \Delta t) \left[\bar{\phi} - \frac{\Delta t}{\tau + \frac{\Delta t}{2}} (\bar{\phi} - \phi^{eq}) \right] (t) + \left[\frac{\Delta t}{2\tau + \Delta t} \phi^{eq} \right] (t + \Delta t), \quad (3.13)$$

which combined with change of variable Eq. (3.9) allows to rewrite the Crank-Nicolson scheme as

$$\phi(t + \Delta t) = \left[\frac{2\tau}{2\tau + \Delta t} \right] (t + \Delta t) \left[\phi^{eq} + \frac{2\tau - \Delta t}{2\tau} (\phi - \phi^{eq}) \right] (t) + \left[\frac{\Delta t}{2\tau + \Delta t} \phi^{eq} \right] (t + \Delta t), \quad (3.14)$$

whose remarkable property is that it remains explicit as long as $(t + \Delta t)$ updated values of τ and ϕ^{eq} are known prior to ϕ . This property is also shared by the implicit scheme, which can be written as

$$\phi(t + \Delta t) = \left[\frac{\tau}{\tau + \Delta t} \right] (t + \Delta t) \left[\phi(t) + \left(\frac{\Delta t}{\tau} \phi^{eq} \right) (t + \Delta t) \right], \quad (3.15)$$

by using Eq. (3.7). In order to compare explicit, Crank-Nicolson and implicit schemes Eqs. (3.6,3.14,3.15), they are used to obtain numerical solutions of Eq. (3.2). The numerical setup is as follows, the initial solution is $\phi_0 = 1$, the target relaxed value is $\phi^{eq} = 0$ and $N = 20 / \Delta t$ timesteps are simulated.

Results are reported on Figure 3.1, we are mainly interested by the effect of the sole non dimensional parameter, $\Delta t / \tau$. In order to get deeper knowledge about those schemes, a similar test case but with $N = 10^4 / \Delta t$ is performed, where only the total error over the complete simulation $\sum |\phi - \phi_a| / N$ is reported on Figure 3.2 as a function of $\Delta t / \tau$. The characteristic time is τ , therefore, one would expect that Δt should be much smaller than τ in order to properly discretize Eq. (3.2).

It is seen on Figure 3.1 that all numerical schemes Eqs. (3.6,3.14,3.15) leads to accu-

3. Lattice-Boltzmann scheme – 3.1. Relaxation equation

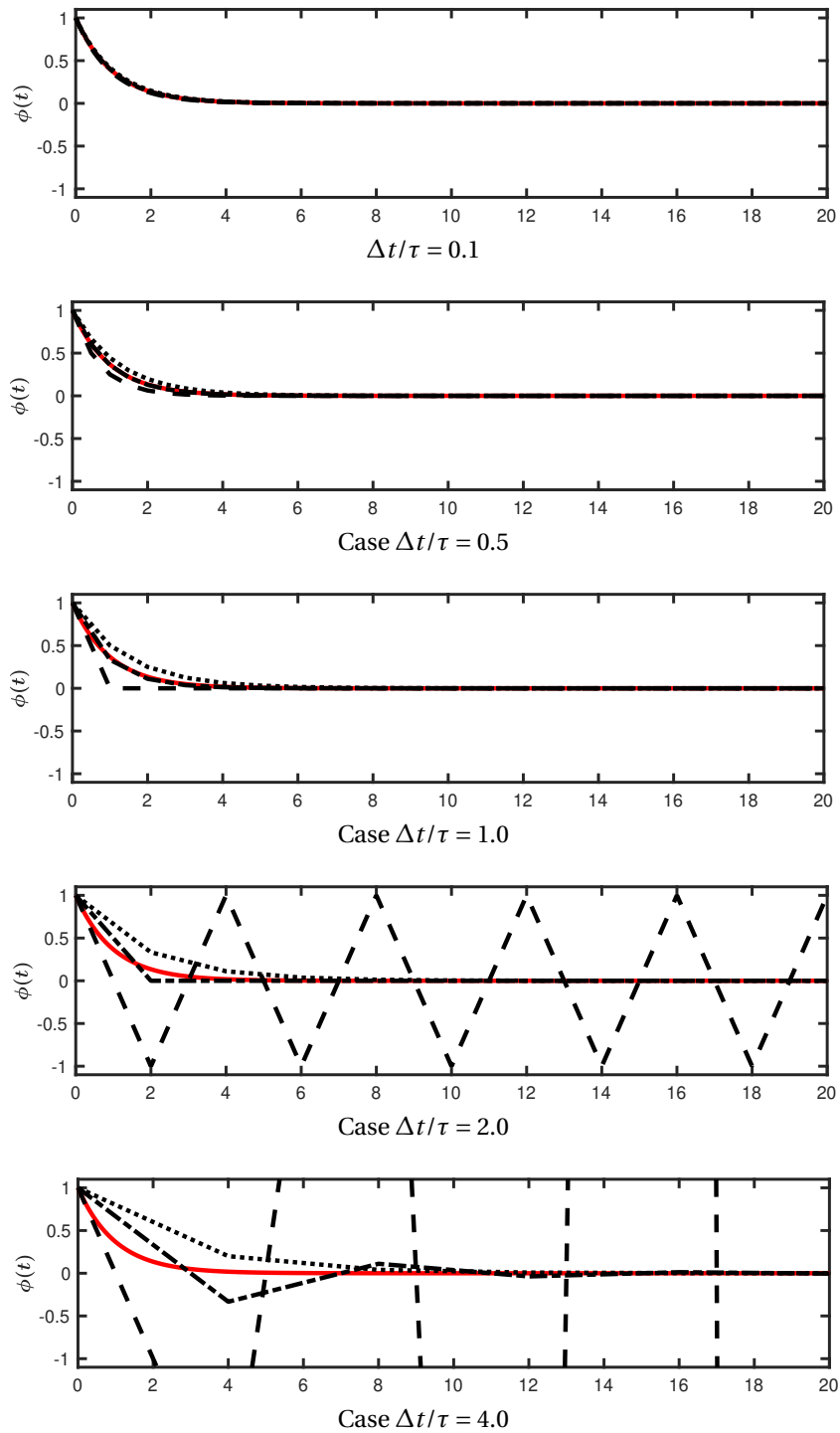


Figure 3.1. – Solutions of the relaxation Eq. (3.2) by different schemes.
— is analytical Eq. (3.3); - - - is explicit Eq. (3.6);
- · - is Crank-Nicolson Eq. (3.14); ···· is implicit Eq. (3.15).

rate solution when $\Delta t/\tau \ll 1$, however, for higher values of this parameter, interesting

3. Lattice-Boltzmann scheme – 3.2. Space and time discretization

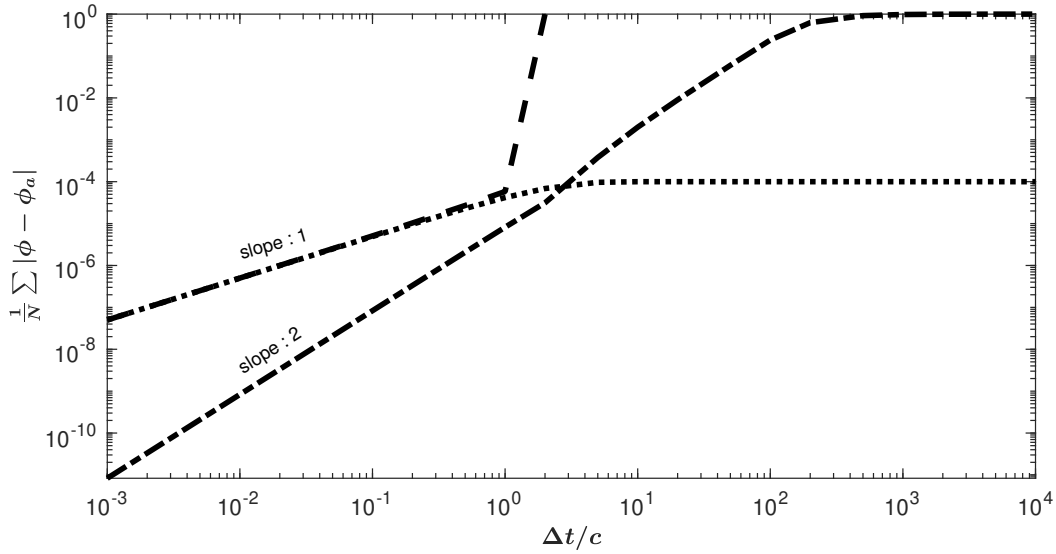


Figure 3.2. – Convergence study of the relaxation test case as a function of $\Delta t/\tau$. --- is explicit Eq. (3.6); -.- is Crank-Nicolson Eq. (3.14); is implicit Eq. (3.15).

tendencies can be reported. First, it seems that the Crank-Nicolson scheme is more accurate than the explicit and implicit schemes for $\Delta t/\tau \leq 1$, this is confirmed by Figure 3.2 where it is seen that Crank-Nicolson is 2^{nd} order accurate while explicit and implicit schemes are only 1^{st} order accurate.

The explicit and Crank-Nicolson instantly and exactly relaxed toward ϕ^{eq} in one time step for respectively $\Delta t = \tau$ and $\Delta t = 2\tau$. For $\Delta t = 2\tau$, the explicit scheme oscillates around ϕ^{eq} , the solution is said to be over-relaxed. More specifically, it infinitely oscillates with an amplitude $2\phi_0$ centered around ϕ^{eq} , switching from $\pm\phi_0$ to $\mp\phi_0$ between each timestep. For larger values $\Delta t > 2\tau$, the explicit scheme is unstable as it is over-relaxed but with an amplification over time, as can be seen on Figure 3.2, however, the Crank-Nicolson scheme remains unconditionally stable for all $\Delta t/\tau$. For $\Delta t > 2\tau$, Crank-Nicolson solution is also over relaxed with a slow damping rate of the oscillations, an higher Δt leading to a slower damping rate.

The implicit scheme, on the other hand, is unconditionally stable and is free of the over-relaxation phenomenon, however, it is seen that it leads to under-relaxed solution, ϕ always converges slower than expected, this delay increases as $\Delta t/\tau \rightarrow \infty$, as can be seen on Figure 3.1.

3.2. Space and time discretization

Now that the relaxation toy model was discretized, we understand concepts such as over and under relaxation associated to discretized relaxation equations. By making full use of the constant velocity advection $c_{i\alpha}$, it is possible to integrate Eq. (2.51) along the characteristic line $\frac{dx}{dt} = c_{i\alpha}$ and to use the Crank-Nicolson rule. Integration over the characteristic line of Eq. (3.1) with an additional arbitrary force term F_i in the

3. Lattice-Boltzmann scheme – 3.2. Space and time discretization

right-hand-side exactly leads to

$$f_i(t + \Delta t, \mathbf{x} + \mathbf{c}_i \Delta t) = f_i(t, \mathbf{x}) + \int_0^{\Delta t} [\Omega_i + F_i](t + s, \mathbf{x} + \mathbf{c}_i s) ds. \quad (3.16)$$

The integral of the right-hand-side of Eq. (3.16) should be evaluated. Using the trapezoidal rule – Crank-Nicolson scheme [4, 24, 80], the same as in Sec. 3.1 – one finds that

$$f_i(t + \Delta t, \mathbf{x} + \mathbf{c}_i \Delta t) = f_i(t, \mathbf{x}) + \frac{\Delta t}{2} \{[\Omega_i + F_i](t, \mathbf{x}) + [\Omega_i + F_i](t + \Delta t, \mathbf{x} + \mathbf{c}_i \Delta t)\} + \mathcal{O}(\Delta t^3). \quad (3.17)$$

Which is an implicit second order accurate $\mathcal{O}(\Delta t^2)$ scheme. Neglecting $\mathcal{O}(\cdot)$ for compactness and defining the intermediate variable $\bar{f}_i = f_i - \frac{\Delta t}{2}[\Omega_i + F_i]$ one gets that

$$\bar{f}_i(t + \Delta t, \mathbf{x} + \mathbf{c}_i \Delta t) = \left\{ \bar{f}_i + \Delta t [\Omega_i + F_i] \right\} (t, \mathbf{x}) \quad (3.18)$$

which is now an explicit scheme for the numerical variable \bar{f}_i . Now shifting Eq. (3.18) by a distance $-\mathbf{c}_i \Delta t$, we are led to an equivalent expression

$$\bar{f}_i(t + \Delta t, \mathbf{x}) = \left\{ \bar{f}_i + \Delta t [\Omega_i + F_i] \right\} (t, \mathbf{x} - \mathbf{c}_i \Delta t). \quad (3.19)$$

From this, it is clear that knowing the last time step variables $[\bar{f}_i, \Omega_i, F_i](t, \mathbf{x})$ allows to know the updated variable $\bar{f}_i(t + \Delta t, \mathbf{x})$. Recalling that \bar{f}_i is merely a numerical variable – similarly to $\bar{\phi}$ in Sec. 3.1 – we should rather try to obtain $f_i(t + \Delta t, \mathbf{x})$. Alternatively, f_i could be split into its equilibrium and non-equilibrium components,

$$f_i^{neq} = f_i - f_i^{eq}. \quad (3.20)$$

Using the definition of \bar{f}_i ,

$$[f_i^{eq} + f_i^{neq}](t + \Delta t, \mathbf{x}) - \frac{\Delta t}{2} [\Omega_i + F_i](t + \Delta t, \mathbf{x}) = \bar{f}_i(t + \Delta t, \mathbf{x}), \quad (3.21)$$

in which the right-hand-side is known from the last time step solution thanks to Eq. (3.19). Then, we compute 0^{th} , 1^{st} and 2^{nd} order moments of Eq. (3.21) and since

3. Lattice-Boltzmann scheme – 3.2. Space and time discretization

Eq. (2.5) these moments applied to Ω_i are identically 0 we can find

$$\Pi^{f^{eq},(0)}(t + \Delta t, \mathbf{x}) = \Pi^{f,(0)}(t + \Delta t, \mathbf{x}) = \rho(t + \Delta t, \mathbf{x}) = \left[\bar{\Pi}^{\bar{f},(0)} + \frac{\Delta t}{2} \Pi^{E,(0)} \right] (t + \Delta t, \mathbf{x}), \quad (3.22)$$

$$\Pi_{\alpha}^{f^{eq},(1)}(t + \Delta t, \mathbf{x}) = \Pi_{\alpha}^{f,(1)}(t + \Delta t, \mathbf{x}) = [\rho u_{\alpha}] (t + \Delta t, \mathbf{x}) = \left[\bar{\Pi}_{\alpha}^{\bar{f},(1)} + \frac{\Delta t}{2} \Pi_{\alpha}^{E,(1)} \right] (t + \Delta t, \mathbf{x}), \quad (3.23)$$

$$\Pi_{\alpha\alpha}^{f^{eq},(2)}(t + \Delta t, \mathbf{x}) = \Pi_{\alpha\alpha}^{f,(2)}(t + \Delta t, \mathbf{x}) = [\rho E] (t + \Delta t, \mathbf{x}) = \left[\bar{\Pi}_{\alpha\alpha}^{\bar{f},(2)} + \frac{\Delta t}{2} \Pi_{\alpha\alpha}^{E,(2)} \right] (t + \Delta t, \mathbf{x}, t). \quad (3.24)$$

At this stage $\bar{\Pi}_{\alpha_1 \dots \alpha_n}^{\bar{f},(n)}$ is known because it was updated from the knowledge of the last time step solution through the streaming, Eq. (3.19). An intermediary conclusion can be drawn here, if the n^{th} order raw force moment $\Pi_{\alpha_1 \dots \alpha_n}^{F,(n)}$ depends on $\Pi_{\alpha_1 \dots \alpha_n}^{f,(n)}$, then the numerical scheme may become implicit. If it depends on gradients of $\Pi_{\alpha_1 \dots \alpha_n}^{f,(n)}$, it can even become implicit *and* non-local. A very simple way to overcome the possible high numerical cost of solving implicit and/or non-local problems is simply to replace $\Pi_{\alpha_1 \dots \alpha_n}^{F,(n)}(t + \Delta t, \mathbf{x})$ by $\Pi_{\alpha_1 \dots \alpha_n}^{F,(n)}(t, \mathbf{x})$, which formally introduces a $\mathcal{O}(\Delta t)$ error in the usually $\mathcal{O}(\Delta t^2)$ order accurate LB scheme.

Now, by noticing that f^{eq} is *only* a function of macroscopic variables ρ , u_{α} and E , it is possible to reconstruct the updated equilibrium $f_i^{eq}(t + \Delta t, \mathbf{x})$ by solving Eqs. (3.22-3.24). Going back to Eq. (3.21) and moving to the right-hand-side all known quantities one gets

$$f_i^{neq}(t + \Delta t, \mathbf{x}) - \frac{\Delta t}{2} \Omega_i(t + \Delta t, \mathbf{x}) = \left[\bar{f}_i - f_i^{eq} + \frac{\Delta t}{2} F_i \right] (t + \Delta t, \mathbf{x}). \quad (3.25)$$

Using the change of variable $\bar{f}_i = f_i - \frac{\Delta t}{2} [\Omega_i + F_i]$, we can similarly define

$$\bar{f}_i^{neq} = \bar{f}_i - f_i^{eq} + \frac{\Delta t}{2} F_i, \quad (3.26)$$

$$= f_i^{neq} - \frac{\Delta t}{2} \Omega_i, \quad (3.27)$$

which leads to the non-equilibrium numerical scheme,

$$f_i^{neq}(t + \Delta t, \mathbf{x}) - \frac{\Delta t}{2} \Omega_i(t + \Delta t, \mathbf{x}) = \bar{f}_i^{neq}(t + \Delta t, \mathbf{x}). \quad (3.28)$$

In order to compute the updated non-equilibrium distribution, we need to solve an implicit equation because Ω_i is a function of f_i^{neq} . However, the BGK collision kernel

3. Lattice-Boltzmann scheme – 3.2. Space and time discretization

$\Omega_i = -\frac{1}{\tau} f_i^{neq}$ allows a simple explicit evaluation,

$$\left[\left(1 + \frac{\Delta t}{2\tau} \right) f_i^{neq} \right] (t + \Delta t, \mathbf{x}) = \bar{f}_i^{neq} (t + \Delta t, \mathbf{x}). \quad (3.29)$$

From Eq. (3.29) and assuming that Eqs. (3.22-3.24) have been solved with a $\mathcal{O}(\Delta t^2)$ accuracy, one could obtain a fully explicit scheme by getting f_i^{neq} from Eq. (3.29). Now, going back to Eq. (3.19) and rearranging it using Eq. (3.26), this yields

$$\bar{f}_i(t + \Delta t, \mathbf{x}) = \left\{ f_i^{eq} + \bar{f}_i^{neq} + \Delta t \left[\Omega_i + \frac{1}{2} F_i \right] \right\} (t, \mathbf{x} - \mathbf{c}_i \Delta t). \quad (3.30)$$

For the BGK collision kernel the link between $\bar{f}_{i,BGK}^{neq}$ and $f_{i,BGK}^{neq}$ non-equilibriums – Eq. (3.27) – then reduces to

$$\bar{f}_{i,BGK}^{neq} = \left(1 + \frac{\Delta t}{2\tau} \right) f_i^{neq}. \quad (3.31)$$

Therefore, the BGK collision kernel $\Omega_{i,BGK} = -\frac{1}{\tau} f_i^{neq}$ can also be written in a fully equivalent way

$$\Omega_{i,BGK} = -\frac{1}{\tau + \frac{\Delta t}{2}} \bar{f}_i^{neq}. \quad (3.32)$$

Introducing the classical notation, we define the numerical relaxation time $\bar{\tau}$ by

$$\bar{\tau} = \tau + \frac{\Delta t}{2}. \quad (3.33)$$

Finally, collecting Eqs. (3.30,3.32,3.33) leads to the classical $\mathcal{O}(\Delta t^2)$ LB-BGK numerical scheme that is found in many classical textbooks [4, 35–37],

$$\boxed{\bar{f}_i(t + \Delta t, \mathbf{x}) = \left[f_i^{eq} + \left(1 - \frac{\Delta t}{\bar{\tau}} \right) \bar{f}_i^{neq} + \frac{\Delta t}{2} F_i \right] (t, \mathbf{x} - \mathbf{c}_i \Delta t),} \quad (3.34)$$

where the non equilibrium is computed through Eq. (3.26). Note that when we are not interested by computing the stress tensor $\Pi_{\alpha\beta}^{neq}$, the computation of f_i^{neq} from \bar{f}_i^{neq} is unnecessary. Here, we have only presented the classical Crank-Nicolson discretization, but higher multistep schemes could also be used [66]. The very simple algorithm described here was obtained through a rigorous discretization of Eq. (2.51) using the assumption of a BGK collision kernel Eq. (3.32). However, while the procedure we have just described here is a rigorous and well-paved *deduction*, an equivalent demonstration from the continuous equations is sometimes not possible for other collision kernels Ω_i . We shall now discuss this topic.

3.3. Lattice-Boltzmann collision kernels

The need for sophisticated collision kernels lies in the lack of stability of the BGK collision model [81, 82]. Noticing that f_i^{eq} only depends on a few number of variables (ρ , u_α and E which means 5 variables for a 3D solver) all the other $q-5$ non-hydrodynamic variables hidden in a DdQq LB solver are actually hidden inside \bar{f}_i^{neq} . Therefore, the vast majority of variables solved by a LB solver are not physically meaningful for macroscopic Physics. The common strategy to increase numerical stability is to change the collision model Ω_i . A change of collision kernel only impacts non-hydrodynamic moments, therefore, a lot of different strategies could be employed to design Ω_i .

3.3.1. Multiple Relaxation Time kernels

A straightforward generalization of the single relaxation collision Eq. (3.32) is obtained by choosing to relax with different characteristic times each of the q independent variables during the collision. This is achieved using an MRT model [4, 83],

$$\Omega_i = M_{ij} f_j^{neq}, \quad (3.35)$$

where M_{ij} is a matrix depending on several relaxations times $\tau_1, \tau_2, \dots, \tau_q$. Equipped with this new collision, we are now solving a numerical scheme consistent in the sense of Lax [14, 22, 23] to the following DVBE-MRT continuous equation,

$$\frac{\partial f_i}{\partial t} + c_{i\alpha} \frac{\partial f_i}{\partial x_\alpha} = M_{ij} f_j^{neq} + F_i, \quad (3.36)$$

Now, let us try to see what is the actual link between \bar{f}_i^{neq} and f_i^{neq} . Using both Eq. (3.27) and Eq. (3.35) leads to

$$\bar{f}_i^{neq} = f_i^{neq} - \frac{\Delta t}{2} M_{ij} f_j^{neq}. \quad (3.37)$$

$$\bar{f}_i^{neq} = \left(\delta_{ij} - \frac{\Delta t}{2} M_{ij} \right) f_j^{neq}. \quad (3.38)$$

Making the *ansatz* that $\left(\delta_{ij} - \frac{\Delta t}{2} M_{ij} \right)$ is invertible we could obtain f_i^{neq} as a function of \bar{f}_i^{neq} ,

$$f_i^{neq} = \left[\left(\boldsymbol{\delta} - \frac{\Delta t}{2} \mathbf{M} \right)^{-1} \right]_{ij} \bar{f}_j^{neq}. \quad (3.39)$$

Then, injecting Eq. (3.39) inside Eq. (3.27) we obtain for an arbitrary MRT model the collision kernel Ω_i as a function of \bar{f}_j^{neq} and M_{ij} only,

$$\Delta t \Omega_i = 2 \left\{ \left[\left(\boldsymbol{\delta} - \frac{\Delta t}{2} \mathbf{M} \right)^{-1} \right]_{ij} - \delta_{ij} \right\} \bar{f}_j^{neq}. \quad (3.40)$$

3. Lattice-Boltzmann scheme – 3.3. Lattice-Boltzmann collision kernels

Before going further, let us highlight a particular choice of MRT model where all relaxation times are identical, $M_{ij} = \tau^{-1} \delta_{ij}$ [4], which is nothing but the BGK kernel. In this case Eq. (3.40) reduces to the classical BGK model,

$$\Delta t \Omega_{i,BGK} = -\frac{\Delta t}{\bar{\tau}} \bar{f}_i^{neq} = -\frac{\Delta t}{\tau} f_i^{neq}. \quad (3.41)$$

where we used the classical shorthand $\bar{\tau} = \tau + \Delta t/2$. Having identified that MRT models are nothing but a generalization of BGK, let us try to understand further what we means by "multiple relaxation time". To allow for a simple understanding, the LB scheme for arbitrary collision Ω_i and force term F_i , Eq. (3.30), needs to be split into 2 different steps, the so-called collide,

$$f_i^{col}(t, \mathbf{x}) = \left\{ f_i^{eq} + \bar{f}_i^{neq} + \Delta t \left[\Omega_i + \frac{1}{2} F_i \right] \right\} (t, \mathbf{x}), \quad (3.42)$$

and stream,

$$\bar{f}_i(t + \Delta t, \mathbf{x}) = f_i^{col}(t, \mathbf{x} - \mathbf{c}_i \Delta t). \quad (3.43)$$

Now, collision step can be obtained for an arbitrary MRT model using Eqs. (3.40,3.42),

$$f_i^{col}(t, \mathbf{x}) = \left\{ f_i^{eq} + \bar{f}_i^{neq} + \left[\left(\boldsymbol{\delta} - \frac{\Delta t}{2} \mathbf{M} \right)^{-1} \right]_{ij} - \delta_{ij} \right\} \bar{f}_j^{neq} + \frac{\Delta t}{2} F_i \right\} (t, \mathbf{x}). \quad (3.44)$$

Depending on matrix M_{ij} , different quantities can be relaxed [84]. For exemple, with the BGK kernel, all non-equilibrium moments are relaxed with the same characteristic time τ . For the TRT model [4], even and odd non-equilibrium moments are relaxed with different characteristic times τ^+ and τ^- . For the raw-moment MRT [84] raw moments are relaxed, for the central-moment MRT [84] central moments are relaxed. In essence, a MRT model is a model that relaxes different moments with different relaxation rates. To make things as simple as possible, we do not specify *which* moments are relaxed, let us simply note that the collision Eq. (3.42) could be recast from the distribution space to the moment space. In which case we denote by \mathcal{M} the vector of the relaxed moments \mathcal{M}_j , they correspond to even/odd moments for TRT, raw moments for raw-MRT, and central moments for central-MRT/cascaded [85, 86]. Then, the q f_i -relaxations summarized by Eq. (3.42) could be replaced by q equivalent \mathcal{M}_j -relaxations,

$$\mathcal{M}_j^{f^{col}}(t, \mathbf{x}) = \left[\mathcal{M}_j^{f_i^{eq}} + \left(1 - \frac{\Delta t}{\frac{\Delta t}{2} + \tau_{\mathcal{M}_j}} \right) \mathcal{M}_j^{\bar{f}_j^{neq}} + \frac{\Delta t}{2} \mathcal{M}_j^{F_i} \right] (t, \mathbf{x}), \quad (3.45)$$

where $\tau_{\mathcal{M}_j}$ is the relaxation rate associated to moment \mathcal{M}_j . A very special value of $\tau_{\mathcal{M}_j}$ should be mentioned, when

$$\tau_{\mathcal{M}_j} = \frac{\Delta t}{2}, \quad (3.46)$$

3. Lattice-Boltzmann scheme – 3.3. Lattice-Boltzmann collision kernels

the post-collision moment \mathcal{M}_j^{fcol} reduces to

$$\mathcal{M}_j^{fcol}(t, \mathbf{x}) = \mathcal{M}_j^{fi^{eq}}(t, \mathbf{x}), \quad (3.47)$$

which corresponds to the *filtration* of moment $\mathcal{M}_j^{\bar{f}^{neq}}$. In other words, the rank of the system is reduced because the next time step solution $t + \Delta t$ does not depend anymore on $\mathcal{M}_j^{\bar{f}^{neq}}$. Comparing to the relaxation toy-model presented in Sec. 3.1, this corresponds to a forced *instantaneous* relaxation of $\mathcal{M}_j^{f^{neq}}$ – remember that $\mathcal{M}_j^{f^{neq}} \propto \mathcal{M}_j^{\bar{f}^{neq}} - \text{to } 0$. Moment $\mathcal{M}_j^{f^{neq}}$ is said to be *filtered* or *regularized*. Note that other MRT models sometimes use

$$\tau_{\mathcal{M}_j} = \text{cste} \Delta t, \quad \text{cste} \neq \frac{1}{2}, \quad (3.48)$$

in which case moment $\mathcal{M}_j^{f^{neq}}$ is not anymore filtered. However, this means that the *a priori* physical relaxation time $\tau_{\mathcal{M}_j}$, which is a continuous parameter, is now enslaved to Δt , necessarily leading to a $\mathcal{O}(\Delta t)$ accurate scheme. Comparing with the relaxation toy model behavior presented in Sec. 3.1, this means that the relaxation of \mathcal{M}_j^f toward $\mathcal{M}_j^{fi^{eq}}$ is faster for lower Δt . This is another example where a LB practice cannot be reasonably explained by a kinetic theory approach. Rather than that, both choices Eqs. (3.46,3.48) can be seen as numerical tricks to enhance the accuracy and/or stability of the overall scheme.

3.3.2. Regularized kernels

Regularized kernels are a class of collision models in which *some* of the non-equilibrium moments are filtered Eq. (3.46). As we have just mentioned it, they could be understood as specific MRT models [84]. Here, we generalize the filtered/regularized kernel. The collision is slightly changed and now reads

$$\mathcal{M}_j^{fcol}(t, \mathbf{x}) = \left[\mathcal{M}_j^{fi^{eq}} + \left(1 - \frac{\Delta t}{\frac{\Delta t}{2} + \tau_{\mathcal{M}_j}} \right) \tilde{\mathcal{M}}_j + \frac{\Delta t}{2} \mathcal{M}_j^{Fi} \right] (t, \mathbf{x}), \quad (3.49)$$

where we consider that $\tilde{\mathcal{M}}_j$ is a tunable field that we use to replace $\mathcal{M}_j^{\bar{f}^{neq}}$. When $\tilde{\mathcal{M}}_j = 0$, the regularized kernel previously defined is recovered. In Sec. 4.2 we will show how the continuous model is changed by $\tilde{\mathcal{M}}_j$ and in Sec. 4.4, we will show that its tuning allows to recover different mechanical constitutive models.

In practice, by filtering most of the non-equilibrium undesired moments, regularized kernels drastically reduce the number of possible free parameters in a LB model. When a fully general LB scheme is used, equilibrium, collision kernel, relaxation rates, force terms and boundary conditions should be modeled for each of

the q independent moments. However, when a regularized kernel is employed, the amount of tunable degrees of freedom is drastically reduced because most of the non-equilibrium moments are filtered out. Additionally, regularized kernels have already been implemented in industrial codes such as PowerFLOW [87] and ProLB [29].

In this manuscript, we chose to use regularized kernels because,

- The concept is easy to grasp and the interpretation of the implementation is crystal clear : they filter/replace some non-hydrodynamic modes at the beginning of each timestep and therefore reduce the rank of the solver.
- They are already well-validated.

3.3.3. Other kernels

For the sake of completeness, let us quickly comment on alternative collision kernels.

3.3.3.1. Entropic kernels

The main idea of this method is to compute the non-equilibrium distribution such that it verifies a numerical \mathcal{H} -theorem [88], which can be considered equivalent to the 2^{nd} thermodynamic law [4, 7, 45]. While some promising results were obtained for compressible flows [88–91], we feel that using the continuous \mathcal{H} -theorem in a discontinuous context, with a discretized velocity space and only using it *locally* in order to modify the collision – therefore ignoring the streaming – is debatable.

3.3.3.2. Cumulant kernels

In cumulant LBM [92–95] instead of relaxing *moments* (linear functions of f_i), other quantities are relaxed, the *cumulants* [96] (non-linear functions of f_i). The collision describes the relaxation of q independent variables, and cumulant LB simply chose to write this relaxation process in a different space than moment space or distribution space.

3.4. Boundary conditions in the lattice-Boltzmann method

While the bounce-back boundary is usually presented as the typical LB boundary condition, we would like to stretch that bounce back has its own underlying assumptions. The bounce back of distributions on a wall implicitly assumes that particles with the associated velocity will, during a time interval t_{bounce} , bounce back, in other words,

$$f_i(t + t_{bounce}, \mathbf{x}) = f_{\bar{i}}(t, \mathbf{x}), \quad (3.50)$$

3. Lattice-Boltzmann scheme – 3.5. The Lattice-Boltzmann Scheme, from time t to $t + \Delta t$

where $f_{\bar{i}}$ denotes the distribution associated to velocity $\mathbf{c}_{\bar{i}} = -\mathbf{c}_i$. The distributions are *reflected back* between time t and $t + t_{\text{bounce}}$. Note that two different classical bounce back exists, namely the fullway $t_{\text{bounce}} = \Delta t$ and halfway $t_{\text{bounce}} = \Delta t/2$ [4]. On the vast majority of lattices, $\|\mathbf{c}_i\| = \|\mathbf{c}_{\bar{i}}\|$ and the boundary condition is assumed to be located at a distance $t_{\text{bounce}}\|\mathbf{c}_i\|$ [4] such that distributions spent the same amount of time $t_{\text{bounce}}/2$ for both outward and return. It means that no interchange occurs between translational (kinetic) and internal energies during the wall/particles collision. Implicitly, this means that bounce-back assumed elastic collisions of particles, which in turn means hard-sphere particles. Note that this discussion also applies to the specular reflection boundary condition [45, 50], which is equivalent to a symmetry or free-slip boundary [4], where only the wall-normal velocity components are reversed. Additionally, let us mention that other classical LB boundary conditions – such as the wet-node approach [4] – only use macroscopic considerations in order to impose constraints to reconstruct distributions near boundaries.

Which means that we don't know what is imposed on higher order moments than mass, momentum and energy when classical LB boundary conditions are used. We would like to avoid this uncertainty.

Fortunately, a particular boundary condition exists in the context of regularized models [97]. The basic principle is to reconstruct the collide population on the boundary condition located at \mathbf{x}_b :

- i) We use classical NSF boundary conditions (Dirichlet, Neumann, etc) to compute macroscopic values on the boundary $[\rho(\mathbf{x}_b), u_\alpha(\mathbf{x}_b), T(\mathbf{x}_b)]$.
- ii) We use finite difference schemes to compute approximated gradients on the boundary nodes $\nabla^{FD}\rho(\mathbf{x}_b), \nabla^{FD}u_\alpha(\mathbf{x}_b)$ and $\nabla^{FD}T(\mathbf{x}_b)$.
- iii) We reconstruct an approximated f_i^{col} using i) for equilibrium, i) and ii) for non-equilibrium and force term following

$$f_i^{col}(\mathbf{x}_b) = f_i^{eq}[\rho(\mathbf{x}_b), u_\alpha(\mathbf{x}_b), T(\mathbf{x}_b)] + \left\{ \left(1 - \frac{\Delta t}{\bar{\tau}}\right) \bar{f}_i^{neq} + \frac{\Delta t}{2} F_i \right\} [\rho(\mathbf{x}_b), u_\alpha(\mathbf{x}_b), T(\mathbf{x}_b), \nabla^{FD}\rho(\mathbf{x}_b), \nabla^{FD}u_\alpha(\mathbf{x}_b), \nabla^{FD}T(\mathbf{x}_b)], \quad (3.51)$$

In the context of regularized kernels, the expression of \bar{f}_i^{neq} as a function of macroscopic gradients is particularly simple – see Sections 4.1 and 4.4 – and effectively only depends on the stress-tensor.

3.5. The Lattice-Boltzmann Scheme, from time t to $t + \Delta t$

Now, everything was set in place, intrinsic details of the discretization of the DVBE Eq. (3.1) have been provided. In what follows, we simply provide the step by step procedure for implementation of a LB scheme without all the discussion and explanations previously mentioned. Therefore, the aim of this Section is to answer to the

3. Lattice-Boltzmann scheme – 3.5. The Lattice-Boltzmann Scheme, from time t to $t + \Delta t$

following question :

How to get the updated $t + \Delta t$ solution out of the last time step t solution with a LB solver ?

3.5.1. Lattice-Boltzmann definitions

To facilitate the reading, let us now recall the variables that appear in a LB solver. For future reference, important quantities in this Section are summarized in Table 3.1. Details can be found about Hermite polynomials and the D3Q19 lattice in Appendix A. However, for the sake of clarity, let us remind here the first few Hermite polynomials. The 0^{th} to 3^{rd} order Hermite polynomials read

$$\mathcal{H}_i^{(0)} = 1, \quad \mathcal{H}_{i\alpha}^{(1)} = c_{i\alpha}, \quad \mathcal{H}_{i\alpha\beta}^{(2)} = c_{i\alpha}c_{i\beta} - c_s^2\delta_{\alpha\beta}, \quad (3.52)$$

$$\mathcal{H}_{i\alpha\beta\gamma}^{(3)} = c_{i\alpha}c_{i\beta}c_{i\gamma} - c_s^2[c_{i\alpha}\delta_{\beta\gamma} + c_{i\beta}\delta_{\gamma\alpha} + c_{i\gamma}\delta_{\alpha\beta}], \quad (3.53)$$

where the lattice sound speed is $c_s = \Delta x / (\sqrt{3}\Delta t)$ for standard lattices. Higher order polynomials do not generally belong to the Hermite basis of standard lattices or are unnecessary at this point of the manuscript. For a given Hermite basis and an arbitrary population f we recall that discrete Hermite moments $a_{\alpha_1 \dots \alpha_n}^{f,(n)}$ and macroscopic (raw) moments $\Pi_{\alpha_1 \dots \alpha_n}^{f,(n)}$ are expressed as

$$a_{\alpha_1 \dots \alpha_n}^{f,(n)} = \sum_{i=0}^{q-1} \mathcal{H}_{i\alpha_1 \dots \alpha_n}^{(n)} f_i, \quad (3.54)$$

$$\Pi_{\alpha_1 \dots \alpha_n}^{f,(n)} = \sum_{i=0}^{q-1} c_{i\alpha_1} \dots c_{i\alpha_n} f_i. \quad (3.55)$$

Since the number of discrete velocities is finite, there always exists an order n involving a non-zero isotropy defect $D_{\alpha_1 \dots \alpha_n}^{(n)}$ between continuous and discrete moments,

$$D_{\alpha_1 \dots \alpha_n}^{f,(n)} = \int c_{\alpha_1} \dots c_{\alpha_n} f d\mathbf{c} - \Pi_{\alpha_1 \dots \alpha_n}^{f,(n)}. \quad (3.56)$$

For D3Q19 – and nearest-neighbors lattices – this isotropy defect appears from the third order ($n = 3$), see for example Eq. (2.49). Next, it is convenient to recall several populations besides f , appearing at different stages of a LB algorithm :

- \mathbf{f} : The total population is the most important population because mass, momentum, etc are macroscopic moments of this population,

$$\rho = \Pi^{f,(0)}, \quad \rho u_\alpha = \Pi_\alpha^{f,(1)}. \quad (3.57)$$

- f^{eq} : The equilibrium population, easily obtained from Eq. (2.31) when all

3. Lattice-Boltzmann scheme – 3.5. The Lattice-Boltzmann Scheme, from time t to $t + \Delta t$

equilibrium Hermite moments $a_{\alpha_1 \dots \alpha_n}^{f^{eq},(n)}$ are known,

$$f_i^{eq} = \omega_i \left\{ \mathcal{H}^{(0)} a^{f^{eq},(0)} + \frac{\mathcal{H}_{i\alpha}^{(1)}}{c_s^2} a_{\alpha}^{f^{eq},(1)} + \frac{\mathcal{H}_{i\alpha\beta}^{(2)}}{2c_s^4} a_{\alpha\beta}^{f^{eq},(2)} + \dots \right\}, \quad (3.58)$$

which is traditionally obtained by projecting the Maxwellian distribution – Eq. (2.6) – onto the truncated Hermite basis [65], similarly to the Grad approach presented in Sec. 2.1.2.

— f^{neq} : The non-equilibrium population.

$$f_i^{neq} = f_i - f_i^{eq}. \quad (3.59)$$

Additionally to those physical distributions, some *numerical* distribution should be defined. They ensure the 2^{nd} order accuracy of the scheme, see Sec. 3.2.

— \bar{f} : The offset distribution, defined by

$$\bar{f}_i = f_i - \frac{\Delta t}{2} (\Omega_i + F_i), \quad (3.60)$$

$$= f_i^{eq} + \bar{f}_i^{neq} - \frac{\Delta t}{2} F_i, \quad (3.61)$$

with F_i a correction force term defined as

$$F_i = \omega_i \left\{ \mathcal{H}^{(0)} a^{F,(0)} + \frac{\mathcal{H}_{i\alpha}^{(1)}}{c_s^2} a_{\alpha}^{F,(1)} + \frac{\mathcal{H}_{i\alpha\beta}^{(2)}}{2c_s^4} a_{\alpha\beta}^{F,(2)} + \dots \right\}. \quad (3.62)$$

Note that the forcing scheme considered both here and in Sec. 3.2 is known as the Guo forcing [98]. It is, to the author's knowledge, the only known forcing scheme to ensure a second order accuracy $\mathcal{O}(\Delta t^2)$ and corresponds to a trapezoidal rule, see Sec. 3.2.

— \bar{f}^{neq} : The offset non-equilibrium distribution, readily obtained from Eqs. (3.60-3.61),

$$\bar{f}_i^{neq} = f_i^{neq} - \frac{\Delta t}{2} \Omega_i = \bar{f}_i - f_i^{eq} + \frac{\Delta t}{2} F_i. \quad (3.63)$$

— f^{col} : The population at the end of a collision step, sometimes called as pre-streaming population. It can be expressed in different but equivalent ways,

$$f_i^{col} = f_i + \frac{\Delta t}{2} (\Omega_i + F_i), \quad (3.64)$$

$$f_i^{col} = \bar{f}_i + \Delta t (\Omega_i + F_i), \quad (3.65)$$

$$f_i^{col} = f_i^{eq} + \bar{f}_i^{neq} + \Delta t \Omega_i + \frac{\Delta t}{2} F_i, \quad (3.66)$$

the last one being probably the most popular one.

Notation	Representation	Equation
f_i	Distribution	$f_i^{eq} + f_i^{neq}$
f_i^{eq}	Equilibrium distribution	3.58
f_i^{neq}	Non-equilibrium distribution	3.59
\bar{f}, \bar{f}^{neq}	Offset distributions	3.60, 3.63
f_i^{col}	Population after collision	3.64
F_i	Forcing term	3.62
$\mathcal{H}^{(k)}$	Hermite polynomials	3.52, 3.53
$a_{\alpha_1 \dots \alpha_n}^{f, (n)}$	Hermite moments	3.54
$\Pi_{\alpha_1 \dots \alpha_n}^{f, (n)}$	Raw moments	3.55
$D_{\alpha_1 \dots \alpha_n}^{f, (n)}$	Lattice isotropy defects	3.56

Table 3.1. – Main LB notations used throughout the manuscript

Indeed, in actual LB solvers, f^{neq} is *never* actually computed, only \bar{f}^{neq} is explicitly computed. Therefore, it is important to give some more details on the link between Ω_i and the offset non-equilibrium distribution \bar{f}^{neq} . While most of these definitions, f_i^{eq} , f_i , f_i^{neq} , \bar{f}_i^{neq} , f_i^{col} already exist in the literature, it is often unclear which one is derived from which. As it was shown in Sec. 3.2, each of these specific distributions has its specific place in the LB scheme ensuring a $\mathcal{O}(\Delta t^2)$ error discretization of the DVBE Eq. (2.51). One should be extremely careful when manipulating all those distributions. For example, the difference between \bar{f} and f is sometimes unclear. Even worse, most of the time, the overline of \bar{f} is simply dropped without mentioning it, which leads to numerous misinterpretations in the literature. In the next Section, we provide the step by step explanation of the LB algorithm which is followed to get the updated $t + \Delta t$ solution from the initial t solution.

3.5.2. Structure of a generic lattice-Boltzmann scheme

The LB scheme encompasses both time and space integration. However, it is often referred to as "stream & collide" and presented as a very simple scheme. Combined with the coating due to distributions, Hermite polynomials and vague mesoscopic interpretations, it often makes the LB algorithm opaque.

Thanks to the equivalence between distributions and moments provided by the Gauss-Hermite quadrature – see Sec. 2.1.2 –, we can choose to describe the LB solution by the knowledge of either $f_i(t, \mathbf{x})$ or its raw moments $\Pi^{(n)}(t, \mathbf{x})$. Being already used for fluid dynamics, moments are more easily understood by fluid dynamicists than

3. Lattice-Boltzmann scheme – 3.5. The Lattice-Boltzmann Scheme, from time t to $t + \Delta t$

distributions. Therefore, more emphasis will be put on moments than distributions, contrarily to more traditional descriptions of the LBM. The LB algorithm reads as follows :

Step 1, initialization. The algorithm starts at time t . Full knowledge of raw moments $\Pi^{(n)}(t, \mathbf{x})$ – or equivalently Hermite moments $a^{(n)}(t, \mathbf{x})$ – is assumed. Throughout the equivalence between moments and distributions, we also know the force, equilibrium and non-equilibrium distributions, F_i , f_i^{eq} and f_i^{neq} ,

$$F_i(t, \mathbf{x}) = \omega_i \left\{ \mathcal{H}^{(0)} a^{F,(0)} + \frac{\mathcal{H}_{i\alpha}^{(1)}}{c_s^2} a_{\alpha}^{F,(1)} + \frac{\mathcal{H}_{i\alpha\beta}^{(2)}}{2c_s^4} a_{\alpha\beta}^{F,(2)} + \dots \right\} (t, \mathbf{x}), \quad (3.67)$$

$$f_i^{eq}(t, \mathbf{x}) = \omega_i \left\{ \mathcal{H}^{(0)} a^{f^{eq},(0)} + \frac{\mathcal{H}_{i\alpha}^{(1)}}{c_s^2} a_{\alpha}^{f^{eq},(1)} + \frac{\mathcal{H}_{i\alpha\beta}^{(2)}}{2c_s^4} a_{\alpha\beta}^{f^{eq},(2)} + \dots \right\} (t, \mathbf{x}), \quad (3.68)$$

$$f_i^{neq}(t, \mathbf{x}) = \omega_i \left\{ \mathcal{H}^{(0)} a^{f^{neq},(0)} + \frac{\mathcal{H}_{i\alpha}^{(1)}}{c_s^2} a_{\alpha}^{f^{neq},(1)} + \frac{\mathcal{H}_{i\alpha\beta}^{(2)}}{2c_s^4} a_{\alpha\beta}^{f^{neq},(2)} + \dots \right\} (t, \mathbf{x}). \quad (3.69)$$

Step 2, collision. The collision is considered as one of the 2 main steps of LB schemes. For classical models it looks quite simple. However, a more general description of this step for an arbitrary collision model should be presented hereafter. First, the collision operator Ω_i is obtained as a function of $\Pi^{(n)}(t, \mathbf{x})$ and f_i^{neq} ,

$$\Omega_i(t, \mathbf{x}) = \Omega_i [f_i^{neq}(t, \mathbf{x}), \Pi^{(n)}(t, \mathbf{x})], \quad (3.70)$$

then the collide population is defined as

$$f_i^{col}(t, \mathbf{x}) = \left[f_i + \frac{\Delta t}{2} (\Omega_i + F_i) \right] (t, \mathbf{x}). \quad (3.71)$$

Sometimes, it is easier to define Ω_i and f_i^{col} as a function of the temporary variable \bar{f}_i^{neq} ,

$$\bar{f}_i^{neq}(t, \mathbf{x}) = \left[f_i^{neq} - \frac{\Delta t}{2} \Omega_i \right] (t, \mathbf{x}). \quad (3.72)$$

or equivalently as a function of \bar{f}_i , f_i^{eq} and F_i ,

$$\bar{f}_i^{neq}(t, \mathbf{x}) = \left[\bar{f}_i - f_i^{eq} + \frac{\Delta t}{2} F_i \right] (t, \mathbf{x}), \quad (3.73)$$

in which case one would define the collision operator Ω_i as

$$\Omega_i(t, \mathbf{x}) = \Omega_i \left[\bar{f}_i(t, \mathbf{x}), f_i^{eq}(t, \mathbf{x}), F_i(t, \mathbf{x}), \Pi^{(n)}(t, \mathbf{x}) \right]. \quad (3.74)$$

3. Lattice-Boltzmann scheme – 3.5. The Lattice-Boltzmann Scheme, from time t to $t + \Delta t$

Eq. (3.40) is an example of such expression for the MRT model. The collided population is then obtained

$$f_i^{col} = f_i + \frac{\Delta t}{2} (\Omega_i + F_i), \quad (3.75)$$

$$\bar{f}_i^{col} = \bar{f}_i + \Delta t (\Omega_i + F_i), \quad (3.76)$$

$$f_i^{col} = f_i^{eq} + \bar{f}_i^{neq} + \Delta t \Omega_i + \frac{\Delta t}{2} F_i. \quad (3.77)$$

Note here that f_i^{col} should not be considered as the "population after collision" in a physical sense, but only in a numerical one. Indeed, $f_i + \Delta t \Omega_i$ could be roughly interpreted in absence of streaming as the physical distribution having undergone all collisions. But $\Delta t / \Omega_i / 2$ is missing to be allowed to attribute this meaning to f_i^{col} .

Step 3, streaming. The advantage of the LB scheme partly lies in the simplicity of the following step. It is known as streaming and corresponds to the shifting of all populations on the cartesian grid,

$$\bar{f}_i(t + \Delta t, \mathbf{x}) = f_i^{col}(t, \mathbf{x} - \mathbf{c}_i \Delta t). \quad (3.78)$$

At this moment of the algorithm, the temporary variable \bar{f}_i was updated, it is known everywhere at time $t + \Delta t$. A very common pitfall is to consider that \bar{f}_i has some kind of physical meaning. However, it should be clear now from previous discussions and Sec. 3.2 that $\bar{f}_i(t + \Delta t, \mathbf{x})$ should *not* be interpreted as a distribution carrying a physical meaning but rather as a temporary numerical variable meant to simplify the overall algorithm whose final goal is to get $f_i(t + \Delta t, \mathbf{x})$, or equivalently its moments $\Pi^{f,(n)}(t + \Delta t, \mathbf{x})$.

Therefore, we should not conclude that the timestep is finished because $\bar{f}_i(t + \Delta t, \mathbf{x})$ was updated. We must now compute the actual variable of interest, either $f_i(t + \Delta t, \mathbf{x})$ or $\Pi^{(n)}(t + \Delta t, \mathbf{x})$.

Step 4, reconstruction. In order to get the updated distributions $f_i(t + \Delta t, \mathbf{x})$, let us combine Eqs. (3.72-3.73,3.78), this leads to,

$$f_i(t + \Delta t, \mathbf{x}) = f_i^{col}(t, \mathbf{x} - \mathbf{c}_i \Delta t) + \frac{\Delta t}{2} (\Omega_i + F_i)(t + \Delta t, \mathbf{x}), \quad (3.79)$$

which is potentially an implicit equation depending on the functional dependencies between f_i , F_i and Ω_i . Now that distributions f_i have been updated, it is possible to get the updated moments $\Pi_{\alpha_1 \dots \alpha_n}^{f,(n)}(t + \Delta t, \mathbf{x})$ using Eqs. (3.55, 3.79) as

$$\Pi_{\alpha_1 \dots \alpha_n}^{f,(n)}(t + \Delta t, \mathbf{x}) = \Pi_{\alpha_1 \dots \alpha_n}^{f_i^{col}(t, \mathbf{x} - \mathbf{c}_i \Delta t), (n)} + \frac{\Delta t}{2} (\Pi_{\alpha_1 \dots \alpha_n}^{\Omega, (n)} + \Pi_{\alpha_1 \dots \alpha_n}^{F, (n)})(t + \Delta t, \mathbf{x}). \quad (3.80)$$

Now, and only now, we can safely say that the updated solution was obtained. Using 4 distinct steps – **initialization**, **collision**, **streaming** and **reconstruction** – it was possible to get the updated solution $\Pi_{\alpha_1 \dots \alpha_n}^{f, (n)}(t + \Delta t, \mathbf{x})$ as a function of the initial solution $\Pi_{\alpha_1 \dots \alpha_n}^{f, (n)}(t, \mathbf{x})$. Equivalently, the updated distributions $f_i(t + \Delta t, \mathbf{x})$ were obtained as a function of the initial ones, $f_i(t, \mathbf{x})$. Therefore, we can consider the timestep $(t, \mathbf{x}) \rightarrow (t + \Delta t, \mathbf{x})$ to be finished. It can be recursively performed m th time in order to get the solution at time $t + m \Delta t$.

These steps are the main ingredients responsible for the method's computing efficiency [18, 21, 99], and low dissipation [100]. While sometimes presented differently [4, 35–37] this structure is shared by most LB schemes using Hermite polynomials and on-lattice discretizations (*i.e.* $\|c_i\| \Delta t = \Delta x$).

In this chapter we *deduced* the complete path from the continuous equations to the numerical scheme. In the next Chapter, we will retrace our steps in the opposite direction, going from the numerical scheme to the continuous equations.

LB solvers are often coupled to finite difference schemes. This coupling being a *numerical* coupling, it goes out of the scope of the DVBE discretization. Therefore, it is safer to learn how to retrace our steps back in order to make sure that a coupled LB schemes is still consistent – in the sense of Lax [14, 22, 23] – to the expected continuous model.

3.6. Recap

In this Chapter, we first illustrated how a discretized relaxation equation behaves for different numerical schemes. We highlighted the phenomena of under and over relaxation and identified the main properties of the Crank-Nicolson scheme. Then, we used it to discretize the DVBE, leading to the scheme actually implemented in a LBM solver. We shown how MRT and regularized kernels were linked, explained the boundary conditions we use and provided a step-by-step summarize of the algorithm to update the solution from time t to $t + \Delta t$. While the content of this Chapter does not presents anything new, the ambiguous distinction between $(\bar{f}_i, \bar{\tau})$ and (f_i, τ) often makes the origin of the LB scheme blurry. This Chapter aims to show unequivocally how the LBM is deduced from the DVBE and the Crank-Nicolson scheme and how collision kernels and force terms are implemented.

4. Taylor expansion based description of the lattice-Boltzmann scheme

This Chapter mainly follows the content of:

G. Farag, S. Zhao, G. Chiavassa, P. Boivin. Consistency study of Lattice-Boltzmann schemes macroscopic limit. *Physics of Fluids*, 2021.

<https://doi.org/10.1063/5.0039490>

Sommaire

4.1	Taylor expansion	65
4.2	Taylor expansion for filtered kernels	68
4.3	Application : Athermal Lattice-Boltzmann Method	71
4.3.1	Numerical scheme	71
4.3.2	Continuous equivalent equations	73
4.3.3	Domain of validity in term of dimensionless numbers	74
4.4	Application : Interpretation of collision models	76
4.4.1	Modeling of lag effects in constitutive equations	77
4.4.2	BGK kernel	79
4.4.3	Regularized kernels	79
4.4.4	Recursive Regularized kernels	80
4.4.5	Hybrid Recursive Regularization kernels	80
4.4.6	Traceless Recursive Regularized kernels	81
4.5	Application : Thermal Lattice-Boltzmann Method, ρ -based model	82
4.5.1	Recursive Regularized- ρ numerical scheme	83
4.5.2	Continuous equivalent equations	84
4.6	Comparison with other Taylor expansions	86
4.6.1	Previous Taylor expansions for lattice-Boltzmann	86
4.6.2	Taylor expansion proposed by <i>Wissocq and Sagaut, 2021</i>	89
4.7	Limits of the proposed Taylor expansion	91
4.8	Recap	94

This chapter presents a deductive description of the LB scheme based on reasonable

4. Taylor expansion based description of the lattice-Boltzmann scheme – 4.1. Taylor expansion

premises. We know from the beginning that the LB scheme is not fully equivalent to a NSF model. Instead of relying on unexplained premises that conveniently hide these differences, we propose to emphasize them and to deduce *a posteriori* what are the actual conditions for a LB scheme to provide an approximate NSF solution. Through the use of classical numerical tools,

- The consistency analysis, see [14, 22–24]
- The dimensional analysis, see Sec. 1.2
- The Taylor series expansion, see Eq. (4.1)

we will show that a satisfactory description of the LBM could be obtained from cheaper assumptions than what the literature is used to. This chapter is organized as follows.

Using the Taylor series expansion, the equivalent modified equations are obtained and discussed for classical BGK/MRT kernels in Sec. 4.1 and for filtered/regularized models in Sec. 4.2. In Sec. 4.3, this methodology is coupled to a dimensional analysis study and is applied to the classical athermal LB scheme in order to identify *a posteriori* what are the actual consistency conditions. In Sec. 4.4, selected collision kernels are presented and their meaning in term of macroscopic models is deduced. In Sec. 4.5, the classical ρ -based thermal LB model is analyzed throughout the scope of this newly proposed framework. The last part, Sec. 4.6, is dedicated to a discussion of Taylor expansions for LB, more specifically those using the Crank-Nicolson scheme.

4.1. Taylor expansion

In this Section, we propose to show the opposite to what was presented in Sec. 3.2. Using the well known Taylor expansion, we will go back from the discretized scheme to the continuous equations by assuming that both Δt and Δx can be made arbitrarily small in order to ensure the convergence of the Taylor series.

Starting from the basic LB algorithm presented in Sec. 3.5.2, we first introduce the distribution's Taylor Expansion in space of any smooth distribution f at $(t, \mathbf{x} - \mathbf{c} \Delta t)$ around (t, \mathbf{x}) . Its Taylor series then reads

$$f(t, \mathbf{x} - \mathbf{c} \Delta t) = f(t, \mathbf{x}) + \sum_{k=1}^{\infty} \frac{(-\Delta t)^k}{k!} \left(c_{\alpha_j} \frac{\partial}{\partial x_{\alpha_j}} \right)^k f(t, \mathbf{x}), \quad (4.1)$$

where α_j is a dummy index such that $c_{\alpha_j} \partial / \partial x_{\alpha_j} = c_x \partial / \partial x + c_y \partial / \partial y + c_z \partial / \partial z$. Taking the n^{th} order macroscopic moment of the streaming Eq. (3.78) leads to the moment streaming equation

$$\Pi_{\alpha_1 \dots \alpha_n}^{\bar{f}(t+\Delta t, \mathbf{x}), (n)} = \Pi_{\alpha_1 \dots \alpha_n}^{f^{col}(t, \mathbf{x} - \mathbf{c}_i \Delta t), (n)}. \quad (4.2)$$

Similarly, Eq. (3.60) can be recast into a moment equation

$$\Pi_{\alpha_1 \dots \alpha_n}^{\bar{f}(t+\Delta t, \mathbf{x}), (n)} = \Pi_{\alpha_1 \dots \alpha_n}^{f, (n)}(t + \Delta t, \mathbf{x}) - \frac{\Delta t}{2} \left(\Pi_{\alpha_1 \dots \alpha_n}^{\Omega(t+\Delta t, \mathbf{x}), (n)} + \Pi_{\alpha_1 \dots \alpha_n}^{F(t+\Delta t, \mathbf{x}), (n)} \right). \quad (4.3)$$

4. Taylor expansion based description of the lattice-Boltzmann scheme – 4.1. Taylor expansion

Combining Eqs. (4.2-4.3) finally leads to

$$\Pi_{\alpha_1 \dots \alpha_n}^{f,(n)}(t + \Delta t, \mathbf{x}) = \Pi_{\alpha_1 \dots \alpha_n}^{f^{col}(t, \mathbf{x} - \mathbf{c}_i \Delta t), (n)} + \frac{\Delta t}{2} \left(\Pi_{\alpha_1 \dots \alpha_n}^{\Omega(t + \Delta t, \mathbf{x}), (n)} + \Pi_{\alpha_1 \dots \alpha_n}^{F(t + \Delta t, \mathbf{x}), (n)} \right). \quad (4.4)$$

This equation is the update rule for $(t + \Delta t)$ moments. It is nothing but the LB numerical scheme written explicitly for the n^{th} order moment $\Pi_{\alpha_1 \dots \alpha_n}^{f(t + \Delta t, \mathbf{x}), (n)}$. We shall now Taylor expand $\Pi_{\alpha_1 \dots \alpha_n}^{f^{col}(t, \mathbf{x} - \mathbf{c}_i \Delta t), (n)}$, using Eq. (4.1),

$$\Pi_{\alpha_1 \dots \alpha_n}^{f^{col}(t, \mathbf{x} - \mathbf{c}_i \Delta t), (n)} = \sum_{i=0}^{q-1} c_{i\alpha_1} \dots c_{i\alpha_n} \left\{ 1 + \sum_{k=1}^{\infty} \frac{(-\Delta t)^k}{k!} \left(c_{i\alpha_{n+j}} \frac{\partial}{\partial x_{\alpha_{n+j}}} \right)^k \right\} f_i^{col}(t, \mathbf{x}). \quad (4.5)$$

Using the fact that the discrete velocities $c_{i\alpha_n}$ are constant leads to

$$\Pi_{\alpha_1 \dots \alpha_n}^{f^{col}(t, \mathbf{x} - \mathbf{c}_i \Delta t), (n)} = \Pi_{\alpha_1 \dots \alpha_n}^{f^{col}(t, \mathbf{x}), (n)} + \sum_{k=1}^{\infty} \frac{(-\Delta t)^k}{k!} \left(\frac{\partial}{\partial x_{\alpha_{n+j}}} \right)^k \Pi_{\alpha_1 \dots \alpha_{n+j}}^{f^{col}(t, \mathbf{x}), (n+k)}. \quad (4.6)$$

Let us use Eq. (4.6) evaluated for the $(n + 1)$ -order moment along with Eq. (4.2) to get

$$\Delta t \frac{\partial \Pi_{\alpha_1 \dots \alpha_{n+2}}^{f^{col}(t, \mathbf{x}), (n+2)}}{\partial x_{\alpha_{n+2}}} = \Pi_{\alpha_1 \dots \alpha_{n+1}}^{f^{col}(t, \mathbf{x}), (n+1)} - \Pi_{\alpha_1 \dots \alpha_{n+1}}^{\bar{f}(t + \Delta t, \mathbf{x}), (n+1)} + \mathcal{O}(\Delta t^2), \quad (4.7)$$

which can be injected back into Eq. (4.6), then using Eq. (4.2) yields

$$\Pi_{\alpha_1 \dots \alpha_n}^{\bar{f}(t + \Delta t, \mathbf{x}), (n)} - \Pi_{\alpha_1 \dots \alpha_n}^{f^{col}(t, \mathbf{x}), (n)} = -\frac{\Delta t}{2} \frac{\partial}{\partial x_{\alpha_{n+1}}} \left[\Pi_{\alpha_1 \dots \alpha_{n+1}}^{f^{col}(t, \mathbf{x}), (n+1)} + \Pi_{\alpha_1 \dots \alpha_{n+1}}^{\bar{f}(t + \Delta t, \mathbf{x}), (n+1)} \right] + \mathcal{O}(\Delta t^3). \quad (4.8)$$

On the other hand, Eqs. (3.62,3.64,3.60) lead to

$$\Pi_{\alpha_1 \dots \alpha_n}^{f^{col}(t, \mathbf{x}), (n)} = \left[\Pi_{\alpha_1 \dots \alpha_n}^{f,(n)} + \frac{\Delta t}{2} \left(\Pi_{\alpha_1 \dots \alpha_n}^{\Omega,(n)} + \Pi_{\alpha_1 \dots \alpha_n}^{F,(n)} \right) \right] (t, \mathbf{x}), \quad (4.9)$$

$$\Pi_{\alpha_1 \dots \alpha_n}^{\bar{f}(t + \Delta t, \mathbf{x}), (n)} = \left[\Pi_{\alpha_1 \dots \alpha_n}^{f,(n)} - \frac{\Delta t}{2} \left(\Pi_{\alpha_1 \dots \alpha_n}^{\Omega,(n)} + \Pi_{\alpha_1 \dots \alpha_n}^{F,(n)} \right) \right] (t + \Delta t, \mathbf{x}). \quad (4.10)$$

At this point it is curious to note that the collision forcing $\Pi_{\alpha_1 \dots \alpha_n}^{\Omega,(n)}$ and the external forcing $\Pi_{\alpha_1 \dots \alpha_n}^{F,(n)}$ have the exact same treatment in the algorithm. From a numerical scheme point of view, the discretization of the collision term Ω_i and the discretization of the forcing term F_i are identical. Thanks to these two last equations note that

$$\Pi_{\alpha_1 \dots \alpha_n}^{f^{col}(t, \mathbf{x}), (n)} + \Pi_{\alpha_1 \dots \alpha_n}^{\bar{f}(t + \Delta t, \mathbf{x}), (n)} = \Pi_{\alpha_1 \dots \alpha_n}^{f,(n)} + \Pi_{\alpha_1 \dots \alpha_n}^{f(t + \Delta t, \mathbf{x}), (n)} + \mathcal{O}(\Delta t^2). \quad (4.11)$$

Injecting Eq. (4.11) and Eq. (4.10) respectively in the right hand side and left hand side

4. Taylor expansion based description of the lattice-Boltzmann scheme – 4.1. Taylor expansion

of Eq. (4.8) leads to the general second order numerical scheme :

$$\begin{aligned} \Pi_{\alpha_1 \dots \alpha_n}^{f(t+\Delta t, \mathbf{x}), (n)} - \Pi_{\alpha_1 \dots \alpha_n}^{f(t, \mathbf{x}), (n)} &= -\frac{\Delta t}{2} \frac{\partial}{\partial x_{\alpha_{n+1}}} \left[\Pi_{\alpha_1 \dots \alpha_{n+1}}^{f, (n+1)}(t, \mathbf{x}) + \Pi_{\alpha_1 \dots \alpha_{n+1}}^{f, (n+1)}(t + \Delta t, \mathbf{x}) \right] \\ &+ \frac{\Delta t}{2} \left[\left(\Pi_{\alpha_1 \dots \alpha_n}^{\Omega, (n)} + \Pi_{\alpha_1 \dots \alpha_n}^{F, (n)} \right)(t, \mathbf{x}) + \left(\Pi_{\alpha_1 \dots \alpha_n}^{\Omega, (n)} + \Pi_{\alpha_1 \dots \alpha_n}^{F, (n)} \right)(t + \Delta t, \mathbf{x}) \right] + \mathcal{O}(\Delta t^3), \end{aligned} \quad (4.12)$$

or equivalently

$$\frac{\Pi_{\alpha_1 \dots \alpha_n}^{f(t+\Delta t, \mathbf{x}), (n)} - \Pi_{\alpha_1 \dots \alpha_n}^{f(t, \mathbf{x}), (n)}}{\Delta t} = \frac{1}{2} \left\{ \mathcal{S}(t + \Delta t, \mathbf{x}) + \mathcal{S}(t, \mathbf{x}) \right\} + \mathcal{O}(\Delta t^2), \quad (4.13)$$

where \mathcal{S} is the source term defined by

$$\mathcal{S} = -\frac{\partial \Pi_{\alpha_1 \dots \alpha_{n+1}}^{f, (n+1)}}{\partial x_{\alpha_{n+1}}} + \Pi_{\alpha_1 \dots \alpha_n}^{\Omega, (n)} + \Pi_{\alpha_1 \dots \alpha_n}^{F, (n)}. \quad (4.14)$$

As already highlighted in the literature on the f equation itself [80] we recognize in Eqs. (4.13,4.14) a second order accurate Crank-Nicolson scheme whose continuous limit $\Delta t \rightarrow 0$ is

$$\frac{\partial \Pi_{\alpha_1 \dots \alpha_n}^{f, (n)}}{\partial t} + \frac{\partial \Pi_{\alpha_1 \dots \alpha_{n+1}}^{f, (n+1)}}{\partial x_{\alpha_{n+1}}} = \Pi_{\alpha_1 \dots \alpha_n}^{\Omega, (n)} + \Pi_{\alpha_1 \dots \alpha_n}^{F, (n)} + \mathcal{O}(\Delta t^2). \quad (4.15)$$

Which is nothing but the discrete velocity Boltzmann Eq. (3.1). Note that for the BGK collision kernel, $\Pi_{\alpha_1 \dots \alpha_n}^{\Omega, (n)} = -\frac{1}{\tau} \Pi_{\alpha_1 \dots \alpha_n}^{f^{neq}, (n)}$. This layered structure between moments $\Pi_{\alpha_1 \dots \alpha_n}^{f, (n)}$ and $\Pi_{\alpha_1 \dots \alpha_{n+1}}^{f, (n+1)}$ shows that non-equilibrium moments follow their own evolution equation, they are not algebraically enslaved to lower order moments as suggested by the Chapman-Enskog expansion through the scale separation hypothesis. Mandatory conditions for a LB solution to approximate a NSF solution will be discussed later in this manuscript for some specific models.

For now, let us say that LBM can be seen as a smart change of variables from macroscopic moments to distribution functions. First the macroscopic information is stored inside the Hermite basis through f^{col} (first change of variable from $\Pi^{(n)}$ to f). Then the transport is performed in the distribution space during the streaming, followed by the macroscopic reconstruction that filters only the relevant information for each macroscopic moment $\Pi^{(n)}$ (second change of variable from f to $\Pi^{(n)}$), prompting us to draw a parallel between classical CFD and LBM, which is now only seen as a macroscopic model – Eq. (4.15) – discretized by a Crank-Nicolson scheme, Eqs. (4.13,4.14). More specifically, each lattice model is consistent to a specific Grad- q system Eq. (4.15), see Sec. 2.1.2.

In the following we will illustrate the proposed formalism on the athermal LB model, on several collision kernels and on the ρ -based recursive regularized model. We shall also demonstrate that although Eq. (4.15) could have been easily guessed from

4. Taylor expansion based description of the lattice-Boltzmann scheme – 4.2. Taylor expansion for filtered kernels

Eq. (3.1), spurious terms will appear during the *numerical* coupling between a LB algorithm and other numerical schemes. Because these terms are purely stemming from a numerical coupling, they can not be described by the Chapman-Enskog expansion alone.

4.2. Taylor expansion for filtered kernels

We have just proved that the DVBE discretized by Crank-Nicolson scheme (in other words, the LB scheme) is second order accurate and consistent to Eq. (4.15), which is also equivalent to Eq. (3.1) due to the equivalence between distributions and moments. When using a classical BGK/MRT kernel, relaxations times τ_j are independent from the time step Δt . However, when using a filtered or regularized kernel – see Sec. 3.3.2 – we have seen that it was somehow equivalent to a specific MRT model where some relaxation terms were set to $\Delta t/2$. In which case some moments are filtered, therefore reducing the rank of the system, and the link with Eqs. (4.15,3.1) is blurred. Because those kernels filtered moments, it is easier to describe what happens on moments than on distributions. In order to be as consistent as possible with the literature and following Sections of the manuscript, let us assume that the only non-equilibrium moments that we do not filter are the 2^{nd} order ones,

$$\Pi_{\alpha\beta}^{f^{col},(2)}(t, \mathbf{x}) = \left[\Pi_{\alpha\beta}^{f^{eq},(2)} + \left(1 - \frac{\Delta t}{\frac{\Delta t}{2} + \tau}\right) \bar{\Pi}_{\alpha\beta}^{f^{neq},(2)} + \frac{\Delta t}{2} \Pi_{\alpha\beta}^{F,(2)} \right] (t, \mathbf{x}). \quad (4.16)$$

Higher order have their corresponding relaxation times equal to $\Delta t/2$ such that they are filtered, see Sec. 3.3.2. We make an exception for the 3^{rd} order one, that we take as

$$\Pi_{\alpha\beta\gamma}^{f^{col},(3)}(t, \mathbf{x}) = \left[\Pi_{\alpha\beta\gamma}^{f^{eq},(3)} + \left(1 - \frac{\Delta t}{\frac{\Delta t}{2} + \tau}\right) \tilde{\Pi}_{\alpha\beta\gamma}^{(3)} + \frac{\Delta t}{2} \Pi_{\alpha\beta\gamma}^{F,(3)} \right] (t, \mathbf{x}), \quad (4.17)$$

where $\tilde{\Pi}_{\alpha\beta\gamma}^{(3)}$ is a tunable tensor. Clearly, when it is not a function of $\bar{\Pi}_{\alpha\beta\gamma}^{f^{neq},(3)}$, all the information coming from the last time step throughout $\bar{\Pi}_{\alpha\beta\gamma}^{f^{neq},(3)}$ are lost. We say that $\bar{\Pi}_{\alpha\beta\gamma}^{f^{neq},(3)}$ was *filtered*. We are now interested in the effect of this filtering on the numerical scheme of the LB stress tensor $\Pi_{\alpha\beta}^{f^{neq},(2)}$. Following the same procedure as in the last Section, we write the LB stress tensor numerical scheme as

$$\Pi_{\alpha\beta}^{f,(2)}(t + \Delta t, \mathbf{x}) = \Pi_{\alpha\beta}^{f^{col}(t, \mathbf{x} - \mathbf{c}_i \Delta t), (2)} + \frac{\Delta t}{2} \left(\Pi_{\alpha\beta}^{\Omega(t + \Delta t, \mathbf{x}), (2)} + \Pi_{\alpha\beta}^{F(t + \Delta t, \mathbf{x}), (2)} \right), \quad (4.18)$$

with

$$\Pi_{\alpha\beta}^{f^{col}(t, \mathbf{x} - \mathbf{c}_i \Delta t), (2)} = \Pi_{\alpha\beta}^{f^{col}(t, \mathbf{x}), (2)} - \Delta t \frac{\partial \Pi_{\alpha\beta\gamma}^{f^{col}(t, \mathbf{x}), (3)}}{\partial x_\gamma} + \frac{\Delta t^2}{2} \frac{\partial^2 \Pi_{\alpha\beta\gamma\delta}^{f^{col}(t, \mathbf{x}), (4)}}{\partial x_\gamma \partial x_\delta} + \mathcal{O}(\Delta t^3). \quad (4.19)$$

4. Taylor expansion based description of the lattice-Boltzmann scheme – 4.2. Taylor expansion for filtered kernels

Note that the following

$$\Pi_{\alpha\beta\gamma}^{f^{col}(t,\mathbf{x}-\mathbf{c}_i\Delta t),(3)} = \Pi_{\alpha\beta\gamma}^{f^{col}(t,\mathbf{x}),(3)} - \Delta t \frac{\partial \Pi_{\alpha\beta\gamma\delta}^{f^{col}(t,\mathbf{x}),(4)}}{\partial x_\delta} + \mathcal{O}(\Delta t^2), \quad (4.20)$$

is also true. Using Eqs. (4.19,4.20),

$$\Pi_{\alpha\beta}^{f^{col}(t,\mathbf{x}-\mathbf{c}_i\Delta t),(2)} - \Pi_{\alpha\beta}^{f^{col}(t,\mathbf{x}),(2)} = -\frac{\Delta t}{2} \frac{\partial}{\partial x_\gamma} \left[\Pi_{\alpha\beta\gamma}^{f^{col}(t,\mathbf{x}),(3)} + \Pi_{\alpha\beta\gamma}^{f^{col}(t,\mathbf{x}-\mathbf{c}_i\Delta t),(3)} \right] + \mathcal{O}(\Delta t^3). \quad (4.21)$$

Now, because we are filtering the 3rd order moment, the 3rd order projection of the streaming is not anymore valid, in other words,

$$\Pi_{\alpha\beta\gamma}^{\bar{f}(t+\Delta t,\mathbf{x}),(3)} \neq \Pi_{\alpha\beta\gamma}^{f^{col}(t,\mathbf{x}-\mathbf{c}_i\Delta t),(3)}, \quad (4.22)$$

due to the filtering, the updated 3rd order moment that will be used as initial condition for the next time step is

$$\Pi_{\alpha\beta\gamma}^{\bar{f}(t+\Delta t,\mathbf{x}),(3)} = \Pi_{\alpha\beta\gamma}^{f^{eq}(t+\Delta t,\mathbf{x}),(3)} + \tilde{\Pi}_{\alpha\beta\gamma}^{(3)}(t+\Delta t,\mathbf{x}) - \frac{\Delta t}{2} \Pi_{\alpha\beta\gamma}^{F(t+\Delta t,\mathbf{x}),(3)}. \quad (4.23)$$

If this last equation is not clear enough, remember that in Eq. (4.17), $\tilde{\Pi}_{\alpha\beta\gamma}^{(3)}$ replaced $\Pi_{\alpha\beta\gamma}^{\bar{f}^{neq},(3)}$. Similarly, in Eq. (4.23), which is obtained from 3rd order projection of Eq. (3.73), the moment $\tilde{\Pi}_{\alpha\beta\gamma}^{(3)}$ replaced $\Pi_{\alpha\beta\gamma}^{\bar{f}^{neq},(3)}$. As a consequence, Eq. (4.21) could only be written as

$$\begin{aligned} \Pi_{\alpha\beta}^{f^{col}(t,\mathbf{x}-\mathbf{c}_i\Delta t),(2)} - \Pi_{\alpha\beta}^{f^{col}(t,\mathbf{x}),(2)} &= -\frac{\Delta t}{2} \frac{\partial}{\partial x_\gamma} \left[\Pi_{\alpha\beta\gamma}^{f^{col}(t,\mathbf{x}),(3)} + \Pi_{\alpha\beta\gamma}^{\bar{f}(t+\Delta t,\mathbf{x}),(3)} \right] \\ &\quad - \frac{\Delta t}{2} \frac{\partial}{\partial x_\gamma} \left[\Pi_{\alpha\beta\gamma}^{f^{col}(t,\mathbf{x}-\mathbf{c}_i\Delta t),(3)} - \Pi_{\alpha\beta\gamma}^{\bar{f}(t+\Delta t,\mathbf{x}),(3)} \right] + \mathcal{O}(\Delta t^3). \\ &= -\frac{\Delta t}{2} \frac{\partial}{\partial x_\gamma} \left[\Pi_{\alpha\beta\gamma}^{f^{col}(t,\mathbf{x}),(3)} + \Pi_{\alpha\beta\gamma}^{\bar{f}(t+\Delta t,\mathbf{x}),(3)} \right] + \Delta t \mathcal{O}_{reg}^{(3)} + \mathcal{O}(\Delta t^3), \end{aligned} \quad (4.24)$$

where $\mathcal{O}_{reg}^{(3)}$ is the error introduced by the replacement of $\Pi_{\alpha\beta\gamma}^{\bar{f}^{neq},(3)}$ by $\tilde{\Pi}_{\alpha\beta\gamma}^{(3)}$ in Eq. (4.17). The rest of the demonstration is identical to the last Section, except that Eqs. (4.17,4.23) should be used and that $\mathcal{O}_{reg}^{(3)}$ is kept until the end, finally yielding,

$$\frac{\partial \Pi_{\alpha\beta}^{f,(2)}}{\partial t} + \frac{\partial \Pi_{\alpha\beta\gamma}^{f,(3)}}{\partial x_\gamma} = -\frac{1}{\tau} \Pi_{\alpha\beta}^{f^{neq},(2)} + \Pi_{\alpha\beta}^{F,(2)} + \mathcal{O}_{reg}^{(3)} + \mathcal{O}(\Delta t^2), \quad (4.26)$$

4. Taylor expansion based description of the lattice-Boltzmann scheme – 4.2. Taylor expansion for filtered kernels

with $\Pi_{\alpha\beta\gamma}^{f,(3)}$ obtained by identification of Eq. (4.23) with 3^{rd} order projections of Eqs. (3.72,3.73),

$$\Pi_{\alpha\beta\gamma}^{f,(3)} = \Pi_{\alpha\beta\gamma}^{f^{eq},(3)} + \frac{2\tau}{2\tau + \Delta t} \tilde{\Pi}_{\alpha\beta\gamma}^{(3)}. \quad (4.27)$$

Tuning $\tilde{\Pi}_{\alpha\beta\gamma}^{(3)}$ allows to freely modify the flux of $\Pi_{\alpha\beta}^{f,(2)}$. However, there is a cost, which is that we created an error, $\mathcal{O}_{reg}^{(3)}$. Using Eqs. (4.17,4.23), we immediately find,

$$\mathcal{O}_{reg}^{(3)} = -\frac{1}{2} \frac{\partial}{\partial x_\gamma} \left[\Pi_{\alpha\beta\gamma}^{f^{col}(t, \mathbf{x} - \mathbf{c}_i \Delta t), (3)} - \tilde{\Pi}_{\alpha\beta\gamma}^{f(t+\Delta t, \mathbf{x}), (3)} \right] = \mathcal{O}(\Delta t). \quad (4.28)$$

When $\tilde{\Pi}_{\alpha\beta\gamma}^{(3)} = \tilde{\Pi}_{\alpha\beta\gamma}^{f^{neq},(3)}$, then $\mathcal{O}_{reg}^{(3)}$ is 0 and we recover the classical case presented in the last Section. We can directly modify the flux $\Pi_{\alpha\beta\gamma}^{f,(3)}$ by tuning $\tilde{\Pi}_{\alpha\beta\gamma}^{(3)}$, but it reduces the order of accuracy of the scheme used to discretize $\Pi_{\alpha\beta}^{f,(2)}$ equation to $\mathcal{O}(\Delta t)$. Note here that we did not specified anything about the LB model we used, except that the 3^{rd} order moment was filtered.

In this respect, we can draw a general conclusion, when $(n+1)^{th}$ order moment is overwritten by an arbitrary value, it deteriorates the order of accuracy of the n^{th} order moment scheme to $\mathcal{O}(\Delta t)$. This has already been observed on the projected regularized collision kernel [81]. In this Section, we deduced that this $\mathcal{O}(\Delta t)$ error appears inside the discretization of the gradients of 3^{rd} order non-equilibrium moments inside the stress-tensor evolution equation. While this error is presumably small, it should be observed during a careful grid convergence analysis. Instead, a 2^{nd} order accuracy was observed with regularized kernels [74, 76, 101]. A schematic argument to explain why a 1^{st} order accuracy was not observed is to consider that the numerical error of a regularized LB model could be written as

$$\Delta t A(t, \mathbf{x}) + \Delta t^2 B(t, \mathbf{x}) + \mathcal{O}(\Delta t^3). \quad (4.29)$$

With A and B two unknown functions. If $A(t, \mathbf{x})$ is extremely small, $A(t, \mathbf{x}) \ll \Delta t B(t, \mathbf{x})$, the dominant error measured by an empirical grid convergence is $\mathcal{O}(\Delta t^2)$. However, as Δt goes to 0, $A(t, \mathbf{x}) > \Delta t B(t, \mathbf{x})$ and the *actual* order of accuracy, $\mathcal{O}(\Delta t)$, should be measured. Empirical measurements of a $\mathcal{O}(\Delta t^2)$ accuracy of regularized kernels only means that the grid convergence study was not conducted with a sufficiently fine grid such that $A(t, \mathbf{x}) \ll \Delta t B(t, \mathbf{x})$.

Generally speaking, all collision kernel where Eq. (4.22) is verified are also $\mathcal{O}(\Delta t)$ accurate. Which means that a non-negligible part of the LB literature is using $\mathcal{O}(\Delta t)$ schemes. From a practical point of view, a low value of the overall numerical error is more important than the order – $\mathcal{O}(\Delta t)$ or $\mathcal{O}(\Delta t^2)$ – of the error. In this aspect, regularized LB models are able to produce solutions with low numerical dissipation and dispersion, even with a $\mathcal{O}(\Delta t)$ error. This will be checked empirically later in this manuscript.

4.3. Application : Athermal Lattice-Boltzmann Method

The last 2 Sections showed that each macroscopic moment follows its own evolution equation Eq. (4.15), advocating a change of paradigm. Instead of considering LB as a kinetic solver let us consider it as a kind of Grad- q solver for an extended set of thermo-hydrodynamic equations. Some of them are desired conservation laws such as mass and momentum conservations, others corresponds to higher order equations in the *finite* hierarchy of q equations related to the lattice $DdQq$. Therefore, f and all other populations previously defined lose their kinetic meaning and are now merely considered as temporary numerical variables in the macroscopic CFD solver known as "lattice-Boltzmann".

4.3.1. Numerical scheme

For the sake of clarity we first apply the proposed Taylor expansion on the classical athermal LB model on standard lattices [4] with a force term specifically designed to get rid of the classical $\mathcal{O}(\text{Ma}^3)$ error of standard lattices [4]. This model, traditionally said to be athermal in the LB literature, is used in practice to solve isothermal flows. Following the proposed Taylor expansion formalism we define the initial solution simply by initial macroscopic fields $\rho(t, \mathbf{x})$, $u_\alpha(t, \mathbf{x})$. From this initial condition we would like to find a LB algorithm that predicts $\rho(t + \Delta t, \mathbf{x})$ and $u_\alpha(t + \Delta t, \mathbf{x})$ following an approximate Navier-Stokes system, hopefully matching mass and momentum conservation Eqs. (1.20,1.21). Let us now detail step-by-step the algorithm that defines the classical athermal LB scheme.

- **Step 1 : Equilibrium construction** Because we restrict ourselves to standard lattices, some third-order Hermite polynomials $\mathcal{H}_i^{(3)}$ do not belong to the Hermite basis. For this reason we do not expand further than the third order, isotropy defects being corrected by an appropriate force term. The equilibrium reads

$$f_i^{eq} = \omega_i \left\{ \mathcal{H}^{(0)} \rho + \frac{\mathcal{H}_{i\alpha}^{(1)}}{c_s^2} \rho u_\alpha + \frac{\mathcal{H}_{i\alpha\beta}^{(2)}}{2c_s^4} [\rho u_\alpha u_\beta] + \frac{\mathcal{H}_{i\gamma}^{(3r)}}{6c_s^6} a_\gamma^{(3r)} \right\}. \quad (4.30)$$

where $a_\gamma^{(3r)}$ is only a function of $a_{\alpha\beta\gamma}^{(3)} = \rho u_\alpha u_\beta u_\gamma$, as can be seen in Appendix A.

- **Step 2 : Force construction** The forcing population is extended to second order,

$$F_i \equiv \omega_i \left\{ \mathcal{H}^{(0)} a^{F,(0)} + \frac{\mathcal{H}_{i\alpha}^{(1)}}{c_s^2} a_\alpha^{F,(1)} + \frac{\mathcal{H}_{i\alpha\beta}^{(2)}}{2c_s^4} a_{\alpha\beta}^{F,(2)} \right\}, \quad (4.31)$$

with its Hermite moments defined in order to properly encompass the mass and

4. Taylor expansion based description of the lattice-Boltzmann scheme – 4.3.
Application : Athermal Lattice-Boltzmann Method

momentum sources \dot{m} and $\rho\mathcal{F}_\alpha$, see Eqs. (1.20-1.21). Those force moments are

$$a_{\alpha\beta}^{F,(2)} = -\frac{\partial D_{\alpha\beta\gamma}^{f^{eq,(3)}}}{\partial x_\gamma} + \rho c_s^2 \frac{2}{3} \frac{\partial u_\gamma}{\partial x_\gamma} \delta_{\alpha\beta} + \rho\mathcal{F}_\alpha u_\beta + \rho\mathcal{F}_\beta u_\alpha - \dot{m} u_\alpha u_\beta, \quad (4.32)$$

$$a_\alpha^{F,(1)} = \rho\mathcal{F}_\alpha, \quad (4.33)$$

$$a^{F,(0)} = \dot{m}, \quad (4.34)$$

with $D_{\alpha\beta\gamma}^{f^{eq,(3)}}$ the isotropy defect of the equilibrium population, related to the lattice and the equilibrium function and \dot{m} and \mathcal{F}_α the mass and momentum arbitrary forcing terms, see Eqs. (1.1-1.2).

- **Step 3 : Non-equilibrium construction** The non-equilibrium population is obtained as

$$\bar{f}_i^{neq} = \bar{f}_i - f_i^{eq} + \frac{\Delta t}{2} F_i. \quad (4.35)$$

- **Step 4 : Collision** With f_i^{eq} , F_i and \bar{f}_i^{neq} built in the previous steps, compute the collided population f_i^{col} as

$$f_i^{col}(t, \mathbf{x}) = f_i^{eq}(t, \mathbf{x}) + \bar{f}_i^{neq}(t, \mathbf{x}) + 2 \left\{ \left[\left(\boldsymbol{\delta} - \frac{\Delta t}{2} \mathbf{M} \right)^{-1} \right]_{ij} - \delta_{ij} \right\} \bar{f}_j^{neq} + \frac{\Delta t}{2} F_i(t, \mathbf{x}). \quad (4.36)$$

Where \mathbf{M} is the collision matrix associated to a collision kernel written as Eq. (3.35). For the BGK kernel it would become

$$f_i^{col}(t, \mathbf{x}) = f_i^{eq}(t, \mathbf{x}) + \left(1 - \frac{\Delta t}{\bar{\tau}} \right) \bar{f}_i^{neq}(t, \mathbf{x}) + \frac{\Delta t}{2} F_i(t, \mathbf{x}). \quad (4.37)$$

- **Step 5 : Streaming** Shift the populations according to

$$\bar{f}_i(t + \Delta t, \mathbf{x}) = f_i^{col}(t, \mathbf{x} - \mathbf{c}_i \Delta t). \quad (4.38)$$

- **Step 6 : Update macroscopic variables** Using the macroscopic update rule Eq. (4.4) for $n = 0, 1, 2$ respectively leads to

$$\rho(t + \Delta t, \mathbf{x}) = \sum_{i=0}^{q-1} \bar{f}_i(t + \Delta t, \mathbf{x}) + \frac{\Delta t}{2} \dot{m}(t + \Delta t, \mathbf{x}), \quad (4.39)$$

$$\rho u_\alpha(t + \Delta t, \mathbf{x}) = \sum_{i=0}^{q-1} c_{i\alpha} \bar{f}_i(t + \Delta t, \mathbf{x}) + \frac{\Delta t}{2} [\rho\mathcal{F}_\alpha](t + \Delta t, \mathbf{x}), \quad (4.40)$$

$$\Pi_{\alpha\beta}^{f,(2)}(t + \Delta t, \mathbf{x}) = \Pi_{\alpha\beta}^{\bar{f}(t+\Delta t, \mathbf{x}), (2)} + \frac{\Delta t}{2} \left(\Pi_{\alpha\beta}^{\Omega(t+\Delta t, \mathbf{x}), (2)} + \Pi_{\alpha\beta}^{F(t+\Delta t, \mathbf{x}), (2)} \right). \quad (4.41)$$

By splitting $\Pi_{\alpha\beta}^{f,(2)}(t + \Delta t, \mathbf{x})$ into its equilibrium and non-equilibrium parts and using the MRT definition of the collision kernel Eq. (3.35), the above leads to the

4. Taylor expansion based description of the lattice-Boltzmann scheme – 4.3.
Application : Athermal Lattice-Boltzmann Method

stress-tensor scheme,

$$\left(1 + \frac{\Delta t}{2\tau}\right) \Pi_{\alpha\beta}^{f^{neq}(t+\Delta t, \mathbf{x}), (2)} = \bar{\Pi}_{\alpha\beta}^{f(t+\Delta t, \mathbf{x}), (2)} - \Pi_{\alpha\beta}^{f^{eq}(t+\Delta t, \mathbf{x}), (2)} + \frac{\Delta t}{2} \Pi_{\alpha\beta}^{F(t+\Delta t, \mathbf{x}), (2)}, \quad (4.42)$$

where we assumed that Ω_i is an arbitrary MRT model Eq. (3.40), and τ is the relaxation time – hidden inside M_{ij} – associated to the second order moments $\Pi_{\alpha\beta}^{f, (2)}$. The difference between MRT and BGK can not be seen when we are only looking at second order moments, τ is simply the relaxation time associated to second order moments, independently of the collision kernel. However, differences would appear between those 2 kernels when looking at higher order moments.

4.3.2. Continuous equivalent equations

Now that macroscopic quantities, namely mass, velocity and stress-tensor $\rho(t + \Delta t, \mathbf{x})$, $u_\alpha(t + \Delta t, \mathbf{x})$ and $\Pi_{\alpha\beta}^{f^{neq}, (2)}(t + \Delta t, \mathbf{x})$ have been explicitly updated let us analyze the equivalent continuous equations of System (4.39, 4.40, 4.42) and compare it with the target set of equations Eqs. (1.20, 1.21, 1.23). Using the continuous limit Eq. (4.15) of the LB scheme and neglecting $\mathcal{O}(\Delta t^2)$ terms leads to an extended Grad- q system whose first equations are :

$$\frac{\partial \rho}{\partial t} + \frac{\partial \rho u_\beta}{\partial x_\beta} = \dot{m} \quad (4.43)$$

$$\frac{\partial \rho u_\alpha}{\partial t} + \frac{\partial \left[\rho u_\alpha u_\beta + \rho c_s^2 \delta_{\alpha\beta} + \Pi_{\alpha\beta}^{f^{neq}, (2)} \right]}{\partial x_\beta} = \rho \mathcal{F}_\alpha, \quad (4.44)$$

$$\frac{\partial \Pi_{\alpha\beta}^{f, (2)}}{\partial t} + \frac{\partial \Pi_{\alpha\beta\gamma}^{f, (3)}}{\partial x_\gamma} = -\frac{1}{\tau} \Pi_{\alpha\beta}^{f^{neq}, (2)} + \Pi_{\alpha\beta}^{F, (2)}. \quad (4.45)$$

Identification procedure immediately tells us that the equation of state and stress tensor in this model are $p = \rho c_s^2$ and $-\Pi_{\alpha\beta}^{f^{neq}, (2)}$. We also see that contrary to the usual NSF model this system has an evolution equation for the stress-tensor, Eq. (4.45), whereas only its trace (total energy) is included in the NSF model. This evolution equation involves $\Pi_{\alpha\beta\gamma}^{f^{neq}, (3)}$ through $\Pi_{\alpha\beta\gamma}^{f, (3)}$, which shows how higher order non-hydrodynamic moments are coupled to low order moments ρ , ρu_α and $\Pi_{\alpha\beta}^{f^{neq}, (2)}$. The term

$$\frac{\partial \Pi_{\alpha\beta}^{f^{neq}, (2)}}{\partial t} = \frac{\partial (\rho u_\alpha u_\beta + \rho c_s^2 \delta_{\alpha\beta})}{\partial t}, \quad (4.46)$$

4. Taylor expansion based description of the lattice-Boltzmann scheme – 4.3.
Application : Athermal Lattice-Boltzmann Method

hidden inside Eq. (4.45) can be replaced using Eq. (4.43,4.44), combining those two equations one can obtain the kinetic tensor $\rho u_\alpha u_\beta$ equation

$$\frac{\partial \rho u_\alpha u_\beta}{\partial t} + \frac{\partial \rho u_\alpha u_\beta u_\gamma}{\partial x_\gamma} + u_\alpha \frac{\partial \left[p \delta_{\gamma\beta} + \Pi_{\gamma\beta}^{f^{neq},(2)} \right]}{\partial x_\gamma} + u_\beta \frac{\partial \left[p \delta_{\alpha\gamma} + \Pi_{\alpha\gamma}^{f^{neq},(2)} \right]}{\partial x_\gamma} = \rho \mathcal{F}_\alpha u_\beta + \rho \mathcal{F}_\beta u_\alpha - \dot{m} u_\alpha u_\beta, \quad (4.47)$$

not to be confused with the kinetic energy evolution equation, corresponding to half the trace of the tensor evolution Eq. (4.47). Using the second order raw moment of the equilibrium population (4.32,4.34) in Eq. (4.45) and the athermal equation of state $p = \rho c_s^2$ finally leads to

$$\begin{aligned} -\Pi_{\alpha\beta}^{f^{neq},(2)} &= \tau \rho c_s^2 \left[\frac{\partial u_\alpha}{\partial x_\beta} + \frac{\partial u_\beta}{\partial x_\alpha} - \delta_{\alpha\beta} \frac{2}{3} \frac{\partial u_\gamma}{\partial x_\gamma} \right] \\ &+ \tau \left[\frac{\partial \Pi_{\alpha\beta}^{f^{neq},(2)}}{\partial t} + \frac{\partial \Pi_{\alpha\beta\gamma}^{f^{neq},(3)}}{\partial x_\gamma} \right] - \tau \left[u_\alpha \frac{\partial \Pi_{\beta\gamma}^{f^{neq},(2)}}{\partial x_\gamma} + u_\beta \frac{\partial \Pi_{\alpha\gamma}^{f^{neq},(2)}}{\partial x_\gamma} \right] \end{aligned} \quad (4.48)$$

with $\tau \rho c_s^2 = \mu$ obtained by identification with the usual definition of the stress tensor Eq. (1.18). Note that the effect of the collision kernel is entirely hidden inside $\Pi_{\alpha\beta\gamma}^{f^{neq},(3)}$. Again, it is important to note that this last equation is not algebraic as the truncated Chapman-Enskog expansion asserts but rather an evolution equation for the unknown $\Pi_{\alpha\beta}^{f^{neq},(2)}$. Note that from a macroscopic point of view, a change of collision kernel can be interpreted as a change of stress tensor evolution model throughout the modification of $\Pi_{\alpha\beta\gamma}^{f^{neq},(3)}$.

4.3.3. Domain of validity in term of dimensionless numbers

It seems that mass and momentum are correctly recovered by the LB scheme, see Eq. (4.43,4.44). The next step is to demonstrate in which cases the Lattice Boltzmann stress-tensor Eq. (1.18) could approximate the Navier-Stokes algebraic stress tensor, Eq. (1.18). In other words,

$$-\Pi_{\alpha\beta}^{f^{neq},(2)} \approx \mathcal{T}_{\alpha\beta} = \mu \left[\frac{\partial u_\alpha}{\partial x_\beta} + \frac{\partial u_\beta}{\partial x_\alpha} - \frac{2\delta_{\alpha\beta}}{3} \frac{\partial u_\gamma}{\partial x_\gamma} \right]. \quad (4.49)$$

To that end, let us nondimensionalize Eq. (4.48). First we need to identify what is the shortest physical time scale t_s , corresponding to the fastest and dominant physical phenomenon. Depending on the situation, mainly two relevant candidates exist: the viscous timescale $t_\mu = \rho L_0^2 / \mu$ and the convective timescale $t_c = L_0 / U_0$. If the shortest

4. Taylor expansion based description of the lattice-Boltzmann scheme – 4.3.
Application : Athermal Lattice-Boltzmann Method

timescale is t_s , then the appropriate nondimensionalization reads

$$\frac{\partial}{\partial t} = \frac{1}{t_s} \frac{\partial}{\partial t^*}, \quad \frac{\partial}{\partial x} = \frac{1}{L_0} \frac{\partial}{\partial x^*}, \quad (4.50)$$

$$\Pi_{\alpha\beta}^{f^{neq},(2)} = \Pi_0 \Pi_{\alpha\beta}^{*,f^{neq},(2)}, \quad \Pi_{\alpha\beta\gamma}^{f^{neq},(3)} = Q_0 \Pi_{\alpha\beta\gamma}^{*,f^{neq},(3)}, \quad (4.51)$$

$$u = U_0 u^*, \quad \rho = \rho_0 \rho^*, \quad T = T_0 T^*. \quad (4.52)$$

where * superscript quantities are $\mathcal{O}(1)$ and non-dimensional. Applying this change of variable we are left with

$$\begin{aligned} -\Pi_{\alpha\beta}^{*,f^{neq},(2)} &= \mathcal{T}_{\alpha\beta}^* + \frac{\mu Q_0}{\rho_0 c_s^2 L_0 \Pi_0} \frac{1}{\rho^*} \frac{\partial \Pi_{\alpha\beta\gamma}^{*,f^{neq},(3)}}{\partial x_\gamma^*} \\ &+ \frac{\widetilde{\text{Ma}}^2}{\text{Re}} \frac{1}{\rho^*} \left[u_\alpha^* \frac{\partial \Pi_{\beta\gamma}^{*,f^{neq},(2)}}{\partial x_\gamma^*} + u_\beta^* \frac{\partial \Pi_{\alpha\gamma}^{*,f^{neq},(2)}}{\partial x_\gamma^*} \right] + \frac{\mu}{\rho_0 c_s^2 t_s} \frac{1}{\rho^*} \frac{\partial \Pi_{\alpha\beta}^{*,f^{neq},(2)}}{\partial t^*}, \end{aligned} \quad (4.53)$$

where the Reynolds number $\text{Re} = t_\mu / t_c$ and athermal Mach number

$$\widetilde{\text{Ma}} = U_0 / c_s, \quad (4.54)$$

have been used. Note that in the athermal case $\widetilde{\text{Ma}}$ is enslaved to the CFL number [14] because $c_s = \Delta x / (\sqrt{3} \Delta t)$, leading to

$$\text{CFL} = \frac{U_0 + c_s}{\Delta x / \Delta t} = \frac{\widetilde{\text{Ma}} + 1}{\sqrt{3}}. \quad (4.55)$$

The stability criterion $\text{CFL} \leq 1$ boils down to the usual athermal Mach limit $\widetilde{\text{Ma}} \leq \sqrt{3} - 1 \approx 0.732$, which is consistent with previous studies [81, 82]. If the convective scaling is chosen the stress-tensor becomes

$$-\Pi_{\alpha\beta}^{*,f^{neq},(2)} = \mathcal{T}_{\alpha\beta}^* + \mathcal{O}\left(\frac{\mu Q_0}{\rho_0 c_s^2 L_0 \Pi_0}\right) + \mathcal{O}\left(\frac{\widetilde{\text{Ma}}^2}{\text{Re}}\right). \quad (4.56)$$

To verify our initial *ansatz* Eq. (4.49), a *sufficient* condition is that $\mathcal{O}(\cdot)$ should be negligible. For non-zero gradients, $\mathcal{O}(\cdot)$ could only vanish because $\widetilde{\text{Ma}}^2 / \text{Re}$ and $(\mu Q_0) / (\rho_0 c_s^2 L_0 \Pi_0)$ are much smaller than 1. Therefore, $\widetilde{\text{Ma}}^2 / \text{Re} \ll 1$ and $(\mu Q_0) / (\rho_0 c_s^2 L_0 \Pi_0) \ll 1$ are *necessary* conditions for *ansatz* Eq. (4.49) to be valid for non trivial flows.

The last term of $\mathcal{O}(\cdot)$ can be neglected for the diffusive and convective timescale respectively if $\widetilde{\text{Ma}}^2 / \text{Re}^2$ and $\widetilde{\text{Ma}}^2 / \text{Re}$ are small enough. On the other hand the factor $\mu Q_0 / \rho_0 c_s^2 L_0 \Pi_0$ corresponding to the ratio between scalings of third and second order non-equilibrium moments is lattice and collision kernel dependent. Because the isotropy defect completely modifies the convective term in the evolution equation of $\Pi_{\alpha\beta\gamma}^{f^{neq},(3)}$, it leads to an evolution equation whose meaning is unclear for standard

4. Taylor expansion based description of the lattice-Boltzmann scheme – 4.4.
Application : Interpretation of collision models

lattices. However, when the recursive regularized kernel [72] is used we get $Q_0 = U_0 \Pi_0$ and the stress-tensor becomes

$$-\Pi_{\alpha\beta}^{*,f^{neq},(2)} = \mathcal{T}_{\alpha\beta}^* + \mathcal{O}\left(\frac{\widetilde{\text{Ma}}^2}{\text{Re}}\right). \quad (4.57)$$

One sees here that the usual "small Knudsen" assumption is not even sufficient because more complicated terms appeared in the scaling analysis. To get back the proper Navier-Stokes stress-tensor one has to carefully analyze one by one each of these spurious terms. Additionally in LB the 3^{rd} order non-equilibrium moment is related to the heat-flux, suggesting that the Prandtl number Pr may also intervene inside Q_0 when the energy equation is also solved by LB.

The Taylor expansion showed that the consistency condition was not as simple as the Chapman-Enskog expansion suggests. The small Knudsen assumption is not enough and both the choice of the lattice and the collision kernel changes the consistency defect in Eq. (4.57). More discrete velocities means that the isotropy defect is pushed away from the Navier-Stokes and the stress-tensor equation, but it also means that more moments equations are also solved. Those equations are likely to modify or even undermine the validity of the solution because they are completely uncontrolled and do not even correspond to a physical/kinetic modeling due to the isotropy defect $D_{\alpha\dots\alpha_n}^{f,(n)}$.

4.4. Application : Interpretation of collision models

Now that we analyzed a simple athermal BGK LB scheme let us discuss the collision kernel by reviewing a sample of techniques that can be used to increase robustness of LB schemes. From the Taylor expansion we've seen that mass and momentum conservation equations were correctly discretized up to $\mathcal{O}(\Delta t^2)$ errors by the LB scheme. On the other hand, the system is not closed through an algebraic constitutive equation as in usual CFD solvers. Instead we inherit Eq. (4.48) from the hierarchy of moments. Rearranging its terms leads to

$$\frac{\partial \Pi_{\alpha\beta}^{f^{neq},(2)}}{\partial t} + \frac{\partial \Pi_{\alpha\beta\gamma}^{f^{neq},(3)}}{\partial x_\gamma} - u_\alpha \frac{\partial \Pi_{\beta\gamma}^{f^{neq},(2)}}{\partial x_\gamma} - u_\beta \frac{\partial \Pi_{\alpha\gamma}^{f^{neq},(2)}}{\partial x_\gamma} = -\frac{1}{\tau} \left(\Pi_{\alpha\beta}^{f^{neq},(2)} + \mathcal{T}_{\alpha\beta} \right), \quad (4.58)$$

where $\mathcal{T}_{\alpha\beta}$ is the NSF stress tensor. Higher order contributions $\Pi_{\alpha\beta\gamma}^{f^{neq},(3)}$, as already discussed, do not necessarily match a meaningful behavior, especially for standard lattices because of isotropy defects. Therefore, a question that could drive us towards the use of a particular kernel is a correct modeling of the stress tensor by Eq. (4.58). Being the only moment that does not appear in the hydrodynamic equations Eqs. (4.43-4.44) the non-equilibrium tensor $\Pi_{\alpha\beta\gamma}^{f^{neq},(3)}$ is our only degree of freedom to modify the mod-

4. Taylor expansion based description of the lattice-Boltzmann scheme – 4.4.
Application : Interpretation of collision models

eling of Eq. (4.58) towards a *physically meaningful* stress tensor transport equation. But first, let us rewrite Eq. (4.58) schematically as

$$\frac{\partial \Pi_{\alpha\beta}^{f^{neq},(2)}}{\partial t} + \mathcal{K}_{\alpha\beta} = -\frac{1}{\tau} \left(\Pi_{\alpha\beta}^{f^{neq},(2)} + \mathcal{T}_{\alpha\beta} \right). \quad (4.59)$$

Nondimensionalization and multiplication by -1 leads to

$$\frac{\partial -\Pi_{\alpha\beta}^{*,f^{neq},(2)}}{\partial t^*} - \frac{t_s}{\Pi_0} \mathcal{K}_{\alpha\beta} = -\frac{t_s}{\tau} \left(-\Pi_{\alpha\beta}^{*,f^{neq},(2)} - \mathcal{T}_{\alpha\beta}^* \right). \quad (4.60)$$

For example for convective flows with the athermal LB model,

$$\frac{t_s}{\tau} = \frac{\rho c_s^2 L_0}{\mu U_0} = \frac{\text{Re}}{\widetilde{\text{Ma}}^2}. \quad (4.61)$$

We already rigorously demonstrated in Sec. 4.3.3 for the athermal model what are the necessary conditions for $\mathcal{K}_{\alpha\beta}$ to be neglected. However, let us note that Eq. (4.60) looks very similar to the relaxation equation Eq. (3.2) we discussed in Sec. 3.1. In the analytical solution, Eq. (3.3), we see that the convergence of ϕ towards ϕ^{eq} is faster for lower values of τ . In the same way, we could conclude that the convergence of $-\Pi_{\alpha\beta}^{*,f^{neq},(2)}$ towards $\mathcal{T}_{\alpha\beta}^*$ is faster for lower values of $\widetilde{\text{Ma}}^2/\text{Re}$. For sufficiently low $\widetilde{\text{Ma}}$ or sufficiently high Re the convergence of $-\Pi_{\alpha\beta}^{*,f^{neq},(2)}$ towards $\mathcal{T}_{\alpha\beta}^*$ modeled by Eq. (4.60) seems to mimic $-\Pi_{\alpha\beta}^{*,f^{neq},(2)} \approx \mathcal{T}_{\alpha\beta}^*$. In other words, the LB equation is not only a relaxation equation for f_i^{neq} , it also provides a consistent relaxation model of $-\Pi_{\alpha\beta}^{*,f^{neq},(2)}$ towards its NSF value $\mathcal{T}_{\alpha\beta}^*$. For athermal lattice-Boltzmann, because $c_s = \Delta x / (\sqrt{3} \Delta t)$, lower Mach means lower timestep, such that Eq. (4.60) is more efficient in approximating $-\Pi_{\alpha\beta}^{*,f^{neq},(2)} \approx \mathcal{T}_{\alpha\beta}^*$ as the CFL is reduced.

4.4.1. Modeling of lag effects in constitutive equations

We have just highlighted that LB mechanical constitutive equation encompasses a lag effect due to $\partial/\partial t$. Neglecting $\mathcal{K}_{\alpha\beta}$, what LB is doing for the treatment of viscous terms is to replace a diffusion equation by another model. To get a better understanding, let us consider the following heat equation [102, 103],

$$\frac{\partial T}{\partial t} = \kappa \frac{\partial^2 T}{\partial x_\alpha^2}. \quad (4.62)$$

Mimicking the LB strategy, it could be replaced by

$$\frac{\partial T}{\partial t} = -\frac{\partial q_\alpha}{\partial x_\alpha}, \quad \frac{\partial q_\alpha}{\partial t} = -\frac{1}{\tau} \left(q_\alpha + \kappa \frac{\partial T}{\partial x_\alpha} \right). \quad (4.63)$$

4. Taylor expansion based description of the lattice-Boltzmann scheme – 4.4.
Application : Interpretation of collision models

Note that this modeling alleviates the paradox of infinite velocity propagation of diffusion [104, 105] in parabolic models such as Eq. (4.62). This choice of modeling of heat flux q_α is either called *hyperbolic diffusion* [106], *hyperbolic heat equation* [104, 107] or *Maxwell-Cattaneo model* [105]. Rewriting the last equation we get,

$$\left(1 + \tau \frac{\partial}{\partial t}\right) q_\alpha = -\kappa \frac{\partial T}{\partial x_\alpha}, \quad (4.64)$$

where the additional $\tau \frac{\partial}{\partial t}$ term to the Fourier law [5, 43] accounts for the required lag to reach steady heat conduction [108, 109]. While not as common as the parabolic [102] model Eq. (4.62), the – very small – values of τ have been experimentally measured for some materials, as mentioned in [105]. Eq. (4.64) is therefore a relevant model in some heat conduction applications. However, this new model is not reference frame invariant. Considering 2 reference frames (x_α, t) and (x'_α, t') translated from one another with velocity v_α , they are related by

$$x_\alpha = x'_\alpha + v_\alpha t', \quad (4.65)$$

$$t = t', \quad (4.66)$$

$$u_\alpha = u'_\alpha + v_\alpha, \quad (4.67)$$

then we can write that

$$\frac{\partial}{\partial t'} = \frac{\partial t}{\partial t'} \frac{\partial}{\partial t} + \frac{\partial x_\alpha}{\partial t'} \frac{\partial}{\partial x_\alpha} = \frac{\partial}{\partial t} + v_\alpha \frac{\partial}{\partial x_\alpha}, \quad (4.68)$$

$$\frac{\partial}{\partial x'_\alpha} = \frac{\partial t}{\partial x'_\alpha} \frac{\partial}{\partial t} + \frac{\partial x_\alpha}{\partial x'_\alpha} \frac{\partial}{\partial x_\alpha} = \frac{\partial}{\partial x_\alpha}, \quad (4.69)$$

which shows that the functional form of Eq. (4.64) is not the same in both reference frames. A solution to this problem is to replace the time derivative $\partial/\partial t$ by other derivatives. For example, using the material derivative [5, 40] D/Dt ,

$$\frac{D\phi}{Dt} = \frac{\partial\phi}{\partial t} + u_\gamma \frac{\partial\phi}{\partial x_\gamma} = \frac{\partial\phi}{\partial t'} + u'_\gamma \frac{\partial\phi}{\partial x'_\gamma} = \frac{D\phi}{Dt'}, \quad (4.70)$$

leads to reference frame invariant functional form of the Maxwell-Cattaneo model. The material derivative is not the only derivative enforcing reference frame invariance. For a symmetric tensor $\Pi_{\alpha\beta}$, the upper convected derivative [110–112] $\delta^{up}/\delta t$, also called Lie-Oldroyd derivative, could be used. In continuum mechanics it corresponds to the rate of change of a tensor property of a small parcel of fluid that is written in the coordinate system rotating and stretching with the fluid velocity u_α . Additionally, the

4. Taylor expansion based description of the lattice-Boltzmann scheme – 4.4.
Application : Interpretation of collision models

lower convected derivative $\delta^{low}/\delta t$ is also defined,

$$\frac{\delta^{up}\Pi_{\alpha\beta}}{\delta t} = \frac{D\Pi_{\alpha\beta}}{Dt} - \Pi_{\alpha\gamma} \frac{\partial u_\beta}{\partial x_\gamma} - \Pi_{\gamma\beta} \frac{\partial u_\gamma}{\partial x_\alpha}, \quad (4.71)$$

$$\frac{\delta^{low}\Pi_{\alpha\beta}}{\delta t} = \frac{D\Pi_{\alpha\beta}}{Dt} + \Pi_{\alpha\gamma} \frac{\partial u_\beta}{\partial x_\gamma} + \Pi_{\gamma\beta} \frac{\partial u_\gamma}{\partial x_\alpha}. \quad (4.72)$$

Using these derivatives to replace the time derivative inside Eq. (4.64) lead to an invariant functional form between coordinates (x_α, t) and (x'_α, t') . The choice of frame-invariant time derivative seems to be a research topic on its own [113, 114] in the field of advanced constitutive equations modeling.

To conclude this small discussion, let simply note that other derivatives – *e.g.* material, upper convected, lower convected – do exist in the literature in order to model lag effects with

$$(1 + \tau \nabla_t) q_\alpha = -\kappa \frac{\partial T}{\partial x_\alpha}, \quad (4.73)$$

where ∇_t is preferably a frame-invariant – *galilean invariant* – derivative.

4.4.2. BGK kernel

With a BGK collision operator, $\Pi_{\alpha\beta\gamma}^{f^{neq},(3)}$ purely stems from higher order non-hydrodynamic equations. In this case, assuming that the lattice is large enough such that $D_{\alpha\beta\gamma}^{f^{neq},(3)} = 0$ – this property is only enforced on some non-diagonal components of tensor $\Pi_{\alpha\beta\gamma}^{(3)}$ for standard lattices – we can write for example the $\Pi_{xx}^{f^{neq},(2)}$ evolution equation,

$$\frac{\partial \Pi_{xx}^{f^{neq},(2)}}{\partial t} - 2u_x \frac{\partial \Pi_{x\gamma}^{f^{neq},(2)}}{\partial x_\gamma} = -\frac{1}{\tau} \left(\Pi_{xx}^{f^{neq},(2)} + \mathcal{T}_{xx} \right) - \frac{\partial \Pi_{xx\gamma}^{f^{neq},(3)}}{\partial x_\gamma}. \quad (4.74)$$

In the left hand side we recognize a transport term in the x direction with an unexpected backward propagation $-2u_x$ while the first term in the right hand side is a relaxation term that steers the variable $\Pi_{xx}^{f^{neq},(2)}$ towards the expected \mathcal{T}_{xx} , see Sec. 3.1. The second term in the right hand side is the coupling with higher-order non-hydrodynamic moments. Because $\Pi_{\alpha\beta\gamma}^{f^{neq},(3)}$ depends on a very complicated cascade of higher order equations, we can not conclude anything on the modeling of the stress tensor by BGK kernel.

4.4.3. Regularized kernels

A particularly efficient way to control the time evolution of the stress tensor was identified in the regularized and recursive regularized collision kernels. The regularization [115, 116] simply discards $\Pi_{\alpha\beta\gamma}^{\bar{f}^{neq},(3)}$ during the collision, leading to a filtered

4. Taylor expansion based description of the lattice-Boltzmann scheme – 4.4.
Application : Interpretation of collision models

non-equilibrium population

$$\bar{f}_i^{\text{neq}} = \omega_i \frac{\mathcal{H}_{i\alpha\beta}^{(2)}}{2c_s^4} \Pi_{\alpha\beta}^{\bar{f}^{\text{neq}},(2)}, \quad (4.75)$$

$$\Pi_{\alpha\beta}^{\bar{f}^{\text{neq}},(2)} = \sum_{i=0}^{q-1} c_{i\alpha} c_{i\beta} \left(\bar{f}_i - f_i^{\text{eq}} + \frac{\Delta t}{2} F_i \right), \quad (4.76)$$

allowing those filtered moments to be compartmentalized from the hydrodynamic moments, and effectively cancelling the last term of Eq. (4.74).

4.4.4. Recursive Regularized kernels

Recursive regularization [72] does not simply removes $\Pi_{\alpha\beta\gamma}^{\bar{f}^{\text{neq}},(3)}$ but replaces it by an approximated value obtained from the CE expansion,

$$\bar{f}_i^{\text{neq}} = \omega_i \left\{ \frac{\mathcal{H}_{i\alpha\beta}^{(2)}}{2c_s^4} \Pi_{\alpha\beta}^{\bar{f}^{\text{neq}},(2)} + \frac{\mathcal{H}_{i\gamma}^{(3r)}}{6c_s^6} \Pi_{\gamma}^{\bar{f}^{\text{neq}},(3r)} \right\}, \quad (4.77)$$

with $\Pi_{\alpha\beta\gamma}^{\bar{f}^{\text{neq}},(3)} = u_{\alpha} \Pi_{\beta\gamma}^{\bar{f}^{\text{neq}},(2)} + u_{\beta} \Pi_{\gamma\alpha}^{\bar{f}^{\text{neq}},(2)} + u_{\gamma} \Pi_{\alpha\beta}^{\bar{f}^{\text{neq}},(2)}$ serving to define $\Pi_{\gamma}^{\bar{f}^{\text{neq}},(3r)}$ as in Appendix A. This leads to a new evolution equation,

$$\frac{\delta^{low} \Pi_{\alpha\beta}^{\bar{f}^{\text{neq}},(2)}}{\delta t} + \Pi_{\alpha\beta}^{\bar{f}^{\text{neq}},(2)} \frac{\partial u_{\gamma}}{\partial x_{\gamma}} = -\frac{1}{\tau} \left(\Pi_{\alpha\beta}^{\bar{f}^{\text{neq}},(2)} + \mathcal{T}_{\alpha\beta} \right), \quad (4.78)$$

where $\delta^{low}/\delta t$ is the lower convected derivative defined in Eq. (4.72). A careful examination of Eq. (4.78) shows that it is a galilean invariant equation [87, 117, 118]. Which is a highly desirable property for any physical model. However, note that the galilean invariance of the *model* does not mean that the numerical solution is also galilean invariant. Due to numerical errors, a reference frame dependent numerical error occurs.

4.4.5. Hybrid Recursive Regularization kernels

Jacob *et al* [119] developed an extension of the recursive regularization by introducing $\sigma \in [0, 1]$ into the non-equilibrium reconstruction Eq. (4.77) as

$$\Pi_{\alpha\beta}^{\bar{f}^{\text{neq}},(2)} = \sigma \sum_{i=0}^{q-1} c_{i\alpha} c_{i\beta} \left(\bar{f}_i - f_i^{\text{eq}} + \frac{\Delta t}{2} F_i \right) - (1 - \sigma) \rho c_s^2 \bar{\tau} \left[\frac{\partial u_{\alpha}}{\partial x_{\beta}} + \frac{\partial u_{\beta}}{\partial x_{\alpha}} - \frac{2\delta_{\alpha\beta}}{3} \frac{\partial u_{\gamma}}{\partial x_{\gamma}} \right]_{FD}, \quad (4.79)$$

where the last term is evaluated from a finite difference scheme. It has been shown [119] that this modification leads, for $\sigma < 1$, to the introduction of a numerical hyper-

4. Taylor expansion based description of the lattice-Boltzmann scheme – 4.4.
Application : Interpretation of collision models

viscosity in the momentum equation. In light of the previous Section, an alternative explanation for the enhanced stability is that $\Pi_{\alpha\beta}^{f^{neq},(2)}$ may deviate from its target relaxed value $\mathcal{T}_{\alpha\beta}$. Using $0 < \sigma < 1$ (resp. $\sigma = 0$) as a weighting parameter is equivalent to a partial (resp. total) reset of $\Pi_{\alpha\beta}^{f^{neq},(2)}$ to its fully relaxed value $\mathcal{T}_{\alpha\beta}$ at the end of each time step, leading to a stronger steering of $\Pi_{\alpha\beta}^{f^{neq},(2)}$ towards $\mathcal{T}_{\alpha\beta}$ by the resulting LB scheme.

4.4.6. Traceless Recursive Regularized kernels

The pressure work is of paramount importance in compressible flows and was already emphasized as a major source of instabilities for thermal LB solutions [82]. Because the non-equilibrium moment $\Pi_{\alpha\beta}^{f^{neq},(2)}$ is the effective stress tensor in LBMs, any spurious term appearing on its trace will act as a spurious pressure in momentum equation. Therefore, artificially enforcing a traceless stress tensor [76] in a d dimensional physical space,

$$\Pi_{\alpha\beta}^{\bar{f}^{neq},(2)} = \sum_{i=0}^{q-1} \left[c_{i\alpha} c_{i\beta} - \frac{\delta_{\alpha\beta}}{d} c_{i\gamma} c_{i\gamma} \right] \left(\bar{f}_i - f_i^{eq} + \frac{\Delta t}{2} F_i \right), \quad (4.80)$$

during the collision allows to get rid of this spurious pressure. We have already seen in this Section that a choice of collision kernel impacts the closure for the $\Pi_{\alpha\beta}^{f^{neq},(2)}$ equation, which does not necessarily lead to a traceless stress tensor. Additionally, it was demonstrated in [120] that the traceless stress tensor can be seen as an additional regularization because it filters the non-equilibrium moment $\Pi_{\alpha\alpha}^{f^{neq},(2)}$, which is supposed to be 0 when the Stokes hypothesis is verified [48]. Using this kernel, and interpreting it as a MRT model – $\mathcal{M}_j = \Pi_{\alpha\alpha}^{(2)}$ in Eq. (3.45) –, this leads to

$$\Pi_{\alpha\alpha}^{f^{col},(2)}(t, \mathbf{x}) = \left[\Pi_{\alpha\alpha}^{f^{eq},(2)} + \left(1 - \frac{\Delta t}{\frac{\Delta t}{2} + \tau_{\Pi_{\alpha\alpha}^{(2)}}} \right) \Pi_{\alpha\alpha}^{\bar{f}^{neq},(2)} + \frac{\Delta t}{2} \Pi_{\alpha\alpha}^{F,(2)} \right] (t, \mathbf{x}). \quad (4.81)$$

Enforcing a traceless $\Pi_{\alpha\beta}^{\bar{f}^{neq},(2)}$ means that it was reconstructed following Eq. (4.80) such that $\Pi_{\alpha\alpha}^{\bar{f}^{neq},(2)} = 0$. For the numerical scheme, which only carries non-equilibrium data throughout the collision, it is equivalent to putting $\Pi_{\alpha\alpha}^{(2)} = \Delta t/2$. When using a recursive regularization, the remnants non filtered variables were ρ , ρu_α , along with all components of $\Pi_{\alpha\alpha}^{\bar{f}^{neq},(2)}$. Now, using the traceless collision, one additional variable was filtered, the trace of the second order non-equilibrium moment, $\Pi_{\alpha\alpha}^{\bar{f}^{neq},(2)}$.

4.5. Application : Thermal Lattice-Boltzmann Method, ρ -based model

As a matter of fact, a fully compressible LBM method can be obtained in a straightforward way by expanding the analytical Maxwellian up to the necessary order and to use the associated required number of distribution function. Unfortunately, such an approach is not tractable for practical flow simulations since it involves at least a 9-th order expansion of the Maxwellian along with the use of 121 distribution functions for 3D computations [38]. In such an approach, mass, momentum and energy conservation are recovered at the same time using a single set of distribution functions, corresponding to the coupled approach for NSF system, in which all equations are solved in monolithic way.

To solve this problem, a commonly used approach is to decouple the energy equation from the mass and momentum conservation equation, leading to a segregated approach, according to the classical nomenclature for CFD methods based on NSF equations. The expected gain here is to be able to keep using a reduced-order expansion of the Maxwellian (compared to the monolithic approach) and a reasonable number of distribution functions, while recovering the full compressible NSF equations dynamics. Within the framework of LBM, this leads to the definition of Double Distribution Function (DDF) methods and Hybrid methods [121]. In the former, the energy equation is solved as the zero-th order of a second set of distribution functions, while in the latter, it is solved using a classical Finite Volume/Finite Difference method for the scalar quantity. Segregated methods raise the issue of the coupling between the block of mass and momentum conservation and the energy equation. Since a restricted Maxwellian expansion is used for the mass/momentum equations, compressibility and thermodynamic effects must be explicitly reintroduced in the associated LB equations[4]. Considering existing DDF and Hybrid methods for high-speed compressible flows, the main coupling ways are [122]: i) to keep using a low-Mach athermal collision model and to enforce the physical pressure gradient as a forcing term, or ii) to use a low-Mach thermal collision model supplemented by some forcing correction terms. These choices are observed to have a deep impact on the features of the resulting numerical method in terms of accuracy and robustness. The first approach leads to some numerical stability problems near discontinuities, while the second is more robust but still necessitates some additional stabilization techniques [74].

In [74, 75, 97, 123–125] a Hybrid ρ -based LBM based on the second approach has been proposed, with successful application to thermal compressible flows in both subsonic and supersonic regimes on a regular D3Q19 lattice. The key features of this method are i) the use of a recursive regularized collision model supplemented by ad hoc correction terms and ii) solving an evolution equation for entropy written in non-conservative form, Eq. (1.6). In this Section, we study this thermal LB scheme throughout the scope of our Taylor expansion formalism.

4.5.1. Recursive Regularized- ρ numerical scheme

This scheme encompasses the thermal effects coming from the FD energy equation inside the 2nd and 3rd order equilibrium moments, leading to a complex equilibrium distribution function compared to the athermal case. This model can be summarized by the following steps :

- **Step 1 : Equilibrium construction** The equilibrium is expanded as

$$f_i^{eq} = \omega_i \left\{ \mathcal{H}^{(0)} \rho + \frac{\mathcal{H}_{i\alpha}^{(1)}}{c_s^2} \rho u_\alpha + \frac{\mathcal{H}_{i\alpha\beta}^{(2)}}{2c_s^4} [\rho u_\alpha u_\beta + \rho c_s^2 (\theta - 1) \delta_{\alpha\beta}] + \frac{\mathcal{H}_{i\gamma}^{(3r)}}{6c_s^6} a_\gamma^{(3r)} \right\}, \quad (4.82)$$

where θ is the normalized temperature,

$$\rho\theta = p/c_s^2, \quad (4.83)$$

and with $a_{\alpha\beta\gamma}^{(3)} = \rho u_\alpha u_\beta u_\gamma + \rho c_s^2 (\theta - 1) [u_\gamma \delta_{\alpha\beta} + u_\beta \delta_{\gamma\alpha} + u_\alpha \delta_{\beta\gamma}]$ serving to define $a_\gamma^{(3r)}$ as in Appendix A.

- **Step 2 : Force construction** The forcing population is simply extended to second order,

$$F_i \equiv \omega_i \left\{ \mathcal{H}^{(0)} a^{F,(0)} + \frac{\mathcal{H}_{i\alpha}^{(1)}}{c_s^2} a_\alpha^{F,(1)} + \frac{\mathcal{H}_{i\alpha\beta}^{(2)}}{2c_s^4} a_{\alpha\beta}^{F,(2)} \right\}, \quad (4.84)$$

with its Hermite moments defined as

$$a_{\alpha\beta}^{F,(2)} = -\frac{\partial D_{\alpha\beta\gamma}^{f^{eq,(3)}}}{\partial x_\gamma} + p \left(\frac{2}{3} - \frac{r}{C_v} \right) \frac{\partial u_\gamma}{\partial x_\gamma} \delta_{\alpha\beta} \quad (4.85)$$

$$+ \frac{r \delta_{\alpha\beta}}{C_v} \left(\rho \dot{q} + \dot{m} \frac{u_\gamma^2}{2} \right) + \rho \mathcal{F}_\alpha u_\beta + \rho \mathcal{F}_\beta u_\alpha - \dot{m} (u_\alpha u_\beta + c_s^2 \delta_{\alpha\beta}),$$

$$a_\alpha^{F,(1)} = \rho \mathcal{F}_\alpha, \quad (4.86)$$

$$a^{F,(0)} = \dot{m}. \quad (4.87)$$

- **Step 3 : Non-equilibrium construction** The offset non-equilibrium population \bar{f}_i^{neq} is built using the recursive regularized collision kernel, Eq. (4.77).
- **Step 4 : Collision** Thanks to previous steps f_i^{eq} , F_i and \bar{f}_i^{neq} have been built, compute the collided population f_i^{col} such that

$$f_i^{col}(t, \mathbf{x}) = f_i^{eq}(t, \mathbf{x}) + \left(1 - \frac{\Delta t}{\bar{\tau}} \right) \bar{f}_i^{neq}(t, \mathbf{x}) + \frac{\Delta t}{2} F_i(t, \mathbf{x}). \quad (4.88)$$

- **Step 5 : Streaming** Shift the populations according to

$$\bar{f}_i(t + \Delta t, \mathbf{x}) = f_i^{col}(t, \mathbf{x} - \mathbf{c}_i \Delta t). \quad (4.89)$$

4. Taylor expansion based description of the lattice-Boltzmann scheme – 4.5.
Application : Thermal Lattice-Boltzmann Method, ρ -based model

- **Step 6 : Coupling update** Discretize a thermodynamic equation – e.g among Eqs. (1.22,5.1,5.2). Let us arbitrarily choose the total energy, therefore, we use a consistent and convergent explicit scheme that can be written as

$$[\rho E](t + \Delta t, \mathbf{x}) = [\rho E](t, \mathbf{x}) + \Delta t \square_{\rho E}(t, \mathbf{x}) + \mathcal{O}(\Delta t^m) + \mathcal{O}(\Delta x^n), \quad (4.90)$$

with $m \geq 1$, $n \geq 1$ and $\square_{\rho E}$ an operator that represents discretized spatial operators in Eq. (1.22).

- **Step 7 : Update macroscopic variables** Using the macroscopic update rule Eq. (4.3) for $n = 0, 1, 2$ respectively leads to

$$\rho(t + \Delta t, \mathbf{x}) = \sum_{i=0}^{q-1} \bar{f}_i(t + \Delta t, \mathbf{x}) + \frac{\Delta t}{2} \dot{m}(t + \Delta t, \mathbf{x}), \quad (4.91)$$

$$\rho u_\alpha(t + \Delta t, \mathbf{x}) = \sum_{i=0}^{q-1} c_{i\alpha} \bar{f}_i(t + \Delta t, \mathbf{x}) + \frac{\Delta t}{2} [\rho \mathcal{F}_\alpha](t + \Delta t, \mathbf{x}), \quad (4.92)$$

$$\left(1 + \frac{\Delta t}{2\tau}\right) \Pi_{\alpha\beta}^{f^{neq}(t+\Delta t, \mathbf{x}), (2)} = \bar{\Pi}_{\alpha\beta}^{\bar{f}(t+\Delta t, \mathbf{x}), (2)} - \Pi_{\alpha\beta}^{f^{eq}(t+\Delta t, \mathbf{x}), (2)} + \frac{\Delta t}{2} \Pi_{\alpha\beta}^{F(t+\Delta t, \mathbf{x}), (2)}. \quad (4.93)$$

Then every other macroscopic variables could be obtained from the knowledge of $\rho(t + \Delta t, \mathbf{x})$, $u_\alpha(t + \Delta t, \mathbf{x})$ and $[\rho E](t + \Delta t, \mathbf{x})$. For example, $T(t + \Delta t, \mathbf{x})$ can be obtained as $T(t + \Delta t, \mathbf{x}) = T(\rho(t + \Delta t, \mathbf{x}), s(t + \Delta t, \mathbf{x}))$. Note that the coupling between finite difference solved energy and LB mainly happens in the term $\bar{\Pi}_{\alpha\alpha}^{\bar{f}(t+\Delta t, \mathbf{x}), (2)} - \Pi_{\alpha\alpha}^{f^{eq}(t+\Delta t, \mathbf{x}), (2)}$, because here the second order equilibrium $\rho u_\alpha^2 + p$, updated from both LB and finite differences, meets with $\bar{\Pi}_{\alpha\alpha}^{\bar{f}(t+\Delta t, \mathbf{x}), (2)}$, which only comes from LB. Therefore, the quantity $\bar{\Pi}_{\alpha\alpha}^{\bar{f}(t+\Delta t, \mathbf{x}), (2)} - \Pi_{\alpha\alpha}^{f^{eq}(t+\Delta t, \mathbf{x}), (2)}$ acts as a kind of garbage collector (there is no better word to describe this) for the errors appearing due to the coupling between finite difference and LB. In this case, the traceless collision – see Sec. 4.4.6 – seems mandatory to prevent the accumulation of coupling errors inside $\Pi_{\alpha\alpha}^{f^{neq}, (2)}$.

4.5.2. Continuous equivalent equations

Now that macroscopic quantities, namely mass, velocity, stress-tensor and temperature, $\rho(t + \Delta t, \mathbf{x})$, $u_\alpha(t + \Delta t, \mathbf{x})$, $\Pi_{\alpha\beta}^{f^{neq}, (2)}(t + \Delta t, \mathbf{x})$ and $T(t + \Delta t, \mathbf{x})$ have been explicitly updated let us consider the equivalent continuous equations of the system Eqs. (4.90-4.93) and compare it with the target set of equations Eqs. (1.20-1.23). Continuous limit

4. Taylor expansion based description of the lattice-Boltzmann scheme – 4.5.
Application : Thermal Lattice-Boltzmann Method, ρ -based model

of the recursive regularized ρ scheme is

$$\frac{\partial \rho}{\partial t} + \frac{\partial \rho u_\beta}{\partial x_\beta} = \dot{m}, \quad (4.94)$$

$$\frac{\partial \rho u_\alpha}{\partial t} + \frac{\partial \left[\rho u_\alpha u_\beta + p \delta_{\alpha\beta} + \Pi_{\alpha\beta}^{f^{neq},(2)} \right]}{\partial x_\beta} = \rho \mathcal{F}_\alpha, \quad (4.95)$$

$$\frac{\partial \Pi_{\alpha\beta}^{f,(2)}}{\partial t} + \frac{\partial \Pi_{\alpha\beta\gamma}^{f,(3)}}{\partial x_\gamma} = -\frac{1}{\tau} \Pi_{\alpha\beta}^{f^{neq},(n)} + \Pi_{\alpha\beta}^{F,(n)}, \quad (4.96)$$

$$\frac{\partial \rho E}{\partial t} + \frac{\partial \left[(\rho E + p) u_\beta + q_\beta + u_\alpha \Pi_{\alpha\beta}^{f^{neq},(2)} \right]}{\partial x_\beta} = \rho \mathcal{F}_\gamma u_\gamma + \rho \dot{q}, \quad (4.97)$$

where $p = \rho \theta c_s^2 = \rho r T$. We shall now deduce the stress tensor evolution equation. First, using Eqs. (4.94,4.95) to isolate the pressure time derivative $\partial p / \partial t$ inside Eq. (4.97) and assuming that the adiabatic exponent γ is a constant leads to the pressure equation,

$$\frac{C_v}{r} \left(\frac{\partial p}{\partial t} + \frac{\partial p u_\beta}{\partial x_\beta} \right) + p \frac{\partial u_\gamma}{\partial x_\gamma} + \frac{\partial q_\gamma}{\partial x_\gamma} + \Pi_{\beta\gamma}^{f^{neq},(2)} \frac{\partial u_\beta}{\partial x_\gamma} = \rho \dot{q} + \dot{m} \frac{u_\gamma^2}{2}. \quad (4.98)$$

with $C_v / r = 1 / (\gamma - 1)$. Then injecting Eqs. (4.47,4.98,4.85-4.87) into Eqs. (4.96) finally leads to

$$\begin{aligned} -\Pi_{\alpha\beta}^{f^{neq},(2)} &= \tau p \left[\frac{\partial u_\alpha}{\partial x_\beta} + \frac{\partial u_\beta}{\partial x_\alpha} - \delta_{\alpha\beta} \frac{2}{3} \frac{\partial u_\gamma}{\partial x_\gamma} \right] + \tau \left\{ \frac{\partial \Pi_{\alpha\beta}^{f^{neq},(2)}}{\partial t} + \frac{\partial \Pi_{\alpha\beta\gamma}^{f^{neq},(3)}}{\partial x_\gamma} \right\} \\ -\tau \left[u_\alpha \frac{\partial \Pi_{\beta\gamma}^{f^{neq},(2)}}{\partial x_\gamma} + u_\beta \frac{\partial \Pi_{\alpha\gamma}^{f^{neq},(2)}}{\partial x_\gamma} \right] &+ \tau \frac{r \delta_{\alpha\beta}}{C_v} \left[-\frac{\partial q_\gamma}{\partial x_\gamma} - \Pi_{\beta\gamma}^{f^{neq},(2)} \frac{\partial u_\beta}{\partial x_\gamma} \right] \end{aligned} \quad (4.99)$$

where we identify that $\tau p = \mu$. Here we end up with a slightly different evolution equation for the stress tensor when compared to the pressure-based and athermal cases. The higher order non-equilibrium moments are filtered out because $\Pi_{\alpha\beta\gamma}^{f^{neq},(3)}$ was reconstructed following the recursive regularized kernel Eq. (4.77). We use the previously defined nondimensionalization, Eqs. (4.50-4.52), with the additional constraint $Q_0 = U_0 \Pi_0$ obtained from Eq. (4.77). Also, for thermal models, c_s is not anymore related to the physical sound speed, therefore changing the definition of the Mach,

$$\text{Ma} = \frac{U_0}{\sqrt{\gamma r T_0}}, \quad (4.100)$$

4. Taylor expansion based description of the lattice-Boltzmann scheme – 4.6.
Comparison with other Taylor expansions

which can be used in the nondimensionalization,

$$\begin{aligned}
-\Pi_{\alpha\beta}^{*,f^{neq,(2)}} &= \Pi_{\alpha\beta}^{*,NS} + \frac{\gamma \text{Ma}^2}{\text{Re}} \frac{1}{\rho^* T^*} \left\{ \frac{\partial \Pi_{\alpha\beta\gamma}^{*,f^{neq,(3)}}}{\partial x_\gamma^*} - u_\alpha^* \frac{\partial \Pi_{\beta\gamma}^{*,f^{neq,(2)}}}{\partial x_\gamma^*} - u_\beta^* \frac{\partial \Pi_{\alpha\gamma}^{*,f^{neq,(2)}}}{\partial x_\gamma^*} \right\} \\
&+ \frac{\mu}{\rho_0 R T_0 t_s} \frac{1}{\rho^* T^*} \frac{\partial \Pi_{\alpha\beta}^{*,f^{neq,(2)}}}{\partial t^*} + \frac{\gamma}{\text{PrRe}} \frac{\delta_{\alpha\beta}}{\rho^* T^*} \left[\frac{\partial^2 T^*}{\partial x_\gamma^* \partial x_\gamma^*} \right] - \frac{\gamma \text{Ma}^2 (\gamma - 1)}{\text{Re}} \frac{\delta_{\alpha\beta}}{\rho^* T^*} \left[\Pi_{\beta\gamma}^{*,f^{neq,(2)}} \frac{\partial u_\beta^*}{\partial x_\gamma^*} \right],
\end{aligned} \tag{4.101}$$

where the Mach number Ma is defined as $\text{Ma} = U_0 / \sqrt{\gamma p / \rho}$. Assuming that convection is dominant, $t_s = L_0 / U_0$, Eq. (4.101) can be recast into

$$-\Pi_{\alpha\beta}^{*,f^{neq,(2)}} = \Pi_{\alpha\beta}^{*,NS} + \mathcal{O}\left(\frac{\text{Ma}^2}{\text{Re}}\right) + \mathcal{O}\left(\frac{1}{\text{RePr}}\right). \tag{4.102}$$

The second error term $\mathcal{O}\left(\frac{1}{\text{RePr}}\right)$ does not scale with the Kn number and is not predicted by the Chapman-Enskog expansion because it is purely stemming from the numerical coupling between the LB scheme and the finite difference scheme Eq. (4.90).

4.6. Comparison with other Taylor expansions

In this Chapter, we demonstrated that a parsimonious bridge between the LBM and the macroscopic equations was accessible. It relies on well known numerical tools. First, the LB scheme is studied in the continuous limit, showing that LB solves an extended Grad- q system, Eq. (4.15). Then, a nondimensional analysis is performed in order to measure the scaling of the inconsistent terms when compared to the NSF system. This fully deductive formalism only needs a single premise, that Δt is sufficiently small in order for the Taylor series to converge. Then, the consistency conditions in term of nondimensional numbers are *deduced*, showing that Kn is not the only parameter driving the consistency towards a NSF model.

4.6.1. Previous Taylor expansions for lattice-Boltzmann

While the Taylor series expansion was presented as a novelty here, other similar analysis have been performed in the literature. Here, we review all contributions the author is aware of.

- In [126], additionally to the Taylor expansion, a simplified Chapman-Enskog expansion [35, 36] is simultaneously performed.
- In [127–129], a diffusive scaling $x \rightarrow x/\text{Kn}$ and $t \rightarrow t/\text{Kn}^2$ is employed, where $\Delta t \propto \text{Kn}^2$, $\Delta x \propto \text{Kn}$, therefore restricting this analysis to low Mach and low Knudsen. Additionally, only the first order explicit discretization of the LBM is considered, contrarily to the widely used semi-implicit Crank-Nicolson [4, 35–37], employed in this manuscript.

4. Taylor expansion based description of the lattice-Boltzmann scheme – 4.6.
Comparison with other Taylor expansions

- In [130], following [131], the choice $\text{Kn} \propto \Delta t$ is made. Then, both Taylor and Chapman-Enskog expansions are performed with this unique parameter.
- In [92, 93, 95], cumulant LB is discussed. A Taylor expansion is performed with a diffusive scaling $\Delta t \propto \text{Kn}^2$, $\Delta x \propto \text{Kn}$, therefore reducing the validity to low Mach and low Knudsen.
- In [132] a diffusive scaling $\Delta t \propto \text{Kn}^2$, $\Delta x \propto \text{Kn}$ is used, therefore reducing the validity to low Mach and low Knudsen flows.
- In [133], a Taylor expansion with arbitrary scaling $\Delta x \propto \epsilon$, $\Delta t \propto \epsilon^m$, with $m \geq 1$ and ϵ a tiny scaling parameter is performed on a LB model for Burgers, Korteweg–de Vries, and Kuramoto–Sivashinsky equations.
- In [134–136], an acoustic scaling is employed, $\Delta t \propto \Delta x$. Additionally, the ratio between the timestep and the relaxation $\Delta t/\bar{\tau}$ – or $\Delta t/\tau$ when an explicit scheme is employed – is assumed constant.

It is worth mentioning that the diffusive scaling – used by most LB models – leads to $\Delta t \propto \Delta x^2$, which allows to get the relaxation time $\bar{\tau}$ as a free parameter. In exchange, we *voluntarily* ignore the Mach number similitude [4]. Therefore, in diffusive scaling, the Mach number is uncontrolled, but as long as it is sufficiently small, its value is not relevant for the considered incompressible flows. This trick allows to get $\bar{\tau}$ as a tunable free parameter for low Mach simulations. More specifically, for most LB models the relaxation time $\bar{\tau}$ reads

$$\bar{\tau} = \frac{\mu}{\rho c_s^2} + \frac{\Delta t}{2}. \quad (4.103)$$

The diffusive scaling can be written with a fixed parameter K as

$$\Delta t = K \Delta x^2. \quad (4.104)$$

Since the sound speed for standard lattices is $c_s = \Delta x/(\Delta t\sqrt{3})$ [4] (the general case being $c_s = \text{cste}\Delta x/\Delta t$) we can write

$$\frac{\bar{\tau}}{\Delta t} = \frac{3\mu K}{\rho} + \frac{1}{2}. \quad (4.105)$$

In other words, neglecting force term F_i and using a diffusive scaling and a BGK kernel, the collision is made *independent* of Δt ,

$$f_i^{col}(t, \mathbf{x}) = f_i^{eq}(t, \mathbf{x}) + \left(1 - \frac{1}{\frac{3\mu K}{\rho} + \frac{1}{2}}\right) \bar{f}_i^{neq}(t, \mathbf{x}). \quad (4.106)$$

Therefore, tuning K allows to arbitrarily choose $\bar{\tau}$ and keeps $(1 - \Delta t/\bar{\tau})$ independent of Δt , which is the assumption employed by many authors of Taylor expansion based descriptions of the LB scheme. However, the diffusive scaling has some drawbacks,

4. Taylor expansion based description of the lattice-Boltzmann scheme – 4.6.
Comparison with other Taylor expansions

because the sound speed becomes grid refinement sensitive,

$$c_s = \frac{1}{\sqrt{3}K \Delta x}, \quad (4.107)$$

such that both Mach and CFL are also grid dependent,

$$\text{Ma} = \sqrt{3}uK \Delta x, \quad (4.108)$$

$$\text{CFL} = uK \Delta x + \frac{1}{\sqrt{3}}. \quad (4.109)$$

However, as long as Ma is sufficiently small, its value is irrelevant. Of course, as the physical Mach number is increased, grid-dependent Ma is not anymore acceptable and diffusive scaling should be dropped and replaced by acoustic scaling, $\Delta x / \Delta t = \text{cste}$ which leads to a proper similitude relations for Ma and CFL when a grid refinement is performed, as it was implicitly demonstrated in this manuscript.

When both the acoustic scaling $\Delta x / \Delta t = \text{cste}$ and the $\Delta t / \bar{\tau} = \text{cste}$ hypothesis are used altogether [134–136], something interesting can be highlighted. Again, let us consider the classical LB scheme on standard lattice [4]. Then using $c_s = \Delta x / (\Delta t \sqrt{3})$ the offset relaxation time reads

$$\bar{\tau} = \frac{3\mu}{\rho \frac{\Delta x^2}{\Delta t^2}} + \frac{\Delta t}{2}. \quad (4.110)$$

Using the acoustic scaling $\Delta x / \Delta t = A = \text{cste}$, this implies

$$\frac{\bar{\tau}}{\Delta t} = \frac{3\mu}{\rho A \Delta x} + \frac{1}{2}. \quad (4.111)$$

Following premises $A = \text{cste}$ and $\Delta t / \bar{\tau} = \text{cste}$, this leads to $\mu / (\rho \Delta x) = B = \text{cste}$. The Reynolds number is therefore expressed as

$$\text{Re} = \frac{uL}{B \Delta x}. \quad (4.112)$$

Which is a grid dependent Reynolds number with non-grid dependent Mach,

$$\text{Ma} = \frac{\sqrt{3}u}{A}. \quad (4.113)$$

Alternatively, the Reynolds can be made non-grid dependent by using $\text{Ma} \propto \Delta x$, which sacrifices the similitude of the Mach number during a grid refinement. Therefore, the acoustic scaling $\Delta x / \Delta t = \text{cste}$ combined with hypothesis $\Delta t / \bar{\tau} = \text{cste}$ does not allow the similitude of all nondimensional numbers, one of them is necessarily grid dependent.

The grid-dependency observed in many Taylor expansions analysis arises from the fact that a *physical parameter* – τ , already present in Eq. (2.51) even before the space-

4. Taylor expansion based description of the lattice-Boltzmann scheme – 4.6.
Comparison with other Taylor expansions

time discretization – is assumed to be a function of a *numerical parameter*, Δt or Δx . Using notions discussed in Sec. 1.2, this formally reduces the rank n of the dimensional problem Eq. (1.27) to $n - 1$, effectively removing one of the $n - k$ nondimensional numbers available to describe the system. With hypothesis $\Delta t/\bar{\tau} = \text{cste}$, only $n - k - 1$ nondimensional parameters are available. To approximate the full compressible and viscous NSF system, a LB scheme and its theoretical description *must* consider τ – or equivalently $\bar{\tau}$ – and Δt as *independent* parameters in order to maintain similitude for all $n - k$ nondimensional numbers when a grid refinement is performed. Additionally, an acoustic scaling is necessary in order to properly tackle the Mach similitude.

4.6.2. Taylor expansion proposed by *Wissocq and Sagaut*, 2021

Very few months after the publication of our Taylor expansion analysis, another contribution was proposed by Wissocq *et al* [120]. As its author mentioned, our Taylor analysis could only be truncated for a vanishing Δt or a "sufficiently small" Δt , in the sense that Δt is completely negligible compared to all characteristic times of our model, including τ . Considering results presented in Sec. 3.1, it seems that the Crank-Nicolson scheme employed to derive the LB scheme – see Sec. 3.2 – roughly leads to accurate solutions as long as $\Delta t/\tau \leq 2$. However, as it was rightly mentioned in [120], many LB simulations are performed with extremely high values of $\Delta t/\tau$. Indeed $\tau \propto \mu$, so in order to mimic Euler solvers, high values of coefficient $\Delta t/\tau$ are necessary, leading to an over-relaxation with damped amplitude over time, see Sec. 3.1.

Rigorously, because the timestep Δt can be much larger than τ in real compressible applications, it is extremely important to understand that the convergence of the Taylor series expansion presented in this manuscript is not necessarily ensured. Therefore, truncation and numerical errors analysis with our Taylor expansion is questionable. However, our formalism is still able to predict the exact continuous limit $\Delta t \rightarrow 0$ – in other words, the consistency – which makes it a suitable tool to design new lattice Boltzmann models in a very parsimonious fashion because $\Delta t \rightarrow 0$ was our sole *ansatz*. In order to allow for numerical error analysis, [120] made different choices, let us compare these choices to our present formalism

- First, while we *a posteriori* nondimensionalized our equations and stressed that different timescales would lead to a different scaling of error terms, they chose to *a priori* nondimensionalize it from kinetic theory principles, using $L/(\Delta x/\Delta t)$ as the characteristic timescale, with L defined as a characteristic length of the flow also serving to nondimensionalize space. By doing so, note that only one nondimensional number Kn appears in the continuous equation,

$$\frac{\partial f_i}{\partial t^*} + c_{i\alpha}^* \frac{\partial f_i}{\partial x_\alpha^*} = -\frac{1}{\text{Kn}} (f_i - f_i^{eq}), \quad (4.114)$$

where $\text{Kn} = \tau \Delta x/(L \Delta t)$. To be as general as possible, a second nondimensional parameter – Strouhal Sh – should have been evidenced [83]. This additional

4. Taylor expansion based description of the lattice-Boltzmann scheme – 4.6.
Comparison with other Taylor expansions

number is known to be important for some low Knudsen viscous phenomena [7].

- Second, for some applications, $\Delta t/\tau$ is sometimes high. A classical Δt expansion as we performed in the present manuscript

$$f(t + \Delta t) = f(t) + \Delta t \frac{\partial f}{\partial t} + \mathcal{O}(\Delta t^2), \quad (4.115)$$

does not necessarily converges. It is therefore questionable to truncate it. Authors of [120] claimed to circumvent this problem with the following trick, which is to nondimensionalize as

$$f(t + \Delta t) = f\left(\frac{L}{\Delta x/\Delta t} \left[t^* + \text{Kn} \frac{\Delta t}{\tau} \right]\right), \quad (4.116)$$

$$= f(t^*) + \text{Kn} \frac{\Delta t}{\tau} \frac{\partial f}{\partial t^*} + \mathcal{O}\left(\text{Kn}^2 \frac{\Delta t^2}{\tau^2}\right). \quad (4.117)$$

Note that this is formally identical to Eq. (4.115), the expansion presented in this manuscript. It is only written in a different system of units. Now, instead of considering $\Delta t \rightarrow 0$, they considered a fixed coefficient $\Delta t/\tau = \text{cste}$ and assumed that $\text{Kn} \rightarrow 0$. Expansion Eq. (4.117) is *viewed* as a Kn expansion while our expansion is *viewed* as a Δt expansion. However, when it comes to actually truncating these expansions to analyze their leading errors, both Δt and Kn are fixed by the simulation. Which means that both expansions lead to the same results because Eqs. (4.115,4.117) are similar, see Sec. 1.2, they are only written in different units system. Therefore, for an actual application with fixed Δt and fixed Kn, both expansions converge – or not – identically.

- Third, using Eq. (4.114), it is possible to express f_i^{neq} as an infinite sum only involving f_i^{eq} by re-injecting successively Eq. (4.114) in itself,

$$f_i^{neq} = -\text{Kn} \left(\frac{\partial}{\partial t^*} + c_{i\alpha}^* \frac{\partial}{\partial x_\alpha^*} \right) f_i, \quad (4.118)$$

$$= -\text{Kn} \left(\frac{\partial}{\partial t^*} + c_{i\alpha}^* \frac{\partial}{\partial x_\alpha^*} \right) f_i^{eq} + \text{Kn}^2 \left(\frac{\partial}{\partial t^*} + c_{i\alpha}^* \frac{\partial}{\partial x_\alpha^*} \right)^2 f_i^{eq} + \mathcal{O}(\text{Kn}^3). \quad (4.119)$$

With this choice, time derivatives of every non equilibrium moments – e.g. $\partial \Pi_{\alpha\beta}^{neq,(2)} / \partial t$ – are expressed as a function of successive derivatives of f_i^{eq} , which effectively hides all numerical schemes encompassed in the LBM but the mass and momentum ones.

These assumptions do allow to try to understand more easily how numerical errors could alter the numerical solution. However, note that by doing so, Taylor expansions presented in [137] and [120] achieved different goals. Our Taylor expansion provides a consistency analysis, classical in numerical schemes analysis – see [14, 22, 23] – which corresponds to an "iso-Physics" expansion because physical nondimensional numbers are kept frozen with vanishing timestep $\Delta t \rightarrow 0$. Their Taylor expansion

4. Taylor expansion based description of the lattice-Boltzmann scheme – 4.7. Limits of the proposed Taylor expansion

presented an *hydrodynamic limit* study, which assumed a fixed ratio $\Delta t/\tau$, which corresponds to an expansion with "iso-discretization" of the relaxation and non-constant Physics because Knudsen $\text{Kn} \propto \text{Ma}/\text{Re} \rightarrow 0$.

Additionally, using Eq. (4.119) allows an easy interpretation because the stress-tensor numerical scheme evidenced by our formalism is now hidden. On the other hand, there *is* a stress-tensor scheme and the collision kernel is also a constitutive equation modeling, see Sec. 4.4. This modeling could be unphysical or the non-hydrodynamic modes hidden inside it could be unstable, in which case the study of numerical errors made in [120] could be unable to tackle it. A more rigorous way would be to study the numerical scheme and continuous limits of *all* equations involved in a LB solver, which is practically difficult. Therefore, while the assumptions employed by [120] allow an elegant expansion, we prefer to stick with our description of the LB scheme, simply because it is more deductive and closer to what is usually done in a numerical scheme analysis.

4.7. Limits of the proposed Taylor expansion

Now, we would like to finish this chapter by reminding the main contributions and drawbacks of our formalism.

Unlike any other expansions of the LB scheme we found in the literature, our contribution is able to deduce from the sole assumption $\Delta t \rightarrow 0$ the full equivalent set of moment equations solved by a LB scheme for arbitrary values of similar parameters Ma, Re, Kn, etc. To this day, every expansion we are aware of missed some terms or the similitude of either the Mach or Reynolds number, both crucial to compressible viscous flows.

This expansion is nothing but a very classical tool in the CFD literature and would not be considered as a novelty if applied to any other numerical scheme. However, the near monopoly of the kinetic interpretation of the LB scheme seems to have overshadowed its numerical straightforward interpretation.

Even if Δt is not necessarily smaller than all characteristic times, it is still useful to build our LB schemes with the continuous limit assumption $\Delta t \rightarrow 0$ in order to check that the target nondimensional numbers of a simulation does not lead to dominant consistency errors. Typically, from the Crank-Nicolson discretization presented in Sec. 3.1 we could roughly estimate that $\Delta t/\tau < 2$ is probably necessary for the convergence of our Taylor series. However, note that most compressible simulations are actually performed with $\Delta t/\tau \gg 2$ and still provide good results. This means that numerical errors could – at least sometimes – be neglected even for $\Delta t/\tau \gg 2$. This is puzzling and we do not have any rigorous argument to advocate for this assumption. However let us mention that this unexpected convergence of relaxation models discretized by Crank-Nicolson is known from the literature, see [107], where they used $\Delta t/\tau \approx 10^2$.

To illustrate that Crank-Nicolson convergence with highly under-resolved relaxation

4. Taylor expansion based description of the lattice-Boltzmann scheme – 4.7. Limits of the proposed Taylor expansion

is far from being a completely wrong *ansatz*, let us go back to a simpler toy model. We have seen from the previous Section that the relaxation only applies to non-equilibrium moments. Therefore, in a LB model, Eq. (4.59) discretized by a Crank-Nicolson scheme with a timestep $\Delta t/\tau \gg 1$ describes the under-resolved relaxation of the effective stress-tensor toward the target NSF stress-tensor.

To reproduce this situation, a very simple toy-model is also discretized by Crank-Nicolson,

$$\frac{d\phi}{dt} = -\frac{1}{\tau} \left[\phi - \sin\left(\frac{2\pi t}{\lambda^{eq}}\right) \right]. \quad (4.120)$$

It is very close to Sec. 3.1 except that now the relaxation target is a time dependent function $\sin\left(\frac{2\pi t}{\lambda^{eq}}\right)$. We previously mentioned that in LB simulations, Δt is generally too high compared to τ . However, note that other characteristic times of the flow are usually sufficiently large to be properly discretized by Δt . Which means that the sole characteristic time much shorter than Δt is τ , the relaxation time.

One could argue that t_μ the characteristic diffusive time is also related to relaxation via $\tau \propto \mu$. Indeed, $t_\mu \propto \mu^{-1}$, such that in a LB solver, low viscosity means slow viscous effects but fast relaxation. Two characteristic times τ and λ^{eq} can be found in Eq. (4.120). Here λ^{eq} is the characteristic time of the equilibrium and τ the characteristic time of relaxation, which means that τ/λ^{eq} could be interpreted as the Knudsen number of this model. When $\tau/\lambda^{eq} \ll 1$, the system is close to equilibrium and the relaxation is expected to be almost instantaneous, when $\tau/\lambda^{eq} \geq 1$, both equilibrium and relaxation acts on the same timescale and the solution is expected to depart from equilibrium.

In what follow, we chose a small $\Delta t/\lambda^{eq} = 0.025$ coefficient because we are only interested by the effects of under-resolved relaxation near equilibrium. To illustrate it, an extreme value $\Delta t/\tau = 10^6$ was chosen, corresponding to $\tau/\lambda^{eq} = 2.5 \times 10^{-8}$. The simulation is 40 iterations long, corresponding to $t_{end} = \lambda^{eq} = 40 \Delta t$. Analytical and numerical solutions can be found in Figure 4.1 for two different initial conditions.

Because the timestep Δt is much larger than the characteristic relaxation time, the red analytical solution is relaxed to $\phi^{eq} = \sin\left(\frac{2\pi t}{\lambda^{eq}}\right)$ long before the first timestep $t = \Delta t$. On the top plot the initial solution $\phi_0 = \phi(t = 0)$ is taken far away from the initial equilibrium solution $\phi_0^{eq} = \phi^{eq}(t = 0)$, then the solution keeps memory of this initial error throughout the complete simulation.

This error can be reduced simply by initializing the simulation to the initial equilibrium value $\phi_0 = \phi_0^{eq}$, as it can be seen on the bottom plot. Additionally, we checked for different timesteps (not shown), and spurious oscillations seem to be almost timestep invariant between $t = 0$ and $t = \lambda^{eq}$ as long as $\Delta t/\tau \gg 1000$. For lower values, a damping of spurious oscillations over time can be observed, we hypothesize that the damping is also present when $\Delta t/\tau = 10^6$ but that its characteristic time is too high to be observed. Figure 4.1 teaches us that for LB solvers, the non-equilibrium stress-tensor should be initialized as close as possible from the NSF target stress-tensor.

In Sec. 4.4.5, the σ parameter introduced by Jacob *et al* [119] was explained as an help for the relaxation process to reach its target equilibrium value. Now, we illustrate this behavior with our simple toy model. After each iteration, the solution ϕ^{CN} produced

4. Taylor expansion based description of the lattice-Boltzmann scheme – 4.7. Limits of the proposed Taylor expansion

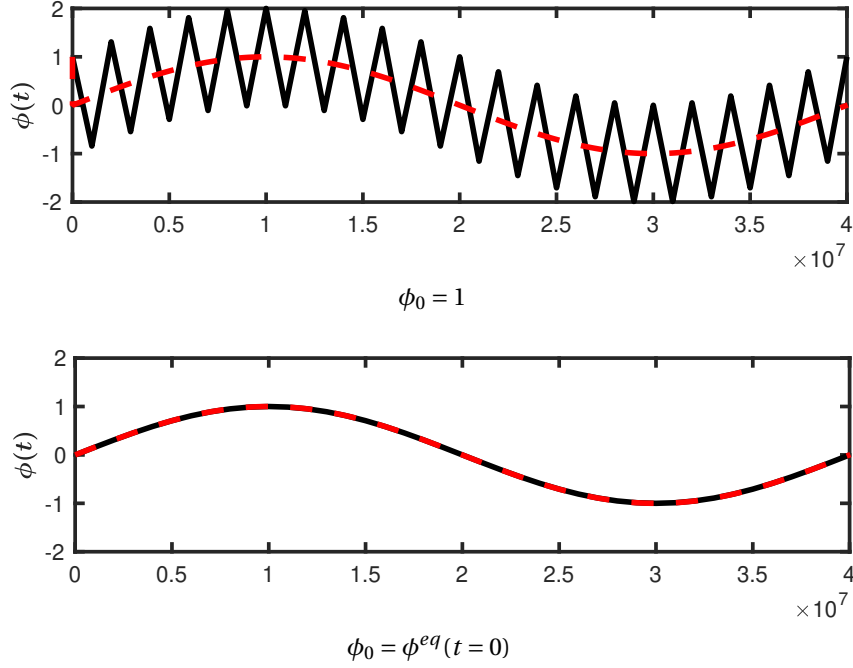


Figure 4.1. – Over-relaxation with $\Delta t/\tau = 10^6$ as a function of $\phi_0 = \phi(t=0)$. Analytical solution is $---$, Crank-Nicolson is $—$.

by the Crank-Nicolson scheme Eq. (3.14) is weighted with its equilibrium value,

$$\phi(t + \Delta t) = \sigma \phi^{CN}(t + \Delta t) + (1 - \sigma) \phi^{eq}(t + \Delta t). \quad (4.121)$$

When $\sigma = 1$, nothing new would happen, the updated solution $\phi(t + \Delta t)$ entirely comes from the Crank-Nicolson scheme, and results of Figure 4.1 are reproduced. However, when $\sigma < 1$, the solution is *guided* to equilibrium. Simulation with previous parameters and $\sigma = 0.9$ can be found on Figure 4.2.

We see that $\sigma < 1$ allows to damp the spurious oscillations due to the over-relaxation. By doing so, the scheme made of Eqs. (3.14,4.121) is not anymore consistent to Eq. (4.120). However, we know that except for the very beginning of the simulation, we should obtain $\phi = \phi^{eq}$, therefore, $\sigma < 1$ *helps* the Crank-Nicolson solution to remain closer to the expected relaxed solution. Therefore, we hypothesize that in a LB scheme, $\sigma < 1$ *helps* the non-equilibrium stress tensor to remain near its equilibrium NSF value. In other words, $\sigma < 1$ damps non-hydrodynamic modes [138, 139] and helps to filter numerical errors of under-resolved relaxation which are now seen as 2 sides of the same coin. From this toy model, it seems that with a Crank-Nicolson scheme, *sometimes*, the convergence of the Taylor expansion with $\Delta t/\tau \gg 1$ is valid, depending on the initial condition. More work should be done to understand the over-relaxation of the stress-tensor, but note that the fact that the LB community seems to be able to mimic so many different NSF solutions with LB is by itself and argument to support that over-relaxation leads to negligible errors or that another mechanism is responsible for the damping of spurious oscillations due to over-relaxation.

4. Taylor expansion based description of the lattice-Boltzmann scheme – 4.8. Recap

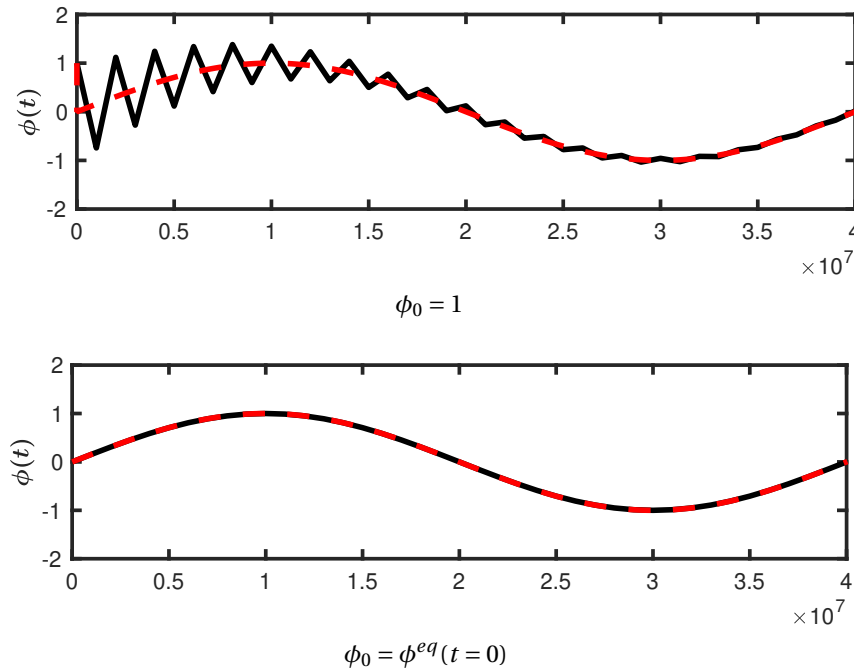


Figure 4.2. – Over-relaxation with $\Delta t/\tau = 10^6$ and $\sigma = 0.9$ as a function of $\phi_0 = \phi(t=0)$. Analytical solution is $-\cdot-\cdot-$, Crank-Nicolson is $—$.

4.8. Recap

In this Chapter, we presented a deductive description of LB schemes. The Taylor expansion of the LB scheme is presented and shows how to go back from the discretized LB scheme to the continuous DVBE. This is particularly useful because most of the improvements of the LB scheme are done on the numerical scheme itself, therefore, the link with the continuous model is not as trivial as usually presented.

Our formalism is generalized to collision kernels in which some information is filtered, such as regularized kernels. We formally show that regularized kernels are $\mathcal{O}(\Delta t)$ accurate, this is an example of non trivial effect of a LB discrete model.

Then we apply our Taylor series expansion to the classical athermal LB model, we show that the consistency condition is indeed more complicated than the low Knudsen assumption of the classical LB framework.

We interpret different collision kernels based on the continuous limit of the LB scheme. The collision kernel is seen to correspond to an implicit choice of unusual mechanical constitutive model. The BGK, regularized, recursive regularized, hybrid recursive regularized along with a new collision kernel known as "traceless" regularization are discussed in light of the new formalism. The recursive regularized kernel is seen to lead to a Galilean invariant continuous model extremely close to other constitutive equations that can be found in the literature of constitutive equations with lag effects.

The newly proposed formalism is then applied to the classical thermal ρ -based

4. Taylor expansion based description of the lattice-Boltzmann scheme – 4.8. Recap

LB model. We show that the low Knudsen assumption is not sufficient to ensure consistency towards NSF. Indeed, Mach, Reynolds and Prandtl are identified to drive different terms in the consistency error of this model.

Our Taylor expansion is also compared to other Taylor series for LBM. We show that other works are indeed restricted to the diffusive scaling – $\Delta t \propto \Delta x^2$ – and/or lead to grid dependent Reynolds or Mach. However, a viscous compressible flow needs similitude of both Mach and Reynolds.

In the last part of this Chapter, we discuss our sole assumption, that Δt is sufficiently small for our series to be safely truncated and we show how the Crank-Nicolson is able to produce accurate solution even for extremely low relaxation times when compared to the timestep Δt .

5. Thermal coupling with finite difference

Sommaire

5.1	Is the entropy equation viable for compressible flows ?	97
5.1.1	Shocks with non-conservative entropy equation	98
5.1.2	Contact surfaces with non-conservative entropy equation	100
5.2	Discretization of the entropy equation	100
5.2.1	Passive scalar advection	100
5.2.2	Finite difference schemes	106
5.2.3	MUSCL-Hancock method	107
5.3	Recap	108

The mass and momentum conservations are solved by the lattice-Boltzmann algorithm. Simultaneously, an additional thermodynamic variable should also be solved in order to approximate Navier-Stokes-Fourier system. On small lattices, this additional variable, the total energy, could not be solved along mass/moment by the lattice-Boltzmann scheme. This is due to the inaccuracy of 3^{rd} and 4^{th} order moments coming from the defect of isotropy Eq. (3.56). Here, different strategies could be employed. We could increase the size of the lattice in order to get back the accurate energy flux. To maintain the stencil as small as possible and avoid a too large amount of fields, we solve the additional thermodynamic variable with a different algorithm. It can be either the Double-Distribution-Function, where a second set of lattice population is used to recover energy conservation, or a more simple finite difference scheme. Here, out of simplicity, we chose the second option.

The usual choice in CFD is to discretize the total energy equation [6, 24] in conservative form. However, from trial and errors, we find that the total energy equation, when coupled to the lattice-Boltzmann mass and momentum conservation, leads to particularly unstable results for a wide range of classical finite difference schemes. We believe it to be due to the interactions of lattice-Boltzmann and finite difference numerical errors. Indeed, remember that 2 independently stable schemes are not necessarily stable once coupled. More specifically, the numerical instabilities we observed are linear instabilities, they are triggered by any supersonic mean flow with superimposed fluctuations.

Nevertheless, an attempt to find a solution was proposed by Zhao *et al* [140], where a

5. Thermal coupling with finite difference – 5.1. Is the entropy equation viable for compressible flows ?

new numerical scheme allows to bring more from the lattice-Boltzmann part into the total energy scheme. However, it is shown in Appendix B that those scheme introduce numerical viscosity.

Regarding what was actually used in this manuscript, in Sec. 5.1, we identify that entropy equation in non-conservative form is a viable candidate to replace total energy in conservative form because,

- Entropy is an eigenmode of the linearized Euler system [141, 142]. In other words for linear flows, the entropy equation in the Euler limit is uncoupled from the LB scheme, which leads to an overall algorithm where numerical errors of the LB and entropy scheme are only weakly coupled.
- For moderately supersonic flows, contact and shock discontinuities are still accurately captured by the entropy equation.

In Sec. 5.2, we mention and justify our different choices in the discretization of the entropy equation.

5.1. Is the entropy equation viable for compressible flows ?

Up to now we have been unable to find a sufficiently robust and accurate numerical scheme for the conservative total energy equation. Hence, we need to resort on other thermodynamic variables than total energy. When the flow is smooth – without any discontinuities – the chain rule can be used to replace Eq. (1.22) by combinations of Eqs. (1.20-1.26). However, not all variables have to be smooth, for example, $\partial \rho u_\beta / \partial x_\beta$ is still properly defined when ρ and u_β both exhibit discontinuities such that ρu_β remains smooth. In this case, the chain rule $\partial \rho u_\beta / \partial x_\beta = \rho \partial u_\beta / \partial x_\beta + u_\beta \partial \rho / \partial x_\beta$ should not be used. Unfortunately, the chain rule is used for any non trivial combinations of Eqs. (1.20-1.26). Therefore, while for smooth flows many combinations of these equations can be performed without affecting the solution, *weak solutions* [102] – i.e. with discontinuities – will be affected. To the best of our knowledge, the Navier-Stokes-Fourier system Eqs. (1.20-1.26) with the total energy equation in conservative form is the unique system whose weak solutions are physical.

Nevertheless, let us check a very specific combination. The Lattice-Boltzmann scheme provide a single algorithm for both mass and momentum Eqs. (1.20,1.21), let us then try to replace the total energy Eq. (1.22). Ordinary replacements are

$$\frac{\partial \rho e}{\partial t} + \frac{\partial \rho e u_\beta}{\partial x_\beta} + p \frac{\partial u_\gamma}{\partial x_\gamma} + \frac{\partial q_\gamma}{\partial x_\gamma} - \Pi_{\alpha\beta}^{neq} \frac{\partial u_\beta}{\partial x_\alpha} = \rho \dot{q} + \dot{m} \frac{u_\gamma^2}{2}, \quad (5.1)$$

$$\rho T \left(\frac{\partial s}{\partial t} + u_\beta \frac{\partial s}{\partial x_\beta} \right) + \frac{\partial q_\gamma}{\partial x_\gamma} - \Pi_{\alpha\beta}^{neq} \frac{\partial u_\beta}{\partial x_\alpha} = \rho \dot{q} + \dot{m} \left(\frac{u_\gamma^2}{2} - e - \frac{p}{\rho} \right). \quad (5.2)$$

In the case of a weak solution, Eqs. (5.1-5.2) are expected to produce unphysical jumps across discontinuities. Let us try to quantify the error introduced by the use of the

5. Thermal coupling with finite difference – 5.1. Is the entropy equation viable for compressible flows ?

entropy Eq. (5.2) instead of the total energy Eq. (1.22). Across a shock in a perfect gas Eq. (1.13), the Rankine-Hugoniot jump conditions [6, 39, 44] can be obtained from Eqs. (1.20-1.26) by assuming vanishing μ and κ . Let us now discuss about the entropy jumps across shocks and contact surfaces.

5.1.1. Shocks with non-conservative entropy equation

- For weak shocks, the Mach number is extremely close to 1, we assume $Ma = 1 + \epsilon$ with $\epsilon \ll 1$, which leads [5] to jump conditions between upstream and downstream states 1 and 2 written as

$$\frac{s_2 - s_1}{C_p} = \mathcal{O}(\epsilon^3), \quad (5.3)$$

$$\frac{p_2 - p_1}{p_1} = \mathcal{O}(\epsilon), \quad (5.4)$$

$$\frac{\rho_2 - \rho_1}{\rho_1} = \mathcal{O}(\epsilon), \quad (5.5)$$

$$\frac{u_2 - u_1}{u_1} = \mathcal{O}(\epsilon). \quad (5.6)$$

Which means that the entropy discontinuity, compared to other variables, is extremely small for weak shocks.

- Non conservative entropy Eq. (5.2) under the Euler assumption and written in the reference frame of the shock reduces to

$$u_\beta \frac{\partial s}{\partial x_\beta} = 0, \quad (5.7)$$

which only admits solutions $s = \text{cste}$ or $u_\beta = 0$. Note that the initial (Rankine-Hugoniot) solution does not satisfies any of those solutions. Therefore, the Rankine-Hugoniot solution is not a steady solution of the entropy equation, and the weak entropy jump will dissociates from the initial discontinuity and will be advected away by the flow. Because the entropy jump is extremely small, the remnants discontinuity near the initial Rankine-Hugoniot jump looks very close to a weak shock solution of the total energy equation, except that it is not exactly stationary and that it is an isentropic discontinuity.

This explains how weak shock-like isentropic discontinuities could happen when using the entropy equation with sufficiently low supersonic Mach. Indeed, those "isentropic weak shocks" are numerically observed in simulations when using the entropy equation. In order to see if the isentropic assumption could be considered valid at least for some specific Mach and γ , let us determine how the entropy jump behaves as a function of those parameters. The Rankine-Hugoniot jump solution for

5. Thermal coupling with finite difference – 5.1. Is the entropy equation viable for compressible flows ?

entropy [6, 39, 44] is

$$f(\gamma, \text{Ma}) = e^{\frac{s_2 - s_1}{r}} = \left[1 + \frac{2\gamma}{\gamma + 1} (\text{Ma}^2 - 1) \right]^{\frac{1}{\gamma - 1}} \left[\frac{(\gamma + 1)\text{Ma}^2}{(\gamma - 1)\text{Ma}^2 + 2} \right]^{\frac{-\gamma}{\gamma - 1}}, \quad (5.8)$$

where Ma is the Mach number of a stationary shock. We use $f(\gamma, \text{Ma})$ because $\frac{s_2 - s_1}{r}$ is defined up to an arbitrary reference constant, hence, to define a % error, we needed a different function. Because the entropy is typically involved throughout $p = e^{s/C_v} \rho^\gamma$, exponential function seemed well indicated. Isentropic discontinuities means that $s_1 = s_2$ such that

$$f_{s_1 = s_2}(\gamma, \text{Ma}) = 1. \quad (5.9)$$

On Figure 5.1 is reported ε_s the percent error between the Rankine-Hugoniot solution Eq. (5.8) and the isentropic solution Eq. (5.9). This error is defined by

$$\varepsilon_s = 100 \frac{f(\gamma, \text{Ma}) - f_{s_1 = s_2}}{f(\gamma, \text{Ma})}. \quad (5.10)$$

Figure 5.1 shows that for a reasonable range of adiabatic exponents the error introduced by the isentropic approximation on a shock remains below an acceptable margin of 5% as long as $\text{Ma} < 1.4$, showing that the entropy Eq. (5.2) could potentially lead to an acceptable accuracy for low supersonic flows. However, for higher values of Ma, the error rapidly increases to unacceptable values, around 25% at $\text{Ma} = 2$.

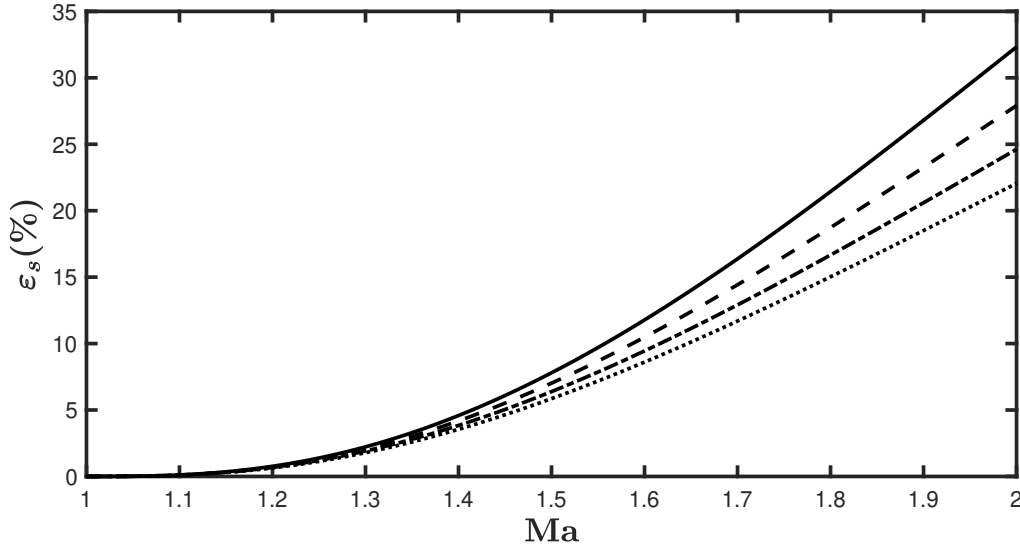


Figure 5.1. – Percent error ε_s between Rankine-Hugoniot and adiabatic functions $e^{\frac{s_2 - s_1}{r}}$ between supersonic state 1 and subsonic state 2 as a function of the Ma number. $\gamma = 1.2$ is —; $\gamma = 1.4$ is - - -; $\gamma = 1.6$ is - · - · and $\gamma = 1.8$ is ····.

5.1.2. Contact surfaces with non-conservative entropy equation

When crossing a contact surface from state 1 to state 2, both normal velocity and pressure are constant, such that mass, momentum and total energy conservation written in the frame reference of the discontinuity ($u_1 = u_2 = 0$) respectively lead to $0 = 0$, $p_1 = p_2$ and $0 = 0$. Similarly, non conservative entropy Eq. (5.2) under the Euler assumptions and written in the reference frame of the contact surface also reduces to $0 = 0$. Therefore, contact surfaces are solutions of both the conservative total energy and non-conservative entropy equations.

5.2. Discretization of the entropy equation

The total energy Eq. (1.22) is the only one providing accurate weak solutions [102]. However, for sufficiently low compressible flows such as $Ma < 1.4$, the entropy equation seems to be an acceptable candidate to replace the total energy equation. This discussion was merely a rationalization and should not be considered as a rigorous demonstration. Its conclusion will be empirically validated by compressible simulations in Chapters 6-7. Of course, here, we only discussed about the vanishing viscosity μ and heat conductivity λ case. For smooth fully resolved solutions, both entropy and total energy equation would lead to identical solutions.

In order to discretize accurately Eq. (5.2), we need to discretize its most important term, the convective one, $u_\beta \partial s / \partial x_\beta$.

5.2.1. Passive scalar advection

In order to properly discretize the convective part of the entropy equation, let us first take a look at a very simple toy-model, the passive scalar ϕ advection by constant velocity a ,

$$\frac{\partial \phi}{\partial t} + a \frac{\partial \phi}{\partial x} = 0, \quad (5.11)$$

whose analytical solution $\phi(t, x)$ is nothing but the initial solution $\phi_0(x)$ shifted by velocity a ,

$$\phi_0(x) = \phi(t = 0, x), \quad \phi(t, x) = \phi_0(x - at). \quad (5.12)$$

Assuming a positive (resp. negative) velocity a means that information travels only from $x = -\infty$ (resp. $x = +\infty$) to $x = +\infty$ (resp. $x = -\infty$). This serves as a guideline to find suitable numerical schemes. No matter the sign of a , more points should be used from the upwind direction because no information comes from the downwind direction, indicating that decentered schemes in the upwind direction should be used

5. Thermal coupling with finite difference – 5.2. Discretization of the entropy equation

in order to discretize Eq. (5.11). For $a > 0$, the easiest choice is

$$\frac{\phi(t + \Delta t) - \phi(t)}{\Delta t} = \frac{\partial \phi}{\partial t} + \mathcal{O}(\Delta t), \quad (5.13)$$

$$\frac{\phi(t, x) - \phi(t, x - \Delta x)}{\Delta x} = \frac{\partial \phi}{\partial x} + \mathcal{O}(\Delta x), \quad (5.14)$$

which is only first order accurate in both space $\mathcal{O}(\Delta x)$ and time $\mathcal{O}(\Delta t)$. Now, let us see what is the effect of these low order errors. Using schemes Eqs. (5.13-5.14) the discretized counterpart of Eq. (5.11) is

$$\phi(t + \Delta t, x) = \phi(t, x) - \frac{a \Delta t}{\Delta x} [\phi(t, x) - \phi(t, x - \Delta x)]. \quad (5.15)$$

Injecting Taylor-series in Eq. (5.15) allows to obtain a *modified equation* [14, 24, 143, 144],

$$\frac{\partial \phi}{\partial t} + a \frac{\partial \phi}{\partial x} = -\frac{1}{2} \left[\Delta t \frac{\partial^2 \phi}{\partial t^2} + a \Delta x \frac{\partial^2 \phi}{\partial x^2} \right] + \mathcal{O}(\Delta t^2, \Delta x^2). \quad (5.16)$$

On the left side we recognize Eq. (5.11), our target equation, on the right side we see here truncation errors $\mathcal{O}(\cdot)$ introduced by discretization, in which we recognize a spurious diffusion term $\frac{\partial^2 \phi}{\partial x^2}$. This means that numerical scheme Eq. (5.15) is expected to create additional unintended diffusion. Additionally, a second order time derivative $\frac{\partial^2 \phi}{\partial t^2}$ was also introduced through numerical errors, in order to interpret it let us notice that we are allowed to rewrite Eq. (5.16) as

$$\frac{\partial \phi}{\partial t} + a \frac{\partial \phi}{\partial x} = \mathcal{O}(\Delta t, \Delta x). \quad (5.17)$$

Taking its first order time or space derivative respectively leads to

$$\frac{\partial^2 \phi}{\partial t^2} + a \frac{\partial^2 \phi}{\partial x \partial t} = \mathcal{O}(\Delta t, \Delta x). \quad (5.18)$$

$$\frac{\partial^2 \phi}{\partial t \partial x} + a \frac{\partial^2 \phi}{\partial x^2} = \mathcal{O}(\Delta t, \Delta x), \quad (5.19)$$

then injecting Eq. (5.19) into Eq. (5.18),

$$\frac{\partial^2 \phi}{\partial t^2} = a^2 \frac{\partial^2 \phi}{\partial x^2} + \mathcal{O}(\Delta t, \Delta x), \quad (5.20)$$

which can be reused in Eq. (5.16) to obtain an interpretable modified equation

$$\frac{\partial \phi}{\partial t} + a \frac{\partial \phi}{\partial x} = \frac{a \Delta x}{2} (1 - \text{CFL}) \frac{\partial^2 \phi}{\partial x^2} + \mathcal{O}(\Delta t^2, \Delta x^2), \quad (5.21)$$

which is an advection-diffusion equation, whose diffusion coefficient is $\frac{a \Delta x}{2} (1 - \text{CFL})$,

5. Thermal coupling with finite difference – 5.2. Discretization of the entropy equation

where the CFL is

$$\text{CFL} = \frac{a\Delta t}{\Delta x}. \quad (5.22)$$

This spurious diffusion coefficient vanishes for a fixed CFL when $\Delta x \rightarrow 0$ or for a fixed gridsize Δx when $\text{CFL} \rightarrow 1$. Because the analytical solution Eq. (5.12) is a frozen pattern moving with velocity a , the spurious diffusion term stemming from the scheme Eq. (5.15) will introduce an additional damping of the solution. For a negative advection velocity a , Eq. (5.15) even leads to a negative diffusion coefficient : gradients are sharpened over time, in other words, this numerical solution is unstable for $a < 0$. Because transport is often the most important phenomenon in compressible flows, extreme care should be taken when choosing an advection numerical scheme. In order to further illustrate that stable and accurate numerical transport is not easily satisfied, Eq. (5.11) is discretized by different numerical schemes and results are presented for a wide range of numerical parameters.

The numerical setup is as follows. First, the periodic domain is of length N , the gridsize is taken as $\Delta x = 1$. Using Eq. (5.22) the advection velocity $a = 1$ along with the tunable CFL is used to define the timestep,

$$\Delta t = \frac{\text{CFL}\Delta x}{a}. \quad (5.23)$$

The initial solution is defined as follows,

$$\phi_0(x) = e^{-\frac{200(x - N/4)^2}{N^2}} + \frac{\tanh\left[\left(x + \frac{N}{12} - \frac{3N}{4}\right) * 10^5\right] - \tanh\left[\left(x - \frac{N}{12} - \frac{3N}{4}\right) * 10^5\right]}{2}, \quad (5.24)$$

which corresponds to a Gaussian profile centered around $N/4$ and a crenel function of half-width $N/12$ centered around $3N/4$, both with amplitude 1, superimposed on a constant value 0. Then, this initial solution is advected for 10 periods in the numerical domain, corresponding to a distance $10N$ for a total of $10N/\text{CFL}$ iterations. Last time step solutions are then plotted. It is expected that the red numerical solutions perfectly matches the black analytical one, as suggested by Eq. (5.12), which just means that the initial solution is advected as a frozen pattern. And after 10 periods the solution exactly went back to its initial position. However, defects between analytical and numerical solutions appears due to truncation errors $\mathcal{O}(\cdot)$. An absence of red numerical solution means that the corresponding numerical scheme returned an unstable solution. Results are presented for a set of 12 different numerical schemes,

- RK1, 30% upwind + 70% centered [145]
- Beam & Warming [14, 24]
- Lax Wendroff [14, 24]
- Fromm [14, 24]
- RK1, MUSCL [146]
- RK2, MUSCL [146]

5. Thermal coupling with finite difference – 5.2. Discretization of the entropy equation

- RK4, centered [82]
- MUSCL Hancock [24]

These algorithms were chosen because they are either traditional in finite difference lectures or because they were used in the Lattice-Boltzmann literature. Chosen numerical parameters are,

- CFL = 0.5, $N = 200$
- CFL = 0.5, $N = 100$
- CFL = 0.9, $N = 200$

A careful examination of figures 5.2 shows that very little of these numerical schemes were able to simultaneously provide accurate on coarse grid ($N = 100$), high CFL (CFL = 0.9). Among these 8 schemes, the MUSCL Hancock method is selected as being the best candidate to provide accurate and stable results on a wide range of numerical parameters while only having a 5 points stencil, which makes it numerically efficient as it only needs to gather datas from points $i - 2$ to $i + 2$ in order to update point i from t to $t + \Delta t$. Lastly, let us quickly discuss about the units in this test case. The problem could have been summarized by a series of parameters,

- Characteristic length of a perturbation x_0 , $[x_0] = m$.
- Characteristic distance of advection L_0 , $[L_0] = m$.
- Velocity advection a , $[a] = m.s^{-1}$.
- Characteristic time of advection t_0 , $[t_0] = s$. However, note that given the velocity a and distance L_0 , $t_0 \propto L_0/a$. This parameter is therefore redundant.
- The space step Δx , $[\Delta x] = m$.
- The time step Δt , $[\Delta t] = s$.
- ϵ , the characteristic amplitude of our perturbation. However, note that the problem we are trying to solve – both continuous and numerical – is linear, therefore, the solution ϕ can be arbitrarily rescaled by any constant. Therefore, ϵ is not a relevant parameter.

Finally, only x_0 , L_0 , a , Δx and Δt are dimensional meaningful parameters. Following Sec. 1.2, 5 – 2 nondimensional numbers could be formed, and the system is better described by a simplified expression,

$$g\left(\frac{x_0}{L_0}, \frac{\Delta x}{x_0}, \text{CFL}\right) = 0. \quad (5.25)$$

Here let us explain a bit further the meaning of these ratios,

- x_0/L_0 corresponds to the ratio between the length of the fluctuation and the distance on which it is advected. x_0 being fixed by the initial condition, another way to describe this ratio is to say that it is equivalent to fixing the number of periods of advection in the periodic box, arbitrarily chosen as 10 in our calculation.
- $\Delta x/x_0$ is related to the amount of discrete points per wavelengths of the perturbation. This adimensional number drives the spatial resolution.

5. Thermal coupling with finite difference – 5.2. Discretization of the entropy equation

- CFL is related to the amount of discrete points per characteristic time $\Delta x/a$. This adimensional number drives the temporal resolution.

This shows that while it would have been tempting to describe this problem by x_0 , L_0 , a , Δx and Δt , it would have led to an unnecessary complicated description while x_0/L_0 , $\Delta x/x_0$ and CFL is the minimal amount of parameters to fully describe the solution. Note that in our simulation we used as parameters i) the number of advection periods that we fixed at 10 ii) the total number of points N iii) the CFL. Therefore, we effectively used this the nondimensional system of units, which is why the advection velocity a was arbitrarily fixed, its value is simply meaningless. Changing it to any arbitrary value while keeping x_0/L_0 , $\Delta x/x_0$ and CFL fixed would *exactly* lead to the same similar solution up to machine precision.

To conclude this part about the advection model Eq. (5.11), let us just keep in mind that the choice of numerical advection scheme is crucial. Thanks to this discussion, we identified the MUSCL-Hancock scheme as a viable candidate to discretize the convective part of the entropy equation.

5. Thermal coupling with finite difference – 5.2. Discretization of the entropy equation

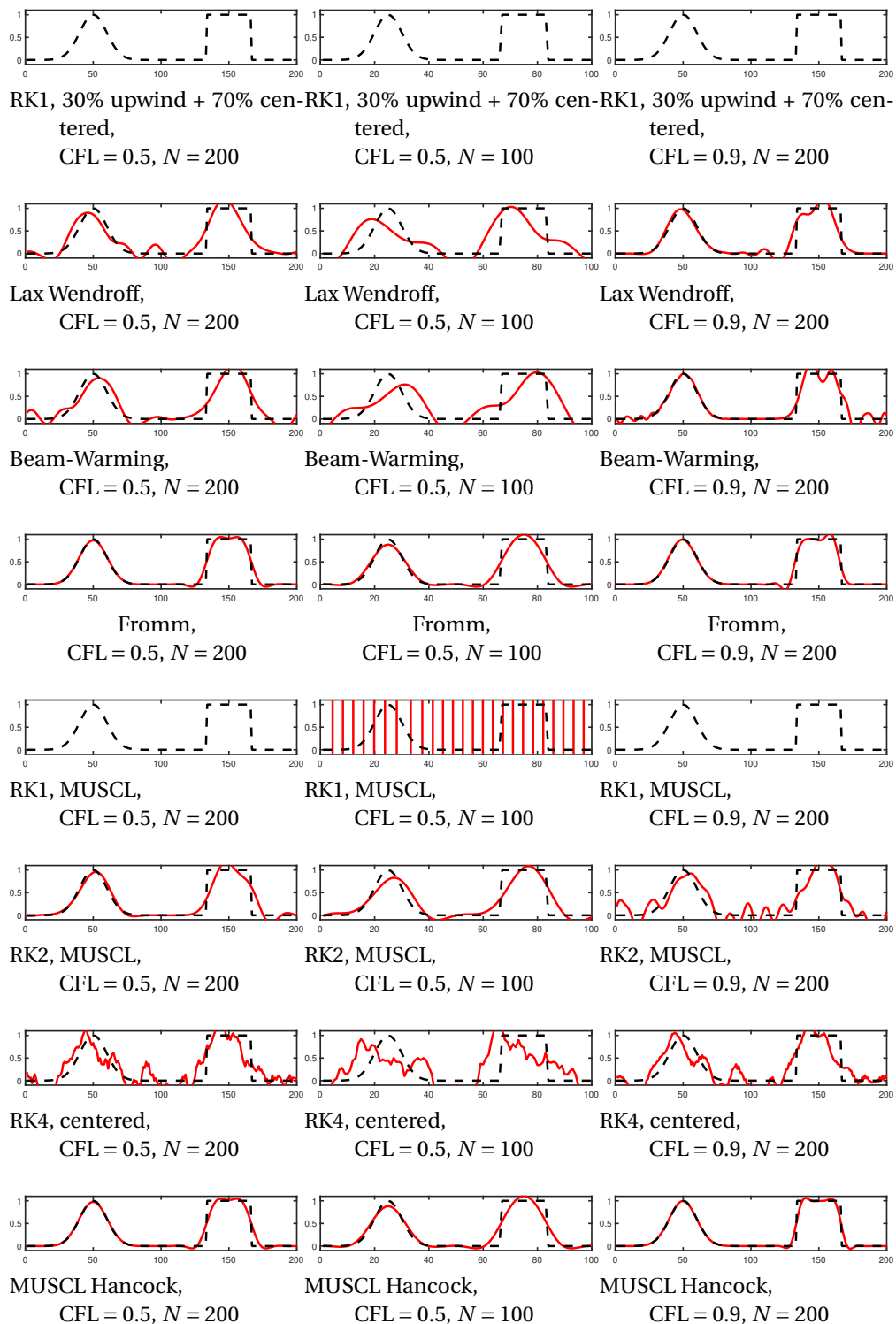


Figure 5.2. – Advection over 10 flow-through-time periods of a passive scalar for different schemes, CFL and grid resolutions

5.2.2. Finite difference schemes

For the sake of clarity, the entropy equation is now written as,

$$\rho T \left(\frac{\partial s}{\partial t} + u_\beta \frac{\partial s}{\partial x_\beta} \right) + \frac{\partial q_\gamma}{\partial x_\gamma} - \Pi_{\gamma\beta}^{neq} \frac{\partial u_\beta}{\partial x_\gamma} = \mathcal{Q}. \quad (5.26)$$

Where $\mathcal{Q} = \rho \dot{q} + \dot{m}(u_\gamma^2/l - e - p/\rho)$. Only keeping the first 2 terms corresponds to the passive scalar advection of variable s by velocity u_β . In order to keep the overall entropy scheme explicit, sufficiently accurate and easily implementable in the code, it was chosen to use a mix of low order and high order numerical schemes. Out of clarity, we only discretize the equation in 1D. In our code, to update the solution from time n to $n+1$, the entropy located in cell i gathers datas from neighboring cells according to

$$\frac{s_i^{n+1} - s_i^n}{\Delta t} + u_i^n \frac{s_{i+\frac{1}{2}}^{MH} - s_{i-\frac{1}{2}}^{MH}}{\Delta x} = \mathcal{S}_i^n + \mathcal{Q}_i^n, \quad (5.27)$$

$$\mathcal{S}_i^n = \lambda \frac{T_{i+1}^n - 2T_i^n + T_{i-1}^n}{\Delta x^2} + \left(\frac{\lambda_{i+1}^n - \lambda_{i-1}^n}{2\Delta x} \right) \left(\frac{T_{i+1}^n - T_{i-1}^n}{2\Delta x} \right) + \mu \frac{4}{3} \left(\frac{u_{i+1}^n - u_{i-1}^n}{2\Delta x} \right)^2, \quad (5.28)$$

$$\mathcal{Q}_i^n = \rho_i^n \dot{q}_i^n + \dot{m}_i^n \left(\frac{u_i^n u_i^n}{2} - e_i^n - \frac{p_i^n}{\rho_i^n} \right), \quad (5.29)$$

where $s_{i+\frac{1}{2}}^{MH}$ is the interpolated value on face $i + \frac{1}{2}$ by MUSCL Hancock method. The heat diffusion and viscous heat are encompassed in \mathcal{S}_i^n , whose discretization was chosen out of trial and error tests. The last term, \mathcal{Q}_i^n , is the local source term. Let us note that this overall scheme is rigorously only first order accurate :

- First, the source term \mathcal{Q}_i^n was discretized using an explicit $\mathcal{O}(\Delta t)$ accurate scheme. This low order scheme is justified by the fact that \mathcal{Q}_i^n often corresponds to sponge zones, which is not a sufficiently stiff term to require extra computational time.
- The heat diffusion was discretized using a $\mathcal{O}(\Delta x^2)$ scheme. This term was not identified as a key term for stability or accuracy, therefore, we stick with this simple scheme.
- The first order gradients in \mathcal{S}_i^n were discretized by centered $\mathcal{O}(\Delta x^2)$ accurate schemes in order to keep their numerical errors non-directional.
- The advection of entropy was discretized by a MUSCL Hancock scheme. Because we used u_i^n instead of $u_i^{n+1/2}$ [24], this scheme achieves an $\mathcal{O}(\Delta t^3, \Delta x^3)$ accuracy only for constant velocity flows. This is due to the difficulty in getting $u_i^{n+1/2}$ in our code. However, note that using $u_i^{n+1/2} = 0.5(u_i^n + u_i^{n+1}) + \mathcal{O}(\Delta t^2)$ and completely changing the structure of our code, it would have been possible to compute $u_i^{n+1/2}$ out of u_i^n and u_i^{n+1} , which does not changes anything in the linear regime but would restore the $\mathcal{O}(\Delta t^3, \Delta x^3)$ accuracy for non-linear flows.
- A dimensional splitting [14, 24] would be rigorously necessary for the extension

5. Thermal coupling with finite difference – 5.2. Discretization of the entropy equation

to 2D/3D. This has not been done and creates a $\mathcal{O}(\Delta t)$ error for regions with streamlines misaligned with either the x , y or z axis.

While more accurate schemes could have been used, our code is mainly destined for industrial applications. Therefore, a trade-off arises between accuracy and efficiency. Given the structure of the code and the targeted applications, the proposed scheme has been identified as a decent compromise between stability, accuracy and low computational cost.

Note that due to human inertia, the code being rather complicated and based on previous works [74, 123], it was chosen to carry on the previous choice to discretize the stress tensor $\mathcal{T}_{\alpha\beta}$ using finite differences, while its numerical approximation was already available from $\Pi_{\alpha\beta}^{neq,(2)}$. While it is merely a guess, using a fully consistent stress tensor between the entropy equation and the momentum conservation could have led to a more natural coupling, which could have brought an extra stability. In what follows, complete details of the MUSCL Hancock method are provided.

5.2.3. MUSCL-Hancock method

Convective part of the entropy equation is discretized as follows

$$\frac{s_i^{n+1} - s_i^n}{\Delta t} + u_i^n \frac{s_{i+\frac{1}{2}}^{MH} - s_{i-\frac{1}{2}}^{MH}}{\Delta x} = 0. \quad (5.30)$$

Where $s_{i+\frac{1}{2}}^{MH}$ and $s_{i-\frac{1}{2}}^{MH}$ are computed using the following steps :

- i) Extrapolated intercell values are evaluated at the left and right sides of the i th cell as

$$s_{i,L} = s_i - \frac{1}{2} \Delta_i, \quad s_{i,R} = s_i + \frac{1}{2} \Delta_i, \quad (5.31)$$

with Δ_i a high order approximation of the slope,

$$\Delta_i = \frac{1}{2} [(1 + \eta)(s_i - s_{i-1}) + (1 - \eta)(s_{i+1} - s_i)], \quad (5.32)$$

and $\eta = \frac{1}{3} [\frac{2\Delta t u_i^n}{\Delta x} - \text{sign}(u_i^n)]$ as suggested in [24].

- ii) Evolving of extrapolated boundary values by a time $\frac{\Delta t}{2}$ is done by

$$\bar{s}_{i,L} = s_{i,L} + \frac{\Delta t u_i^n}{2\Delta x} (s_{i,L} - s_{i,R}), \quad \bar{s}_{i,R} = s_{i,R} + \frac{\Delta t u_i^n}{2\Delta x} (s_{i,L} - s_{i,R}). \quad (5.33)$$

- iii) Then $s_{i+\frac{1}{2}}^{MH}$ and $s_{i-\frac{1}{2}}^{MH}$ are evaluated as

$$s_{i+\frac{1}{2}}^{MH} = \begin{cases} \bar{s}_{i,R} & \text{if } u_i^n \geq 0 \\ \bar{s}_{i+1,L} & \text{if } u_i^n < 0 \end{cases} \quad s_{i-\frac{1}{2}}^{MH} = \begin{cases} \bar{s}_{i-1,R} & \text{if } u_i^n \geq 0 \\ \bar{s}_{i,L} & \text{if } u_i^n < 0 \end{cases} \quad (5.34)$$

For passive scalar advection, this scheme results in a compact 5 points stencil which is $\mathcal{O}(\Delta t^3, \Delta x^3)$ accurate [24].

5.3. Recap

In this Chapter, the thermal coupling of the hybrid LB model is discussed. Due to the inaccurate energy conservation of LB solvers using small lattices, a secondary thermodynamic variable should be discretized. To achieve a fully conservative scheme, the discretization of the total energy equation in conservative form is necessary, to this end, a numerical scheme was derived in Appendix B. However, the entropy being an eigenmode of the linearized Euler system, it is more easily discretized because :

- It mostly behaves as a passive scalar in smooth regions.
- In the linear limit it is uncoupled from the other modes – acoustic and vorticity – that are hidden in the LB solver.

Therefore, the LB scheme being stable on its own, if we select a high accuracy and robust finite difference scheme for the entropy mode, the errors of both schemes will not interact, at least in the linear limit. Therefore, it is much easier to couple a discretized entropy equation and to achieve a robust overall scheme when using the entropy equation, which is why we decided to use it.

Fortunately, we were able to show that while the entropy equation does not lead to a conservative scheme, it does lead to sufficiently accurate jump conditions for the low supersonic regime, which is consistent with previous studies [74, 75, 147–149]. Then, a wide variety of schemes are tested on the passive scalar advection test case in order to determine which scheme could lead to accurate results for the entropy equation. The MUSCL Hancock scheme is selected for its high accuracy and robustness compared to previous schemes employed in the hybrid LBM literature.

6. Pressure-based lattice-Boltzmann model

This Chapter mainly follows the content of:

G. Farag, S. Zhao, T. Coratger, P. Boivin, G. Chiavassa and P. Sagaut. A pressure-based regularized lattice-Boltzmann method for the simulation of compressible flows. *Physics of Fluids*, 2020.

<https://doi.org/10.1063/5.0011839>

Sommaire

6.1	Hybrid Recursive Regularized pressure based model	110
6.2	Continuous equivalent equations	113
6.3	Results	115
6.3.1	Isentropic vortex advection	115
6.3.2	Entropy spot advection	117
6.3.3	Acoustic wave propagation	118
6.3.4	Thermal Couette Flow	118
6.3.5	Shock wave inner structure	120
6.3.6	One-dimensional shock tube	124
6.3.7	Shock-Vortex interaction	124
6.4	Recap	125

In previous chapters, a numerical scheme interpretation of the lattice-Boltzmann method was carried out. Then, this method was used in Sec. 4.5 to analyze a ρ -based thermal model [74]. Now that the numerical scheme for an arbitrary moment $\Pi_{\alpha_1 \dots \alpha_n}^{f, (n)}$ – Eq. (3.80) – was evidenced from the collide and stream algorithm, let us try to see if the ρ -based model presented in Sec. 4.5 is the only possible choice of thermal lattice-Boltzmann scheme verifying mass and momentum conservation. To this end, the coupling between the mass/momentum block and thermal effects is now performed using a kind of predictor-corrector approach, that allows for the use of a very simple athermal-like equilibrium. This will yield the definition of a new segregated, pressure-based hybrid LBM equipped with a traceless hybrid recursive regularized collision model and an entropy equation to encompass thermal effects. **Note that the designation of density or pressure based only corresponds to the 0th**

order moment of the equilibrium and should not be confused with the classical CFD designation of density/pressure-based solvers.

Note that segregated pressure-based LBMs have been investigated by many authors during the last two decades, mostly for low-Mach flows, e.g. low-Mach thermal flows with variable properties [150], low-Mach combustion [151–154], low-Mach multiphase flows [155–168] including phase change and thermal phase change [169–173]. In almost all cases, the double distribution function approach was used to solve the additional equation (e.g. phase index, temperature ...); only very few authors used a hybrid approach with a Finite Difference method for the scalar temperature/energy equation [151, 152, 169, 173]. To the knowledge of the authors, the present hybrid recursive regularized p method is the first one dealing with segregated pressure-based method for high-speed compressible flows in both subsonic and supersonic regimes, using a hybrid finite-difference-based approach to solve the entropy equation.

The general structure of the present model is discussed in Sec. 6.1. The Taylor expansion analysis we presented being generic, we only provided its results for this new model in Sec. 6.2. Numerical results obtained with the new method are displayed in Sec. 6.3.

6.1. Hybrid Recursive Regularized pressure based model

Here, similarly to Sections 4.3 and 4.5, the scheme is recast into a list of consecutive steps. Assuming all variables are known at time t , the algorithm to follow to get the $t + \Delta t$ solution is

- **Step 1 : Equilibrium construction** The equilibrium is expanded following the complete D3Q19 basis, corresponding to polynomials of order 0 to 3 in Appendix A.

$$f_i^{eq} = \omega_i \left\{ \mathcal{H}^{(0)} \rho \theta + \frac{\mathcal{H}_{i\alpha}^{(1)}}{c_s^2} \rho u_\alpha + \frac{\mathcal{H}_{i\alpha\beta}^{(2)}}{2c_s^4} [\rho u_\alpha u_\beta] + \frac{\mathcal{H}_{i\gamma}^{(3r)}}{6c_s^6} a_\gamma^{(3r)} \right\}. \quad (6.1)$$

where $a_\gamma^{(3r)}$ is a function of $a_{\alpha\beta\gamma}^{(3)} = \rho u_\alpha u_\beta u_\gamma$ defined in Appendix A. This basis simply allows to use a simpler force correction term F_i due to a reduced isotropy defect $D_{\alpha\beta\gamma}^{feq,(3)}$. This procedure could also be applied for the ρ -based [149] and does not affect the consistency. Assuming that as in [149] the ρ -based approach also used the complete basis, the main difference with Eq. (4.30) lies in the 0^{th} order, where ρ is replaced by the normalized pressure $\rho\theta = p/c_s^2$. Let us also recall the classical definition of the normalized temperature, Eq. (4.83).

- **Step 2 : Force construction** The forcing term is simply extended to second order,

$$F_i \equiv \omega_i \left\{ \mathcal{H}^{(0)} a^{F,(0)} + \frac{\mathcal{H}_{i\alpha}^{(1)}}{c_s^2} a_\alpha^{F,(1)} + \frac{\mathcal{H}_{i\alpha\beta}^{(2)}}{2c_s^4} a_{\alpha\beta}^{F,(2)} \right\}, \quad (6.2)$$

6. Pressure-based lattice-Boltzmann model – 6.1. Hybrid Recursive Regularized pressure based model

with its Hermite moments defined as

$$\begin{aligned} a_{\alpha\beta}^{F,(2)} &= c_s^2 u_\alpha \frac{\partial \rho(1-\theta)}{\partial x_\beta} + c_s^2 u_\beta \frac{\partial \rho(1-\theta)}{\partial x_\alpha} \\ &+ \delta_{\alpha\beta} \rho c_s^2 \frac{2}{3} \frac{\partial u_\gamma}{\partial x_\gamma} - c_s^2 \delta_{\alpha\beta} \frac{\partial \rho(1-\theta)}{\partial t} - \frac{\partial D_{\alpha\beta\gamma}^{feq,(3)}}{\partial x_\gamma} \\ &+ \rho \mathcal{F}_\alpha u_\beta + \rho \mathcal{F}_\beta u_\alpha - \dot{m} u_\alpha u_\beta, \end{aligned} \quad (6.3)$$

$$a_\alpha^{F,(1)} = \rho \mathcal{F}_\alpha, \quad (6.4)$$

$$a^{F,(0)} = \dot{m}. \quad (6.5)$$

It was observed that the following set of schemes in the force term led to reasonable stability properties for supersonic flows,

$$\frac{\partial \rho(1-\theta)}{\partial x}(t, x) = \frac{[\rho(1-\theta)](t, x + \Delta x) - [\rho(1-\theta)](t, x - \Delta x)}{2 \Delta x} + \mathcal{O}(\Delta x^2), \quad (6.6)$$

$$\frac{\partial \rho(1-\theta)}{\partial t}(t, x) = \frac{[\rho(1-\theta)](t, x) - [\rho(1-\theta)](t - \Delta t, x)}{\Delta t} + \mathcal{O}(\Delta t), \quad (6.7)$$

$$\begin{aligned} \frac{\partial u_\gamma}{\partial x_\gamma}(t, x) &= \frac{1}{\rho(t, x)} \left[\dot{m}(t, x) - u_\gamma(t, x) \frac{\rho(t, x_\gamma + \Delta x) - \rho(t, x_\gamma - \Delta x)}{2 \Delta x} \right. \\ &\quad \left. - \frac{\rho(t, x) - \rho(t - \Delta t, x)}{\Delta t} \right] + \mathcal{O}(\Delta t, \Delta x^2). \end{aligned} \quad (6.8)$$

Note that the unusual velocity divergence scheme Eq. (6.8) was obtained using mass conservation Eq. (1.20). Additionally, on a D3Q19 lattice, the divergence of the isotropy defect is

$$\frac{\partial D_{\alpha\beta\gamma}^{feq,(3)}}{\partial x_\gamma} = \delta_{\alpha\beta} \frac{\partial \rho u_\alpha^3}{\partial x_\alpha} + (1 - \delta_{\alpha\beta}) \frac{\partial \rho u_x u_y u_z}{\partial x_\psi}, \quad (6.9)$$

without summation over repeated index α and with ψ defined by $\psi \neq \alpha$ and $\psi \neq \beta$. It was discretized by the following scheme,

$$\frac{\partial \phi}{\partial x_\gamma} \approx \begin{cases} \frac{\phi(x_\gamma) - \phi(x_\gamma - \Delta x)}{\Delta x} & \text{if } u_\gamma \geq 0 \\ \frac{\phi(x_\gamma + \Delta x) - \phi(x_\gamma)}{\Delta x} & \text{if } u_\gamma < 0 \end{cases}, \quad (6.10)$$

his set of numerical schemes have been found to be optimal for the $Ma \geq 1$ stability of Kovasznay modes simulated in Sec. 6.3.

- **Step 3 : Non-equilibrium construction** Though the pressure-based model does not presuppose the use of a specific collision kernel, we chose to use the traceless hybrid recursive regularized collision kernel, see Sec. 4.4. The non-equilibrium population \bar{f}_i^{neq} is then reconstructed following Eqs. (4.77,4.80) and using the

6. Pressure-based lattice-Boltzmann model – 6.1. Hybrid Recursive Regularized pressure based model

complete basis, similarly to the equilibrium distribution Eq. (6.1).

- **Step 4 : Collision** Thanks to previous steps f_i^{eq} , F_i and \bar{f}_i^{neq} have been built, compute the collided population f_i^{col} such that

$$f_i^{col}(t, \mathbf{x}) = f_i^{eq}(t, \mathbf{x}) + \left(1 - \frac{\Delta t}{\bar{\tau}}\right) \bar{f}_i^{neq}(t, \mathbf{x}) + \frac{\Delta t}{2} F_i(t, \mathbf{x}), \quad (6.11)$$

with the offset relaxation time defined for this model by

$$\bar{\tau} = \frac{\mu}{\rho c_s^2} + \frac{\Delta t}{2}. \quad (6.12)$$

- **Step 5 : Streaming** Shift the populations according to

$$\bar{f}_i(t + \Delta t, \mathbf{x}) = f_i^{col}(t, \mathbf{x} - \mathbf{c}_i \Delta t). \quad (6.13)$$

- **Step 6 : Coupling update** Here, for stability reasons, it was chosen to follow the path of the ρ -based model [74, 123] and to discretize the entropy, Eq. (5.2), see Appendix 5.2.2 for more details. This step provides the knowledge of $s(t + \Delta t, \mathbf{x})$ as a function of the previous time t .
- **Step 7 : Update macroscopic variables** When applied to $n = 0$ the macroscopic update rule Eq. (4.4) usually gives us the updated density $\rho(t + \Delta t, \mathbf{x})$. But here because we modified the equilibrium distribution it leads to an updated pressure $(p^* / c_s^2)(t + \Delta t, \mathbf{x})$ such that

$$\left(\frac{p^*}{c_s^2}\right)(t + \Delta t, \mathbf{x}) = \Pi^{\bar{f}(t+\Delta t, \mathbf{x}), (0)} + \frac{\Delta t}{2} \dot{m}(t + \Delta t, \mathbf{x}). \quad (6.14)$$

which is equivalent to an unphysical equation for the pressure, $\partial(p^* / c_s^2) / \partial t + \partial \rho u_\beta / \partial x_\beta = \dot{m}$, see Eq. (4.15) for $n = 0$. To recover the correct mass conservation equation it is mandatory to modify the 0th order update rule such as :

$$\rho(t + \Delta t, \mathbf{x}) = \Pi^{\bar{f}(t+\Delta t, \mathbf{x}), (0)} + \rho(t, \mathbf{x})[1 - \theta](t, \mathbf{x}) + \frac{\Delta t}{2} \dot{m}(t + \Delta t, \mathbf{x}). \quad (6.15)$$

The update rule for $n = 1, 2$ remains unchanged,

$$\rho u_\alpha(t + \Delta t, \mathbf{x}) = \sum_{i=0}^{q-1} c_{i\alpha} \bar{f}_i(t + \Delta t, \mathbf{x}) + \frac{\Delta t}{2} [\rho \mathcal{F}_\alpha](t + \Delta t, \mathbf{x}), \quad (6.16)$$

$$\left(1 + \frac{\Delta t}{2\tau}\right) \Pi_{\alpha\beta}^{f^{neq}(t+\Delta t, \mathbf{x}), (2)} = \Pi_{\alpha\beta}^{\bar{f}(t+\Delta t, \mathbf{x}), (2)} - \Pi_{\alpha\beta}^{f^{eq}(t+\Delta t, \mathbf{x}), (2)} + \frac{\Delta t}{2} \Pi_{\alpha\beta}^{F(t+\Delta t, \mathbf{x}), (2)} \quad (6.17)$$

Then compute $T(t + \Delta t, \mathbf{x})$, from $s(t + \Delta t, \mathbf{x})$ and $\rho(t + \Delta t, \mathbf{x})$.

6.2. Continuous equivalent equations

Now that macroscopic quantities, namely mass, velocity, stress-tensor and temperature, $\rho(t + \Delta t, \mathbf{x})$, $u_\alpha(t + \Delta t, \mathbf{x})$, $\Pi_{\alpha\beta}^{f^{neq},(2)}(t + \Delta t, \mathbf{x})$ and $T(t + \Delta t, \mathbf{x})$ have been explicitly updated let us analyze the equivalent continuous equations of the system Eqs. (6.15,6.16,6.17) and compare it with the target set of equations Eqs. (1.20,1.21,5.2). Following Chapter 4, the Taylor expansion of the lattice-Boltzmann method coupled with a consistent entropy scheme leads to the system of equations

$$\frac{\partial \rho}{\partial t} + \frac{\partial \rho u_\beta}{\partial x_\beta} = \dot{m}, \quad (6.18)$$

$$\frac{\partial \rho u_\alpha}{\partial t} + \frac{\partial \left[\rho u_\alpha u_\beta + p \delta_{\alpha\beta} + \Pi_{\alpha\beta}^{f^{neq},(2)} \right]}{\partial x_\beta} = \rho \mathcal{F}_\alpha, \quad (6.19)$$

$$\frac{\partial \Pi_{\alpha\beta}^{f,(2)}}{\partial t} + \frac{\partial \Pi_{\alpha\beta\gamma}^{f,(3)}}{\partial x_\gamma} = -\frac{1}{\tau} \Pi_{\alpha\beta}^{f^{neq},(n)} + \Pi_{\alpha\beta}^{E,(n)}, \quad (6.20)$$

$$\rho T \left(\frac{\partial s}{\partial t} + u_\beta \frac{\partial s}{\partial x_\beta} \right) + \frac{\partial q_\gamma}{\partial x_\gamma} - \mathcal{T}_{\alpha\beta} \frac{\partial u_\beta}{\partial x_\gamma} = \rho \dot{q} + \dot{m} \left(\frac{u_\gamma^2}{2} - e - \frac{p}{\rho} \right), \quad (6.21)$$

where equations of state for ideal gas are $p = \rho r T$, $s = C_v \ln(p/\rho^\gamma)$ and caloric constitutive equation is Eq. (1.24). We recognize mass, momentum and entropy conservation along with an evolution equation for the stress tensor, let us analyze this equation. Using the kinetic tensor Eq. (4.47) obtained from mass and momentum conservation, the force terms Eqs. (6.3,6.5) along with the 2nd and 3rd order macroscopic moments of the equilibrium population lead to the stress tensor equation,

$$\begin{aligned} -\Pi_{\alpha\beta}^{f^{neq},(2)} &= \tau \rho c_s^2 \left[\frac{\partial u_\alpha}{\partial x_\beta} + \frac{\partial u_\beta}{\partial x_\alpha} - \delta_{\alpha\beta} \frac{2}{3} \frac{\partial u_\gamma}{\partial x_\gamma} \right] \\ + \tau \left\{ \frac{\partial \Pi_{\alpha\beta}^{f^{neq},(2)}}{\partial t} + \frac{\partial \Pi_{\alpha\beta\gamma}^{f^{neq},(3)}}{\partial x_\gamma} \right\} &- \tau \left[u_\alpha \frac{\partial \Pi_{\beta\gamma}^{f^{neq},(2)}}{\partial x_\gamma} + u_\beta \frac{\partial \Pi_{\alpha\gamma}^{f^{neq},(2)}}{\partial x_\gamma} \right], \end{aligned} \quad (6.22)$$

where we recall from Eq. (6.12) that $\tau \rho c_s^2 = \mu$. This is the exact same evolution equation as in the athermal case, see Sec. 4.3. Because equilibrium is enslaved to low order macroscopic moments the only place where the higher order moments have an impact in thermo-hydrodynamic equations is through $\Pi_{\alpha\beta\gamma}^{f^{neq},(3)}$. Fortunately here we used a filtered collision kernel – see Eq. (3.34) – so that even if higher order macroscopic equations are unphysical their effect on low order macroscopic equations is explicitly filtered during non-equilibrium reconstruction [72, 81]. To find out in which cases the stress-tensor evolution equation is sufficiently close to its expected value we use the same nondimensionalization as in Sections 4.3 and 4.5, except that $Q_0 = U_0 \Pi_0$ is

6. Pressure-based lattice-Boltzmann model – 6.2. Continuous equivalent equations

known because of the collision kernel. This leads to a normalized equation,

$$-\Pi_{\alpha\beta}^{*,f^{neq,(2)}} = \mathcal{F}_{\alpha\beta}^* + \frac{\text{Ma}^2 \gamma r T_0}{\text{Re}} \frac{1}{c_s^2 \rho^*} \frac{\partial \Pi_{\alpha\beta\gamma}^{*,f^{neq,(3)}}}{\partial x_\gamma^*} - \frac{\text{Ma}^2 \gamma r T_0}{\text{Re}} \frac{1}{c_s^2 \rho^*} \left[u_\alpha^* \frac{\partial \Pi_{\beta\gamma}^{*,f^{neq,(2)}}}{\partial x_\gamma^*} + u_\beta^* \frac{\partial \Pi_{\alpha\gamma}^{*,f^{neq,(2)}}}{\partial x_\gamma^*} \right] + \frac{\mu}{\rho_0 c_s^2 t_s} \frac{1}{\rho^*} \frac{\partial \Pi_{\alpha\beta}^{*,f^{neq,(2)}}}{\partial t^*}. \quad (6.23)$$

Note that defining the CFL number [14] as in most classical compressible codes

$$\text{CFL} = \frac{U_0 + \sqrt{\gamma r T_0}}{\Delta x / \Delta t}, \quad (6.24)$$

and reminding that the lattice sound speed is $c_s = \Delta x / (\sqrt{3} \Delta t)$ we can see that

$$\frac{\gamma r T_0}{c_s^2} = \frac{3\text{CFL}^2}{(\text{Ma} + 1)^2}. \quad (6.25)$$

By assuming that our fastest relevant phenomenon is the convection, such that $t_s = L_0 / U_0$, we can rearrange Eq. (6.23) into

$$-\Pi_{\alpha\beta}^{*,f^{neq,(2)}} = \mathcal{F}_{\alpha\beta}^* + \mathcal{O}\left(\frac{\text{Ma}^2 \text{CFL}^2}{\text{Re} (\text{Ma} + 1)^2}\right), \quad (6.26)$$

which is the consistency condition of the pressure-based model [76]. This very simple expression was obtainable only because we used a collision kernel in which the scaling of third order non-equilibrium moments is algebraically enslaved to variables whose scaling is known, see Eq. (4.77). This equation shows an attractive feature of this model : the discretized continuous equations now directly depends on the CFL number, similarly to the athermal model throughout Eq. (4.55) and unlike the ρ -based model, see Eq. (4.102), where the error is not lowered by reducing the CFL.

Consistency errors of athermal (Sec. 4.3), ρ -based (Sec. 4.5) and p -based (present chapter) are recalled in Table 6.1, comparison of the ρ and p based models, at least in term of consistency, clearly favors the use of the p -based model, because unlike the ρ -based model,

- The consistency error decreases with decreasing CFL.
- The error remain bounded when Ma is increased.
- The consistency error goes to 0 as the Ma is decreased.
- The error is Pr independent.

It is of utmost importance to recall that consistency and stability [14, 22, 23], are 2 different properties. Now that the consistency of the lattice-Boltzmann p -based model have been checked, let us validate its stability by numerical simulations.

Model	Stress tensor error	Equation
Athermal model (Sec. 4.3)	$\mathcal{O}\left(\frac{\widetilde{\text{Ma}}^2}{\text{Re}}\right)$	(4.57)
Compressible density-based (Sec. 4.5)	$\mathcal{O}\left(\frac{\text{Ma}^2}{\text{Re}}\right) + \mathcal{O}\left(\frac{1}{\text{Re Pr}}\right)$	(4.102)
Compressible pressure-based (present section)	$\mathcal{O}\left(\frac{\text{Ma}^2 \text{CFL}^2}{\text{Re} (\text{Ma} + 1)^2}\right)$	(6.26)

Table 6.1. – Summary of consistency errors for the stress tensor, for the three models studied. Recall that athermal and thermal Mach numbers $\widetilde{\text{Ma}}$ and Ma have different definitions, see Eqs. (4.54,4.100)

6.3. Results

In this Section, the proposed traceless hybrid recursive regularized p is assessed on different configurations and compared to reference solutions that can be either analytical solutions or numerical solutions obtained by high-order Navier-Stokes Fourier solvers. The validations are aimed at demonstrating the ability of the present model to accurately reproduce fully compressible effects for a wide range of physical parameters, including

- Convection tests at Mach=(0.5, 1, 1.5) for the three fundamental Kovasznay modes: vorticity (Sec. 6.3.1), entropy (Sec. 6.3.2) and acoustic (Sec. 6.3.3). These tests show excellent dissipative and dispersive properties.
- Couette thermal flow tests in Sec. 6.3.4. This Section validates the accuracy of the model regarding the viscous heating and heat diffusion for a wide range of Ma , Pr and γ numbers.
- Validations in the presence of shocks. They include one-dimensional shock tube (Sec. 6.3.6), and shock-vortex interaction (Sec. 6.3.7).

All inviscid simulations are carried out setting the dynamic viscosity to $\mu = 10^{-15}$ in order to mimic an Euler solver. The classical definition for the acoustic CFL number Eqs. (6.24) is adopted throughout all test cases.

6.3.1. Isentropic vortex advection

The first test case is the usual inviscid and isentropic vortex advected by a mean uniform flow in a fully periodic domain. The analytical solution is a frozen pattern simply advected by the mean flow over time. The $[0, 10] \times [0, 10]$ physical domain is discretized by a 200×200 mesh. The isentropic vortex is initialized at its center and

defined as

$$\rho = \left[1 - \frac{(\gamma - 1)}{2} M_v^2 e^{1-r^2/R^2} \right] \frac{1}{\gamma - 1}, \quad p = \rho^\gamma, \quad (6.27)$$

$$u = u_0 - M_v \sqrt{\gamma} e^{(1-r^2/R^2)/2} (y - y_c), \quad (6.28)$$

$$v = M_v \sqrt{\gamma} e^{(1-r^2/R^2)/2} (x - x_c), \quad (6.29)$$

with $r = \sqrt{(x - x_c)^2 + (y - y_c)^2}$. The characteristic radius of the spot is set to $R = 1$, the free stream flow to $u_0 = Ma\sqrt{\gamma}$, $T_0 = 1$, $\rho = 1$, $\gamma = 1.4$ and the strength of the vortex to $M_v = \frac{1}{4\pi\sqrt{\gamma}}$, following [123]. The time-step is fixed to $\Delta t = 0.001725$, corresponding to an acoustic CFL ≈ 0.1 for the $Ma = 1.5$ case. The value of the hybrid recursive regularized weighting parameter is $\sigma = 1$ leading to a stress tensor 100% evaluated by the LBM. The vortex is then advected on a distance of $200R$ corresponding to 20 flow-through-time (FTT). The initial and final density maps with identical colorbars are reported for different values of the Mach number in Fig. 6.1. As expected, the shape of the vortex is perfectly preserved after 20 FTT, regardless of the Mach value (0.5, 1 and 1.5). For each Mach number, the dissipation, defined as $\xi = \frac{\min \rho(20FTT) - \min \rho(t=0)}{1 - \min \rho(t=0)}$

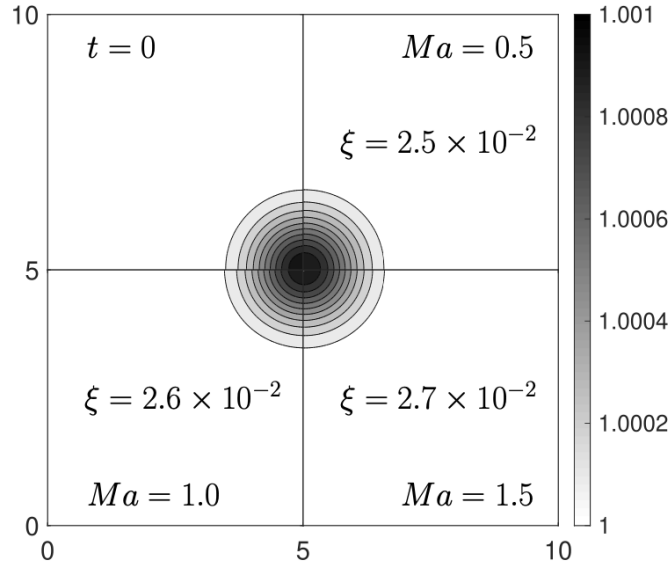


Figure 6.1. – Density fields for the isentropic vortex convection: initial/analytical profile (top left), and solution after 20FTT for $Ma = (0.5, 1.0, 1.5)$. The dissipation ξ is reported in each case.

is also reported in Fig. 6.1, showing that less than 1% of the initial amplitude was lost after 20 FTT. Note that use of $\sigma = 1$ was possible in these simulations, whereas maximum values of σ close to 0.7 were achieved with the hybrid recursive regularized ρ formulation[74] studied in Sec. 4.5. This translates to a decrease in dissipation ξ by about an order of magnitude compared with the hybrid recursive regularized

ρ model[74]. The proposed hybrid recursive regularized p method is then able to compute accurately the advection of a radial flow over a long time without introducing spatial distortion nor spurious dissipation, despite a relatively low spatial resolution.

6.3.2. Entropy spot advection

The convected entropy spot is a benchmark of particular interest for the present model as it is expected for the numerical solution to be mainly dependent on the finite difference part of the solver used for the entropy equation. The LBM is known to exhibit a low numerical dissipation behavior [100], it is then important to check that the finite difference part of the scheme does not deteriorate this property. A good way to verify it is to convect a pure entropy spot over a long distance. The flow is then initialized as

$$\rho = \rho_0 \left(1 + \epsilon e^{-r^2/R^2} \right), \quad (6.30)$$

$$T = T_0 \left(1 - \epsilon e^{-r^2/R^2} \right), \quad (6.31)$$

$$u = u_0, \quad v = 0, \quad (6.32)$$

with a sufficiently low value of $\epsilon = 10^{-3}$ ensuring that the $u \pm c$ acoustic modes are not triggered [174]. All the other parameters remain unchanged compared to the isentropic vortex aside the dissipation which now reads as $\xi = \frac{\max \rho(20FTT) - \max \rho(t=0)}{1 - \max \rho(t=0)}$. Initial and final solutions of the advected entropy spot can be seen on Fig. 6.2, leading to the conclusion that the shape of the entropy spot is well preserved and that less than 3% of the maximum amplitude was lost over the whole simulation.

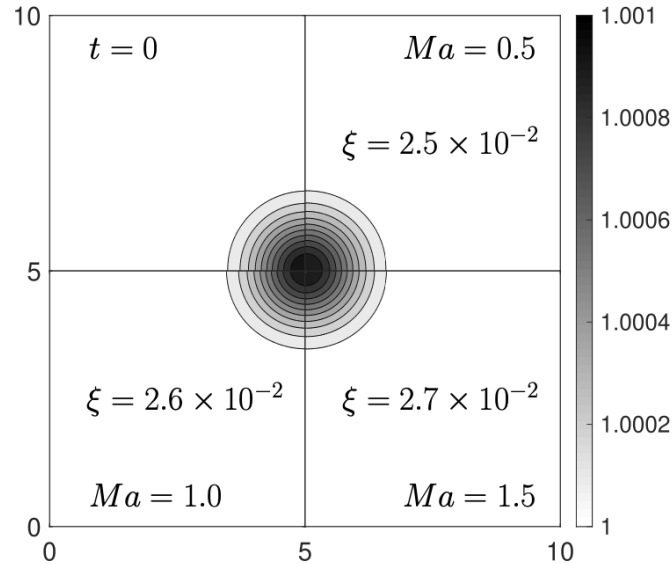


Figure 6.2. – Density fields for the entropy spot convection: initial/analytical profile (top left), and solution after $20FTT$ for $Ma = (0.5, 1.0, 1.5)$.

6.3.3. Acoustic wave propagation

We compute in this part the propagation of a pure acoustic wave over a long distance. The wave is not simply advected by the mean flow, it is propagated with a $u + c$ velocity, which leads to a complex pattern when initialized in a 2D domain. It was then chosen to test the acoustic decay in a 1D periodic simulation with a $[0, 10]$ physical domain discretized by 200 points and $\Delta t = 0.001725$. The acoustic wave is initialized as

$$\rho = \rho_0 \left(1 + \epsilon e^{-r^2/R^2} \right), \quad (6.33)$$

$$T = T_0 \left(1 + (\gamma - 1)\epsilon e^{-r^2/R^2} \right), \quad (6.34)$$

$$u = u_0 + c_0 \epsilon e^{-r^2/R^2}, \quad (6.35)$$

$$v = 0, \quad (6.36)$$

with $r = (x - x_c)$ and $\epsilon = 10^{-3}$. Analytical and numerical solutions are plotted on Fig. 6.3. A good agreement with the analytical solution is observed, with a very low

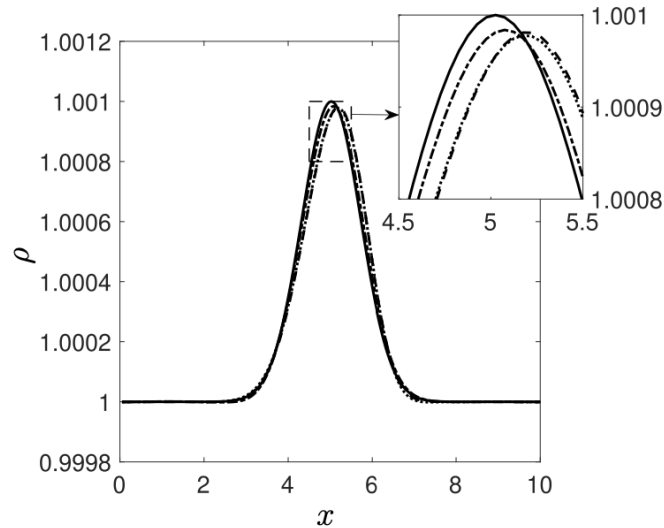


Figure 6.3. – Density fields for the acoustic propagation ($u + c$ mode): initial/analytical profile (solid line), and solution after $20FTT$ at $Ma = 0.5$ (dashed), $Ma = 1.0$ (dotted) and $Ma = 1.5$ (dot-dashed).

numerical dissipation ξ of respectively 1.9×10^{-2} , 2.2×10^{-2} and 1.6×10^{-2} for subsonic, sonic and supersonic cases.

6.3.4. Thermal Couette Flow

The thermal Couette flow is presented here as part of the validation basis of compressible LB models, but credit for this subsection goes to Thomas Coratger, who carried out these validations.

6. Pressure-based lattice-Boltzmann model – 6.3. Results

Having validated the hybrid recursive regularized p model the Euler part of the conservation equations through convection tests, let us now validate the shear stress and heat transfer balance through an analysis of thermal Couette flows.

The test case is two-dimensional and consists of a shear flow between two infinite flat plates: one is static and the other is moving in the x -direction at a constant velocity.

$$U = \text{Ma} \times c_{s,\infty}, \quad (6.37)$$

A shear force is transmitted to the fluid by the no-slip condition at the boundaries where thermal properties are given. Then, the temperature T only depends on y . At steady state, the effects of viscous heat dissipation and thermal conduction balance out.

During simulations, the heat capacity ratio at constant pressure C_p and the Prandtl number $\text{Pr} = (\mu C_p)/\lambda$ are assumed to be constant. For the benchmark, a simplified version of boundary conditions via cut cell approach [97] is adopted. Moreover, two specific thermal configurations are performed in a $2 \times 101 \times 1$ domain. In the first one, the walls are at the same temperature such as $T_{\text{top wall}} = T_{\text{bottom wall}} = \text{const.}$ and the viscosity μ is constant.

This configuration introduces a linear profile of u_x velocity as a function of y and the temperature can be theoretically expressed as [75]:

$$\frac{T}{T_w} = 1 + \frac{y}{H} \zeta \left(1 - \frac{y}{H}\right), \quad (6.38)$$

where T_w is the temperature at the boundary walls, H is the distance between them and $\zeta = \text{Pr} \frac{\gamma-1}{2} \text{Ma}^2$. In the second configuration, the bottom wall is adiabatic with the Neumann temperature boundary condition $q_y = -\lambda(\partial T/\partial y) = 0$ and the top wall is at constant temperature. For this configuration, the viscosity μ is temperature dependent,

$$\frac{\mu}{\mu_0} = \frac{T}{T_0}, \quad (6.39)$$

Then, the velocity and temperature profiles are coupled and can be found analytically as [6]:

$$\frac{T}{T_w} = 1 + \zeta \left[1 - \left(\frac{u_x}{U}\right)^2\right], \quad (6.40)$$

$$\left(1 + \frac{2}{3}\zeta\right) \frac{y}{H} = \frac{u_x}{U} + \zeta \left[\frac{u_x}{U} - \frac{1}{3}\left(\frac{u_x}{U}\right)^3\right], \quad (6.41)$$

The simulations are performed with the following conditions: the CFL varies between 0.23 and 0.77 to ensure the solution stability, the wall temperature is $T_w = 300 \text{ K}$, the initial pressure of the flow is $P_0 = 101325 \text{ Pa}$ and $\sigma = 0.7$.

The two cases are tested through a wide range of supersonic parameters (Ma , Pr and γ).

Fig. 6.4 shows the thermal configuration for a specific set of parameters ($\gamma = 7/5$,

Isothermal bottom - Isothermal top				Adiabatic bottom - Isothermal top			
Ma	Pr	γ	L_2^T Error	Ma	Pr	γ	L_2^T Error
0.35	5	5/3	0.0001499	0.35	5	5/3	0.0001605
1	1.5	5/3	0.0005695	1	1.5	5/3	0.0011649
1.3	0.71	7/5	0.0002404	1.3	0.71	7/5	0.0001973
1.3	0.71	5/3	0.0007031	1.3	0.71	5/3	0.0008085

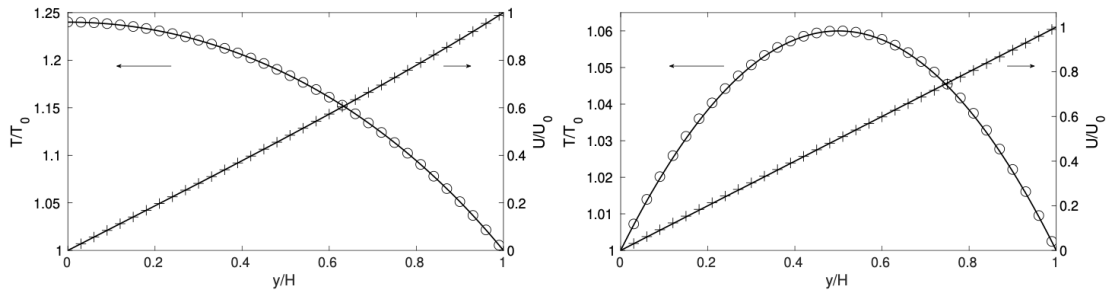
 Table 6.2. – L_2 Error Eq. (6.42) for different performed simulations.


Figure 6.4. – Temperature and velocity profiles of the thermal Couette flow for $\gamma = 7/5$, $Pr = 0.71$ and $Ma = 1.3$. The solid lines — correspond to analytical results; the numerical results + and \circ correspond respectively to the velocity profiles U/U_0 and the temperature profiles T/T_0 . Boundary conditions: isothermal top wall and adiabatic bottom wall (left), isothermal walls (right).

$Pr = 0.71$ and $Ma = 1.3$) while Table 6.2 summarizes all the results with the L_2 error on the temperature defined as:

$$L_2^T = \frac{\sqrt{\sum (T_{i,\text{Simulation}} - T_{i,\text{Theory}})^2}}{\sqrt{\sum T_{i,\text{Theory}}^2}}, \quad (6.42)$$

Figure 6.4 and Table 6.2 show again a good agreement between simulations and analytical solutions, thus validating the viscous and thermal properties of the model. Finally, a convergence study of the model is carried out by varying the grid resolution in the y -direction and measuring the L_2 norm on the temperature. Figure 6.5 shows a second order convergence in space, classical of Lattice-Boltzmann models [4].

6.3.5. Shock wave inner structure

The capability of hybrid recursive regularized p to capture inner shock structures is demonstrated through the comparison with an analytical solution [175].

This particular Navier-Stokes-Fourier solution for a stationary viscous shock is

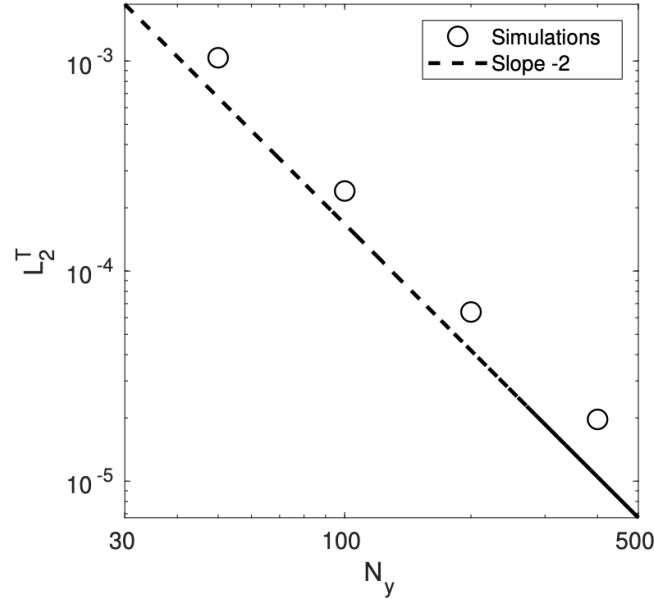


Figure 6.5. – Convergence study : L_2^T norm Eq. (6.42) as a function of the resolution N_y . Carried out in the case of the isothermal top and bottom walls presented in Fig. 6.4.b.

obtained for $Pr = 0.75$ and stands for any values of Ma , Re and γ . The following procedure is used to compare the numerical solution with the analytical one. Initial upstream ϕ_0 and downstream ϕ_1 physical fields are initialized through the Rankine-Hugoniot jump conditions [6] and linked by a smooth sigmoidal profile chosen as

$$\phi = \phi_0 + (1 + \tanh [25(x - x_s)]) \frac{\phi_1 - \phi_0}{2}, \quad (6.43)$$

in which x is the space coordinate and x_s the initial position of the shock. Then from this smooth profile the simulation naturally reaches the steady state solution which is the solution we are looking for. Because this solution has no other characteristic length scale than the shock thickness the initialization may lead to a shift between positions of the analytical and numerical shocks, to circumvent this problem the numerical solution is then shifted such that the maximal entropy coincides between both solutions. Then the abscissa x is normalized such that

$$\xi = \frac{x}{\lambda_0}, \quad (6.44)$$

where λ_0 is the mean free path defined as

$$\lambda_0 = \frac{4}{5} \sqrt{\frac{8\gamma}{\pi}} \frac{Ma}{Re} L_0, \quad (6.45)$$

6. Pressure-based lattice-Boltzmann model – 6.3. Results

with $Ma = \frac{U_0}{\sqrt{\gamma r T_0}}$, $Re = \frac{\rho_0 U_0 L_0}{\mu_0}$ and $L_0 = 1$ a characteristic length scale. This normalization allows to get rid of the Re dependence of the theoretical solution.

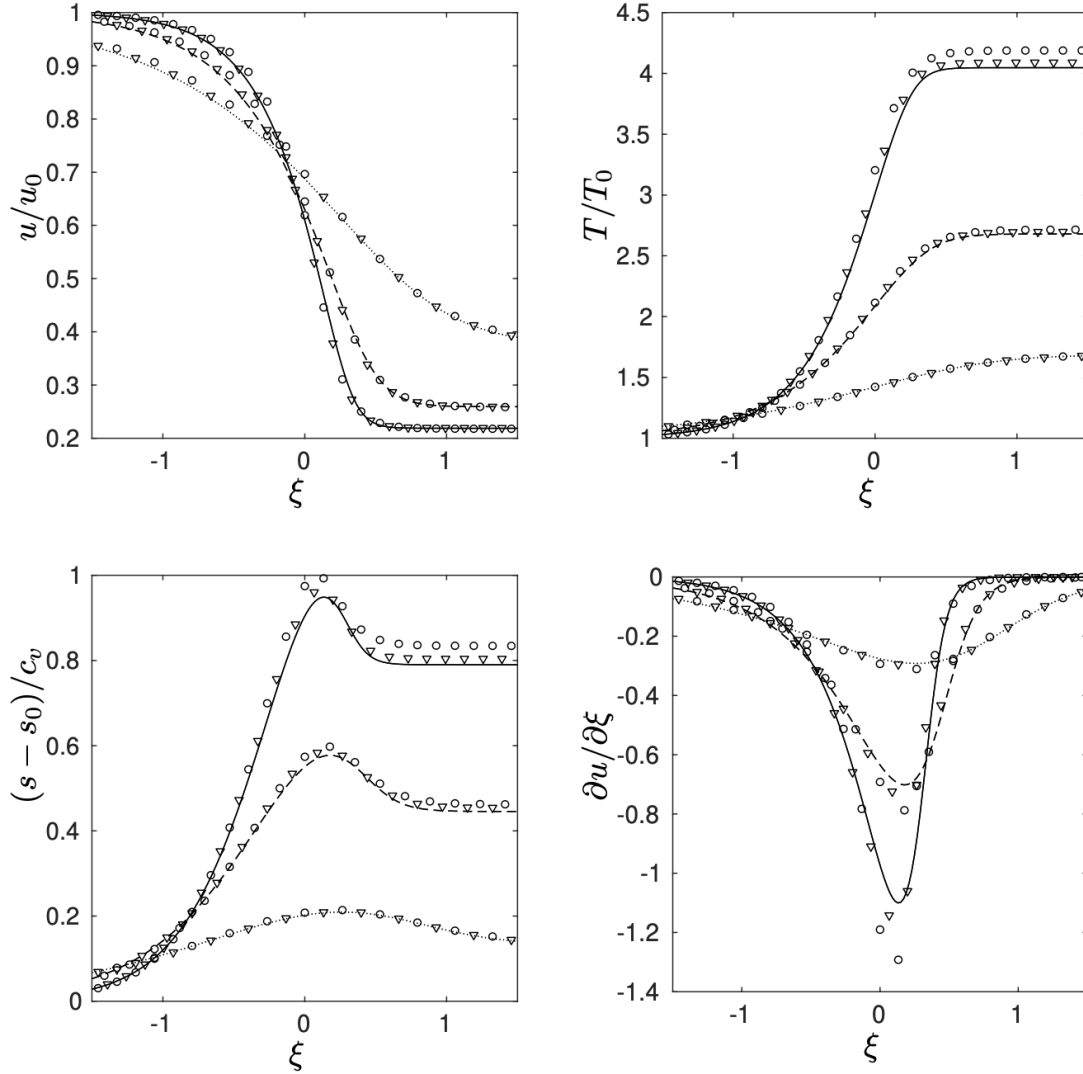


Figure 6.6. – Shock inner structure for different values of Ma . Solid, dashed and dotted lines are analytical solutions [175] for respectively $Ma = 4, 3, 2$. Triangles and circles markers corresponds to numerical solutions with $Re = 1000, 2000$.

Normalized velocity, temperature, entropy and stress profiles near the shock are respectively plotted in Fig. 6.6 and Fig. 6.7 for different Mach numbers, different adiabatic exponents, $\sigma = 1.0$ and a maximum local CFL of 0.2. Because the normalized thickness of the shock depends on the mean free path Eq. (6.45), the number of points

N_0 plotted in Fig 6.6-6.7 is not fixed and is given by

$$N_0 = \frac{12}{5 \times 10^{-4}} \sqrt{\frac{8\gamma}{\pi}} \frac{\text{Ma}}{\text{Re}}, \quad (6.46)$$

which corresponds in our simulations to $N_0 \in [60, 180]$.

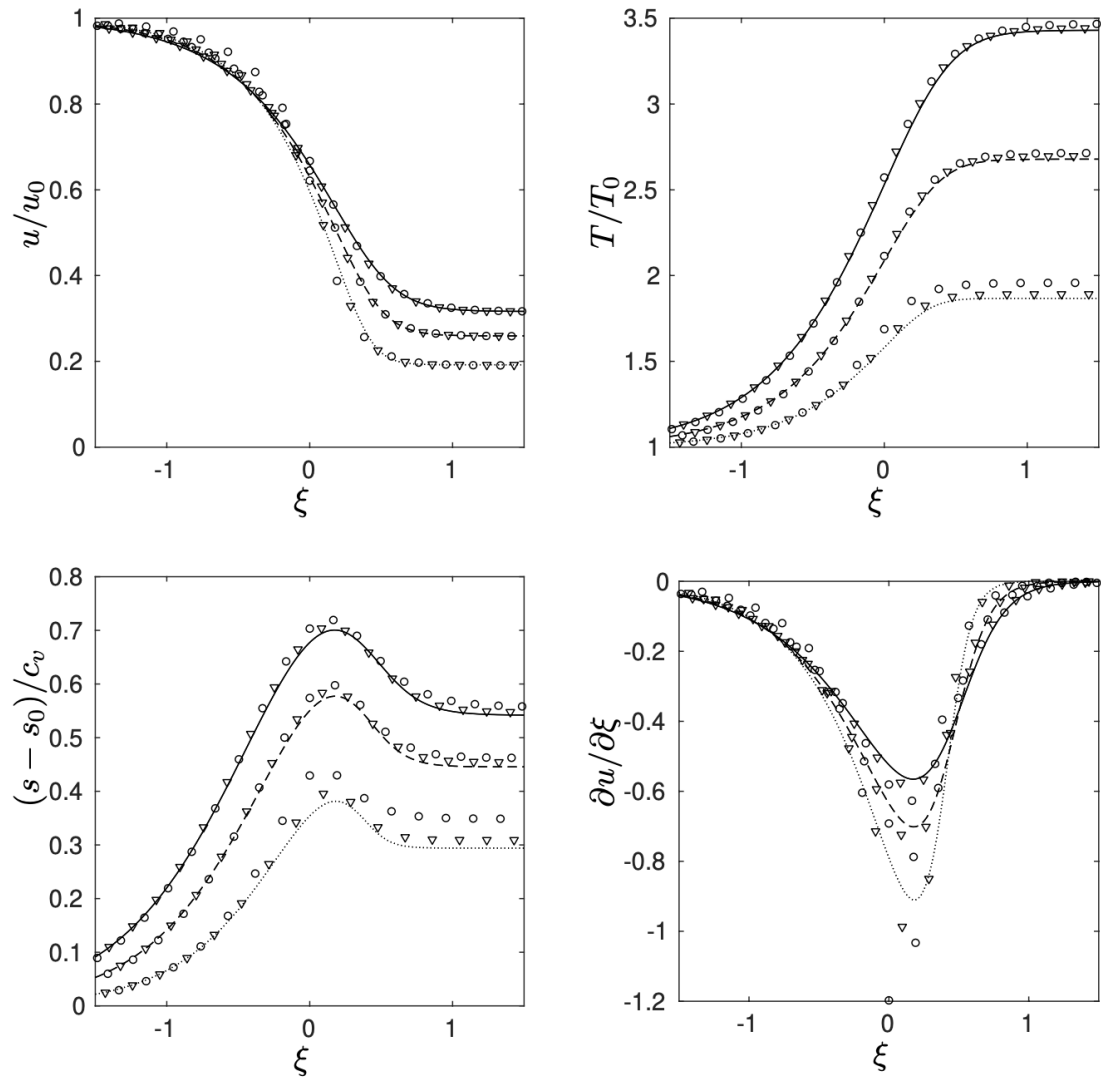


Figure 6.7. – Shock inner structure for different values of γ . Solid, dashed and dotted lines are analytical solutions [175] for respectively $\gamma = 1.6, 1.4, 1.2$. Triangles and circles markers corresponds to numerical solutions with $\text{Re} = 1000, 2000$.

In Fig 6.6 we see that an increase of Re , equivalent to reducing the non-normalized thickness of the shock without changing the jumps, demean the accuracy of the results by coarsening the grid. An higher Ma increases both the number of points inside the shock but also the jumps of physical fields such that the overall effect seems to be

a decrease of accuracy. A decrease of γ reduces both the number of points and the thickness of the shock, leading to a decrease of accuracy. These defects are attributed to numerical errors mainly coming from the wrong entropy jumps, see Sec. 5.1.

6.3.6. One-dimensional shock tube

Here the present model is assessed on a classical 1D Riemann problem. Because we have seen in Sections 5.1 and 6.3.5 that our model was not suitable for too high Mach numbers, a simplified Sod-like [24] shock tube is initialized similarly to [75] with a left state $(\rho_L, u_L, p_L) = (1, 0, 1)$ and a right state $(\rho_R, u_R, p_R) = (3, 0, 3)$ in a domain of total length $L = 1$ with an initial discontinuity located at $x = 0.5$. This test case presents sufficiently small jumps such that even entropy equation leads to sufficiently accurate results. This domain is discretized by 400 points, the time-step is related to the space increment through $\frac{\Delta t}{\Delta x} = 0.2582$, the other parameters are $\gamma = 1.4$, $\sigma = 1$, $\mu = 10^{-15}$. After 350 timesteps the solution is plotted in Fig. 6.8, showing from left to right a shock wave, a slip line and an expansion wave computed with the present model (dashed line). The reference solution was obtained with a classical first order HLLC [24] (solid line) solver using with 10^4 points. Agreement is very good: beside a small overshoot at the contact interface, the different levels are well captured.

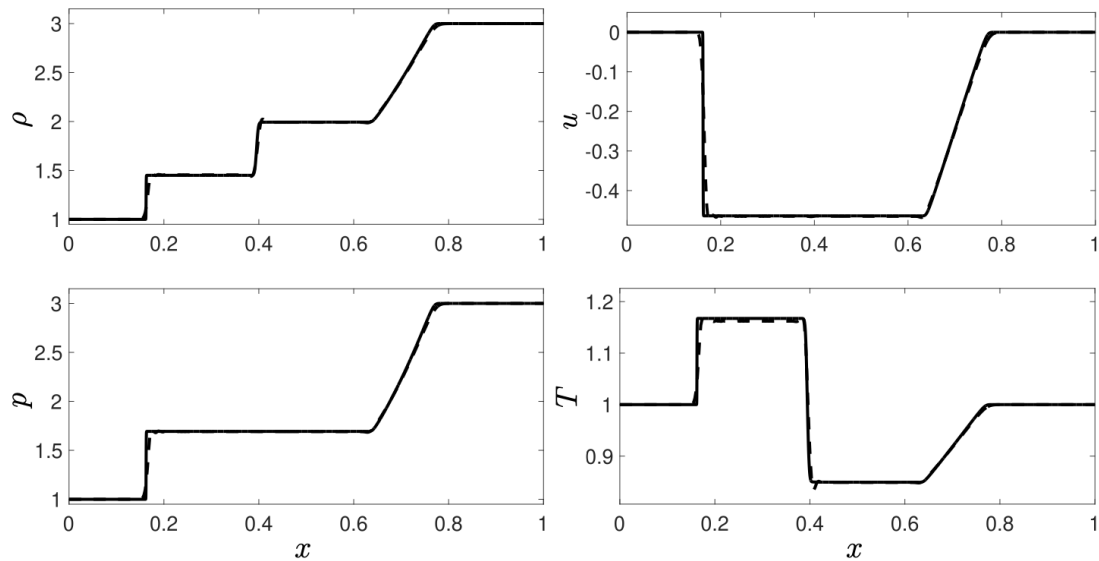


Figure 6.8. – Sod-like shock tube solution. Density, velocity, pressure and temperature profiles as obtained with the hybrid recursive regularized p model (dashed) and reference (solid).

6.3.7. Shock-Vortex interaction

The present model is finally assessed on an unsteady, viscous, compressible flow consisting of the interaction of a stationary shock wave with an isentropic vortex. The

mean field is defined by the Mach number of the shock, M_s , and the left and right initial states are solution of the Rankine-Hugoniot problem,

$$\frac{\rho_R}{\rho_L} = \frac{u_L}{u_R} = \frac{(\gamma + 1)M_s^2}{(\gamma - 1)M_s^2 + 2}, \quad (6.47)$$

$$\frac{p_R}{p_L} = 1 + \frac{2\gamma}{(\gamma + 1)}(M_s^2 - 1). \quad (6.48)$$

Then, an isentropic vortex, as already defined in a previous validation, is superimposed in the upstream region. The vortex will cross the shock and create a complex pattern of pressure waves that will be compared to a reference solution [176]. Physical parameters are set to $M_s = 1.2$, $M_v = 0.25$, $\gamma = 1.4$, $Re = 800$, $Pr = 0.75$, $p_L = 1.0$, $T_L = 1.0$, $u_L = M_s\sqrt{\gamma}$, which corresponds to "case C" in the reference solution [176]. The computational domain is $[0, 28] \times [0, 24]$, discretized by a 1120×960 mesh, shock and vortex positions are respectively $x_s = 8$ and $(x_c, y_c) = (6, 12)$. Numerical parameters were set to $CFL = 0.87$ and $\sigma = 0.7$ where the CFL was based on the upstream region. Instantaneous density fields during the simulation are shown in Fig. 6.9. Nor-

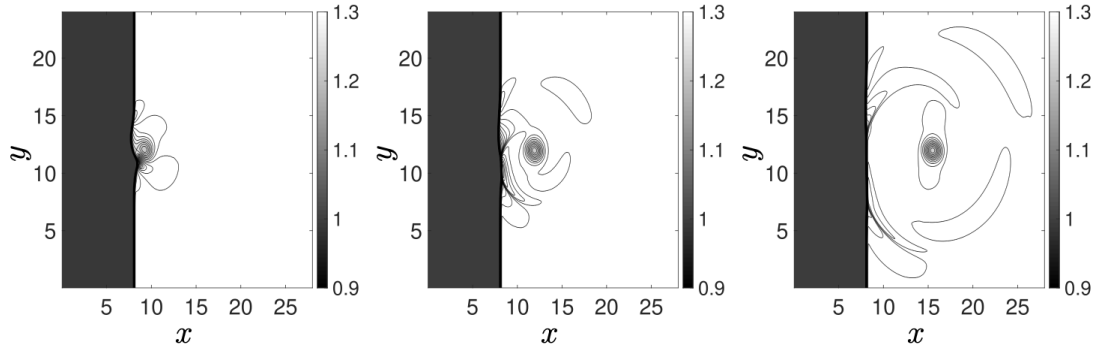


Figure 6.9. – Density field for the shock-vortex interaction at $t = 3T$ (left), $t = 6T$ (center), $t = 10T$ (right).

malized pressure $\Delta p = \frac{p - p_R}{p_R}$ is then plotted on Fig. 6.10 along a radial cut of fixed angle $\theta = -45^\circ$ for $t = 6T$, $t = 8T$ and $t = 10T$ where we defined $T = \frac{R}{c_R}$ as the characteristic convective time of the vortex in the shocked region, showing very little difference with the reference 4th/6th order time/spatial accuracy solution [176]. Precursor and second sound are also plotted on Fig. 6.11 and compared to [176], showing again a good agreement.

6.4. Recap

In this Chapter, a new pressure-based hybrid regularized LBM, referred to as hybrid recursive regularized p model, has been presented, for the simulation of shocked compressible flows for Mach numbers ranging from 0 to 1.2. It is based on a fully explicit segregated approach for the pressure, preserving the robustness of classical

6. Pressure-based lattice-Boltzmann model – 6.4. Recap

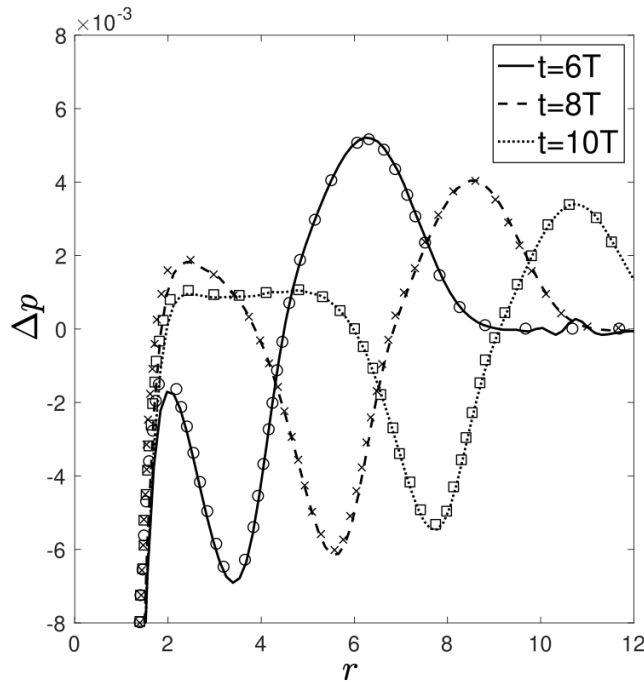


Figure 6.10. – Radial cut at $\theta = -\pi/4$ of the pressure variation Δp . Lines correspond to the present Lattice-Boltzmann solution and symbols denote the reference solution [176].

athermal LBM via the predictor step. Through a variety of numerical experiments, we systematically validated (i) the Eulerian part of the system, via convection tests of the three linearized Euler eigenmodes, (ii) the diffusive and viscous terms, through thermal Couette flows simulations, and (iii) the method’s robustness and accuracy, through a 2D example of shock - vortex interactions.

A theoretical investigation of the proposed solver was conducted in Sec. 6.2 and showed in Table 6.1 that the consistency defects of the model were better fitted for compressible simulations when compared to the previous ρ -based model, see Sec. 4.5.

Additionally, the traceless collision kernel is introduced, it corresponds to the regularization of the trace of the stress tensor, which is supposed to be 0 but is polluted by a non-hydrodynamic mode which is therefore filtered by the newly proposed kernel.

Note that the present p -based model was also successfully implemented and validated for humid air with phase changes [177], academical combustion [178], LES turbulent flame [179] and seems to exhibited advantageous computational efficiency [21] compared to some traditional CFD solvers, at least in the domain of combustion.

More important than numerical validations, this section showed us – mainly throughout the completely unusual Eq. (6.15) – that the traditional kinetic-led lattice-Boltzmann guideline was not the sole one to be able to design new efficient lattice-Boltzmann schemes. The present scheme and its correction step Eq. (6.15) are purely stemming from a FD interpretation of the lattice-Boltzmann scheme. In the next chapter, we will see how *a priori* completely different lattice-Boltzmann models – ρ and p based –

6. Pressure-based lattice-Boltzmann model – 6.4. Recap

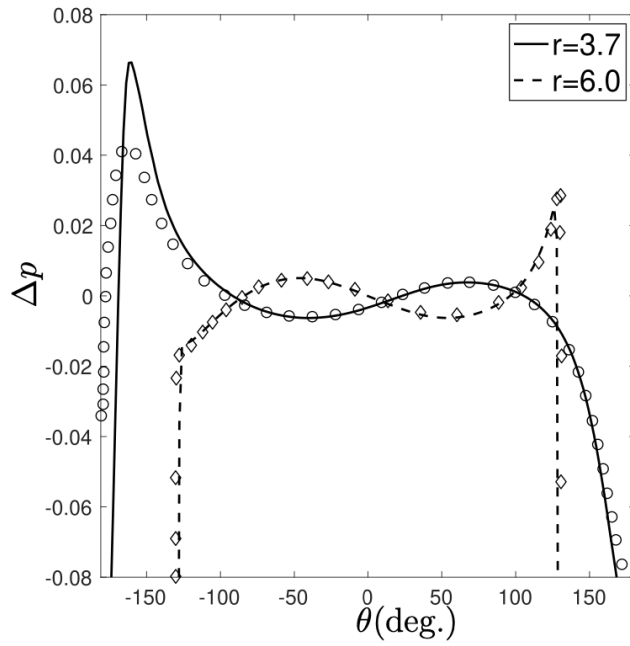


Figure 6.11. – Circumferential pressure variation at $t = 6T$. Solid line corresponds to $r = 3.7$ and dashed line to $r = 6$. Markers refers to the corresponding reference solution [176].

could be bridged into a unified formalism.

7. Unified model, bridging between pressure-based and density-based methods

This Chapter mainly follows the content of:

G. Farag, T. Coratger, G. Wissocq, S. Zhao, P. Boivin and P. Sagaut. A unified hybrid lattice-Boltzmann method for compressible flows: Bridging between pressure-based and density-based methods. *Physics of Fluids*, 2021.

<https://doi.org/10.1063/5.0057407>

Sommaire

7.1	Hybrid recursive regularized lattice Boltzmann models	129
7.1.1	Forceless p -based model	129
7.1.2	Forceless improved- ρ -based model	130
7.1.3	Forceless model comparison	131
7.1.4	Non-equilibrium definition in p -based	133
7.1.5	Consistent BGK p -based	135
7.1.6	Comparison accounting for force terms	135
7.2	Unified model on standard lattice	137
7.2.1	Unified LB scheme	138
7.2.2	Interpretation of δ_{0i}	140
7.2.3	Coupled models	141
7.2.3.1	Thermal coupling	142
7.2.3.2	Non-equilibrium reconstruction	142
7.2.3.3	Force term discretization	143
7.2.3.4	Sensor, artificial bulk viscosity	143
7.2.4	Step-by-step unified scheme	144
7.3	Numerical validations	145
7.3.1	Isentropic vortex	145
7.3.2	Entropy spot	147
7.3.3	Thermal Couette flow	149
7.3.4	2D Riemann problems	149
7.3.5	Compressible double shear layer	151
7.3.6	Shock-vortex interaction	151
7.3.7	Shock-entropy spot interaction	153
7.4	Recap	156

7. Unified model, bridging between pressure-based and density-based methods – 7.1. Hybrid recursive regularized lattice Boltzmann models

A few months after publication of the p -based model [76], a new ρ -based model was proposed by Guo *et al* [149]. This new "improved- ρ -based" model represents a huge step towards the achievement of an high Mach lattice-Boltzmann solver as it was shown to be stable for the isentropic vortex up to a Mach 4 advection.

The purpose of the present chapter is twofold. First, it is proved by theoretical analysis in Sec. 7.1 that segregated p -based and improved- ρ -based regularized collision models are strictly identical in the absence of forcing terms, and therefore can be interpreted as implementation variants of the the same method, which can be re-expressed as a ρ -based method. Then, a unified general formulation that encompasses both segregated p -based and ρ -based along with forcing terms is then given in Sec. 7.2. An important associated result is that differences between preexisting classical ρ -based, p -based and improved- ρ -based methods simply lies in different third and fourth order equilibrium moments and different isotropy force correction strategies. An optimal formulation of the correction forcing terms is proposed along with some additional stabilization techniques.

This unified method, which appears as a modified ρ -based method, is assessed considering a wide set of test cases in Sec. 7.3.

7.1. Hybrid recursive regularized lattice Boltzmann models

In this section, we thoroughly compare the p -based and improved- ρ -based models applied to a regularized kernel. First, we perform a comparison of the pure LB schemes without forcing term. Specifying the equation of state (EOS) is unnecessary at this point as long as the compared schemes employed the same strategy, which is our assumption in what follows. Therefore, for the sake of generality, the normalized temperature $\theta = rT/c_s^2$ can be updated from any EOS without any impact on the present demonstration. The classical EOS choice in LBM is athermal [4] $\theta = 1$, however, as it was demonstrated in Sec. 4.3, it leads to a Mach enslaved to CFL number. A way to circumvent this problem is to use the generalized athermal [82, 120] $\theta = (\Delta x \text{CFL})^2 / [(\Delta t(\text{Ma} + 1)c_s)^2 \gamma]$ or directly the ideal gas equation [74] $p = \rho c_s^2 \theta$.

7.1.1. Forceless p -based model

Full details of this model can be found in [76]. The numerical algorithm is summarized as follows. For regularized kernels, a restricted number of variables is sufficient to describe the system, therefore, the initial solution of the simulation is characterized by $[\rho, \rho u_\alpha, \theta, \Pi_{\alpha\beta}^{neq}](t, \mathbf{x})$. In order to get the updated solution $[\rho, \rho u_\alpha, \theta, \Pi_{\alpha\beta}^{neq}](t + \Delta t, \mathbf{x})$, several steps should be performed :

7. Unified model, bridging between pressure-based and density-based methods – 7.1.
Hybrid recursive regularized lattice Boltzmann models

- The p -based equilibrium distribution $f_i^{p,eq}$ is reconstructed from (t, \mathbf{x}) moments

$$f_i^{p,eq}(t, \mathbf{x}) = \omega_i \left\{ \mathcal{H}^{(0)} \rho \theta + \frac{\mathcal{H}_{i\alpha}^{(1)}}{c_s^2} \rho u_\alpha + \frac{\mathcal{H}_{i\alpha\beta}^{(2)}}{2c_s^4} [\rho u_\alpha u_\beta] + \frac{\mathcal{H}_{i\gamma}^{(3r)}}{6c_s^6} a_\gamma^{(3r)} \right\} (t, \mathbf{x}), \quad (7.1)$$

with $a_{\alpha\beta\gamma}^{(3)} = \rho u_\alpha u_\beta u_\gamma$ serving to define $a_\gamma^{(3r)}$ as in Appendix A.

- The non-equilibrium distribution $\bar{f}_i^{neq}(t, \mathbf{x})$ is also reconstructed from moments $[\rho, \rho u_\alpha, \Pi_{\alpha\beta}^{neq}] (t, \mathbf{x})$ using either the projected [115] or recursive [72, 119] regularization.
- Collision and streaming are performed,

$$f_i^{p,col}(t, \mathbf{x}) = f_i^{p,eq}(t, \mathbf{x}) + \left(1 - \frac{\Delta t}{\tau}\right) \bar{f}_i^{neq}(t, \mathbf{x}), \quad (7.2)$$

$$\bar{f}_i^p(t + \Delta t, \mathbf{x}) = f_i^{p,col}(t, \mathbf{x} - \mathbf{c}_i \Delta t). \quad (7.3)$$

- Then the macroscopic reconstruction reads

$$\rho(t + \Delta t, \mathbf{x}) = \sum_{i=0}^{q-1} \bar{f}_i^p(t + \Delta t, \mathbf{x}) + \rho(t, \mathbf{x}) [1 - \theta(t, \mathbf{x})]. \quad (7.4)$$

$$\rho u_\alpha(t + \Delta t, \mathbf{x}) = \sum_{i=0}^{q-1} c_{i\alpha} \bar{f}_i^p(t + \Delta t, \mathbf{x}), \quad (7.5)$$

$$\Pi_{\alpha\beta}^{\bar{f}^{neq}}(t + \Delta t, \mathbf{x}) = \sum_{i=0}^{q-1} c_{i\alpha} c_{i\beta} \left[\bar{f}_i^p - f_i^{p,eq} \right] (t + \Delta t, \mathbf{x}), \quad (7.6)$$

- To close the system, a finite difference scheme is used to update an additional thermodynamic variable such as entropy [74–76] or total energy [140]. From this additional step, $\theta(t + \Delta t, \mathbf{x})$ is now updated.

Then, one can apply recursively this algorithm from time (t, \mathbf{x}) to time $(t + \Delta t, \mathbf{x})$. This scheme therefore provides the regularized p -based numerical solution $\forall t = N_t \Delta t$ with $N_t \in \mathbb{N}$.

7.1.2. Forceless improved- ρ -based model

In this model [149] a free parameter Θ was introduced. This parameter will be addressed later, but in the present Section we consider the case $\Theta = 0$. Similarly to the p -based algorithm, the initial solution $[\rho, \rho u_\alpha, \theta, \Pi_{\alpha\beta}^{neq}] (t, \mathbf{x})$ is known. In order to get the updated solution $(t + \Delta t, \mathbf{x})$ using the regularized improved- ρ -based model, one should perform the following steps,

7. Unified model, bridging between pressure-based and density-based methods – 7.1.
Hybrid recursive regularized lattice Boltzmann models

- Compute the equilibrium population,

$$f_i^{\rho,eq}(t, \mathbf{x}) = \omega_i \left\{ \mathcal{H}^{(0)} \rho + d_i + \frac{\mathcal{H}_{i\alpha}^{(1)}}{c_s^2} \rho u_\alpha + \frac{\mathcal{H}_{i\alpha\beta}^{(2)}}{2c_s^4} [\rho u_\alpha u_\beta] + \frac{\mathcal{H}_{i\gamma}^{(3r)}}{6c_s^6} a_\gamma^{(3r)} \right\} (t, \mathbf{x}), \quad (7.7)$$

with $a_{\alpha\beta\gamma}^{(3)} = \rho u_\alpha u_\beta u_\gamma$ serving to define $a_\gamma^{(3r)}$ as in Appendix A and with d_i defined as

$$d_i = \begin{cases} \rho[\theta - 1] & \text{if } i \neq 0 \\ \frac{\omega_0 - 1}{\omega_0} \rho[\theta - 1] & \text{if } i = 0 \end{cases} \quad (7.8)$$

with ω_0 the lattice weight for the non-moving population $i = 0$.

- The non-equilibrium population \bar{f}_i^{neq} is computed from a regularized collision kernel [72, 115, 119].
- Collision and streaming are performed

$$f_i^{\rho,col}(t, \mathbf{x}) = f_i^{\rho,eq}(t, \mathbf{x}) + \left(1 - \frac{\Delta t}{\bar{\tau}}\right) \bar{f}_i^{neq}(t, \mathbf{x}), \quad (7.9)$$

$$\bar{f}_i^\rho(t + \Delta t, \mathbf{x}) = f_i^{\rho,col}(t, \mathbf{x} - \mathbf{c}_i \Delta t). \quad (7.10)$$

- The macroscopic reconstruction reads

$$\rho(t + \Delta t, \mathbf{x}) = \sum_{i=0}^{q-1} \bar{f}_i^\rho(t + \Delta t, \mathbf{x}). \quad (7.11)$$

$$\rho u_\alpha(t + \Delta t, \mathbf{x}) = \sum_{i=0}^{q-1} c_{i\alpha} \bar{f}_i^\rho(t + \Delta t, \mathbf{x}), \quad (7.12)$$

$$\Pi_{\alpha\beta}^{\bar{f}^{neq}}(t + \Delta t, \mathbf{x}) = \sum_{i=0}^{q-1} c_{i\alpha} c_{i\beta} \left[\bar{f}_i^\rho - f_i^{\rho,eq} \right] (t + \Delta t, \mathbf{x}). \quad (7.13)$$

- Similarly to the p -based model, to close the system an additional thermodynamic variable is solved through a finite difference scheme, which is sufficient to get $\theta(t + \Delta t, \mathbf{x})$.

This algorithm can be used to update the numerical solution from (t, \mathbf{x}) to $(t + \Delta t, \mathbf{x})$. Applying this procedure recursively finally leads to the regularized improved- ρ -based numerical solution $\forall t = N_t \Delta t$ with $N_t \in \mathbb{N}$.

7.1.3. Forceless model comparison

We now prove that it is possible to bridge between the p -based model (Sec. 7.1.1) and the improved- ρ -based model (Sec. 7.1.2). Starting from the latter, we inject Eq. (7.8)

7. Unified model, bridging between pressure-based and density-based methods – 7.1.
Hybrid recursive regularized lattice Boltzmann models

inside Eq. (7.7), using the p -based equilibrium definition Eq. (7.1) leading to

$$f_i^{\rho,eq}(t, \mathbf{x}) = \begin{cases} f_i^{p,eq}(t, \mathbf{x}) & \text{if } i \neq 0 \\ f_i^{p,eq}(t, \mathbf{x}) - \rho(t, \mathbf{x})[\theta(t, \mathbf{x}) - 1] & \text{if } i = 0 \end{cases} \quad (7.14)$$

To allow for a fair comparison, we assume that i) both models start from the same initial solution and ii) the collision kernel is a function of the initial moments. Considering the initial solution $[\rho, \rho u_\alpha, \Pi_{\alpha\beta}^{neq}](t, \mathbf{x})$, this means that the reconstructed non-equilibrium term \bar{f}_i^{neq} is identical between both models because it has been reconstructed from the same initial condition, with the same procedure. For example, the recursive regularization could be used,

$$\bar{f}_i^{neq} = \omega_i \left\{ \frac{\mathcal{H}_{i\alpha\beta}^{(2)}}{2c_s^4} \Pi_{\alpha\beta}^{\bar{f}^{neq},(2)} + \frac{\mathcal{H}_{i\gamma}^{(3r)}}{6c_s^6} \Pi_{\gamma}^{\bar{f}^{neq},(3r)} \right\}, \quad (7.15)$$

with $\Pi_{\alpha\beta\gamma}^{\bar{f}^{neq},(3)} = u_\alpha \Pi_{\beta\gamma}^{\bar{f}^{neq},(2)} + u_\beta \Pi_{\gamma\alpha}^{\bar{f}^{neq},(2)} + u_\gamma \Pi_{\alpha\beta}^{\bar{f}^{neq},(2)}$ serving to define $\Pi_{\gamma}^{\bar{f}^{neq},(3r)}$ as in Appendix A which clearly shows that choosing the same initial solution $[\rho, \rho u_\alpha, \Pi_{\alpha\beta}^{neq}](t, \mathbf{x})$ trivially leads to $\bar{f}_i^{p,neq} = \bar{f}_i^{\rho,neq}$ in this case. Using both Eq. (7.14) and the equivalence between non-equilibrium populations allows us to write

$$f_i^{\rho,col} = \begin{cases} f_i^{p,col}(t, \mathbf{x}) & \text{if } i \neq 0, \\ f_i^{p,col}(t, \mathbf{x}) - \rho(t, \mathbf{x})[\theta(t, \mathbf{x}) - 1] & \text{if } i = 0, \end{cases} \quad (7.16)$$

This equation established a formal link between collided populations Eqs. (7.2,7.9). Now that collision was analyzed, the streaming step of both models can be linked using Eq. (7.10,7.16),

$$\bar{f}_i^{\rho}(t + \Delta t, \mathbf{x}) = \begin{cases} \bar{f}_i^p(t + \Delta t, \mathbf{x}) & \text{if } i \neq 0 \\ \bar{f}_i^p(t + \Delta t, \mathbf{x}) - \rho(t, \mathbf{x})[\theta(t, \mathbf{x}) - 1] & \text{if } i = 0 \end{cases} \quad (7.17)$$

Here, it is important noticing the temporal evaluation " t " of the $\rho[\theta - 1]$ term. This comes from the non-moving $i = 0$ population, which means that

$$\bar{f}_0^{\rho}(t + \Delta t, \mathbf{x}) = f_0^{\rho,col}(t, \mathbf{x}) = f_0^{p,col}(t, \mathbf{x}) - \rho(t, \mathbf{x})[\theta(t, \mathbf{x}) - 1] \quad (7.18)$$

7. Unified model, bridging between pressure-based and density-based methods – 7.1.
Hybrid recursive regularized lattice Boltzmann models

Injecting Eq. (7.17) inside Eqs. (7.11-7.13) and using the fact that $c_{0\alpha} = 0$ leads to

$$\rho(t + \Delta t, \mathbf{x}) = \sum_{i=0}^{q-1} \bar{f}_i^p(t + \Delta t, \mathbf{x}) + \rho(t, \mathbf{x})[1 - \theta(t, \mathbf{x})], \quad (7.19)$$

$$\rho u_\alpha(t + \Delta t, \mathbf{x}) = \sum_{i=0}^{q-1} c_{i\alpha} \bar{f}_i^p(t + \Delta t, \mathbf{x}), \quad (7.20)$$

$$\Pi_{\alpha\beta}^{\bar{f}^{neq}}(t + \Delta t, \mathbf{x}) = \sum_{i=0}^{q-1} c_{i\alpha} c_{i\beta} [\bar{f}_i^p - f_i^{p,eq}](t + \Delta t, \mathbf{x}). \quad (7.21)$$

Which is exactly identical to Eqs. (7.4-7.6). Therefore, from the initial solution $[\rho, \rho u_\alpha, \Pi_{\alpha\beta}^{neq}](t, \mathbf{x})$, both the p -based and the improved- ρ -based lead to the same updated solution $[\rho, \rho u_\alpha, \Pi_{\alpha\beta}^{neq}](t + \Delta t, \mathbf{x})$. In other words, the hybrid recursive regularized p -based model [76] and improved- ρ -based model [149] are strictly equivalent in the absence of force terms and other coupled physical models. Next, we highlight how a similar bridge can also be obtained for more classical models than the regularized one. Out of simplicity, we chose to demonstrate it on the BGK collision kernel. Before doing so, we shall highlight the fundamental point of how the p -model differs from more classical ρ -based models.

7.1.4. Non-equilibrium definition in p -based

The equivalence between models was obtained by a straight comparison of the numerical schemes corresponding to the p -based model (Sec. 7.1.1) and the improved- ρ -based model (Sec. 7.1.2). In this demonstration it was implicitly assumed that the whole numerical solution can be summarized by the knowledge of moments $[\rho, \rho u_\alpha, \theta, \Pi_{\alpha\beta}^{neq}]$, which is true for regularized collisions [72, 115]. However, for other kernels, higher order moments ($\Pi_{\alpha\beta\gamma}, \Pi_{\alpha\beta\gamma\delta}, \dots$) should also be considered. Here, we provide a general demonstration of the equivalence between the two models presented in Sections 7.1.2 and 7.1.1 on the BGK collision kernel. This collision kernel is the simplest one in which the knowledge of moments $[\rho, \rho u_\alpha, \theta, \Pi_{\alpha\beta}^{neq}]$ is insufficient to reconstruct the complete numerical solution for an arbitrary lattice. The following demonstration could be trivially generalized to other collision models involving more moments than regularized ones. First, let us notice that in classical LB models, mass conservation requires

$$\sum_{i=0}^{q-1} [\bar{f}_i - f_i^{eq}] = 0. \quad (7.22)$$

As a consequence, classically, second order non-equilibrium raw $\Pi_{\alpha\beta}^{neq}$ and Hermite $a_{\alpha\beta}^{neq}$ moments follow

$$\Pi_{\alpha\beta}^{neq} = a_{\alpha\beta}^{neq}. \quad (7.23)$$

7. Unified model, bridging between pressure-based and density-based methods – 7.1.
Hybrid recursive regularized lattice Boltzmann models

On the contrary, in p -based model, because of Eq. (7.4), the definition of the updated density can be recast as

$$\sum_{i=0}^{q-1} (\bar{f}_i^p - f_i^{p,eq})(t, \mathbf{x}) + [\rho(t, \mathbf{x})(\theta(t, \mathbf{x}) - 1) - \rho(t - \Delta t, \mathbf{x})(\theta(t - \Delta t, \mathbf{x}) - 1)] = 0, \quad (7.24)$$

or equivalently,

$$\sum_{i=0}^{q-1} \left\{ (\bar{f}_i^p - f_i^{p,eq})(t, \mathbf{x}) + \delta_{i0} [\rho(t, \mathbf{x})(\theta(t, \mathbf{x}) - 1) - \rho(t - \Delta t, \mathbf{x})(\theta(t - \Delta t, \mathbf{x}) - 1)] \right\} = 0, \quad (7.25)$$

where δ_{i0} is a Kroenecker symbol. A comparison of this last equation with Eq. (7.22) pleads for a different definition of p -based non-equilibrium distribution. Instead of the classical $\bar{f}_i^p - f_i^{p,eq}$, non-equilibrium distribution can now be defined as

$$\begin{aligned} \bar{f}_i^{p,neq}(t, \mathbf{x}) &= (\bar{f}_i^p - f_i^{p,eq})(t, \mathbf{x}) \\ &+ \delta_{i0} [\rho(t, \mathbf{x})(\theta(t, \mathbf{x}) - 1) - \rho(t - \Delta t, \mathbf{x})(\theta(t - \Delta t, \mathbf{x}) - 1)]. \end{aligned} \quad (7.26)$$

This definition of the non-equilibrium verifies

$$\Pi_{\alpha\beta}^{neq} = \sum_{i=0}^{q-1} c_{i\alpha} c_{i\beta} \bar{f}_i^{p,neq} = \sum_{i=0}^{q-1} \mathcal{H}_{i\alpha\beta}^{(2)} \bar{f}_i^{p,neq} = a_{\alpha\beta}^{neq}. \quad (7.27)$$

However, in either [76] or Sec. 7.1.1, Eq. (7.26) was never used. Instead, raw and Hermite moments classically read in p -based as

$$\sum_{i=0}^{q-1} \mathcal{H}_{i\alpha\beta}^{(2)} [\bar{f}_i^p - f_i^{p,eq}] \neq \sum_{i=0}^{q-1} c_{i\alpha} c_{i\beta} [\bar{f}_i^p - f_i^{p,eq}]. \quad (7.28)$$

This does not seem to be consistent with Eq. (7.23). This ambiguity is eliminated by noting that the computation of both $a_{\alpha\beta}^{neq}$ and $\Pi_{\alpha\beta}^{neq}$ is unnecessary in regularized LB algorithms, only raw moments $\Pi_{\alpha\beta}^{neq}$ are necessary. Therefore, defining Hermite moments from raw moments $a_{\alpha\beta}^{neq} \equiv \Pi_{\alpha\beta}^{neq}$ as in both [137] and Sec. 7.1.1 or traceless second order Hermite moments $a_{\alpha\beta}^{neq} \equiv \sum_{i=0}^{q-1} [c_{i\alpha} c_{i\beta} - \frac{\delta_{\alpha\beta}}{3} c_{i\gamma} c_{i\gamma}] (\bar{f}_i - f_i^{eq})$ as in [76] instead of Hermite moments allows to bypass the unusual definition Eq. (7.26). Instead, the non-equilibrium remains defined as

$$\bar{f}_i^{p,neq}(t, \mathbf{x}) \equiv (\bar{f}_i^p - f_i^{p,eq})(t, \mathbf{x}). \quad (7.29)$$

With the natural definition of non-equilibrium Eq. (7.26) for an arbitrary kernel, let us try to compare our two models using the more classical BGK collision kernel, in which Eq. (7.26) would lead to inconsistent results.

7. Unified model, bridging between pressure-based and density-based methods – 7.1.
Hybrid recursive regularized lattice Boltzmann models

7.1.5. Consistent BGK p -based

A p -based model equipped with non-equilibrium Eq. (7.26) reads

$$\begin{aligned} \bar{f}_i^p(t + \Delta t, \mathbf{x}) = & f_i^{eq,p}(t, \mathbf{x} - \mathbf{c}_i \Delta t) + \left(1 - \frac{\Delta t}{\tau + \Delta t/2}\right) \left\{ \bar{f}_i^p(t, \mathbf{x} - \mathbf{c}_i \Delta t) - f_i^{eq,p}(t, \mathbf{x} - \mathbf{c}_i \Delta t) \right. \\ & \left. - \delta_{0i} [\rho(\theta - 1)](t - \Delta t, \mathbf{x}) - [\rho(\theta - 1)](t, \mathbf{x}) \right\}. \end{aligned} \quad (7.30)$$

Then, by adding on both sides $-\delta_{0i}[\rho(\theta - 1)](t, \mathbf{x})$ we get,

$$\begin{aligned} \bar{f}_i^p(t + \Delta t, \mathbf{x}) - \delta_{0i}[\rho(\theta - 1)](t, \mathbf{x}) = & f_i^{eq,p}(t, \mathbf{x} - \mathbf{c}_i \Delta t) - \delta_{0i}[\rho(\theta - 1)](t, \mathbf{x}) \\ & + \left(1 - \frac{\Delta t}{\tau + \Delta t/2}\right) \left\{ \bar{f}_i^p(t, \mathbf{x} - \mathbf{c}_i \Delta t) - f_i^{eq,p}(t, \mathbf{x} - \mathbf{c}_i \Delta t) \right. \\ & \left. - \delta_{0i} [\rho(\theta - 1)](t - \Delta t, \mathbf{x}) - [\rho(\theta - 1)](t, \mathbf{x}) \right\}. \end{aligned} \quad (7.31)$$

Using definitions Eqs. (7.14), (7.17) we finally get

$$\bar{f}_i^p(t + \Delta t, \mathbf{x}) = f_i^{eq,\rho}(t, \mathbf{x} - \mathbf{c}_i \Delta t) + \left(1 - \frac{\Delta t}{\tau + \Delta t/2}\right) \left\{ \bar{f}_i^p(t, \mathbf{x} - \mathbf{c}_i \Delta t) - f_i^{eq,\rho}(t, \mathbf{x} - \mathbf{c}_i \Delta t) \right\}, \quad (7.32)$$

with the equilibrium defined as Eq. (7.7), which is nothing else than the improved- ρ -based model equipped with a BGK collision kernel. This definition formally proves the exact equivalence between improved- ρ -based and a p -based equipped by Eq. (7.26) on BGK collision kernel.

7.1.6. Comparison accounting for force terms

Having demonstrated the equivalence in the absence of force corrective terms in the previous section, it is natural to infer that the force terms of both models should be equivalent up to negligible errors. We denote the corrective force term associated with p -based or improved- ρ -based models by $F_i^{p,\rho}$. From [76] and [149] we find that,

$$F_i^{p,\rho} = \omega_i \frac{\mathcal{H}_{i\alpha\beta}^{(2)}}{2c_s^4} \left[a_{\alpha\beta}^C + a_{\alpha\beta}^{p,\rho} \right], \quad (7.33)$$

where $a_{\alpha\beta}^C$ is the lattice dependent component of the force term shared by both models,

$$a_{\alpha\beta}^C = c_s^2 \left[u_\alpha \frac{\partial \rho(1 - \theta)}{\partial x_\beta} + u_\beta \frac{\partial \rho(1 - \theta)}{\partial x_\alpha} \right] - \frac{\partial D_{\alpha\beta\gamma}^{f^{eq,(3)}}}{\partial x_\gamma}, \quad (7.34)$$

7. Unified model, bridging between pressure-based and density-based methods – 7.1.
Hybrid recursive regularized lattice Boltzmann models

For the D3Q19 basis (see Appendix A) which is the lattice we used,

$$\frac{\partial D_{\alpha\beta\gamma}^{f^{eq,(3)}}}{\partial x_\gamma} = \delta_{\alpha\beta} \frac{\partial \rho u_\alpha^3}{\partial x_\alpha} + (1 - \delta_{\alpha\beta}) \frac{\partial \rho u_x u_y u_z}{\partial x_\psi}, \quad (7.35)$$

without summation over repeated index α and with ψ defined by $\psi \neq \alpha$ and $\psi \neq \beta$. Additionally, $a_{\alpha\beta}^{p,\rho}$ depends on the considered model,

$$a_{\alpha\beta}^p = \delta_{\alpha\beta} c_s^2 \left(\frac{\partial \rho(\theta - 1)}{\partial t} + \rho \frac{2}{D} \frac{\partial u_\gamma}{\partial x_\gamma} \right), \quad (7.36)$$

$$a_{\alpha\beta}^\rho = \delta_{\alpha\beta} c_s^2 \left(u_\gamma \frac{\partial \rho(1 - \theta)}{\partial x_\gamma} + \rho(1 - \theta) \frac{D + 2}{D} \frac{\partial u_\gamma}{\partial x_\gamma} \right). \quad (7.37)$$

A Taylor expansion of the LB scheme [137] shows that in p -based and improved- ρ -based the stress tensor equation reads

$$\begin{aligned} -\Pi_{\alpha\beta}^{f^{neq,(2)}} &= \tau \rho c_s^2 \left[\frac{\partial u_\alpha}{\partial x_\beta} + \frac{\partial u_\beta}{\partial x_\alpha} \right] + \tau \delta_{\alpha\beta} c_s^2 \left[\frac{\partial \rho u_\gamma}{\partial x_\gamma} + \frac{\partial \rho \theta}{\partial t} \right] - \tau a_{\alpha\beta}^{p,\rho} \\ &+ \tau \left[\frac{\partial \Pi_{\alpha\beta}^{f^{neq,(2)}}}{\partial t} + \frac{\partial \Pi_{\alpha\beta\gamma}^{f^{neq,(3)}}}{\partial x_\gamma} \right] - \tau \left[u_\alpha \frac{\partial \Pi_{\beta\gamma}^{f^{neq,(2)}}}{\partial x_\gamma} + u_\beta \frac{\partial \Pi_{\alpha\gamma}^{f^{neq,(2)}}}{\partial x_\gamma} \right]. \end{aligned} \quad (7.38)$$

Note that in the case of the recursive regularized kernel, $\Pi_{\alpha\beta\gamma}^{f^{neq,(3)}}$ being a linear function of $\Pi_{\alpha\beta}^{f^{neq,(2)}}$, injecting Eq. (7.38) into itself similarly to [75, 120] leads to the more tractable equation,

$$-\Pi_{\alpha\beta}^{f^{neq,(2)}} = \tau \rho c_s^2 \left[\frac{\partial u_\alpha}{\partial x_\beta} + \frac{\partial u_\beta}{\partial x_\alpha} \right] + \tau \delta_{\alpha\beta} c_s^2 \left[\frac{\partial \rho u_\gamma}{\partial x_\gamma} + \frac{\partial \rho \theta}{\partial t} \right] - \tau a_{\alpha\beta}^{p,\rho} + \mathcal{O}(\tau^2). \quad (7.39)$$

In order to further analyze the improved- ρ -based, it is necessary to express the time derivative $\frac{\partial \rho \theta}{\partial t}$. Considering a perfect gas equation of state $p = \rho \theta c_s^2$ and combining the mass, momentum and total energy equations one gets the following pressure equation,

$$\frac{1}{\gamma - 1} \left(\frac{\partial \rho \theta}{\partial t} + \frac{\partial \rho \theta u_\beta}{\partial x_\beta} \right) + \rho \theta \frac{\partial u_\gamma}{\partial x_\gamma} - \frac{\partial}{\partial x_\gamma} \left(\lambda \frac{\partial \theta}{\partial x_\gamma} \right) + c_s^{-2} \Pi_{\beta\gamma}^{f^{neq,(2)}} \frac{\partial u_\beta}{\partial x_\gamma} = 0. \quad (7.40)$$

Assuming a Prandtl number $\text{Pr} \geq \mathcal{O}(1)$, it is reasonable to rewrite Eq. (7.40) as

$$\frac{\partial \rho \theta}{\partial t} + \frac{\partial \rho \theta u_\beta}{\partial x_\beta} + \rho \theta (\gamma - 1) \frac{\partial u_\gamma}{\partial x_\gamma} = \mathcal{O}(\tau). \quad (7.41)$$

7. Unified model, bridging between pressure-based and density-based methods – 7.2.
Unified model on standard lattice

Using Eqs. (7.37,7.39,7.41) leads to the improved- ρ -based stress tensor

$$-\Pi_{\alpha\beta}^{f^{neq},(2)} = \tau \rho c_s^2 \left[\frac{\partial u_\alpha}{\partial x_\beta} + \frac{\partial u_\beta}{\partial x_\alpha} - \delta_{\alpha\beta} \frac{2}{D} \frac{\partial u_\gamma}{\partial x_\gamma} \right] + \tau \delta_{\alpha\beta} c_s^2 \rho \theta \left[\frac{D+2}{D} - \gamma \right] \frac{\partial u_\gamma}{\partial x_\gamma} + \mathcal{O}(\tau^2), \quad (7.42)$$

in which an uncontrolled bulk viscosity appears, similarly to what was pointed out in [75]. Note that due to the second law of thermodynamics a positive bulk viscosity $(\frac{D+2}{D} - \gamma) \geq 0$ is mandatory [5]. In both the initial ρ -based model [74] and the improved- ρ -based model [149], bulk viscosity is nonzero. This is due to the mismatch between the actual adiabatic exponent γ of the simulation and the natural adiabatic exponent $\gamma_{LB} = \frac{D+2}{D}$ arising from the chosen D dimensional lattice. Inspired by [75], one can easily get rid of this uncontrolled bulk by replacing Eq. (7.37) by

$$\tilde{a}_{\alpha\beta}^\rho = \delta_{\alpha\beta} c_s^2 \left(u_\gamma \frac{\partial \rho(1-\theta)}{\partial x_\gamma} + \rho \left[\frac{D+2}{D} - \gamma \theta \right] \frac{\partial u_\gamma}{\partial x_\gamma} \right). \quad (7.43)$$

In this case the stress tensor obtained from the improved- ρ -based with zero bulk viscosity defined by Eqs. (7.39,7.43) is now equivalent up to a different $\mathcal{O}(\tau^2)$ error to the p -based one given by Eqs. (7.36,7.39),

$$-\Pi_{\alpha\beta}^{f^{neq},(2)} = \tau \rho c_s^2 \left[\frac{\partial u_\alpha}{\partial x_\beta} + \frac{\partial u_\beta}{\partial x_\alpha} - \delta_{\alpha\beta} \frac{2}{D} \frac{\partial u_\gamma}{\partial x_\gamma} \right] + \mathcal{O}(\tau^2). \quad (7.44)$$

This is due to the fact that $a_{\alpha\beta}^p = \tilde{a}_{\alpha\beta}^\rho + \mathcal{O}(\tau)$, leading to a $\mathcal{O}(\tau^2)$ difference between the p -based stress tensor Eq. (7.44) and the zero-bulk viscosity improved- ρ -based stress tensor obtained from Eqs. (7.39,7.43). This shows that when the corrective force term is taken into account, models [76, 149] become rigorously different, yet a strong connection still exists between them.

7.2. Unified model on standard lattice

In this section, we propose to build a numerical LB scheme meant to unify preexisting compressible models discussed above [74–76, 148]. For the sake of completeness, additional mass source \dot{m} , momentum force $\rho \mathcal{F}_\alpha$ and energy source $\rho \dot{q}$ are included. The LB scheme first provides mass and momentum conservations,

$$\frac{\partial \rho}{\partial t} + \frac{\partial \rho u_\beta}{\partial x_\beta} = \dot{m} \quad (7.45)$$

$$\frac{\partial \rho u_\alpha}{\partial t} + \frac{\partial \left[\rho u_\alpha u_\beta + p \delta_{\alpha\beta} + \Pi_{\alpha\beta}^{neq} \right]}{\partial x_\beta} = \rho \mathcal{F}_\alpha. \quad (7.46)$$

7. Unified model, bridging between pressure-based and density-based methods – 7.2.
Unified model on standard lattice

completed by a second thermodynamic variable solved by FD. Hydrodynamic equations (7.45,7.46) are coupled to thermal effects Eqs. (1.22,5.1,5.2) through the perfect gas EOS $p = \rho r T$, $e = C_v T$ and heat capacities $C_v = r/(\gamma-1)$ and $C_p = \gamma r/(\gamma-1)$. Then, combining Eqs. (7.45,7.46) with any choice among Eqs. (1.22,5.1,5.2) and assuming a constant r and γ values one gets the kinetic tensor and pressure Eqs. (4.47,4.98),

$$\frac{\partial \rho u_\alpha u_\beta}{\partial t} + \frac{\partial \rho u_\alpha u_\beta u_\gamma}{\partial x_\gamma} + u_\alpha \frac{\partial p}{\partial x_\beta} + u_\beta \frac{\partial p}{\partial x_\alpha} + \mathcal{O}(\tau) = \rho \mathcal{F}_\alpha u_\beta + \rho \mathcal{F}_\beta u_\alpha - \dot{m} u_\alpha u_\beta, \quad (7.47)$$

$$\frac{1}{\gamma-1} \left(\frac{\partial p}{\partial t} + \frac{\partial p u_\beta}{\partial x_\beta} \right) + p \frac{\partial u_\gamma}{\partial x_\gamma} + \mathcal{O}(\tau) = \rho \dot{q} + \dot{m} \frac{u_\gamma^2}{2}, \quad (7.48)$$

written in a compact form in which $\mathcal{O}(\tau)$ accounts for viscous and heat conductive terms. Then, the system is closed by computing the heat flux q_α through FD,

$$q_\alpha = -\lambda \frac{\partial T}{\partial x_\alpha}, \quad (7.49)$$

and by using a proper correction term during collision so that LB stress tensor is

$$-\Pi_{\alpha\beta}^{f^{neq,(2)}} = \mu \left[\frac{\partial u_\alpha}{\partial x_\beta} + \frac{\partial u_\beta}{\partial x_\alpha} - \delta_{\alpha\beta} \frac{2}{D} \frac{\partial u_\gamma}{\partial x_\gamma} \right] + \mathcal{O}(\tau^2). \quad (7.50)$$

7.2.1. Unified LB scheme

Now, we provide detailed equations of the unified model. For the sake of clarity, we use the improved- ρ -based format. The unified equilibrium distribution f_i^{eq} is

$$f_i^{eq} = \omega_i \left\{ \rho + \frac{\omega_i - \delta_{0i}}{\omega_i} \rho [\theta - 1] (1 - \zeta) + \frac{\mathcal{H}_{i\alpha}^{(1)}}{c_s^2} \rho u_\alpha + \frac{\mathcal{H}_{i\alpha\beta}^{(2)}}{2c_s^4} [\rho u_\alpha u_\beta + \zeta \delta_{\alpha\beta} \rho c_s^2 (\theta - 1)] + \frac{\mathcal{H}_{i\gamma}^{(3r)}}{6c_s^6} a_\gamma^{(3r)} \right\}, \quad (7.51)$$

in which two arbitrary fields $\zeta(t, \mathbf{x})$ and $\kappa(t, \mathbf{x})$ have been introduced and with $a_{\alpha\beta\gamma}^{(3)} = \rho u_\alpha u_\beta u_\gamma - \kappa \rho c_s^2 (u_\alpha \delta_{\beta\gamma} + u_\beta \delta_{\gamma\alpha} + u_\gamma \delta_{\alpha\beta})$ serving to define $a_\gamma^{(3r)}$ as in Appendix A. A Taylor expansion [137] shows that a force term is necessary to account for mass \dot{m} , momentum $\rho \mathcal{F}_\alpha$ and energy $\rho \dot{q}$ sources. Another force term is also necessary to remove significant errors in the stress tensor introduced by isotropy defects Eq. (3.56). Complete forcing terms can follow two different strategies F_i and G_i , they are equivalent

7. Unified model, bridging between pressure-based and density-based methods – 7.2.
Unified model on standard lattice

up to a $\mathcal{O}(\tau)$ difference and read as

$$F_i = \omega_i \left\{ \mathcal{H}^{(0)} \dot{m} + \frac{\mathcal{H}_{i\alpha}^{(1)}}{c_s^2} \rho \mathcal{F}_\alpha + \frac{\mathcal{H}_{i\alpha\beta}^{(2)}}{2c_s^4} a_{\alpha\beta}^{F,(2)} \right\}, \quad (7.52)$$

$$G_i = \omega_i \left\{ \mathcal{H}^{(0)} \dot{m} + \frac{\mathcal{H}_{i\alpha}^{(1)}}{c_s^2} \rho \mathcal{F}_\alpha + \frac{\mathcal{H}_{i\alpha\beta}^{(2)}}{2c_s^4} a_{\alpha\beta}^{G,(2)} \right\}, \quad (7.53)$$

in which Hermite moments $a_{\alpha\beta}^{F,(2)}$ and $a_{\alpha\beta}^{G,(2)}$ are

$$a_{\alpha\beta}^{F,(2)} = \frac{2}{D} \delta_{\alpha\beta} (1 - \kappa) \rho c_s^2 \frac{\partial u_\gamma}{\partial x_\gamma} - \delta_{\alpha\beta} c_s^2 \frac{\partial \rho (1 - \theta)}{\partial t} - \delta_{\alpha\beta} c_s^2 \frac{\partial \rho \kappa u_\gamma}{\partial x_\gamma} + a_{\alpha\beta}^C + \rho \mathcal{F}_\alpha u_\beta + \rho \mathcal{F}_\beta u_\alpha - \dot{m} u_\alpha u_\beta, \quad (7.54)$$

$$a_{\alpha\beta}^{G,(2)} = \delta_{\alpha\beta} c_s^2 \rho \left(\frac{2}{D} (1 - \kappa) - (\gamma - 1) \theta \right) \frac{\partial u_\gamma}{\partial x_\gamma} + \delta_{\alpha\beta} c_s^2 \frac{\partial \rho (1 - \theta - \kappa) u_\gamma}{\partial x_\gamma} - \dot{m} \left(\delta_{\alpha\beta} c_s^2 + u_\alpha u_\beta - \frac{(\gamma - 1) u_\gamma^2}{2} \delta_{\alpha\beta} \right) + \delta_{\alpha\beta} (\gamma - 1) \rho \dot{q} + a_{\alpha\beta}^C + \rho \mathcal{F}_\alpha u_\beta + \rho \mathcal{F}_\beta u_\alpha, \quad (7.55)$$

where $a_{\alpha\beta}^C$ is the lattice-dependent component of the force term,

$$a_{\alpha\beta}^C = c_s^2 \left[u_\alpha \frac{\partial \rho (1 - \theta - \kappa)}{\partial x_\beta} + u_\beta \frac{\partial \rho (1 - \theta - \kappa)}{\partial x_\alpha} \right] - \frac{\partial D_{\alpha\beta\gamma}^{feq,(3)}}{\partial x_\gamma}, \quad (7.56)$$

For the D3Q19 basis (see Appendix A),

$$-\frac{\partial D_{\alpha\beta\gamma}^{feq,(3)}}{\partial x_\gamma} = \delta_{\alpha\beta} \frac{\partial \rho u_\alpha (\kappa - u_\alpha^2)}{\partial x_\alpha} - (1 - \delta_{\alpha\beta}) \frac{\partial \rho u_x u_y u_z}{\partial x_\psi}, \quad (7.57)$$

in which no summation over repeated index α is done and ψ is chosen as $\psi \neq \alpha$ and $\psi \neq \beta$. It is worth noting that $a_{\alpha\beta}^{F,(2)}$ and $a_{\alpha\beta}^{G,(2)}$ can be considered as generalizations of force term strategies respectively employed in [76] and [75, 149]. Using either F_i or G_i in the usual collide, stream and macroscopic reconstruction procedure then leads to a unified LB numerical scheme which is consistent with Eqs. (7.45,7.46), completed by a stress tensor equation,

$$-\Pi_{\alpha\beta}^{f^{neq,(2)}} = \tau (1 - \kappa) \rho c_s^2 \left[\frac{\partial u_\alpha}{\partial x_\beta} + \frac{\partial u_\beta}{\partial x_\alpha} - \delta_{\alpha\beta} \frac{2}{D} \frac{\partial u_\gamma}{\partial x_\gamma} \right] + \mathcal{O}(\tau^2). \quad (7.58)$$

Identification procedure between Eq. (7.58) and the stress tensor then leads to $\mu = \tau (1 - \kappa) \rho c_s^2$. Using equilibrium Eq. (7.51), force term Eq. (7.53), $\zeta = 1$ and $\kappa = 1 - \theta$, this model recovers the zero-bulk viscosity ρ -based model [75]. With Eq. (7.52), $\zeta = 0$

7. *Unified model, bridging between pressure-based and density-based methods – 7.2.*
Unified model on standard lattice

and $\kappa = 0$, the p -based model [76] is recovered. Lastly, if Eq. (7.53) is used along with $\zeta = \frac{\Theta}{1-\Theta}$ and $\kappa = \Theta$, the zero-bulk viscosity version of the improved- ρ -based model is recovered, where Θ is a free parameter introduced in [149]. Through numerical experiments, the influence of the value proposed by [149] for Θ is found negligible, $\zeta = 0$ and $\kappa = 0$ are therefore chosen to keep the model as simple as possible.

In what follows it was chosen to use F_i instead of G_i . While it still unclear which one of the two corrections is the best one in term of accuracy and stability, there exists some compelling arguments to use F_i ,

- First, because the Prandtl number is implicitly contained in the pressure time derivative in F_i , this force term allows to handle arbitrary values of Pr while the force term G_i , by using Eq. (7.40) is restricted to $\text{Pr} \geq \mathcal{O}(1)$ for consistency reasons.
- Second, by avoiding the use of Eq. (7.40) to assess the consistency of the LB stress-tensor, F_i allows an easier coupling with complex EOS such as the van der Waals equation [43] or Noble Able stiffened gas [180]. Indeed, these EOS would lead to a more complicated pressure equation than Eq. (7.40) in which additional non dimensional numbers introduced by those EOS would also appear in consistency errors of the stress-tensor.
- Lastly, F_i does not involve using the heat release term \dot{q} , it is therefore easier to use in combustion applications.

Force terms F_i and G_i are equivalent – $F_i = G_i + \mathcal{O}(\tau)$ – for monospecies fluids with order unity Pr, which is the case here, but F_i is still shorter to implement, therefore it was retained in what follows.

7.2.2. Interpretation of δ_{0i}

Before moving to the algorithmic description of our scheme, we provide a simple explanation of how the classical ρ -based model [74, 75, 148] differs from recent models such as p -based [76] and improved- ρ -based [149] in which the unusual Kronecker δ_{0i}

7. Unified model, bridging between pressure-based and density-based methods – 7.2.
Unified model on standard lattice

is used, see Eq. (7.51) with $\zeta \neq 1$. Let us project δ_{0i} onto the D3Q19 Hermite basis,

$$a^{\delta_{0i},(0)} = \sum_{i=0}^{q-1} \mathcal{H}_i^{(0)} \delta_{0i} = 1, \quad (7.59)$$

$$a_{\alpha}^{\delta_{0i},(1)} = \sum_{i=0}^{q-1} \mathcal{H}_{i\alpha}^{(1)} \delta_{0i} = 0, \quad (7.60)$$

$$a_{\alpha\beta}^{\delta_{0i},(2)} = \sum_{i=0}^{q-1} \mathcal{H}_{i\alpha\beta}^{(2)} \delta_{0i} = -c_s^2 \delta_{\alpha\beta}, \quad (7.61)$$

$$a_{\alpha\beta\gamma}^{\delta_{0i},(3)} = \sum_{i=0}^{q-1} \mathcal{H}_{i\alpha\beta\gamma}^{(3)} \delta_{0i} = 0, \quad (7.62)$$

$$a^{\delta_{0i},\mathcal{A}_i} = \sum_{i=0}^{q-1} \mathcal{A}_i \delta_{0i} = 2c_s^4, \quad (7.63)$$

$$a^{\delta_{0i},\mathcal{B}_i} = \sum_{i=0}^{q-1} \mathcal{B}_i \delta_{0i} = 2c_s^4, \quad (7.64)$$

$$a^{\delta_{0i},\mathcal{C}_i} = \sum_{i=0}^{q-1} \mathcal{C}_i \delta_{0i} = 2c_s^4. \quad (7.65)$$

Then, we can exactly express δ_{0i} by

$$\delta_{0i} = \omega_i \left\{ \mathcal{H}_i^{(0)} - \frac{\mathcal{H}_{ixx}^{(2)} + \mathcal{H}_{iyy}^{(2)} + \mathcal{H}_{izz}^{(2)}}{2c_s^2} + \frac{\mathcal{A}_i + \mathcal{B}_i + \mathcal{C}_i}{12c_s^4} \right\}. \quad (7.66)$$

Injecting Eq. (7.66) into Eq. (7.51) allows to write

$$\begin{aligned} f_i^{eq} = \omega_i \left\{ \mathcal{H}_i^{(0)} \rho + \frac{\mathcal{H}_{i\alpha}^{(1)}}{c_s^2} \rho u_{\alpha} + \frac{\mathcal{H}_{i\alpha\beta}^{(2)}}{2c_s^4} [\rho u_{\alpha} u_{\beta} + \delta_{\alpha\beta} \rho c_s^2 (\theta - 1)] \right. \\ \left. + \frac{\mathcal{H}_{i\gamma}^{(3r)}}{6c_s^6} a_{\gamma}^{(3r)} - \frac{\mathcal{A}_i + \mathcal{B}_i + \mathcal{C}_i}{12c_s^4} \rho [\theta - 1] (1 - \zeta) \right\}, \quad (7.67) \end{aligned}$$

with $a_{\alpha\beta\gamma}^{(3)} = \rho u_{\alpha} u_{\beta} u_{\gamma} - \kappa \rho c_s^2 (u_{\alpha} \delta_{\beta\gamma} + u_{\beta} \delta_{\gamma\alpha} + u_{\gamma} \delta_{\alpha\beta})$ serving to define $a_{\gamma}^{(3r)}$ as in Appendix A. In other words, recent models such as p -based and improved- ρ -based are equivalent to the classical ρ -based model [74, 75, 148] with additional information projected onto fourth order polynomials \mathcal{A}_i , \mathcal{B}_i and \mathcal{C}_i due to $\zeta \neq 1$ in Eq. (7.51). This is expected to change numerical errors of lattice-Boltzmann regularized schemes without changing the consistency of mass and momentum conservation equations.

7.2.3. Coupled models

The LB scheme being now unified, this section aims at further comparing and unifying the different ingredients that were previously used in the compressible hybrid

recursive regularized literature [74–76, 148]. In this chapter, the chosen basis for simulations is the D3Q19 basis whose details can be found in Appendix A.

7.2.3.1. Thermal coupling

The entropy equation in non-conservative format being mainly an advection equation with source terms, it is easily discretized and leads to robust results, explaining this choice of energy variable, widely present in the LB literature [74–76, 148]. Which is why an entropy equation solved by finite differences is chosen,

$$\frac{\partial s}{\partial t} + u_\beta \frac{\partial s}{\partial x_\beta} = \frac{1}{\rho T} \left[\Pi_{\alpha\beta} \frac{\partial u_\alpha}{\partial x_\beta} + \frac{\partial}{\partial x_\beta} \left(\lambda \frac{\partial T}{\partial x_\beta} \right) \right]. \quad (7.68)$$

In all previous studies, viscous heat and heat conduction were discretized by classical second order centered finite difference schemes while different strategies were employed for the convective term. When applied to a 1D passive scalar equation these advection schemes correspond to :

- In [74], a $\mathcal{O}(\Delta t^2)$ accurate Runge-Kutta temporal integration is adopted along with a $\mathcal{O}(\Delta x^3)$ accurate MUSCL scheme [146] resulting in a 9 points stencil between timesteps t and $t + \Delta t$.
- In [75, 148], the stencil was simplified by replacing the Runge-Kutta 2 integration by a simpler $\mathcal{O}(\Delta t)$ accurate Euler temporal integration. The spatial integration remained identical and the overall scheme leads to a 5 points stencil.
- In [76], time and space were discretized simultaneously by a MUSCL-Hancock [24] method, resulting in a compact $\mathcal{O}(\Delta t^3, \Delta x^3)$ accurate 5 points stencil.

Due to its compactness and its high order of accuracy, the MUSCL-Hancock method is chosen, the only difference being that the flux limiter was removed compared to [76]. Except the convective term, other terms are still discretized by second order centered schemes. Implementation details for the entropy equation can be found in Appendix 5.2.2.

7.2.3.2. Non-equilibrium reconstruction

Here, we follow the hybrid recursive regularized method along with the traceless non-equilibrium reconstruction [76, 137], which has been identified [120] as a supplementary regularization for moment $\Pi_{\gamma\gamma}$. The non-equilibrium second order moment is then calculated using

$$\begin{aligned} \bar{\Pi}_{\alpha\beta}^{\text{neq},(2)}(t, \mathbf{x}) = & \sigma \sum_{i=0}^{q-1} \left[c_{i\alpha} c_{i\beta} - \frac{\delta_{\alpha\beta}}{3} c_{i\gamma} c_{i\gamma} \right] \left(\bar{f}_i(t, \mathbf{x}) - f_i^{\text{eq}}(t, \mathbf{x}) + \frac{\Delta t}{2} F_i(t - \Delta t, \mathbf{x}) \right) \\ & - \left[(1 - \sigma)(1 - \kappa) \rho c_s^2 \bar{T} \left(\frac{\partial u_\alpha}{\partial x_\beta} + \frac{\partial u_\beta}{\partial x_\alpha} - \frac{2\delta_{\alpha\beta}}{D} \frac{\partial u_\gamma}{\partial x_\gamma} \right) \right] (t, \mathbf{x}) \end{aligned} \quad (7.69)$$

7. Unified model, bridging between pressure-based and density-based methods – 7.2.
Unified model on standard lattice

Where σ is the weighting free parameter introduced by Jacob *et al* [119]. Note the $t - \Delta t$ evaluation of F_i . Numerical experiments showed better stability properties for $\text{Ma} \gtrsim 1.7$ simulations than with the usual t evaluation, however, no measurable difference was observed for lower Ma numbers when using t . This change formally introduces a $\mathcal{O}(\Delta t)$ error in the stress tensor, which is of the order of the leading numerical error already introduced by the non-BGK collision kernel [81, 120, 137]. Using, Eq. (7.69), the recursive regularized procedure states that

$$\bar{f}_{\alpha\beta\gamma}^{\text{neq},(3)}(t, \mathbf{x}) = \left[u_\alpha \bar{f}_{\beta\gamma}^{\text{neq},(2)} + u_\beta \bar{f}_{\gamma\alpha}^{\text{neq},(2)} + u_\gamma \bar{f}_{\alpha\beta}^{\text{neq},(2)} \right](t, \mathbf{x}). \quad (7.70)$$

Then, the recursive regularization with D3Q19 lattice (Appendix A) dictates that non-equilibrium should be defined as

$$\bar{f}_i^{\text{neq}} = \omega_i \left\{ \frac{\mathcal{H}_{i\alpha\beta}^{(2)}}{2c_s^4} \bar{f}_{\alpha\beta}^{\text{neq},(2)} + \frac{\mathcal{H}_{i\gamma}^{(3r)}}{6c_s^6} \bar{f}_\gamma^{\text{neq},(3r)} \right\}. \quad (7.71)$$

with $\bar{f}_{\alpha\beta\gamma}^{\text{neq},(3)}$ serving to define $\bar{f}_\gamma^{\text{neq},(3r)}$, similarly to Appendix A.

7.2.3.3. Force term discretization

Here, we detail numerical schemes employed to discretize the force corrective term F_i , Eq. (7.52). Spatial gradients of F_i are systematically discretized by a $\mathcal{O}(\Delta x)$ accurate upwind schemes [75],

$$\frac{\partial \phi}{\partial x_\gamma} \approx \begin{cases} \frac{\phi(x_\gamma) - \phi(x_\gamma - \Delta x)}{\Delta x} & \text{if } u_\gamma \geq 0 \\ \frac{\phi(x_\gamma + \Delta x) - \phi(x_\gamma)}{\Delta x} & \text{if } u_\gamma < 0 \end{cases}, \quad (7.72)$$

except for the velocity divergence operator which is discretized using a $\mathcal{O}(\Delta x^2)$ accurate centered scheme,

$$\frac{\partial \phi}{\partial x_\gamma} \approx \frac{\phi(x_\gamma + \Delta x) - \phi(x_\gamma - \Delta x)}{2\Delta x}. \quad (7.73)$$

7.2.3.4. Sensor, artificial bulk viscosity

We found that the bulk viscosity μ_β added by the filtering process $|\Pi_{\alpha\alpha}^{\text{neq}}| = \min(0.1|\nabla \cdot \mathbf{u}|, |\Pi_{\alpha\alpha}^{\text{neq}}|)$ proposed in [149] sometimes create spurious acoustic noise near curved discontinuities on the vortex/shock and entropy spot/shock interaction test cases. Therefore, a smoother artificial bulk viscosity $\mu_\beta = 0.05 \mu \text{Ma}$ is introduced. Defining Ma as the

7. Unified model, bridging between pressure-based and density-based methods – 7.2.
Unified model on standard lattice

local Mach number allows to write,

$$F_i^{\mu\beta} = \omega_i \frac{\mathcal{H}_{i\alpha\beta}^{(2)}}{2c_s^4} \delta_{\alpha\beta} \rho c_s^2 (\kappa - 1) 0.05 \text{Ma} \frac{\partial u_\gamma}{\partial x_\gamma}, \quad (7.74)$$

which is added only during collision, resulting in an additional first order forcing implementation. This bulk viscosity is meant to damp unstable acoustic modes in very high Mach number simulations. It is worth mentioning that this artificial bulk is only added in the LB part of the algorithm and that the stability of all simulations that will be presented in this article does not depend on it, except for $\text{Ma} \gtrsim 1.7$. Nevertheless, Eq. (7.74) is kept in all test cases performed in this chapter. Using this additional bulk viscosity, it is found that the Mach 4 simulations presented in [149] can be reproduced with the present model. Additionally, to handle discontinuities, a sensor consisting of a normalized numerical Laplacian operator is used to define an artificial kinematic viscosity,

$$\nu_{sc} = s_c \left| \frac{\rho(x - \Delta x) - 2\rho(x) + \rho(x + \Delta x)}{\rho(x - \Delta x) + 2\rho(x) + \rho(x + \Delta x)} \right|, \quad (7.75)$$

where s_c is a free parameter. Then, this artificial viscosity is added to the physical dynamic viscosity, $\mu = \mu_{ph} + \rho\nu_{sc}$. Through numerical experiments, we found that contact discontinuities creates as much or more Gibbs oscillations than shocks, explaining the unusual choice to evaluate Eq. (7.75) using ρ instead of p . This allows our sensor to be triggered by both shocks and contact discontinuities.

7.2.4. Step-by-step unified scheme

All necessary ingredients have been discussed, we shall now detail the step-by-step algorithm to get the updated solution $[\rho, \rho u_\alpha, \theta, \Pi_{\alpha\beta}^{neq}](t + \Delta t, \mathbf{x})$ from the last timestep solution $[\rho, \rho u_\alpha, \theta, \Pi_{\alpha\beta}^{neq}](t, \mathbf{x})$. We remind that for numerical simulations, $\zeta = 0$ and $\kappa = 0$ have been retained along with force term F_i .

- i) Knowing $[\rho, \rho u_\alpha, \theta, \Pi_{\alpha\beta}^{neq}](t, \mathbf{x})$, use the equation of state $s = C_v \ln c_s^2 \theta \rho^{1-\gamma}$ to get the entropy $s(t, \mathbf{x})$ as a function of $\rho(t, \mathbf{x})$ and $\theta(t, \mathbf{x})$.
- ii) Compute the equilibrium distribution $f_i^{eq}(t, \mathbf{x})$ using Eq. (7.51) and the D3Q19 basis, Appendix A.
- iii) Compute either $F_i(t, \mathbf{x})$ and $F_i^{\mu\beta}(t, \mathbf{x})$ using Eqs. (7.52, 7.74).
- iv) Compute the non-equilibrium $\bar{f}_i^{neq}(t, \mathbf{x})$ using Eqs. (7.70-7.71).
- v) Compute the collided population $f_i^{col}(t, \mathbf{x})$ as

$$f_i^{col}(t, \mathbf{x}) = f_i^{eq}(t, \mathbf{x}) + \left(1 - \frac{\Delta t}{\bar{\tau}}\right) \bar{f}_i^{neq}(t, \mathbf{x}) + \Delta t \left(\frac{1}{2} F_i + F_i^{\mu\beta}\right)(t, \mathbf{x}). \quad (7.76)$$

7. Unified model, bridging between pressure-based and density-based methods – 7.3.
Numerical validations

vi) Shift the populations along lattices following the streaming,

$$\bar{f}_i(t + \Delta t, \mathbf{x}) = f_i^{col}(t, \mathbf{x} - \mathbf{c}_i \Delta t). \quad (7.77)$$

vii) Equilibrium moments can now be updated as

$$\rho(t + \Delta t, \mathbf{x}) = \sum_{i=0}^{q-1} \bar{f}_i(t + \Delta t, \mathbf{x}) + \frac{\Delta t}{2} \dot{m}(t + \Delta t, \mathbf{x}), \quad (7.78)$$

$$\rho u_\alpha(t + \Delta t, \mathbf{x}) = \sum_{i=0}^{q-1} c_{i\alpha} \bar{f}_i(t + \Delta t, \mathbf{x}) + \frac{\Delta t}{2} [\rho \mathcal{F}_\alpha](t + \Delta t, \mathbf{x}), \quad (7.79)$$

viii) Solve the entropy equation following numerical schemes presented in Appendix A in order to get the updated $s(t + \Delta t, \mathbf{x})$ and use it along with $\rho(t + \Delta t, \mathbf{x})$ to get the updated normalized temperature $\theta(t + \Delta t, \mathbf{x})$ through $\theta = c_s^{-2} \rho^{\gamma-1} e^{s/C_v}$.

ix) Then, the updated stress tensor can be computed from Eqs. (7.51-7.52,7.69).

After those steps, $[\rho, \rho u_\alpha, \theta, \Pi_{\alpha\beta}^{neq}](t + \Delta t, \mathbf{x})$, the updated solution, is now obtained.

7.3. Numerical validations

7.3.1. Isentropic vortex

An isentropic vortex initialized in a 2D fully periodic box of size $[10 \times 10]$ and discretized by a 200×200 mesh is simulated. This unity radius vortex $R = 1$ is transported over a distance $200R$ corresponding to 20 flow through time periods. The Ma number of the mean free flow $u_0 = \text{Ma}\sqrt{\gamma}$ is tuned to check the capability of the present method to transport on a relatively long distance. $\text{Ma} = 4, 3, 2, 1$ are chosen along with $\text{CFL} = 0.1, 0.15, 0.2, 0.3$.

The hybrid weighting parameter is fixed to $\sigma = 1$, meaning that the stress tensor is completely recovered from the LB scheme. The analytical solution of this Euler simulation is a frozen vortex advected without any dissipation nor dispersion. Therefore, a vanishing $\mu = 10^{-15}$ viscosity is chosen to mimic an Euler solver. The initial solution is

$$\rho = \left[1 - \frac{(\gamma - 1)}{2} M_v^2 e^{1-r^2/R^2} \right] \frac{1}{\gamma - 1}, \quad p = \rho^\gamma, \quad (7.80)$$

$$u = u_0 - M_v \sqrt{\gamma} e^{(1-r^2/R^2)/2} (y - y_c), \quad (7.81)$$

$$v = M_v \sqrt{\gamma} e^{(1-r^2/R^2)/2} (x - x_c), \quad (7.82)$$

with $M_v = 1/(4\pi\sqrt{\gamma})$.

Density fields after exactly 20 periods are plotted on Fig. 7.1, it is seen that the overall circular shape is well conserved by the present solver, even after a relatively long distance of $200R$.

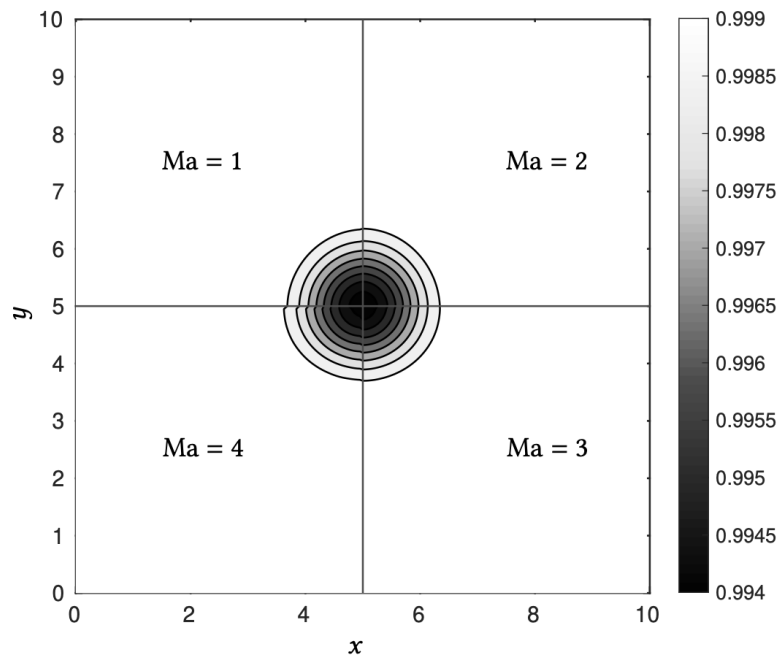


Figure 7.1. – Isentropic vortex : Isotropy comparison after 20 convective times at different Mach numbers.

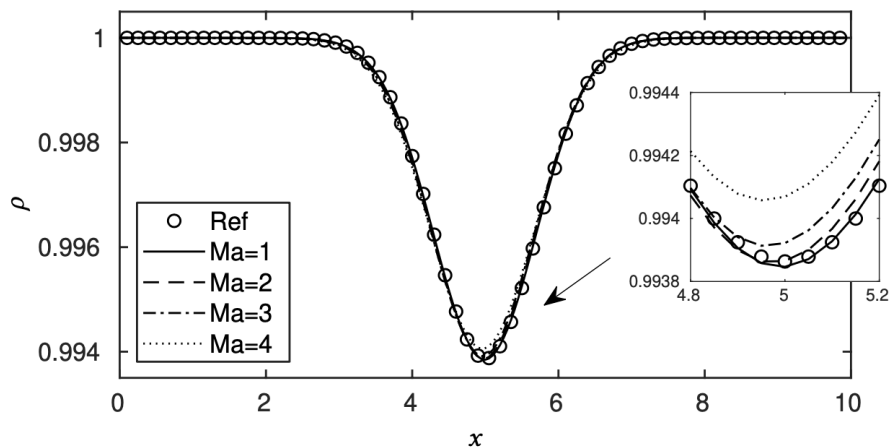


Figure 7.2. – Isentropic vortex : Comparison of $y = 0$ density slices at different Mach numbers after 20 periods.

To further validate the present results, $y = 5$ slices for different Ma numbers are also plotted on Fig. 7.2, showing that while higher Ma values led to higher errors, the damping remained very small for Mach numbers up to $Ma = 4$, exhibiting less than 6% of errors when compared to the reference analytical solution.

7.3.2. Entropy spot

This second test case is very similar to the isentropic vortex except that we now transport an entropy spot, initialized as

$$\rho = \left(1 + \epsilon e^{-r^2/R^2}\right), \quad (7.83)$$

$$p = 1, \quad u = u_0, \quad v = 0. \quad (7.84)$$

The analytical solution is also a frozen pattern advected by the mean flow $u_0 = \text{Ma}\sqrt{\gamma}$ without any changes of shape or amplitude.

All the other numerical and physical parameters are exactly the same as those of the isentropic vortex. Fig. 7.3 presents a comparison between different Ma values.

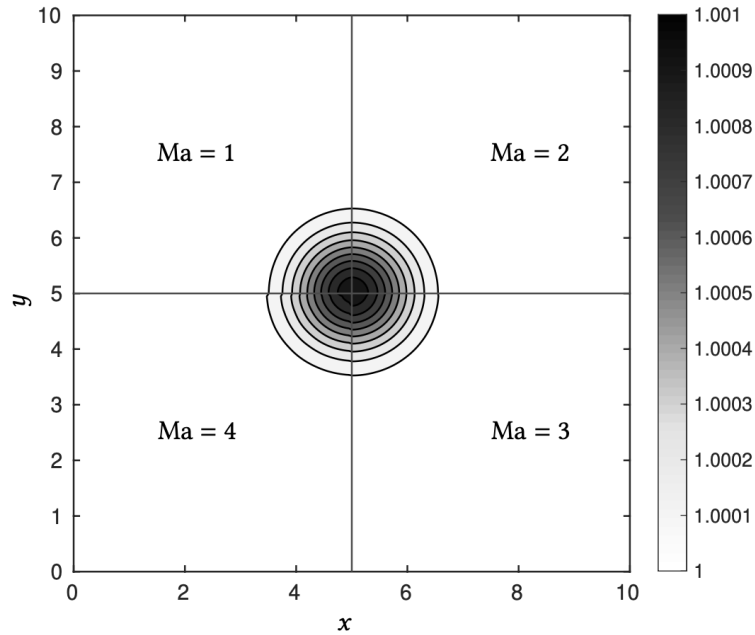


Figure 7.3. – Entropy spot : Isotropy comparison after 20 convective times at different Mach numbers.

After 20 periods the circular shape is well preserved. $y = 5$ slices can be seen on Fig. 7.4 to quantitatively show how the numerical errors introduced by the present method altered the entropy spot.

Again, higher Mach led to more damping, but it remained in an acceptable margin of about 5% errors. Note that the choice of the numerical MUSCL-Hancock scheme for the convective term of Eq. (7.68) is of critical importance for this test case as it can be seen on Fig. 7.5, where different numerical schemes were employed for the $\text{Ma} = 1$ case, a) Lax-Wendroff [24], b) Fromm [24], c) Runge-Kutta 1 with 20% of upwind scheme and 80% of centered scheme, d) MUSCL [74, 75, 148], e) Adams-Bashforth with MUSCL [74, 75, 148], f) MUSCL-Hancock [24, 76, 181].

It is shown that the accurate transport of the entropy mode significantly depends on the discretization of Eq. (7.68), highlighting that numerical properties of Hybrid LB

7. Unified model, bridging between pressure-based and density-based methods – 7.3.
 Numerical validations

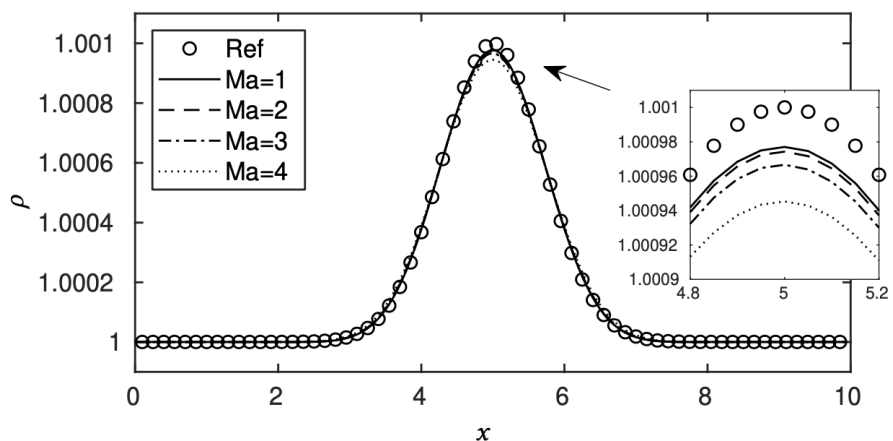


Figure 7.4. – Entropy spot : Comparison of $y = 0$ density slices at different Mach numbers after 20 periods.

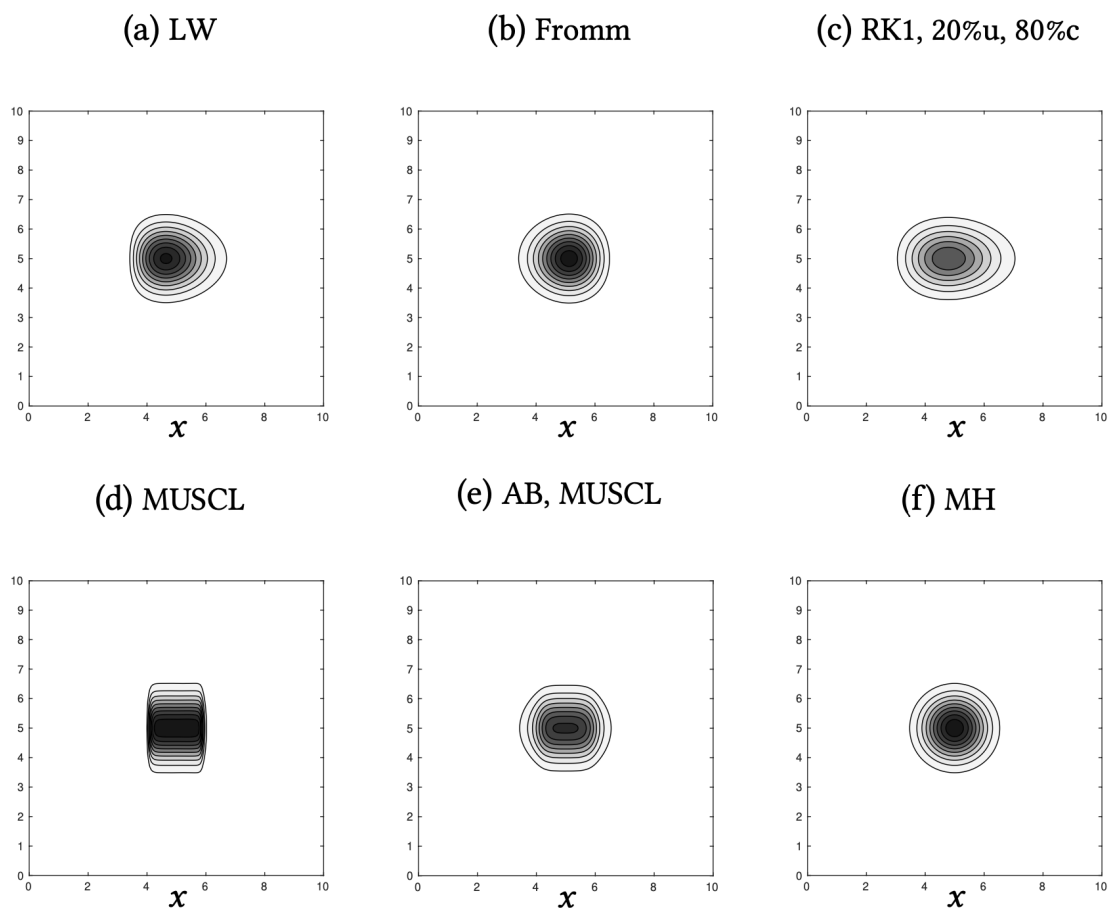


Figure 7.5. – Entropy spot : Comparison of density fields of the $Ma = 1$ advection after 20 periods for different discretizations of the convective term of Eq. (7.68).

schemes are inherited from both the LB part and FD part.

7.3.3. Thermal Couette flow

In this test case, a $H = 1 \times 10^{-4}$ long domain is discretized by a 1×100 grid. Prandtl number Pr is fixed to 0.71. The adiabatic exponent is chosen as $\gamma = 1.4$. Characteristic CFL ranges from 0.2 to 0.5 to ensure the stability of the simulations while the hybrid LB parameter is fixed to $\sigma = 0.9$. A no-slip isothermal wall moving at $Ma = 1.3, 2.3, 3.3$ is placed at $y = H$, and a no-slip wall at $y = 0$, leading to a linear velocity profile with constant shear-stress. Due to the viscous heat term present in the entropy equation Eq. (7.68) the fluid is heated up. When the generated heat is balanced by heat diffusion, a stationary solution is achieved. The Reynolds number does not changes the stationary analytical solution, but it controls the rate of momentum transfer from the moving wall to the inner domain. A Reynolds number of order unity is therefore chosen to allow a fast convergence, after which a constant \mathcal{L}_2 error for temperature and velocity fields of order 1×10^{-3} and 1×10^{-4} are reported for all Mach numbers tested. In Fig. 7.6, the normalized temperature and normalized velocity curves are compared to their analytical counterparts [76]. A satisfactory agreement is observed for both profiles, showing the capability of the present model to handle viscous and heat conduction terms.

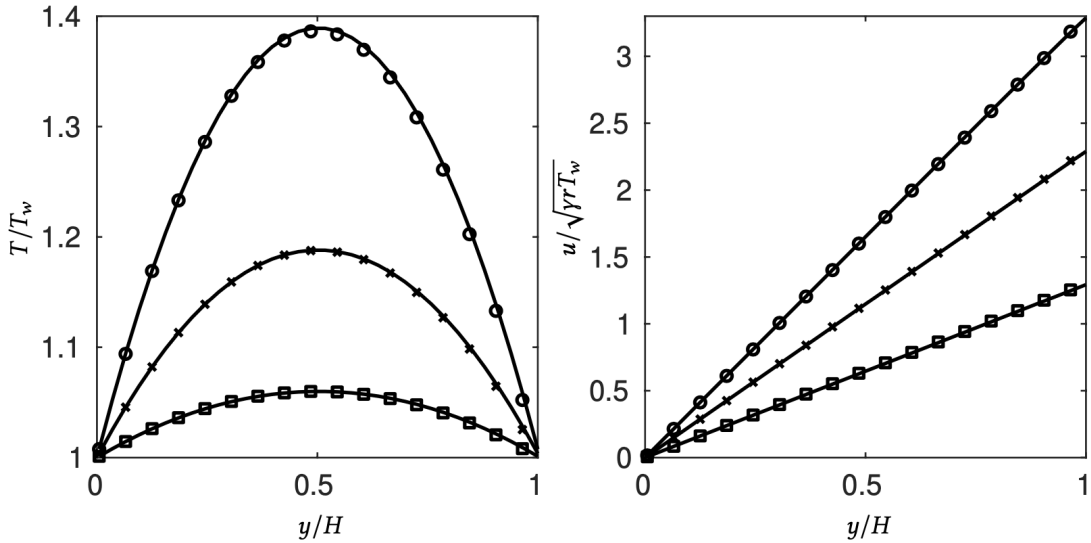


Figure 7.6. – Thermal Couette flow : Left is normalized temperature, right is local Ma number. Squares, crosses and circles are the $Ma = 1.3, 2.3, 3.3$ references, solid lines correspond to numerical solutions with the present model.

7.3.4. 2D Riemann problems

To assess the capability of the present solver to handle discontinuities in a wide range of situations, configurations 4-6-11-12-13-16 in [182] are simulated with the

7. Unified model, bridging between pressure-based and density-based methods – 7.3.
 Numerical validations

same numerical parameters. These test cases are 2D Riemann problems, they are initialized by 4 constant states divided by discontinuities placed along $x = 0.5$ and $y = 0.5$. The exact initial conditions are given in Appendix C.

The hybrid LB parameter is fixed to $\sigma = 1.0$, a square domain of side length $L = 1$ is discretized by a 400×400 grid. Dynamic viscosity is fixed to $\mu = 10^{-15}$ while the adiabatic exponent is $\gamma = 1.4$. A single fixed value of $\Delta t / \Delta x = 0.22$, very close to values adopted by [182], is chosen here.

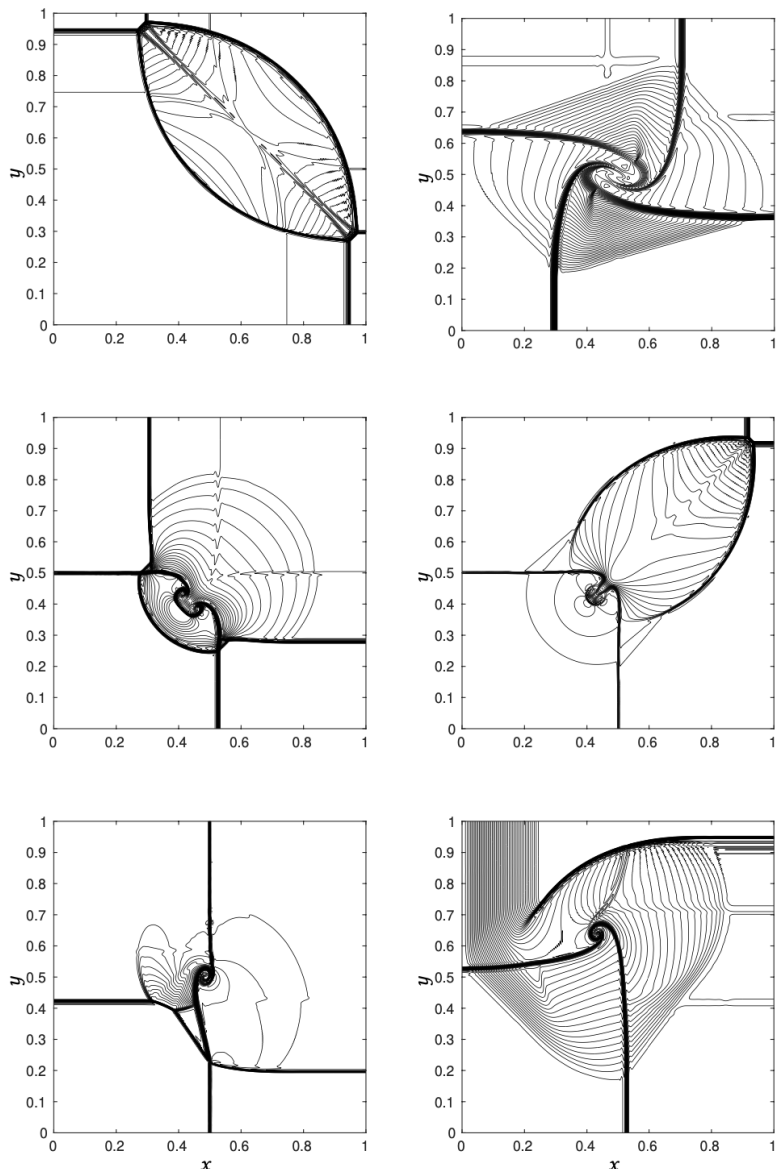


Figure 7.7. – 2D Riemann problems : Density fields of configurations 4-6-11-12-13-16 [182].

Density fields are presented after 500 timesteps for all 6 configurations in Fig. 7.7 where 50 isolines are linearly ranging from $1.05 \times \min(\rho)$ to $0.95 \times \max(\rho)$. The shock

sensor parameter is fixed to $s_c = 0.3$ to reduce Gibbs oscillations near discontinuities. The shape of the complex patterns of shocks, contact discontinuities and rarefaction waves presented in [182] are well reproduced in all 6 configurations.

7.3.5. Compressible double shear layer

To further demonstrate the stability of the proposed solver, a compressible double shear layer problem is specifically designed and tested on different square grids. The fully periodic square $[L \times L]$ domain is discretized by 64×64 , 128×128 , 256×256 , 512×512 and 1024×1024 grids and the initial CFL is fixed to $CFL = 0.28$. For this simulation, $\sigma = 1$ is used. Adiabatic exponent is $\gamma = 1.4$, dynamic viscosity is taken as $\mu = 10^{-15}$ to model an Euler simulation, characteristic Mach number is $Ma = 0.65$ and the simulation is run until $2t_c = \frac{2L}{Ma\sqrt{\gamma}}$. The initial solution,

$$u = \begin{cases} Ma\sqrt{\gamma}\tanh k(y - 0.25), & \text{if } y \leq 0.5 \\ Ma\sqrt{\gamma}\tanh k(0.75 - y), & \text{if } y > 0.5 \end{cases} \quad (7.85)$$

$$v = Ma\sqrt{\gamma}\delta \sin 2\pi(x + 0.25), \quad \rho = 1, \quad T = 1, \quad (7.86)$$

consists of two layers of fluid sliding on each other through a sigmoidal profile of characteristic thickness $k = 80$. A sinusoidal perturbation whose amplitude is controlled by $\delta = 0.05$ by introduced on the spanwise velocity, which eventually leads to the formation of a clockwise and counter-clockwise vortices around $t = t_c$, local Mach number then exceeds its initial value. Because the chosen initial Mach number is sufficiently large, a complex pattern of 4 radial shocks is formed around time $t = 2t_c$ and interacts with the circumferential slip lines wrapping around each vortex.

This can be seen on Fig. 7.8, where vorticity and Mach fields are represent at $t = (t_c, 2t_c)$ for the 512×512 grid.

A quantitative comparison between different grids can be seen on Fig. 7.9, where vorticity and Mach are plotted along the diagonal line of the bottom left quadrant. No sensor viscosity is used in this test case, therefore, the stability of the simulation completely relies on the numerical viscosity and hyperviscosity introduced by truncature errors.

7.3.6. Shock-vortex interaction

The shock-vortex interaction is a complex test case in which both accuracy and stability are tested. The simulation is characterized by a $Ma = 1.2$ stationary shock positioned at $x_s = 8$ and initialized by the Rankine-Hugoniot jump conditions,

$$\frac{\rho_R}{\rho_L} = \frac{u_L}{u_R} = \frac{(\gamma + 1)Ma^2}{(\gamma - 1)Ma^2 + 2}, \quad \frac{p_R}{p_L} = 1 + \frac{2\gamma}{(\gamma + 1)}(Ma^2 - 1). \quad (7.87)$$

In the upstream region is superimposed a $M_v = 0.25$ isentropic vortex Eq. (7.80). Other physical parameters are set to $\gamma = 1.4$, $Re = 800$, $Pr = 0.75$, $p_L = 1.0$, $T_L = 1.0$,

7. Unified model, bridging between pressure-based and density-based methods – 7.3.
 Numerical validations

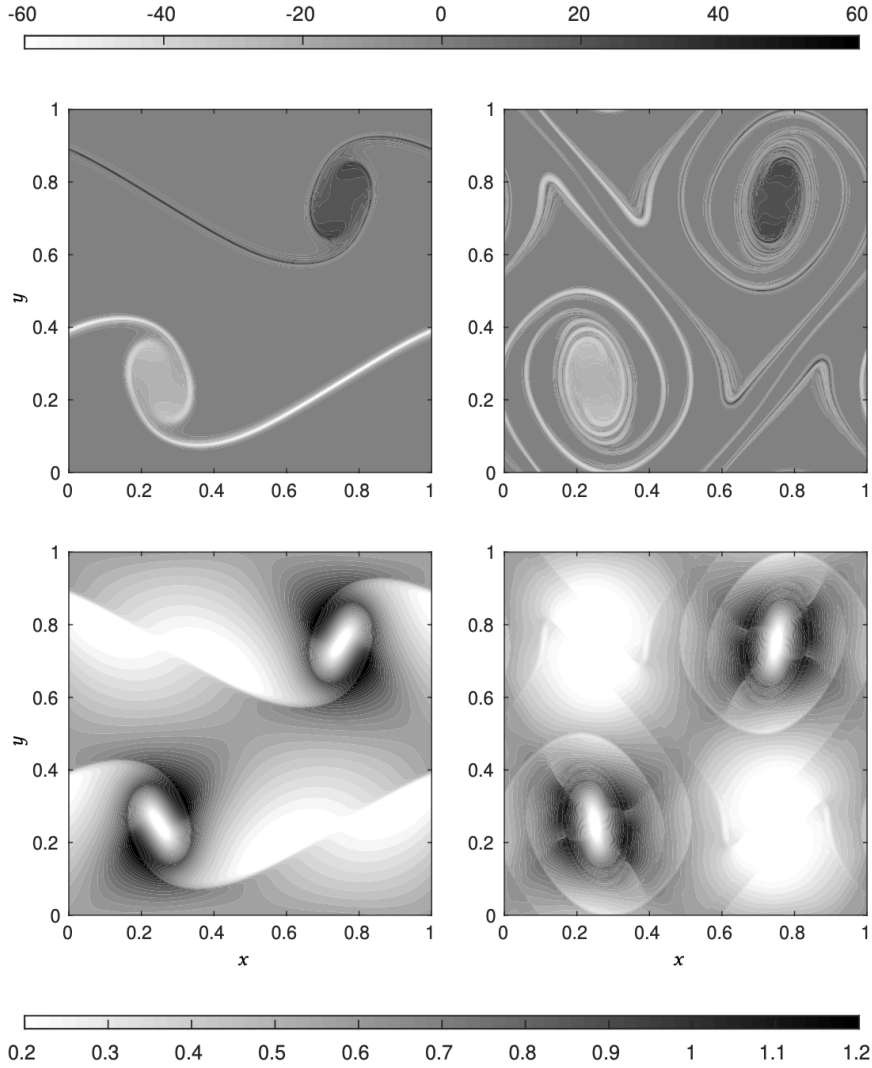


Figure 7.8. – Double shear layer : Vorticity (top) and Mach (bottom) at time t_c (left) and $2t_c$ (right) using the 512×512 grid.

$u_L = M_s \sqrt{\gamma}$. The simulation takes place in a $[0, 28] \times [0, 24]$ computational domain discretized by a 1120×960 grid. The initial position of the vortex is $(x_c, y_c) = (6, 12)$. The maximum CFL, evaluated in the upstream region, is set to 0.83 and the stabilizing parameter of the hybrid lattice LB model is $\sigma = 0.7$.

On Fig. 7.10 is plotted the normalized pressure fluctuation $\Delta p = \frac{p - p_R}{p_R}$ along a radial slice of angle $\theta = -45^\circ$ at different integer multiples of the characteristic time $T = \frac{R}{c_R}$ corresponding to $t = 6T$, $t = 8T$ and $t = 10T$. A circumferential slice around the vortex at time $t = 6T$ is also visible for two different radii. Both the radial and circumferential slices are in good agreement with the reference solution.

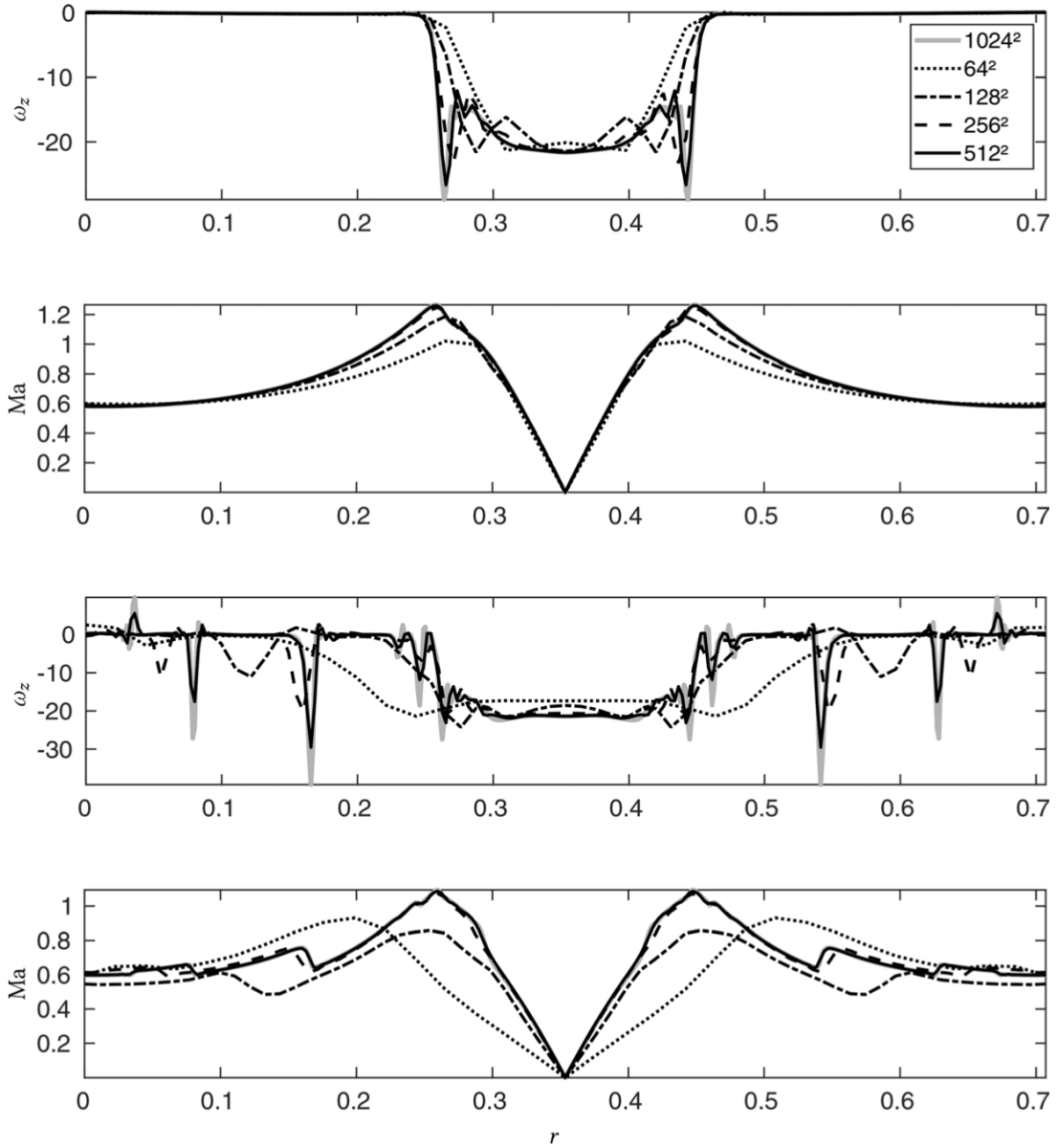


Figure 7.9. – Double shear layer : Vorticity and Mach slices between points $(0, 0)$ and $(0.5, 0.5)$ at time t_c (top) and $2t_c$ (bottom) for different grid resolutions.

7.3.7. Shock-entropy spot interaction

Similarly to the shock-vortex interaction, a stationary shock is placed at $x_s = 10$. The mean flow is initialized through the Rankine-Hugoniot jump conditions Eqs. (7.87). An entropy spot of amplitude $\epsilon = 0.1$, centered at $(x_c, y_c) = (3, 12)$ is placed in the upstream region. Note that $|x_s - x_c|$ is more than 3 times higher than for the last test case to avoid any superposition of the initial profiles of shock and entropy-spot.

Other relevant parameters are set to $\mu = 10^{-15}$, $p_L = 1.0$, $T_L = 1.0$, $u_L = M_s \sqrt{\gamma}$ and $s_c = 0$. Domain and numerical parameters such as Δx and σ are identical to the

7. Unified model, bridging between pressure-based and density-based methods – 7.3.
 Numerical validations

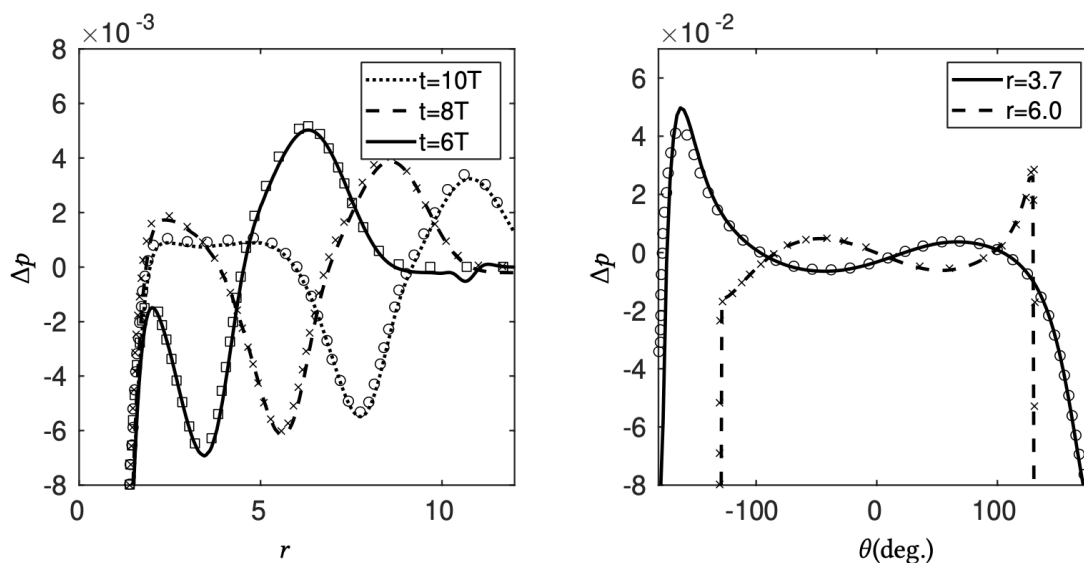


Figure 7.10. – Vortex/shock interaction : Radial (left) and circumferential (right) cuts compared to reference[176] (symbols).

shock-vortex test case, with a lower value of the timestep characterized by CFL = 0.42. The simulation is run until $t = 8$, for three different values of the adiabatic exponent, $\gamma = 1.2, 1.4, 1.6$.

During the simulation, the pure entropy spot crosses the shock wave and creates and pattern of frozen entropy, frozen vorticity and pressure waves [174, 183]. Frozen modes are plotted in the frame reference of the shocked spot on Fig. 7.11 and Fig. 7.12 while the pressure non-evanescent field is plotted on Fig. 7.13 in the frame reference of the shock.

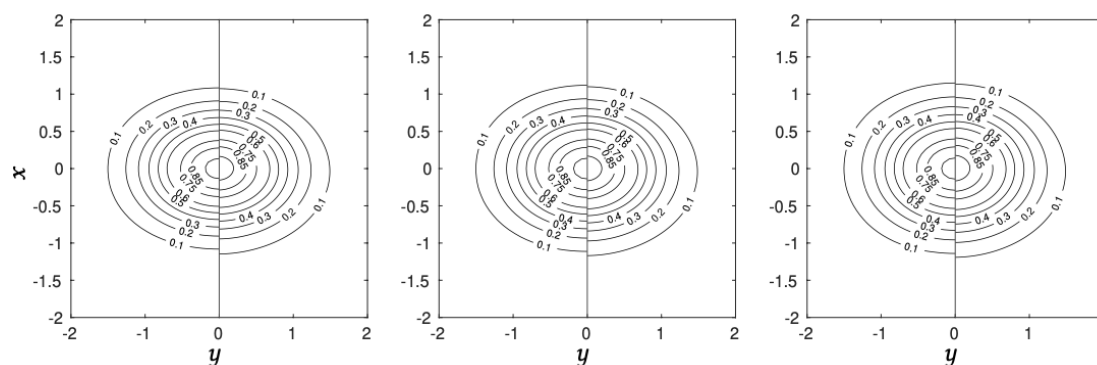


Figure 7.11. – Entropy spot/shock interaction : Normalized transmitted entropy fields $s'/\epsilon C_p$, time $t = 8$. From left to right $\gamma = 1.2, 1.4$ and 1.6 . Analytical [174, 183] and numerical solutions respectively corresponds to $y < 0$ and $y \geq 0$ parts of the plot.

On all these figures, negative y corresponds to analytical solutions [174, 183] while positive y corresponds to the present solver. On a side-note, we mention that these

7.4. Recap

In this Chapter, we derive a unified formalism for all preexisting hybrid thermal models proposed by our group :

- ρ -based model
- p -based model
- improved- ρ -based model

along with a unified formalism for the force correction term. We projected all 3 models on the complete D3Q19 basis, which allow ourselves to find a unique model with free parameters embedded inside it whose tuning allows to get back any of the previous models. From this unified formalism, we particularly emphasize that both the p -based and improved- ρ -based models are actually equivalent implementation variants of each other. Additionally, we performed numerous numerical experiments in order to maximize the stability and the accuracy of the method. The MUSCL Hancock method, traceless hybrid recursive regularized kernel and the force term are identified as key points for the stability of the solutions.

Then, the unified model with optimal parameters is validated on a wide range of compressible test cases, showing the capability of the solver to simulate low supersonic shocked flows (roughly up to $Ma = 1.3$) and high supersonic unshocked flows (up to $Ma = 4.0$).

Conclusion and perspectives

As a fully fledged numerical method able to solve a system of partial differential equations, LBM is a credible solver for wide variety of models. Among its most natural applications, the aeronautical and aerospace fields needs to deal with reasonably to highly compressible flows. Therefore, a LB model for arbitrary Mach numbers should be able to solve mass, momentum and total energy in conservative form in order to recover a correct solution in both smooth and discontinuous regions of the flow.

Therefore, the purpose of this thesis was to improve the existing LB compressible models. Due to their simplicity, regularized LB models were chosen. Hence, this thesis is a direct continuation of pioneering works from Feng *et al* [74], Guo *et al* [148, 149] and Renard *et al* [75], where a LB algorithm for mass/momentum conservation was completed by an entropy equation in non-conservative form.

7.5. Conclusion

Finally, what has been learn and what has been done during those $3 + \epsilon$ years ? The first task was to dig up the literature to learn LBM. The Crank-Nicolson discretization, the difference between \bar{f}_i and f_i , the proper discretization of the force term and the clear definition of the beginning and end of the timestep from time t to $t + \Delta t$ are notions that surprisingly are not so well documented because most of the literature tends to bring to the fore the simplicity of the collide & stream algorithm and rarely recall its derivation and the necessary underlying assumptions. The second task was to interpret the LBM in a deductive fashion, this led to Taylor series interpretation of the LB scheme and to the following original ideas :

- We hypothesized a reason to explain that LBM still provides good results even with $\Delta t/\tau \gg 1$, meaning with an extremely under-resolved relaxation.
- We rigorously derived the order of accuracy of complex LB schemes.
- We explained how "collision kernel" implicitly means "constitutive model" and made a link with the Maxwell-Cattaneo model.
- We explained the mechanism of damping of non-hydrodynamic modes by the hybrid parameter σ .
- We explained why the entropy equation is reasonable for low supersonic and was extensively used [74, 75, 147–149] in the LB literature.

- We proposed a more robust discretization of the entropy equation – the MUSCL Hancock method [24] – and identified it as a key point for robustness and accuracy of the overall hybrid LB scheme.
- We proposed a systematic method to deduce the actual consistency conditions of any LB model and we applied it to the classical athermal model, and some compressible models proposed by our group.
- We proposed a new "traceless" collision kernel, which is an extension of the recursive-regularized kernel and filter an additional non-hydrodynamic mode.
- We derived a new p -based LB model, then we unified it with preexisting ρ /improved- ρ models and explained the actual differences between these models.

Additionally to this background work, the pressure-based and unified models were validated on various subsonic and supersonic test cases (Sec. 6.3 and 7.3), showing good accuracy and robustness, with only 3 free parameters :

- CFL, which is always a free parameter in unstationary codes.
- σ , whose use has been greatly reduced by the traceless collision kernel.
- A free coefficient s_c for the shock sensor, which is only used on shocked flows.

Out of 3 years of numerical experiments using the different LB models discussed in this manuscript, we found that the stability of our family of LB models rely mostly on 3 basic blocs, **equally** important :

- The degrees of freedom in the 3rd and 4th order equilibrium and non-equilibrium.
- The force correction term and its discretization.
- The choice of thermodynamic variable discretized by finite differences and the choice of numerical scheme.

When these 3 aspects are rigorously addressed on minimal test cases, robust LB schemes can be achieved. These schemes are consistent to the NSF system with an unusual constitutive equation. Its order of accuracy highly depends on the collision kernel. It is easily parallelized, provides high accuracy results and has been shown to be a robust solver for compressible flows. In this manuscript, we believe to have provided reasonable premises and an original and parsimonious interpretation of LBM purely as a numerical solver. By doing so, we were able to propose some improvements in the understanding, the stability and accuracy of compressible LB models.

We also would like to mention that the background developments and models proposed in this manuscript were applied to 3D LES applications by our group. The M6 wing from Coratger *et al* [184] and Volvo burner from Tayyab *et al* [179] can be seen on Fig. 7.14 and Fig. 7.15. Both of these applications were carried out with the pressure-based model proposed in Chap. 6. Boivin *et al* [21] also carried out a benchmark of the model in the context of combustion, showing a faster simulation than other investigated solvers.

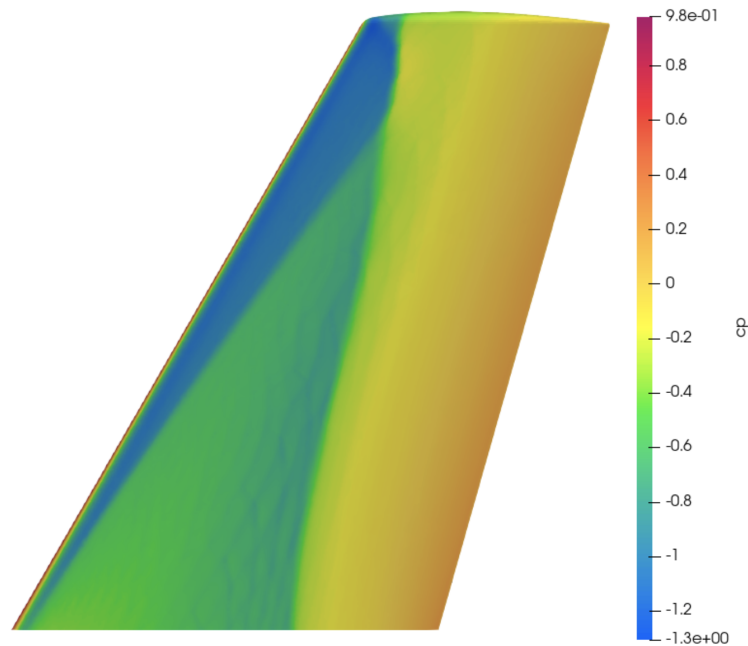


Figure 7.14. – Pressure coefficient on the top surface of the ONERA M6 wing taken from [184], using model proposed in Chap. 6

As a final note, we mention that a side-project has been carried out during this PhD. We extended the "Linear-Interaction-Analysis" method to encompass a heat releasing/absorbing shock wave as well as a Noble-Able-Stiffened-Gas equation of state, see Appendix D. This method was also used to compute analytical solutions for the shock-entropy spot interaction in Sec. 7.3.7.

7.6. Perspectives

In order to improve further the LB models, we believe that now 4 major problems should be addressed :

- First, a robust discretization of the total energy scheme is the key issue that prevents us to reach high Mach shocked solutions. Indeed, improvements could be made even for smooth flows : the employed discretization scheme could be upgraded, particularly using a dimensional splitting and/or using $u_i^{n+1/2}$ instead of u_i^n in the MUSCL-Hancock method are expected to increase at least the order of accuracy and possibly the stability.
- Second, the astonishing capability of the Crank-Nicolson scheme to provide accurate solutions even for highly under-resolved relaxation ($\Delta t/\tau \gg 1$) should be explained and measured on minimal toy models in order to understand more about the errors of LB solvers.
- Third, the continuous limit of the system of equations approximated by the LB solver should be carefully studied. The reason is that different constitutive

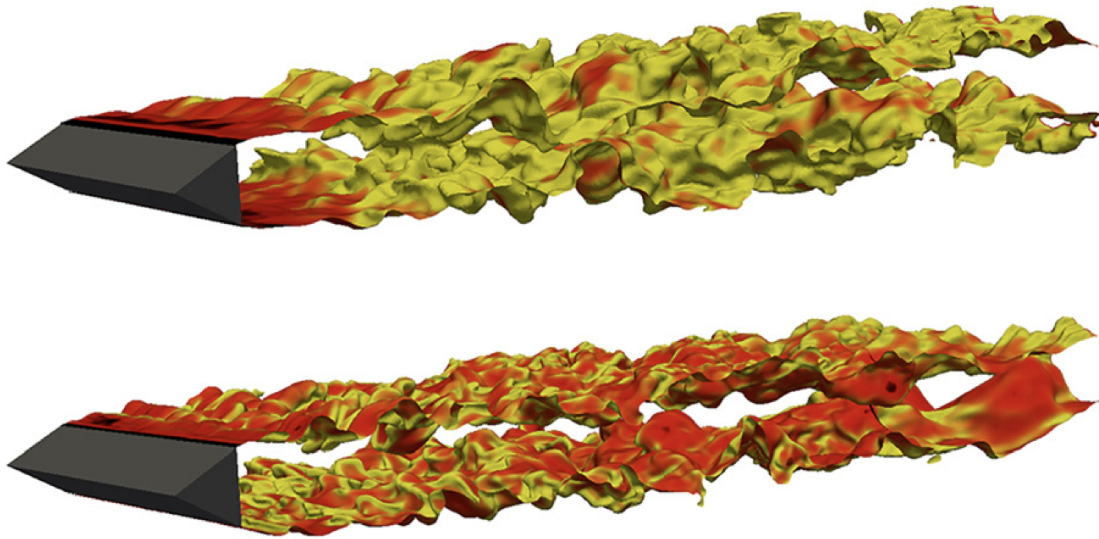


Figure 7.15. – Iso-surface of the progress variable at 0.5 for two configurations of the VOLVO burner taken from [179], using model proposed in Chap. 6

models necessarily lead to different solutions, *e.g.* an extreme case in [185], where the author found that a Maxwell-Cattaneo model – see Sec. 4.4.1 – applied to both heat flux and stress-tensor led to extremely different results when compared to the classical NSF solution and even non-existence of solutions for some moderately strong shocks. The DVBE on standard lattices is linearly very close to NSF [100, 186], but we do not believe a general argument could be found to ensure that it is still true when the solution we are looking for exhibits strong gradients, such as boundary layers or shocks.

- The meaning of all moments involved in a LB simulation should be investigated. While higher-order moments have been investigated in the context of Cumulant LBM [92–95] in order to achieve a 4th-order accuracy, we believe that LB researchers will also have to start looking at those "negligible" terms on other collision kernels in order to extend its capabilities. Calling them "ghost modes" [37] or using the classical Chapman-Enskog expansion makes us forget that as small as they are, those additional terms could predominate or pile up over time, just as a "negligible" negative numerical viscosity could completely ruin a simulation in classical CFD.

Funding

This work was supported by Labex MEC (ANR-10-LABX-0092).

7.7. Scientific communications

Finally, note that research activities conducted during this Ph.D led to the following scientific communications.

Publications

- **G. Farag**, P. Boivin and P. Sagaut. Interaction of two-dimensional spots with a heat releasing/absorbing shock wave: linear interaction approximation results. *Journal of Fluid Mechanics*, 2019. <https://doi.org/10.1017/jfm.2019.324>
(See Appendix D)
- **G. Farag**, S. Zhao, T. Coratger, P. Boivin, G. Chiavassa and P. Sagaut. A pressure-based regularized lattice-Boltzmann method for the simulation of compressible flows. *Physics of Fluids*, 2020. <https://doi.org/10.1063/5.0011839>
(See Chap. 6)
- S. Zhao, **G. Farag**, P. Boivin and P. Sagaut. Toward fully conservative hybrid lattice Boltzmann methods for compressible flows. *Physics of Fluids*, 2020. <https://doi.org/10.1063/5.0033245>
(See Appendix B)
- **G. Farag**, S. Zhao, G. Chiavassa, P. Boivin. Consistency study of Lattice-Boltzmann schemes macroscopic limit. *Physics of Fluids*, 2021. <https://doi.org/10.1063/5.0039490>
(See Chap. 4)
- **G. Farag**, T. Coratger, G. Wissocq, S. Zhao, P. Boivin and P. Sagaut. A unified hybrid lattice-Boltzmann method for compressible flows: Bridging between pressure-based and density-based methods. *Physics of Fluids*, 2021. <https://doi.org/10.1063/5.0057407>
(See Chap. 7)
- T. Coratger, **G. Farag**, S. Zhao, P. Boivin and P. Sagaut. Large-eddy Lattice-Boltzmann modelling of transonic flows. *Physics of Fluids*, 2021. <https://doi.org/10.1063/5.0064944>
- **G. Farag**, P. Boivin and P. Sagaut. Linear Interaction Approximation for shock/disturbance interaction with real gas effects. (under preparation)
- G. Wissocq, T. Coratger, **G. Farag**, S. Zhao, P. Boivin and P. Sagaut. (submitted)

Conference

- **G. Farag**, S. Zhao, T. Coratger, P. Boivin, G. Chiavassa and P. Sagaut. Hybrid regularized Lattice Boltzmann model for compressible flows : interaction of Kovasznay modes with a shock wave. [WCCM-ECCOMAS Congress, 2020.](#)

Appendices

Sommaire

A	The D3Q19 complete basis	163
B	Toward a conservative scheme	166
B.1	<i>U</i> -scheme	166
B.2	<i>C</i> -scheme	167
B.3	<i>UC</i> -scheme	167
B.4	Correction to the <i>U</i> -scheme	168
C	2D Riemann initial states	169
D	Linear Interaction Approximation	170
D.1	Description of the mean flow solution	170
D.2	The Kovaszny modal decomposition for fluctuations	172
D.3	The normal-mode-based LIA	173

A. The D3Q19 complete basis

Here, we provide the details of the lattice that was employed in this manuscript. First, the weights and discrete velocities are,

i	0	1	2	3	4	5	6	7	8	9	10	11	12	13	14	15	16	17	18
ω_i	$\frac{1}{3}$	$\frac{1}{18}$	$\frac{1}{18}$	$\frac{1}{18}$	$\frac{1}{18}$	$\frac{1}{18}$	$\frac{1}{18}$	$\frac{1}{36}$	$\frac{1}{36}$	$\frac{1}{36}$	$\frac{1}{36}$	$\frac{1}{36}$	$\frac{1}{36}$	$\frac{1}{36}$	$\frac{1}{36}$	$\frac{1}{36}$	$\frac{1}{36}$	$\frac{1}{36}$	$\frac{1}{36}$
$\frac{c_{ix}\Delta t}{\Delta x}$	0	+1	-1	0	0	0	0	+1	-1	+1	-1	0	0	+1	-1	+1	-1	0	0
$\frac{c_{iy}\Delta t}{\Delta x}$	0	0	0	+1	-1	0	0	+1	-1	0	0	+1	-1	-1	+1	0	0	+1	-1
$\frac{c_{iz}\Delta t}{\Delta x}$	0	0	0	0	0	+1	-1	0	0	+1	-1	+1	-1	0	0	-1	+1	-1	+1

Table 7.1.

With a lattice constant defined as $c_s = \Delta x / (\sqrt{3} \Delta t)$. The complete basis of Gauss-Hermite polynomials detailed in [181] and used in this study manuscript reads as

$$\mathcal{H}_i^{(0)} \equiv 1, \quad (\text{A1a})$$

$$\mathcal{H}_{i,\alpha}^{(1)} \equiv c_{i\alpha}, \quad (\text{A1b})$$

$$\mathcal{H}_{i,\alpha\beta}^{(2)} \equiv c_{i\alpha}c_{i\beta} - c_s^2\delta_{\alpha\beta}, \quad (\text{A1c})$$

$$\mathcal{H}_{i,\alpha\beta\gamma}^{(3)} \equiv c_{i\alpha}c_{i\beta}c_{i\gamma} - c_s^2(\delta_{\alpha\beta}c_{i\gamma} + \delta_{\beta\gamma}c_{i\alpha} + \delta_{\alpha\gamma}c_{i\beta}), \quad (\text{A1d})$$

$$\begin{aligned} \mathcal{H}_{i,\alpha\beta\gamma\delta}^{(4)} &\equiv c_{i\alpha}c_{i\beta}c_{i\gamma}c_{i\delta} + c_s^4(\delta_{\alpha\beta}\delta_{\gamma\delta} + \delta_{\beta\gamma}\delta_{\delta\alpha} + \delta_{\delta\alpha}\delta_{\beta\gamma}) \\ &- c_s^2(c_{i\alpha}c_{i\beta}\delta_{\gamma\delta} + c_{i\beta}c_{i\gamma}\delta_{\delta\alpha} + c_{i\gamma}c_{i\delta}\delta_{\alpha\beta} + c_{i\delta}c_{i\alpha}\delta_{\beta\gamma} + c_{i\gamma}c_{i\alpha}\delta_{\beta\delta} + c_{i\beta}c_{i\delta}\delta_{\alpha\gamma}), \end{aligned} \quad (\text{A1e})$$

$$\mathcal{H}_{i,1}^{(3r)} \equiv \mathcal{H}_{i,xxxy}^{(3)} + \mathcal{H}_{i,yzzz}^{(3)}, \quad (\text{A1f})$$

$$\mathcal{H}_{i,2}^{(3r)} \equiv \mathcal{H}_{i,xzzz}^{(3)} + \mathcal{H}_{i,xyyy}^{(3)}, \quad (\text{A1g})$$

$$\mathcal{H}_{i,3}^{(3r)} \equiv \mathcal{H}_{i,yyyz}^{(3)} + \mathcal{H}_{i,xxxx}^{(3)}, \quad (\text{A1h})$$

$$\mathcal{H}_{i,4}^{(3r)} \equiv \mathcal{H}_{i,xxxy}^{(3)} - \mathcal{H}_{i,yzzz}^{(3)}, \quad (\text{A1i})$$

$$\mathcal{H}_{i,5}^{(3r)} \equiv \mathcal{H}_{i,xzzz}^{(3)} - \mathcal{H}_{i,xyyy}^{(3)}, \quad (\text{A1j})$$

$$\mathcal{H}_{i,6}^{(3r)} \equiv \mathcal{H}_{i,yyyz}^{(3)} - \mathcal{H}_{i,xxxx}^{(3)}. \quad (\text{A1k})$$

Leading to 16 linearly independent Hermite polynomials. To form a complete basis, 3 additional orthogonal polynomials should be defined,

$$\mathcal{A}_i = \frac{4}{9}(3 + 2\sqrt{3})\mathcal{D}_{xyz}^{(4)} + \frac{4}{9}(3 - \sqrt{3})\mathcal{D}_{xzy}^{(4)} + \frac{4}{9}(3 - \sqrt{3})\mathcal{D}_{zyx}^{(4)}, \quad (\text{A2})$$

$$\mathcal{B}_i = \frac{4}{9}(3 + 2\sqrt{3})\mathcal{D}_{xzy}^{(4)} + \frac{4}{9}(3 - \sqrt{3})\mathcal{D}_{xyz}^{(4)} + \frac{4}{9}(3 - \sqrt{3})\mathcal{D}_{zyx}^{(4)}, \quad (\text{A3})$$

$$\mathcal{C}_i = \frac{4}{9}(3 + 2\sqrt{3})\mathcal{D}_{zyx}^{(4)} + \frac{4}{9}(3 - \sqrt{3})\mathcal{D}_{xzy}^{(4)} + \frac{4}{9}(3 - \sqrt{3})\mathcal{D}_{xyz}^{(4)}, \quad (\text{A4})$$

where $\mathcal{D}_{xyz}^{(4)} = \mathcal{H}_{ixxyy}^{(4)} + \frac{c_s^2}{2}\mathcal{H}_{izz}^{(2)}$. Additionally, let's remark that

$$\sum_{i=0}^{q-1} \omega_i \mathcal{A}_i \mathcal{A}_i = \sum_{i=0}^{q-1} \omega_i \mathcal{B}_i \mathcal{B}_i = \sum_{i=0}^{q-1} \omega_i \mathcal{C}_i \mathcal{C}_i = 24c_s^8. \quad (\text{A5})$$

And the Hermite moments corresponding to this basis are

$$a^{(0)} \equiv \sum_{i=0}^{q-1} \mathcal{H}_i^{(0)} f_i, \quad (\text{A6a})$$

$$a_\alpha^{(1)} \equiv \sum_{i=0}^{q-1} \mathcal{H}_{i,\alpha}^{(1)} f_i, \quad (\text{A6b})$$

$$a_{\alpha\beta}^{(2)} \equiv \sum_{i=0}^{q-1} \mathcal{H}_{i,\alpha\beta}^{(2)} f_i, \quad (\text{A6c})$$

$$a_{\alpha\beta\gamma}^{(3)} \equiv \sum_{i=0}^{q-1} \mathcal{H}_{i,\alpha\beta\gamma}^{(3)} f_i, \quad (\text{A6d})$$

$$a_1^{(3r)} \equiv 3 \left(a_{xxy}^{(3)} + a_{yzz}^{(3)} \right), \quad (\text{A6e})$$

$$a_2^{(3r)} \equiv 3 \left(a_{xzz}^{(3)} + a_{xyy}^{(3)} \right), \quad (\text{A6f})$$

$$a_3^{(3r)} \equiv 3 \left(a_{yyz}^{(3)} + a_{xxz}^{(3)} \right), \quad (\text{A6g})$$

$$a_4^{(3r)} \equiv a_{xxy}^{(3)} - a_{yzz}^{(3)}, \quad (\text{A6h})$$

$$a_5^{(3r)} \equiv a_{xzz}^{(3)} - a_{xyy}^{(3)}, \quad (\text{A6i})$$

$$a_6^{(3r)} \equiv a_{yyz}^{(3)} - a_{xxz}^{(3)}, \quad (\text{A6j})$$

$$a_{\mathcal{A}}^{(4)} \equiv \sum_{i=0}^{q-1} \mathcal{A}_i f_i, \quad (\text{A6k})$$

$$a_{\mathcal{B}}^{(4)} \equiv \sum_{i=0}^{q-1} \mathcal{B}_i f_i, \quad (\text{A6l})$$

$$a_{\mathcal{C}}^{(4)} \equiv \sum_{i=0}^{q-1} \mathcal{C}_i f_i. \quad (\text{A6m})$$

Therefore, on D3Q19, any function f_i can be written as

$$f_i = w_i \left\{ \sum_{n=0}^2 \frac{1}{n! c_s^{2n}} a^{(n)} : \mathcal{H}_i^{(n)} + \frac{\mathcal{H}_{i\gamma}^{(3r)}}{6c_s^6} a_\gamma^{(3r)} + \frac{\mathcal{A}_i a_{\mathcal{A}}^{(4)} + \mathcal{B}_i a_{\mathcal{B}}^{(4)} + \mathcal{C}_i a_{\mathcal{C}}^{(4)}}{24c_s^8} \right\}. \quad (\text{A7})$$

Note that an equivalent orthogonal D3Q19 basis can also be found in [84]. More details about lattices can be found in [4].

B. Toward a conservative scheme

In Zhao *et al* [140] were derived two different numerical schemes. Those schemes are meant to discretize the total energy transport in conservative form by including some of the numerical information coming from populations f_i . The idea is to be able to discretize a conservative form using the lattice-Boltzmann distributions and without defining completely new distributions. First, let us expand the streamed population multiplied by a variable ϕ , Eq. (3.78),

$$\left[\phi f_i^{col}\right](t, \mathbf{x} - \mathbf{c}_i \Delta t) = \left[\phi f_i^{col}\right](t, \mathbf{x}) - c_{i\alpha} \Delta t \frac{\partial [\phi f_i^{col}]}{\partial x_\alpha}(t, \mathbf{x}) + \mathcal{O}(\Delta t^2). \quad (\text{B1})$$

Taking the 0^{th} order moment and rearranging terms leads to

$$\frac{\partial [\rho \phi u_\alpha]}{\partial x_\alpha}(t, \mathbf{x}) = \frac{1}{\Delta t} \sum_{i=0}^{q-1} \left\{ \left[\phi f_i^{col}\right](t, \mathbf{x}) - \left[\phi f_i^{col}\right](t, \mathbf{x} - \mathbf{c}_i \Delta t) \right\} + \mathcal{O}(\Delta t) \quad (\text{B2})$$

which is a first order approximation of the divergence of $\rho \phi u_\alpha$. Following this kinds of strategies, different schemes were derived in [140].

B.1. U -scheme

In [140], the U -scheme was named *upwind*, however, numerically there are no preferred directions based on the velocity. In order to avoid any misconceptions, we prefer to name it differently, hence we call it U -scheme.

$$[\rho E](t + \Delta t, \mathbf{x}) = [\rho E](t, \mathbf{x}) - \sum_{i=0}^{q-1} \left\{ [H f_i^{col}](t, \mathbf{x}) - [H f_i^{col}](t, \mathbf{x} - \mathbf{c}_i \Delta t) \right\}, \quad (\text{B3})$$

where $H = E + p/\rho$ is the total enthalpy. This scheme is meant to discretize the Euler part ($\mathcal{T}_{\alpha\beta} = 0$ and $q_\alpha = 0$) of Eqs. (1.3) and one could easily Taylor expand it to show that this scheme is effectively consistent [14, 22, 23] to the inviscid total energy equation.

In order to understand what are the numerical properties of this scheme, let us restrict ourselves to a more naive situation, the transport of a passive scalar ϕ by a constant mean flow. In this case f_i^{col} , ρ and u_α are constants and the scheme reduces to

$$\phi(t + \Delta t, \mathbf{x}) = \phi(t, \mathbf{x}) - \sum_{i=0}^{q-1} \frac{f_i^{col}}{\rho} \left\{ \phi(t, \mathbf{x}) - \phi(t, \mathbf{x} - \mathbf{c}_i \Delta t) \right\}, \quad (\text{B4})$$

whose Taylor expansion leads to a modified equation,

$$\frac{\partial \phi}{\partial t} + u_\gamma \frac{\partial \phi}{\partial x_\gamma} = \frac{\Delta t}{2} \frac{p}{\rho} \frac{\partial^2 \phi}{\partial x_\gamma^2} + \mathcal{O}(\Delta t^2) \quad (\text{B5})$$

which is an advection-diffusion equation with positive diffusion coefficient $\frac{\Delta t}{2} \frac{p}{\rho}$. While this diffusion is always positive for the passive scalar ϕ , it leads to a sign dependent diffusion when applied to the total energy ρE due to the coupling with mass and momentum conservations.

B.2. C-scheme

The C-scheme is effectively a *centered* scheme, it is defined as

$$[\rho E](t + \Delta t, \mathbf{x}) = [\rho E](t, \mathbf{x}) - \sum_{i=0}^{q-1} \left\{ f_i^{col}(t, \mathbf{x}) \frac{H(t, \mathbf{x} + \mathbf{c}_i \Delta t) + H(t, \mathbf{x})}{2} \right. \quad (\text{B6})$$

$$\left. - f_i^{col}(t, \mathbf{x} - \mathbf{c}_i \Delta t) \frac{H(t, \mathbf{x} - \mathbf{c}_i \Delta t) + H(t, \mathbf{x})}{2} \right\}. \quad (\text{B7})$$

Which is also consistent [14, 22, 23] to the Euler part of Eqs. (1.3). The transport of a passive scalar ϕ by a constant mean flow using this scheme is

$$\phi(t + \Delta t, \mathbf{x}) = \phi(t, \mathbf{x}) - \sum_{i=0}^{q-1} \frac{f_i^{col}}{\rho} \left\{ \frac{\phi(t, \mathbf{x} + \mathbf{c}_i \Delta t) - \phi(t, \mathbf{x} - \mathbf{c}_i \Delta t)}{2} \right\}, \quad (\text{B8})$$

whose Taylor expansion leads to a modified equation,

$$\frac{\partial \phi}{\partial t} + u_\gamma \frac{\partial \phi}{\partial x_\gamma} = -\frac{\Delta t}{2} u_\alpha u_\beta \frac{\partial^2 \phi}{\partial x_\alpha \partial x_\beta} + \mathcal{O}(\Delta t^2). \quad (\text{B9})$$

B.3. UC-scheme

A free parameter κ that allows to switch between both schemes can be introduced

$$\phi(t + \Delta t, \mathbf{x}) = \phi(t, \mathbf{x}) - \kappa \sum_{i=0}^{q-1} \frac{f_i^{col}}{\rho} \left\{ \phi(t, \mathbf{x}) - \phi(t, \mathbf{x} - \mathbf{c}_i \Delta t) \right\} \quad (\text{B10})$$

$$- (1 - \kappa) \sum_{i=0}^{q-1} \frac{f_i^{col}}{\rho} \left\{ \frac{\phi(t, \mathbf{x} + \mathbf{c}_i \Delta t) - \phi(t, \mathbf{x} - \mathbf{c}_i \Delta t)}{2} \right\}, \quad (\text{B11})$$

whose Taylor expansion leads to a modified equation,

$$\frac{\partial \phi}{\partial t} + u_\gamma \frac{\partial \phi}{\partial x_\gamma} = \frac{\Delta t}{2} \{ (\kappa - 1) u_\alpha u_\beta + \kappa \frac{p}{\rho} \delta_{\alpha\beta} \} \frac{\partial^2 \phi}{\partial x_\alpha \partial x_\beta} + \mathcal{O}(\Delta t^2), \quad (\text{B12})$$

suggesting that $\kappa = 1$ is the only value that would lead to a positive numerical diffusion coefficient in front of every second order derivatives. As it was already mentioned, when those schemes are applied to the total energy ρE , they would lead to a sign dependent diffusion due to the coupling with mass and momentum conservations.

B.4. Correction to the U -scheme

An improvement to the U -scheme can be obtained by adding a tunable correction Ψ ,

$$[\rho E](t + \Delta t, \mathbf{x}) = [\rho E](t, \mathbf{x}) - \sum_{i=0}^{q-1} \left\{ [Hf_i^{col}](t, \mathbf{x}) - [Hf_i^{col}](t, \mathbf{x} - \mathbf{c}_i \Delta t) \right\} + \Delta t \Psi. \quad (\text{B13})$$

A Taylor analysis shows that this scheme is first order accurate with a modified equation

$$\frac{\partial \rho E}{\partial t} + \frac{\partial \rho H u_\beta}{\partial x_\beta} = \frac{\Delta t}{2} \frac{\partial}{\partial x_\gamma} \left\{ \frac{\partial \rho u_\gamma H}{\partial t} + \frac{\partial (\rho u_\gamma u_\beta + \delta_{\gamma\beta} p) H}{\partial x_\beta} \right\} + \mathcal{O}(\Delta t^2) + \Psi. \quad (\text{B14})$$

Making the assumption that viscous and heat diffusion terms could be neglected, a more careful study of the leading error shows that

$$\frac{\partial \rho E}{\partial t} + \frac{\partial \rho H u_\beta}{\partial x_\beta} = \frac{\Delta t}{2} \frac{\partial}{\partial x_\gamma} \left\{ -u_\beta u_\gamma \frac{\partial p}{\partial x_\beta} + p u_\gamma \frac{2-\gamma}{\gamma-1} \frac{\partial u_\beta}{\partial x_\beta} + p \frac{\partial H}{\partial x_\gamma} \right\} + \mathcal{O}(\Delta t^2) + \Psi. \quad (\text{B15})$$

Therefore, $\Psi = -\frac{\Delta t}{2} \frac{\partial}{\partial x_\gamma} \left\{ -u_\beta u_\gamma \frac{\partial p}{\partial x_\beta} + p u_\gamma \frac{2-\gamma}{\gamma-1} \frac{\partial u_\beta}{\partial x_\beta} + p \frac{\partial H}{\partial x_\gamma} \right\}$ could lead to a more accurate scheme by removing the dominant truncature error. However, none of the schemes presented in this section were used in this manuscript because they create a numerical viscosity.

C. 2D Riemann initial states

We provide in this appendix all initial states [182] used in Sec. 7.3.4 for the chosen two dimensional Riemann problems.

$$(p, \rho, u, v)_{\text{Config.4}} = \begin{cases} (1.1, 1.1, 0.0, 0.0) & \text{if } x \geq 0.5, y \geq 0.5 \\ (0.35, 0.5065, 0.8939, 0.0) & \text{if } x < 0.5, y \geq 0.5 \\ (1.1, 1.1, 0.8939, 0.8939) & \text{if } x < 0.5, y < 0.5 \\ (0.35, 0.5065, 0.0, 0.8939) & \text{if } x \geq 0.5, y < 0.5 \end{cases} \quad (\text{C1})$$

$$(p, \rho, u, v)_{\text{Config.6}} = \begin{cases} (1.0, 1.0, 0.75, -0.5) & \text{if } x \geq 0.5, y \geq 0.5 \\ (1.0, 2.0, 0.75, 0.5) & \text{if } x < 0.5, y \geq 0.5 \\ (1.0, 1.0, -0.75, 0.5) & \text{if } x < 0.5, y < 0.5 \\ (1, 3, -0.75, -0.5) & \text{if } x \geq 0.5, y < 0.5 \end{cases} \quad (\text{C2})$$

$$(p, \rho, u, v)_{\text{Config.11}} = \begin{cases} (1.0, 1.0, 0.1, 0.0) & \text{if } x \geq 0.5, y \geq 0.5 \\ (0.4, 0.5313, 0.8276, 0.0) & \text{if } x < 0.5, y \geq 0.5 \\ (0.4, 0.8, 0.1, 0.0) & \text{if } x < 0.5, y < 0.5 \\ (0.4, 0.5313, 0.1, 0.7276) & \text{if } x \geq 0.5, y < 0.5 \end{cases} \quad (\text{C3})$$

$$(p, \rho, u, v)_{\text{Config.12}} = \begin{cases} (0.4, 0.5313, 0.0, 0.0) & \text{if } x \geq 0.5, y \geq 0.5 \\ (1.0, 1.0, 0.7276, 0.0) & \text{if } x < 0.5, y \geq 0.5 \\ (1.0, 0.8, 0.0, 0.0) & \text{if } x < 0.5, y < 0.5 \\ (1.0, 1.0, 0.0, 0.7276) & \text{if } x \geq 0.5, y < 0.5 \end{cases} \quad (\text{C4})$$

$$(p, \rho, u, v)_{\text{Config.13}} = \begin{cases} (1.0, 1.0, 0.0, -0.3) & \text{if } x \geq 0.5, y \geq 0.5 \\ (1.0, 2.0, 0.0, 0.3) & \text{if } x < 0.5, y \geq 0.5 \\ (0.4, 1.0626, 0.0, 0.8145) & \text{if } x < 0.5, y < 0.5 \\ (0.4, 0.5313, 0.0, 0.4276) & \text{if } x \geq 0.5, y < 0.5 \end{cases} \quad (\text{C5})$$

$$(p, \rho, u, v)_{\text{Config.16}} = \begin{cases} (0.4, 0.5313, 0.1, 0.1) & \text{if } x \geq 0.5, y \geq 0.5 \\ (1.0, 1.0222, -0.6179, 0.1) & \text{if } x < 0.5, y \geq 0.5 \\ (1.0, 0.8, 0.1, 0.1) & \text{if } x < 0.5, y < 0.5 \\ (1.0, 1.0, 0.1, 0.8276) & \text{if } x \geq 0.5, y < 0.5 \end{cases} \quad (\text{C6})$$

D. Linear Interaction Approximation

A side project was carried out during a previous internship and 4-5 months of the present Ph.D. Being out of the scope of the lattice-Boltzmann method for compressible flows, we only report here a brief overview. This project included some extensions of the Linear Interaction Approximation (LIA) theory,

- In a published article [183], we extended LIA to heat releasing/absorbing shocks along with a new consistent Chu’s disturbance energy [142] definition. The heat releasing case was considered by [187] to model thin detonations.
- In an article in progress, LIA was extended to the Noble Able Stiffened Gas equation of state along with a new consistent Chu’s disturbance energy [142] definition.

We now provide an extremely brief overview of the basic principles of the method, applied to heat releasing/absorbing shocks. Full details could be found in [183].

The propagation of a hydrodynamic shock wave across an heterogeneous medium is a very important topic in many fields of application, e.g. aerospace engineering, nuclear engineering but also astrophysics. Such an interaction is known to emit a complex field, which is a mixture of acoustic, entropy and vortical waves according to Kovasznay’s decomposition [141, 188, 189]. In the limit of small disturbances, the emitted field can be accurately predicted considering a linearized theory, namely the Linear Interaction Approximation (LIA), see [189] for an exhaustive discussion. This theory was pioneered in the 1950s by [190–193] and is still under development [174, 194–197].

D.1. Description of the mean flow solution

Considering the case of an 1D flow along the x axis and a normal shock wave and denoting (u_x, u_r, u_ϕ) the component of velocity in cylindrical coordinates (in the discontinuity reference frame, the x axis being taken normal to the planar shock wave), the upstream and downstream mean quantities (resp. subscripts 1,2) relate through the Hugoniot jump conditions for mass, momentum and energy:

$$\begin{aligned} \rho_1 u_{x1} &= \rho_2 u_{x2}, \\ p_1 + \rho_1 u_{x1}^2 &= p_2 + \rho_2 u_{x2}^2, \\ h_1 + \frac{u_{x1}^2}{2} &= h_2 + \frac{u_{x2}^2}{2}, \end{aligned} \tag{D1}$$

with u_r and u_ϕ being conserved through the shock:

$$u_{r1} = u_{r2}, \quad u_{\phi1} = u_{\phi2}. \tag{D2}$$

The enthalpy h jump condition may be reformulated as

$$c_p T_1 + \frac{u_{x1}^2}{2} = c_p T_2 + \frac{u_{x2}^2}{2} - \Delta Q, \quad (\text{D3})$$

where ΔQ accounts for heat release/heat absorption at the shock wave. $\Delta Q > 0$ was considered by [187] to model thin detonations, while $\Delta Q < 0$ should be used to account for physical mechanisms restricted to a thin region downstream the shock front that act as an energy sink, e.g. radiative losses or condensation [41].

Introducing the sound speeds on either side of the shock c_1, c_2 in the jump conditions lead to the following relation between the upstream and downstream Mach Numbers, respectively M_1 and M_2 :

$$M_2^2 = \frac{1 + \gamma M_1^2 - (M_1^2 - 1)\sqrt{1 - \beta}}{1 + \gamma M_1^2 + \gamma(M_1^2 - 1)\sqrt{1 - \beta}}, \quad \beta = \frac{2(\gamma^2 - 1)M_1^2 q}{(1 - M_1^2)^2}, \quad (\text{D4})$$

where the normalized heat coefficient has been introduced

$$q = \frac{\Delta Q}{c_1^2}. \quad (\text{D5})$$

The compression factor $m = \rho_2 / \rho_1 = u_1 / u_2$ is obtained through

$$\frac{1}{m} = \frac{1 + \gamma M_1^2}{(\gamma + 1)M_1^2} + \frac{1 - M_1^2}{(\gamma + 1)M_1^2} \sqrt{1 - \beta}. \quad (\text{D6})$$

Note that c_p and γ , appearing in the above relations are assumed identical on both side of the shock, thereby considerably reducing the equations. When the assumption does not hold, the present study still present valuable benchmarks for numerical codes, in which thermodynamic properties may be artificially set to constants.

All other classical relations for $T_2 / T_1, p_2 / p_1, \dots$ are formally identical to those of the classical normal shock case, M_2 and m being now given by the above formula. The consistency constraint which ensures that both m and M_2 remain positive is

$$q_{\min} < q < q_{\max}, \quad (\text{D7})$$

where

$$q_{\min} = \frac{1}{1 - \gamma} - \frac{M_1^2}{2}, \quad q_{\max} = \frac{(1 - M_1^2)^2}{2(\gamma^2 - 1)M_1^2}. \quad (\text{D8})$$

One recovers the physical behavior that the downstream flow is accelerated in the case $q > 0$ compared to the neutral shock case $q = 0$, while it is decelerated in the opposite case $q < 0$, due to the balance between kinetic energy and internal energy. In the asymptotic limit $q = q_{\max}$, the system satisfies the so-called Chapman-Jouguet condition $M_2 = 1$ [see, e.g. 198]. The other limit, $q = q_{\min}$ corresponds to an infinite mass compression ratio, impossible to sustain in practice.

D.2. The Kovasznay modal decomposition for fluctuations

The Linear Interaction Approximation relies on a small disturbance hypothesis and the use of linearized equations to describe fluctuation propagation on either side of the shock. For each quantity (e.g. u), let us identify the fluctuation part (u') and the mean (\bar{u}) as

$$u = \bar{u} + u', \quad p = \bar{p} + p', \quad \dots \quad (\text{D9})$$

and assume the fluctuation part is small ($u'/\bar{u} \ll 1$). In the reference frame tied to the planar shock front the 2D perturbation field then satisfies

$$\frac{\partial \rho'}{\partial t} + \bar{u} \frac{\partial \rho'}{\partial x} + \bar{\rho} \frac{\partial u'_j}{\partial x_j} = 0, \quad (\text{D10})$$

$$\frac{\partial u'_i}{\partial t} + \bar{u} \frac{\partial u'_i}{\partial x} + \frac{1}{\bar{\rho}} \frac{\partial p'}{\partial x_i} = 0, \quad (\text{D11})$$

$$\frac{\partial p'}{\partial t} + \bar{u} \frac{\partial p'}{\partial x} + \gamma \bar{p} \frac{\partial u'_j}{\partial x_j} = 0, \quad (\text{D12})$$

which can be recast as a system of evolution equations for Kovasznay's physical modes:

$$\frac{\partial s'}{\partial t} + \bar{u} \frac{\partial s'}{\partial x} = 0, \quad (\text{D13})$$

$$\frac{\partial \omega'_{\parallel}}{\partial t} + \bar{u} \frac{\partial \omega'_{\parallel}}{\partial x} = 0, \quad (\text{D14})$$

$$\frac{\partial \omega'_{\perp}}{\partial t} + \bar{u} \frac{\partial \omega'_{\perp}}{\partial x} = 0, \quad (\text{D15})$$

$$\left(\frac{\partial}{\partial t} + \bar{u} \frac{\partial}{\partial x} \right)^2 p' = c^2 \nabla^2 p', \quad (\text{D16})$$

where $\omega' = \nabla \times \mathbf{u}'$ denotes the fluctuating vorticity, and $\omega'_{\perp} = (\omega' \cdot \mathbf{n})\mathbf{n}$ and $\omega'_{\parallel} = \omega' - \omega'_{\perp}$ are the shock-normal and the shock-parallel components of vorticity, respectively, with \mathbf{n} the unit normal vector of the planar shock wave. The shock-normal and the shock-tangential components correspond to the toroidal and poloidal components of the velocity field in the reference frame tied to the planar shock front, respectively [189]. One recognizes the entropy mode, the toroidal and poloidal vorticity modes, the fast and slow acoustic modes and the concentration mode. It is worth noting that Kovasznay's modes correspond to the eigenmodes of the linearized propagation operator, which are orthonormal according to the inner product associated to Chu's definition of compressible disturbance energy [142]. Let us now introduce propagating plane wave disturbances of the general form

$$\phi' = A_i(\mathbf{k}) e^{i(\mathbf{k} \cdot \mathbf{x} - \Omega t)}. \quad (\text{D17})$$

Here, $A_i(\mathbf{k})$ denotes the amplitude of upstream Kovasznay mode of type i , with $i = s, a, v, t$ for entropy, acoustic, concentration and poloidal/toroidal vorticity mode, re-

spectively. \mathbf{k} is the perturbation wave vector, associated with pulsation $\Omega = \bar{u}_1 k \cos \alpha$, where α is the angle of the incident perturbation with respect to the shock, as illustrated in Fig. D1.

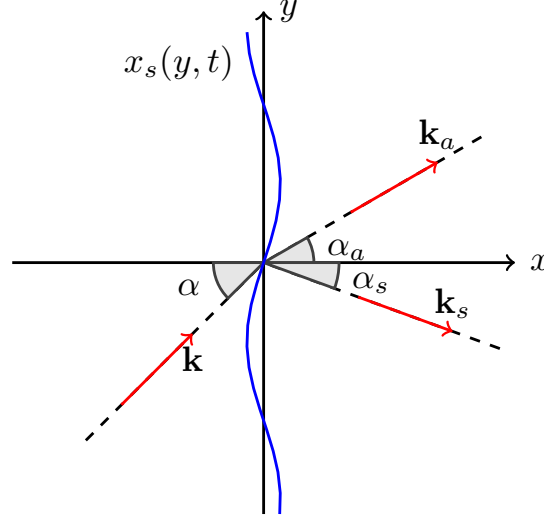


Figure D1. – Sketch of the LIA configuration. The corrugated shock mean front position is at $x = 0$. The incident perturbation has wave vector \mathbf{k} , at angle α with respect to the shock normal. Emitted waves may be acoustic waves, with wave vector \mathbf{k}_a , or non-acoustic ones, with wave vector \mathbf{k}_s .

D.3. The normal-mode-based LIA

The shock jump relations for a normal planar shock wave read

$$\begin{aligned}
 \bar{\rho}_1 \left(u'_{x1} - \frac{\partial x_s}{\partial t} \right) + \bar{u}_1 \rho'_1 &= \bar{\rho}_2 \left(u'_{x2} - \frac{\partial x_s}{\partial t} \right) + \bar{u}_2 \rho'_2, \\
 p'_1 + \rho'_1 \bar{u}_1^2 + 2\bar{\rho}_1 \bar{u}_1 u'_{x1} &= p'_2 + \rho'_2 \bar{u}_2^2 + 2\bar{\rho}_2 \bar{u}_2 u'_{x2}, \\
 h'_1 + \bar{u}_1 \left(u'_{x1} - \frac{\partial x_s}{\partial t} \right) &= h'_2 + \bar{u}_2 \left(u'_{x2} - \frac{\partial x_s}{\partial t} \right), \\
 \bar{u}_1 \frac{\partial x_s}{\partial y} + u'_{r1} &= \bar{u}_2 \frac{\partial x_s}{\partial y} + u'_{r2}, \\
 u'_{\phi 1} &= u'_{\phi 2},
 \end{aligned} \tag{D18}$$

Where we denote the shock fluctuating displacement with respect to its equilibrium position,

$$x_s = x_s(y, t) = A_x e^{i(k_y y - \Omega t)}, \tag{D19}$$

as depicted in Fig. D1. The normalized shock relations (D18) could be recast into a linear system,

$$M Z_i = B_i, \tag{D20}$$

where M and B_i are known. This system is deduced by injecting upstream disturbances of amplitude A_i and downstream disturbances of amplitude $A_i Z_i$ inside (D18). The transfer function vector Z_i contains the intensity Z_{ij} of each emitted Kovasznay mode j for a given incident mode i ,

$$Z_i = (Z_{it}, Z_{iv}, Z_{is}, Z_{ia}, Z_{ix})^T. \quad (\text{D21})$$

Then, a given pattern of upstream perturbation can be decomposed into Fourier modes (D17) obtained via a 2D polar Fourier transform [174, 183] with (k, α) the polar coordinates in the Fourier space. The downstream perturbation is then calculated by computing Z_i for each Fourier modes, which allows to recombine the downstream perturbation. In other words, knowing only the upstream perturbation (shape, amplitude), shock Mach number, adiabatic exponent γ and heat release ΔQ , we can analytically compute the downstream perturbation.

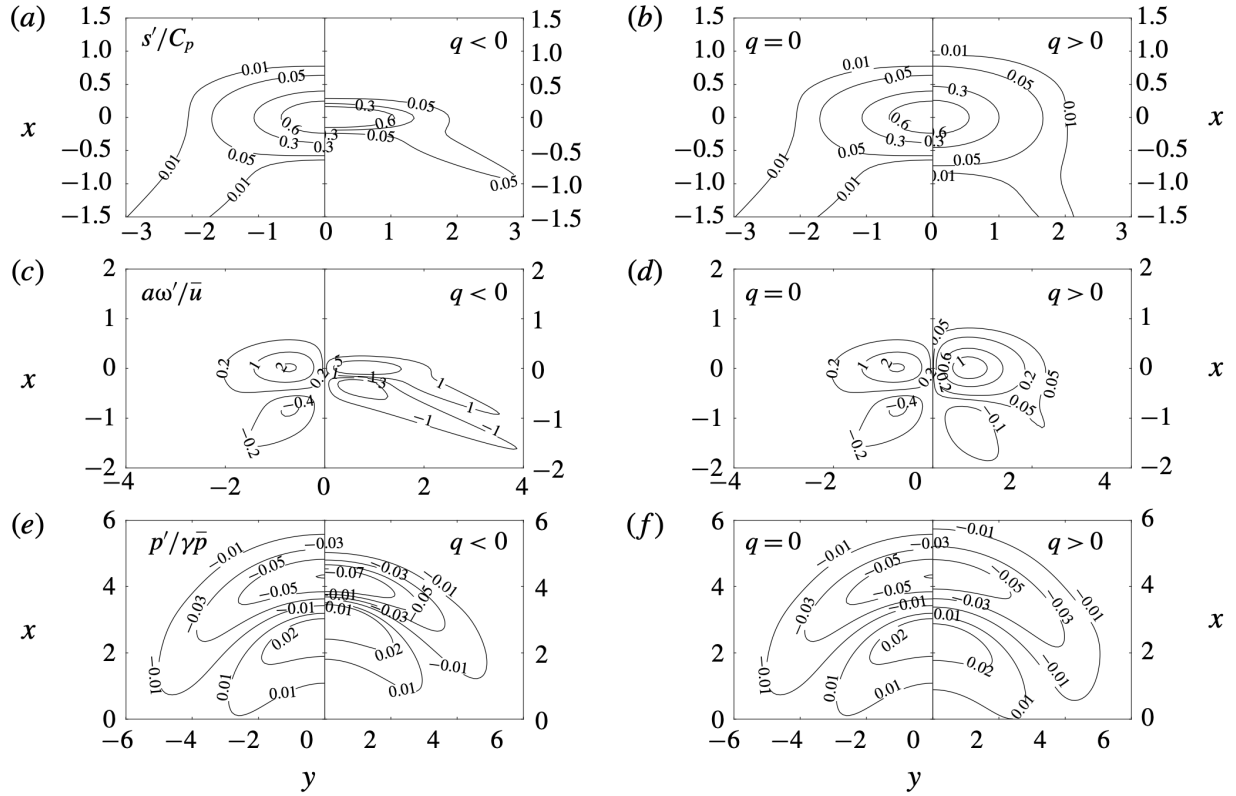


Figure D2. – Incident Gaussian entropy spot: analytical emitted entropy, vorticity perturbations (from a to f). (a,c,e) Adiabatic versus endothermic case. (b,d,f) Adiabatic versus exothermic.

A similar work is currently being written in which the LIA has been extended to the Noble Able Stiffened Gas equation of state [180, 199, 200].

Bibliography

- [1] Gregory A Tokaty. A history and philosophy of fluid mechanics. Courier Corporation, 1994 (cit. on p. 15).
- [2] John D Anderson Jr and John David Anderson. A history of aerodynamics: and its impact on flying machines. 8. Cambridge university press, 1998 (cit. on p. 15).
- [3] Peter OK Krehl. History of shock waves, explosions and impact: a chronological and biographical reference. Springer Science & Business Media, 2008 (cit. on p. 15).
- [4] Timm Krüger, Halim Kusumaatmaja, Alexandr Kuzmin, et al. “The lattice Boltzmann method”. In: Springer International Publishing 10 (2017), pp. 978–3 (cit. on pp. 15–18, 31, 35, 39, 40, 42, 43, 46, 50, 52–54, 56, 57, 63, 71, 82, 86–88, 120, 129, 165).
- [5] Lev Davidovich Landau and Evgeny Mikhailovich Lifshitz. “Fluid mechanics”. In: flme (1959) (cit. on pp. 15, 22, 23, 25, 26, 28, 30, 78, 98, 137).
- [6] Hans Wolfgang Liepmann and Anatol Roshko. Elements of gasdynamics. Courier Corporation, 2001 (cit. on pp. 15, 22–26, 28, 30, 32, 37, 96, 98, 99, 119, 121).
- [7] Carlo Cercignani. “The boltzmann equation”. In: The Boltzmann equation and its applications. Springer, 1988, pp. 40–103 (cit. on pp. 15, 28, 29, 31, 33, 42, 43, 56, 90).
- [8] Bastien Chopard, Jean L Falcone, and Jonas Latt. “The lattice Boltzmann advection-diffusion model revisited”. In: The European Physical Journal Special Topics 171.1 (2009), pp. 245–249 (cit. on p. 16).
- [9] Irina Ginzburg, Dominique d’Humières, and Alexander Kuzmin. “Optimal stability of advection-diffusion lattice Boltzmann models with two relaxation times for positive/negative equilibrium”. In: Journal of Statistical Physics 139.6 (2010), pp. 1090–1143 (cit. on p. 16).
- [10] Maxime Escande, Praveen Kumar Kolluru, Louis Marie Cléon, et al. “Lattice Boltzmann Method for wave propagation in elastic solids with a regular lattice: Theoretical analysis and validation”. In: arXiv preprint arXiv:2009.06404 (2020) (cit. on p. 16).

- [11] Linhao Zhong, Shide Feng, Ping Dong, et al. “Lattice Boltzmann schemes for the nonlinear Schrödinger equation”. In: Physical Review E 74.3 (2006), p. 036704 (cit. on p. 16).
- [12] Alessandro De Rosis. “Modeling epidemics by the lattice Boltzmann method”. In: Physical Review E 102.2 (2020), p. 023301 (cit. on p. 16).
- [13] Zhiqiang Zhou and Jingtang Ma. “Lattice Boltzmann methods for solving partial differential equations of exotic option pricing”. In: Frontiers of Mathematics in China 11.1 (2016), pp. 237–254 (cit. on p. 16).
- [14] Randall J LeVeque. Finite difference methods for ordinary and partial differential equations. SIAM, 2007 (cit. on pp. 16, 17, 53, 63, 65, 75, 90, 101, 102, 106, 114, 166, 167).
- [15] David R Noble, John G Georgiadis, and Richard O Buckius. “Comparison of accuracy and performance for lattice Boltzmann and finite difference simulations of steady viscous flow”. In: International Journal for Numerical Methods in Fluids 23.1 (1996), pp. 1–18 (cit. on p. 16).
- [16] Sebastian Geller, Manfred Krafczyk, Jonas Tölke, et al. “Benchmark computations based on lattice-Boltzmann, finite element and finite volume methods for laminar flows”. In: Computers & fluids 35.8-9 (2006), pp. 888–897 (cit. on p. 16).
- [17] Florian Schornbaum and Ulrich Rude. “Massively parallel algorithms for the lattice Boltzmann method on nonuniform grids”. In: SIAM Journal on Scientific Computing 38.2 (2016), pp. C96–C126 (cit. on p. 16).
- [18] Michael F Barad, Joseph G Kocheemoolayil, and Cetin C Kiris. “Lattice Boltzmann and Navier-stokes cartesian cfd approaches for airframe noise predictions”. In: 23rd AIAA Computational fluid dynamics conference. 2017, p. 4404 (cit. on pp. 16, 63).
- [19] Karl-Robert Wichmann, Martin Kronbichler, Rainald Löhner, et al. “A runtime based comparison of highly tuned lattice Boltzmann and finite difference solvers”. In: The International Journal of High Performance Computing Applications (2021), p. 10943420211006169 (cit. on p. 16).
- [20] Jonas Latt, Christophe Coreixas, and Joël Beny. “Cross-platform programming model for many-core lattice Boltzmann simulations”. In: Plos one 16.4 (2021), e0250306 (cit. on p. 16).
- [21] Pierre Boivin, M Tayyab, and S Zhao. “Benchmarking a lattice-Boltzmann solver for reactive flows: Is the method worth the effort for combustion?” In: Physics of Fluids 33.7 (2021), p. 071703 (cit. on pp. 16, 63, 126, 158).

- [22] Peter D Lax and Robert D Richtmyer. “Survey of the stability of linear finite difference equations”. In: Communications on pure and applied mathematics 9.2 (1956), pp. 267–293 (cit. on pp. 17, 53, 63, 65, 90, 114, 166, 167).
- [23] Robert D Richtmyer and Keith W Morton. “Difference methods for initial-value problems”. In: Malabar (1994) (cit. on pp. 17, 53, 63, 65, 90, 114, 166, 167).
- [24] Eleuterio F Toro. Riemann solvers and numerical methods for fluid dynamics: a practical introduction. Springer Science & Business Media, 2013 (cit. on pp. 17, 50, 65, 96, 101–103, 106–108, 124, 142, 147, 158).
- [25] Jh Bertrand. “Sur l’homogénéité dans les formules de physique”. In: Cahiers de recherche de l’Academie de Sciences 86 (1878), pp. 916–920 (cit. on pp. 17, 27).
- [26] Aimé Vaschy. “Sur les lois de similitude en physique”. In: Annales télégraphiques. Vol. 19. 1892, pp. 25–28 (cit. on pp. 17, 27).
- [27] Edgar Buckingham. “On physically similar systems; illustrations of the use of dimensional equations”. In: Physical review 4.4 (1914), p. 345 (cit. on pp. 17, 27).
- [28] Leonid P Yarin. The Pi-Theorem: applications to fluid mechanics and heat and mass transfer. Vol. 1. Springer Science & Business Media, 2012 (cit. on pp. 17, 27).
- [29] ProLB High-fidelity lattice Boltzmann CFD in exceptional turnaround times. <http://www.prolb-cfd.com>. Accessed: October 2021 (cit. on pp. 17, 56).
- [30] CS group. <https://www.csgroup.eu/en/>. Accessed: October 2021 (cit. on p. 17).
- [31] Airbus. <https://www.airbus.com>. Accessed: October 2021 (cit. on p. 17).
- [32] Renault group. <https://www.renaultgroup.com>. Accessed: October 2021 (cit. on p. 17).
- [33] LMFA, Laboratoire de Mécanique des Fluides et d’Acoustique, UMR 5509. <http://lmfa.ec-lyon.fr/?lang=en>. Accessed: October 2021 (cit. on p. 17).
- [34] M2P2, Laboratoire de Mécanique, Modélisation et Procédés Propres, UMR 7340. <http://www.m2p2.fr>. Accessed: October 2021 (cit. on p. 17).
- [35] AA Mohamad. Lattice Boltzmann Method. Vol. 70. Springer, 2011 (cit. on pp. 17, 42, 43, 52, 63, 86).
- [36] Zhaoli Guo and Chang Shu. Lattice Boltzmann method and its applications in engineering. Vol. 3. World Scientific, 2013 (cit. on pp. 17, 42, 43, 52, 63, 86).

- [37] Sauro Succi. The lattice Boltzmann equation: for complex states of flowing matter. Oxford University Press, 2018 (cit. on pp. [17](#), [33](#), [35](#), [36](#), [42](#), [43](#), [52](#), [63](#), [86](#), [160](#)).
- [38] Xiaowen Shan et al. “General solution of lattices for Cartesian lattice Bhatnagar-Gross-Krook models”. In: Physical Review E 81.3 (2010), p. 036702 (cit. on pp. [18](#), [82](#)).
- [39] John D Anderson. Modern compressible flow. Tata McGraw-Hill Education, 2003 (cit. on pp. [22](#), [25](#), [98](#), [99](#)).
- [40] Etienne Guyon, Jean-Pierre Hulin, Luc Petit, et al. Physical hydrodynamics. Oxford University Press, 2015 (cit. on pp. [22](#), [25](#), [26](#), [28](#), [30](#), [78](#)).
- [41] Ya B Zel'Dovich and Yu P Raizer. Physics of shock waves and high-temperature hydrodynamic phenomena. Courier Corporation, 2002 (cit. on pp. [22](#), [26](#), [171](#)).
- [42] Douglas Adams. The Hitchhiker's Guide to the Galaxy. 1979 (cit. on p. [23](#)).
- [43] Stephen J Blundell and Katherine M Blundell. Concepts in thermal physics. OUP Oxford, 2009 (cit. on pp. [23](#), [24](#), [30](#), [37](#), [78](#), [140](#)).
- [44] Antoine Sellier. Introduction aux écoulements compressibles et aux fluides hétérogènes. Editions Ecole Polytechnique, 2001 (cit. on pp. [23](#), [24](#), [98](#), [99](#)).
- [45] Carlo Cercignani. Rarefied gas dynamics: from basic concepts to actual calculations. Vol. 21. Cambridge University Press, 2000 (cit. on pp. [25](#), [29](#), [31](#), [32](#), [37](#), [56](#), [57](#)).
- [46] Sylvie Vaclair. “Eléments de physique statistique”. In: (1993) (cit. on pp. [25](#), [28](#), [37](#)).
- [47] R Becker. Impact waves and detonation. National Advisory Committee for Aeronautics, 1929 (cit. on p. [25](#)).
- [48] Guido Buresti. “A note on Stokes' hypothesis”. In: Acta Mechanica 226.10 (2015), pp. 3555–3559 (cit. on pp. [26](#), [81](#)).
- [49] Leonid Ivanovich Sedov and AG Volkovets. Similarity and dimensional methods in mechanics. CRC press, 2018 (cit. on p. [27](#)).
- [50] Graeme Austin Bird. “Molecular gas dynamics”. In: NASA STI/Recon Technical Report A 76 (1976), p. 40225 (cit. on pp. [28](#), [32](#), [57](#)).
- [51] Guy R McNamara and Gianluigi Zanetti. “Use of the Boltzmann equation to simulate lattice-gas automata”. In: Physical review letters 61.20 (1988), p. 2332 (cit. on p. [29](#)).
- [52] Ludwig Boltzmann. “Weitere studien über das wärmeleichgewicht unter gasmolekülen”. In: Kinetische Theorie II. Springer, 1970, pp. 115–225 (cit. on p. [32](#)).

- [53] Prabhu Lal Bhatnagar, Eugene P Gross, and Max Krook. “A model for collision processes in gases. I. Small amplitude processes in charged and neutral one-component systems”. In: Physical review 94.3 (1954), p. 511 (cit. on p. 32).
- [54] Laure Saint-Raymond. Hydrodynamic limits of the Boltzmann equation. 1971. Springer Science & Business Media, 2009 (cit. on p. 32).
- [55] Cédric Villani. “Limites hydrodynamiques de l’équation de Boltzmann”. In: Séminaire Bourbaki 2000 (2001), pp. 365–405 (cit. on p. 32).
- [56] Alexander Gorban and Ilya Karlin. “Hilbert’s 6th problem: exact and approximate hydrodynamic manifolds for kinetic equations”. In: Bulletin of the American Mathematical Society 51.2 (2014), pp. 187–246 (cit. on pp. 32, 42).
- [57] David Hilbert. “Begründung der kinetischen Gastheorie”. In: Mathematische Annalen 72.4 (1912), pp. 562–577 (cit. on p. 33).
- [58] David Hilbert. “Grundzüge einer allgemeinen Theorie der linearen Integralgleichungen”. In: Integralgleichungen und Gleichungen mit unendlich vielen Unbekannten. Springer, 1989, pp. 8–171 (cit. on p. 33).
- [59] John K Hunter. “Asymptotic analysis and singular perturbation theory”. In: Department of Mathematics, University of California at Davis (2004), pp. 1–3 (cit. on pp. 33, 42).
- [60] S Chapman and TG Cowling. The Mathematical Theory of Non-Uniform Gases, 3rd edn. Cambridge Math. 1970 (cit. on pp. 33, 42, 43).
- [61] George Eugène Uhlenbeck, George W Ford, Gordon William Ford, et al. Lectures in statistical mechanics. Vol. 1. Proquest/Csa Journal Division, 1963 (cit. on pp. 34, 42).
- [62] Harold Grad. “On the kinetic theory of rarefied gases”. In: Communications on pure and applied mathematics 2.4 (1949), pp. 331–407 (cit. on pp. 35, 36).
- [63] Harold Grad. “Note on N-dimensional hermite polynomials”. In: Communications on Pure and Applied Mathematics 2.4 (1949), pp. 325–330 (cit. on pp. 36, 39).
- [64] Uriel Frisch, Brosl Hasslacher, and Yves Pomeau. “Lattice-gas automata for the Navier-Stokes equation”. In: Physical review letters 56.14 (1986), p. 1505 (cit. on p. 38).
- [65] Xiaowen Shan, Xue-Feng Yuan, and Hudong Chen. “Kinetic theory representation of hydrodynamics: a way beyond the Navier-Stokes equation”. In: Journal of Fluid Mechanics 550 (2006), p. 413 (cit. on pp. 39, 59).

- [66] Dominik Wilde, Andreas Krämer, Knut Küllmer, et al. “Multistep lattice Boltzmann methods: Theory and applications”. In: International Journal for Numerical Methods in Fluids 90.3 (2019), pp. 156–169 (cit. on pp. [41](#), [52](#)).
- [67] Harold Grad. “Asymptotic theory of the Boltzmann equation”. In: The physics of Fluids 6.2 (1963), pp. 147–181 (cit. on p. [42](#)).
- [68] Hans Christian Öttinger. Beyond equilibrium thermodynamics. John Wiley & Sons, 2005 (cit. on p. [42](#)).
- [69] AV Bobylev. “The Chapman-Enskog and Grad methods for solving the Boltzmann equation”. In: DoSSR 262.1 (1982), pp. 71–75 (cit. on p. [42](#)).
- [70] AV Bobylev. “Instabilities in the Chapman-Enskog expansion and hyperbolic Burnett equations”. In: Journal of statistical physics 124.2-4 (2006), pp. 371–399 (cit. on p. [42](#)).
- [71] Henning Struchtrup. “Macroscopic transport equations for rarefied gas flows”. In: Macroscopic Transport Equations for Rarefied Gas Flows. Springer, 2005, pp. 145–160 (cit. on p. [42](#)).
- [72] Christophe Coreixas, Gauthier Wissocq, Guillaume Puigt, et al. “Recursive regularization step for high-order lattice Boltzmann methods”. In: Physical Review E 96.3 (2017), p. 033306 (cit. on pp. [42](#), [76](#), [80](#), [113](#), [130](#), [131](#), [133](#)).
- [73] Irina Ginzburg. “Consistent lattice Boltzmann schemes for the Brinkman model of porous flow and infinite Chapman-Enskog expansion”. In: Physical Review E 77.6 (2008), p. 066704 (cit. on p. [42](#)).
- [74] Yongliang Feng, Pierre Boivin, Jérôme Jacob, et al. “Hybrid recursive regularized thermal lattice Boltzmann model for high subsonic compressible flows”. In: Journal of Computational Physics 394 (2019), pp. 82–99 (cit. on pp. [42](#), [70](#), [82](#), [107–109](#), [112](#), [116](#), [117](#), [129](#), [130](#), [137](#), [140–142](#), [147](#), [157](#)).
- [75] Florian Renard, Yongliang Feng, Jean-François Boussuge, et al. “Improved compressible hybrid lattice Boltzmann method on standard lattice for subsonic and supersonic flows”. In: Computers & Fluids 219 (2021), p. 104867 (cit. on pp. [42](#), [82](#), [108](#), [119](#), [124](#), [130](#), [136](#), [137](#), [139–143](#), [147](#), [157](#)).
- [76] G Farag, S Zhao, T Coratger, et al. “A pressure-based regularized lattice-Boltzmann method for the simulation of compressible flows”. In: Physics of Fluids 32.6 (2020), p. 066106 (cit. on pp. [42](#), [70](#), [81](#), [114](#), [129](#), [130](#), [133–135](#), [137](#), [139](#), [140](#), [142](#), [147](#), [149](#)).
- [77] Nicolò Frapolli, Shyam S Chikatamarla, and Iliya V Karlin. “Entropic lattice Boltzmann model for compressible flows”. In: Physical Review E 92.6 (2015), p. 061301 (cit. on p. [42](#)).

- [78] Nicolò Frapolli, Shyam S Chikatamarla, and Ilya V Karlin. “Entropic lattice Boltzmann model for gas dynamics: Theory, boundary conditions, and implementation”. In: Physical Review E 93.6 (2016), p. 063302 (cit. on p. 42).
- [79] Nicolò Frapolli, Shyam S Chikatamarla, and Iliya V Karlin. “Lattice kinetic theory in a comoving galilean reference frame”. In: Physical review letters 117.1 (2016), p. 010604 (cit. on p. 42).
- [80] Paul J Dellar. “An interpretation and derivation of the lattice Boltzmann method using Strang splitting”. In: Computers & Mathematics with Applications 65.2 (2013), pp. 129–141 (cit. on pp. 50, 67).
- [81] Gauthier Wissocq, Christophe Coreixas, and Jean-François Bousuge. “Linear stability and isotropy properties of athermal regularized lattice Boltzmann methods”. In: Physical Review E 102.5 (2020), p. 053305 (cit. on pp. 53, 70, 75, 113, 143).
- [82] Florian Renard, Gauthier Wissocq, Jean-François Bousuge, et al. “A linear stability analysis of compressible hybrid lattice Boltzmann methods”. In: Journal of Computational Physics (2021), p. 110649 (cit. on pp. 53, 75, 81, 103, 129).
- [83] Pierre Lallemand, Li-shi Luo, Manfred Krafczyk, et al. “The lattice Boltzmann method for nearly incompressible flows”. In: Journal of Computational Physics 431 (2021), p. 109713 (cit. on pp. 53, 89).
- [84] Christophe Coreixas, Bastien Chopard, and Jonas Latt. “Comprehensive comparison of collision models in the lattice Boltzmann framework: Theoretical investigations”. In: Physical Review E 100.3 (2019), p. 033305 (cit. on pp. 54, 55, 165).
- [85] Pietro Asinari. “Generalized local equilibrium in the cascaded lattice Boltzmann method”. In: Physical Review E 78.1 (2008), p. 016701 (cit. on p. 54).
- [86] Linlin Fei and Kai H Luo. “Cascaded lattice Boltzmann method for thermal flows on standard lattices”. In: International Journal of Thermal Sciences 132 (2018), pp. 368–377 (cit. on p. 54).
- [87] Hudong Chen, Raoyang Zhang, and Pradeep Gopalakrishnan. Lattice boltzmann collision operators enforcing isotropy and galilean invariance. US Patent 10,867,088. 2020 (cit. on pp. 56, 80).
- [88] Nicolò Frapolli, Shyam Chikatamarla, and Ilya Karlin. “Theory, analysis, and applications of the entropic lattice Boltzmann model for compressible flows”. In: Entropy 22.3 (2020), p. 370 (cit. on p. 56).
- [89] Mohammad Hossein Saadat, Fabian Bösch, and Ilya V Karlin. “Lattice Boltzmann model for compressible flows on standard lattices: Variable Prandtl number and adiabatic exponent”. In: Physical Review E 99.1 (2019), p. 013306 (cit. on p. 56).

- [90] Mohammad Hossein Saadat, Benedikt Dorschner, and Ilya Karlin. “Extended lattice Boltzmann model”. In: Entropy 23.4 (2021), p. 475 (cit. on p. 56).
- [91] MH Saadat, SA Hosseini, B Dorschner, et al. “Extended lattice Boltzmann model for gas dynamics”. In: Physics of Fluids 33.4 (2021), p. 046104 (cit. on p. 56).
- [92] Martin Geier, Martin Schönherr, Andrea Pasquali, et al. “The cumulant lattice Boltzmann equation in three dimensions: Theory and validation”. In: Computers & Mathematics with Applications 70.4 (2015), pp. 507–547 (cit. on pp. 56, 87, 160).
- [93] Martin Geier, Andrea Pasquali, and Martin Schönherr. “Parametrization of the cumulant lattice Boltzmann method for fourth order accurate diffusion part I: Derivation and validation”. In: Journal of Computational Physics 348 (2017), pp. 862–888 (cit. on pp. 56, 87, 160).
- [94] Martin Geier, Andrea Pasquali, and Martin Schönherr. “Parametrization of the cumulant lattice Boltzmann method for fourth order accurate diffusion part II: Application to flow around a sphere at drag crisis”. In: Journal of Computational Physics 348 (2017), pp. 889–898 (cit. on pp. 56, 160).
- [95] Martin Geier and Andrea Pasquali. “Fourth order Galilean invariance for the lattice Boltzmann method”. In: Computers & Fluids 166 (2018), pp. 139–151 (cit. on pp. 56, 87, 160).
- [96] Ronald Aylmer Fisher et al. “090: The Derivation of the Pattern Formulae of Two-Way Partitions From Those of Simpler Patterns.” In: (1931) (cit. on p. 56).
- [97] Yongliang Feng, S Guo, Jérôme Jacob, et al. “Solid wall and open boundary conditions in hybrid recursive regularized lattice Boltzmann method for compressible flows”. In: Physics of Fluids 31.12 (2019), p. 126103 (cit. on pp. 57, 82, 119).
- [98] Zhaoli Guo, Chuguang Zheng, and Baochang Shi. “Discrete lattice effects on the forcing term in the lattice Boltzmann method”. In: Physical review E 65.4 (2002), p. 046308 (cit. on p. 59).
- [99] Rainald Löhner. “Towards overcoming the LES crisis”. In: International Journal of Computational Fluid Dynamics 33.3 (2019), pp. 87–97 (cit. on p. 63).
- [100] Simon Marié, Denis Ricot, and Pierre Sagaut. “Comparison between lattice Boltzmann method and Navier–Stokes high order schemes for computational aeroacoustics”. In: Journal of Computational Physics 228.4 (2009), pp. 1056–1070 (cit. on pp. 63, 117, 160).
- [101] M Tayyab, S Zhao, Y Feng, et al. “Hybrid regularized lattice-Boltzmann modelling of premixed and non-premixed combustion processes”. In: Combustion and Flame 211 (2020), pp. 173–184 (cit. on p. 70).

- [102] John R Ockendon, Sam Howison, Andrew Lacey, et al. Applied partial differential equations. Oxford University Press on Demand, 2003 (cit. on pp. 77, 78, 97, 100).
- [103] D John and JR Anderson. “Computational fluid dynamics: the basics with applications”. In: P. Perback, International ed., Published (1995), pp. 4–30 (cit. on p. 77).
- [104] Kumar K Tamma and Raju R Namburu. “Hyperbolic heat-conduction problems-Numerical simulations via explicit Lax-Wendroff-based finite element formulations”. In: Journal of thermophysics and heat transfer 5.2 (1991), pp. 232–239 (cit. on p. 78).
- [105] CI Christov. “On frame indifferent formulation of the Maxwell–Cattaneo model of finite-speed heat conduction”. In: Mechanics Research Communications 36.4 (2009), pp. 481–486 (cit. on p. 78).
- [106] Hiroaki Nishikawa. “Robust and accurate viscous discretization via upwind scheme–I: Basic principle”. In: Computers & Fluids 49.1 (2011), pp. 62–86 (cit. on p. 78).
- [107] Philip L Roe and Mohit Arora. “Characteristic-based schemes for dispersive waves I. The method of characteristics for smooth solutions”. In: Numerical Methods for Partial Differential Equations 9.5 (1993), pp. 459–505 (cit. on pp. 78, 91).
- [108] DS Chandrasekharaiah. “Hyperbolic thermoelasticity: a review of recent literature”. In: (1998) (cit. on p. 78).
- [109] PM Jordan, W Dai, and RE Mickens. “A note on the delayed heat equation: Instability with respect to initial data”. In: Mechanics Research Communications 35.6 (2008), pp. 414–420 (cit. on p. 78).
- [110] James G Oldroyd. “On the formulation of rheological equations of state”. In: Proceedings of the Royal Society of London. Series A. Mathematical and Physical Sciences 200.1063 (1950), pp. 523–541 (cit. on p. 78).
- [111] Felipe Angeles. “Non-hyperbolicity of the inviscid Cattaneo-Christov system for compressible fluid flow in several space dimensions”. In: arXiv preprint arXiv:2109.09652 (2021) (cit. on p. 78).
- [112] Brian J Edwards and Antony N Beris. “Remarks concerning compressible viscoelastic fluid models”. In: Journal of non-newtonian fluid mechanics 36 (1990), pp. 411–417 (cit. on p. 78).
- [113] Jean-Luc Thiffeault. “Covariant time derivatives for dynamical systems”. In: Journal of Physics A: Mathematical and General 34.29 (2001), p. 5875 (cit. on p. 79).
- [114] T Matolcsi and P Ván. “Can material time derivative be objective?” In: Physics Letters A 353.2-3 (2006), pp. 109–112 (cit. on p. 79).

- [115] Jonas Latt and Bastien Chopard. “Lattice Boltzmann method with regularized pre-collision distribution functions”. In: Mathematics and Computers in Simulation 72.2-6 (2006), pp. 165–168 (cit. on pp. [79](#), [130](#), [131](#), [133](#)).
- [116] Keijo K Mattila, Paulo C Philippi, and Luiz A Hegele Jr. “High-order regularization in lattice-Boltzmann equations”. In: Physics of Fluids 29.4 (2017), p. 046103 (cit. on p. [79](#)).
- [117] Hudong Chen, Pradeep Gopalakrishnan, and Raoyang Zhang. “Recovery of Galilean invariance in thermal lattice Boltzmann models for arbitrary Prandtl number”. In: International Journal of Modern Physics C 25.10 (2014), p. 1450046 (cit. on p. [80](#)).
- [118] Hudong Chen, Raoyang Zhang, and Pradeep Gopalakrishnan. “Filtered lattice Boltzmann collision formulation enforcing isotropy and Galilean invariance”. In: Physica Scripta 95.3 (2020), p. 034003 (cit. on p. [80](#)).
- [119] Jérôme Jacob, Orestis Malaspinas, and Pierre Sagaut. “A new hybrid recursive regularised Bhatnagar–Gross–Krook collision model for Lattice Boltzmann method-based large eddy simulation”. In: Journal of Turbulence 19.11-12 (2018), pp. 1051–1076 (cit. on pp. [80](#), [92](#), [130](#), [131](#), [143](#)).
- [120] Gauthier Wissocq and Pierre Sagaut. Hydrodynamic limits and numerical errors of isothermal lattice Boltzmann schemes. 2021. arXiv: [2104.14217](#) [[physics.flu-dyn](#)] (cit. on pp. [81](#), [89–91](#), [129](#), [136](#), [142](#), [143](#)).
- [121] Qing Li, Kai Hong Luo, QJ Kang, et al. “Lattice Boltzmann methods for multiphase flow and phase-change heat transfer”. In: Progress in Energy and Combustion Science 52 (2016), pp. 62–105 (cit. on p. [82](#)).
- [122] Pradeep Gopalakrishnan, Raoyang Zhang, and Hudong Chen. Temperature coupling algorithm for hybrid thermal lattice boltzmann method. US Patent 10,762,252. 2020 (cit. on p. [82](#)).
- [123] Yong-Liang Feng, Shao-Long Guo, Wen-Quan Tao, et al. “Regularized thermal lattice Boltzmann method for natural convection with large temperature differences”. In: International Journal of Heat and Mass Transfer 125 (2018), pp. 1379–1391 (cit. on pp. [82](#), [107](#), [112](#), [116](#)).
- [124] Yongliang Feng, Muhammad Tayyab, and Pierre Boivin. “A Lattice-Boltzmann model for low-Mach reactive flows”. In: Combustion and Flame 196 (2018), pp. 249–254 (cit. on p. [82](#)).
- [125] Muhammad Tayyab, Yongliang Feng, and Pierre Boivin. “Updated Hybrid Lattice-Boltzmann Model for Low-Mach Reactive Flows”. In: Mediterranean Combustion Symposium. 2019 (cit. on p. [82](#)).

- [126] Jinhua Lu, Haiyan Lei, Chang Shu, et al. “The more actual macroscopic equations recovered from lattice Boltzmann equation and their applications”. In: Journal of Computational Physics 415 (2020), p. 109546 (cit. on p. 86).
- [127] Michael Junk and Axel Klar. “Discretizations for the incompressible Navier–Stokes Equations based on the lattice Boltzmann method”. In: SIAM journal on scientific computing 22.1 (2000), pp. 1–19 (cit. on p. 86).
- [128] Michael Junk. “A finite difference interpretation of the lattice Boltzmann method”. In: Numerical Methods for Partial Differential Equations: An International Journal 17.4 (2001), pp. 383–402 (cit. on p. 86).
- [129] Michael Junk, Axel Klar, and Li-Shi Luo. “Asymptotic analysis of the lattice Boltzmann equation”. In: Journal of Computational Physics 210.2 (2005), pp. 676–704 (cit. on p. 86).
- [130] Yinfeng Dong, Jianying Zhang, and Guangwu Yan. “A higher-order moment method of the lattice Boltzmann model for the conservation law equation”. In: Applied mathematical modelling 34.2 (2010), pp. 481–494 (cit. on p. 87).
- [131] Yan Guangwu. “A lattice Boltzmann equation for waves”. In: Journal of Computational Physics 161.1 (2000), pp. 61–69 (cit. on p. 87).
- [132] David J Holdych, David R Noble, John G Georgiadis, et al. “Truncation error analysis of lattice Boltzmann methods”. In: Journal of Computational Physics 193.2 (2004), pp. 595–619 (cit. on p. 87).
- [133] Hiroshi Otomo, Bruce M Boghosian, and François Dubois. “Two complementary lattice-Boltzmann-based analyses for nonlinear systems”. In: Physica A: Statistical Mechanics and its Applications 486 (2017), pp. 1000–1011 (cit. on p. 87).
- [134] François Dubois. “Equivalent partial differential equations of a lattice Boltzmann scheme”. In: Computers & Mathematics with Applications 55.7 (2008), pp. 1441–1449 (cit. on pp. 87, 88).
- [135] François Dubois and Pierre Lallemand. “Towards higher order lattice Boltzmann schemes”. In: Journal of Statistical mechanics: theory and experiment 2009.06 (2009), P06006 (cit. on pp. 87, 88).
- [136] François Dubois. “Nonlinear fourth order Taylor expansion of lattice Boltzmann schemes”. In: Asymptotic Analysis Preprint (2019), pp. 1–41 (cit. on pp. 87, 88).
- [137] G Farag, S Zhao, G Chiavassa, et al. “Consistency study of Lattice-Boltzmann schemes macroscopic limit”. In: Physics of Fluids 33.3 (2021), p. 037101 (cit. on pp. 90, 134, 136, 138, 142, 143).

- [138] Thomas Astoul, Gauthier Wissocq, Jean-françois Boussuge, et al. “Lattice boltzmann method for computational aeroacoustics on non-uniform meshes: a direct grid coupling approach”. In: arXiv preprint arXiv:2004.14887 (2020) (cit. on p. 93).
- [139] Thomas Astoul, Gauthier Wissocq, Jean-François Boussuge, et al. “Analysis and reduction of spurious noise generated at grid refinement interfaces with the lattice Boltzmann method”. In: Journal of Computational Physics 418 (2020), p. 109645 (cit. on p. 93).
- [140] S Zhao, G Farag, Pierre Boivin, et al. “Toward fully conservative hybrid lattice Boltzmann methods for compressible flows”. In: Physics of Fluids 32.12 (2020), p. 126118 (cit. on pp. 96, 130, 166).
- [141] Boa-Teh Chu and Leslie SG Kovásznyay. “Non-linear interactions in a viscous heat-conducting compressible gas”. In: Journal of Fluid Mechanics 3.5 (1958), pp. 494–514 (cit. on pp. 97, 170).
- [142] Boa-Teh Chu. “On the energy transfer to small disturbances in fluid flow (Part I)”. In: Acta Mechanica 1.3 (1965), pp. 215–234 (cit. on pp. 97, 170, 172).
- [143] RF Warming and BJ Hyett. “The modified equation approach to the stability and accuracy analysis of finite-difference methods”. In: Journal of computational physics 14.2 (1974), pp. 159–179 (cit. on p. 101).
- [144] Alain Lerat and Roger Peyret. “Noncentered schemes and shock propagation problems”. In: Computers & Fluids 2.1 (1974), pp. 35–52 (cit. on p. 101).
- [145] Bruno Després and François Dubois. Systèmes hyperboliques de lois de conservation: Application à la dynamique des gaz. Editions Ecole Polytechnique, 2005 (cit. on p. 102).
- [146] Kyu Hong Kim, Chongam Kim, and Oh-Hyun Rho. “Methods for the accurate computations of hypersonic flows: I. AUSMPW+ scheme”. In: Journal of computational physics 174.1 (2001), pp. 38–80 (cit. on pp. 102, 142).
- [147] Pradeep Gopalakrishnan, Raoyang Zhang, and Hudong Chen. Lattice Boltzmann Based Solver for High Speed Flows. US Patent App. 16/274,403. 2019 (cit. on pp. 108, 157).
- [148] S Guo, Y Feng, J Jacob, et al. “An efficient lattice Boltzmann method for compressible aerodynamics on D3Q19 lattice”. In: Journal of Computational Physics (2020), p. 109570 (cit. on pp. 108, 137, 140–142, 147, 157).
- [149] S Guo, Y Feng, and P Sagaut. “Improved standard thermal lattice Boltzmann model with hybrid recursive regularization for compressible laminar and turbulent flows”. In: Physics of Fluids 32.12 (2020), p. 126108 (cit. on pp. 108, 110, 129, 130, 133, 135, 137, 139, 140, 143, 144, 157).

- [150] Y. Cao. “Variable property-based lattice Boltzmann flux solver for thermal flows in the low Mach limit”. In: Int. J. Heat Mass Transfer 101 (2016), pp. 254–264 (cit. on p. 110).
- [151] Olga Filippova and Dieter Hänel. “A novel lattice BGK approach for low Mach number combustion”. In: J. Comput. Phys. 158.2 (2000), pp. 139–160 (cit. on p. 110).
- [152] O. Filippova and D. Haenel. “A novel numerical scheme for reactive flows at low Mach numbers”. In: Computers Physics Communications 129 (2000), pp. 267–274 (cit. on p. 110).
- [153] M. Ashna and M.H. Rahimian. “LBM simulation of head-on collision of evaporating and burning droplets in coalescence regime”. In: Int. J. Heat Mass Transfer 109 (2017), pp. 520–536 (cit. on p. 110).
- [154] Taehun Lee, Ching-Long Lin, and Lea-Der Chen. “A lattice Boltzmann algorithm for calculation of the laminar jet diffusion flame”. In: J. Comput. Phys. 215.1 (2006), pp. 133–152 (cit. on p. 110).
- [155] R. Zhang, X. He, and S. Chen. “Interface and surface tension in incompressible lattice Boltzmann multiphase model”. In: Comput. Phys. Commun. 129 (2000), pp. 121–130 (cit. on p. 110).
- [156] Taehun Lee and Ching-Long Lin. “A stable discretization of the lattice Boltzmann equation for simulation of incompressible two-phase flows at high density ratio”. In: J. Comput. Phys. 206.1 (2005), pp. 16–47 (cit. on p. 110).
- [157] Xiaoyi He, Shiyi Chen, and Raoyang Zhang. “A lattice Boltzmann scheme for incompressible multiphase flow and its application in simulation of Rayleigh–Taylor instability”. In: J. Comput. Phys. 152.2 (1999), pp. 642–663 (cit. on p. 110).
- [158] R. Zhang, X. He, G. Doolen, et al. “Surface tension effects on two-dimensional two-phase Kelvin-Helmholtz instabilities”. In: Adv. Water Resour. 24 (2001), pp. 461–478 (cit. on p. 110).
- [159] X. He, R. Zhang, S. Chen, et al. “On the three-dimensional Rayleigh-Taylor instability”. In: Phys. Fluids 11 (1999), pp. 1143–1152 (cit. on p. 110).
- [160] Takaji Inamuro, Tajima Ogata, S Tajima, et al. “A lattice Boltzmann method for incompressible two-phase flows with large density differences”. In: J. Comput. Phys. 198.2 (2004), pp. 628–644 (cit. on p. 110).
- [161] S. Mukherjee and J. Abrahams. “A pressure-evolution-based multi-relaxation-time high-density-ratio two-phase lattice-Boltzmann model”. In: Computers and Fluids 36 (2007), pp. 1149–1158 (cit. on p. 110).
- [162] K.W. Connington, M.Z. Miskin, T. Lee, et al. “Lattice-Boltzmann simulations of particle-laden liquid bridges: effect of volume fraction and wettability”. In: International Journal of Multiphase Flows 76 (2015), pp. 32–46 (cit. on p. 110).

- [163] Taehun Lee. “Effects of incompressibility on the elimination of parasitic currents in lattice Boltzmann equation method for binary fluids”. In: *Computers and Mathematics with Applications* 58 (2009), pp. 987–994 (cit. on p. 110).
- [164] A. Fakhari, M. Geier, and T. Lee. “A mass-conserving lattice Boltzmann method with dynamic grid refinement for immiscible two-phase flows”. In: *J. Comput. Phys.* 315 (2016), pp. 434–457 (cit. on p. 110).
- [165] K.C. Sahu and S.P. Vanka. “A multiphase lattice Boltzmann study of buoyancy-induced mixing in a tilted channel”. In: *Computers and Fluids* 50 (2011), pp. 199–215 (cit. on p. 110).
- [166] K. Connington and T. Lee. “Lattice Boltzmann simulations of forced wetting transitions of drops on superhydrophobic surfaces”. In: *J. Comput. Phys.* 250 (2013), pp. 601–615 (cit. on p. 110).
- [167] T. Lee and L. Liu. “Lattice Boltzmann simulations of micron-scale drop impact on dry surfaces”. In: *J. Comput. Phys.* 229 (2010), pp. 8045–8063 (cit. on p. 110).
- [168] L. Amaya-Bower and T. Lee. “Single bubble rising dynamics for moderate Reynolds number using Lattice Boltzmann method”. In: *Computers and Fluids* 39 (2010), pp. 1191–1207 (cit. on p. 110).
- [169] R.H.H. Abadi and M.H. Rahimian. “hybrid lattice Boltzmann finite difference model for simulation of phase change in a ternary fluid”. In: *Int. J. Heat Mass Transfer* 127 (2018), pp. 704–716 (cit. on p. 110).
- [170] E. Reyhanian, M.H. Rahimian, and S. Farsid Chini. “Investigation of 2D drop evaporation on a smooth and homogeneous surface using Lattice Boltzmann method”. In: *Int. Commun. Heat Mass Transfer* 89 (2018), pp. 64–72 (cit. on p. 110).
- [171] H. Safari, M.H. Rahimian, and M. Krafczyk. “Extended Lattice Boltzmann method for simulation of thermal phase change in two-phase fluid flow”. In: *Physical Review E* 88 (2013), p. 013304 (cit. on p. 110).
- [172] H. Safari, M.H. Rahimian, and M. Krafczyk. “Consistent simulation of droplet evaporation based on phase-field multiphase lattice Boltzmann method”. In: *Physical Review E* 90 (2014), p. 033305 (cit. on p. 110).
- [173] M. Mohammadi-Shad and T. Lee. “Phase-field lattice Boltzmann modelling of boiling using a sharp-interface energy solver”. In: *Physical Review E* 96 (2017), p. 013306 (cit. on p. 110).
- [174] David Fabre, Laurent Jacquin, and Jörn Sesterhenn. “Linear interaction of a cylindrical entropy spot with a shock”. In: *Physics of Fluids* 13.8 (2001), pp. 2403–2422 (cit. on pp. 117, 154, 155, 170, 174).

- [175] Manoj Singh and Arvind Patel. “Shock wave structure in a non-ideal gas under temperature and density-dependent viscosity and heat conduction”. In: Theoretical and Computational Fluid Dynamics 33.6 (2019), pp. 537–559 (cit. on pp. [120](#), [122](#), [123](#)).
- [176] Osamu Inoue and Yuji Hattori. “Sound generation by shock–vortex interactions”. In: Journal of Fluid Mechanics 380 (1999), pp. 81–116 (cit. on pp. [125–127](#), [154](#)).
- [177] Isabelle Cheylan, Song Zhao, Pierre Boivin, et al. “Compressible pressure-based Lattice-Boltzmann applied to humid air with phase change”. In: Applied Thermal Engineering 191 (2021), p. 116868 (cit. on p. [126](#)).
- [178] Muhammad Tayyab, Basile Radisson, Christophe Almarcha, et al. “Experimental and numerical lattice-Boltzmann investigation of the Darrieus–Landau instability”. In: Combustion and Flame 221 (2020), pp. 103–109 (cit. on p. [126](#)).
- [179] M Tayyab, S Zhao, and Pierre Boivin. “Lattice-Boltzmann modeling of a turbulent bluff-body stabilized flame”. In: Physics of Fluids 33.3 (2021), p. 031701 (cit. on pp. [126](#), [158](#), [160](#)).
- [180] Olivier Le Métayer and Richard Saurel. “The Noble-Abel Stiffened-Gas equation of state”. In: Physics of Fluids (1994-present) 28.4 (2016), p. 046102 (cit. on pp. [140](#), [174](#)).
- [181] G Farag, T Coratger, G Wissocq, et al. “A unified hybrid lattice-Boltzmann method for compressible flows: Bridging between pressure-based and density-based methods”. In: Physics of Fluids 33.8 (2021), p. 086101 (cit. on pp. [147](#), [163](#)).
- [182] Peter D Lax and Xu-Dong Liu. “Solution of two-dimensional Riemann problems of gas dynamics by positive schemes”. In: SIAM Journal on Scientific Computing 19.2 (1998), pp. 319–340 (cit. on pp. [149–151](#), [169](#)).
- [183] G Farag, Pierre Boivin, and P Sagaut. “Interaction of two-dimensional spots with a heat releasing/absorbing shock wave: linear interaction approximation results”. In: Journal of Fluid Mechanics 871 (2019), pp. 865–895 (cit. on pp. [154](#), [155](#), [170](#), [174](#)).
- [184] T Coratger, G Farag, S Zhao, et al. “Large-eddy lattice-Boltzmann modeling of transonic flows”. In: Physics of Fluids 33.11 (2021), p. 115112 (cit. on pp. [158](#), [159](#)).
- [185] FJ Uribe. “Shock waves: the Maxwell-Cattaneo case”. In: Physical Review E 93.3 (2016), p. 033110 (cit. on p. [160](#)).
- [186] P-A Masset and G Wissocq. “Linear hydrodynamics and stability of the discrete velocity Boltzmann equations”. In: Journal of Fluid Mechanics 897 (2020) (cit. on p. [160](#)).

- [187] César Huete, Antonio L Sánchez, and Forman A Williams. “Theory of interactions of thin strong detonations with turbulent gases”. In: Physics of Fluids 25.7 (2013), p. 076105 (cit. on pp. 170, 171).
- [188] Leslie SG Kovaszny. “Turbulence in supersonic flow”. In: Journal of the Aeronautical Sciences 20.10 (1953), pp. 657–674 (cit. on p. 170).
- [189] Pierre Sagaut and Claude Cambon. Homogeneous turbulence dynamics. Vol. 10. Springer, 2008 (cit. on pp. 170, 172).
- [190] H.S. Ribner. “Shock-turbulence interaction and the generation of noise”. In: NACA Technical Note 3255 (1954) (cit. on p. 170).
- [191] Herbert S Ribner. “Convection of a pattern of vorticity through a shock wave”. In: (1954) (cit. on p. 170).
- [192] Herbert S Ribner. The sound generated by interaction of a single vortex with a shock wave. Tech. rep. Citeseer, 1959 (cit. on p. 170).
- [193] Franklin K Moore. “Unsteady oblique interaction of a shock wave with a plane disturbance”. In: (1953) (cit. on p. 170).
- [194] J Griffond. “Linear interaction analysis applied to a mixture of two perfect gases”. In: Physics of Fluids 17.8 (2005), p. 086101 (cit. on p. 170).
- [195] J Griffond. “Linear interaction analysis for Richtmyer-Meshkov instability at low Atwood numbers”. In: Physics of Fluids 18.5 (2006), p. 054106 (cit. on p. 170).
- [196] J Griffond, O Souldard, and D Souffland. “A turbulent mixing Reynolds stress model fitted to match linear interaction analysis predictions”. In: Physica Scripta 2010.T142 (2010), p. 014059 (cit. on p. 170).
- [197] Jérôme Griffond and Olivier Souldard. “Evolution of axisymmetric weakly turbulent mixtures interacting with shock or rarefaction waves”. In: Physics of Fluids 24.11 (2012), p. 115108 (cit. on p. 170).
- [198] Yakov Borissovich Zeldovich. “On the theory of the propagation of detonation in gaseous systems”. In: (1950) (cit. on p. 171).
- [199] P Boivin, MA Cannac, and O Le Métayer. “A thermodynamic closure for the simulation of multiphase reactive flows”. In: International Journal of Thermal Sciences 137 (2019), pp. 640–649 (cit. on p. 174).
- [200] Matei Ioan Radulescu. “Compressible flow in a Noble–Abel stiffened gas fluid”. In: Physics of Fluids 32.5 (2020), p. 056101 (cit. on p. 174).

“ His heart beat madly and the noise of life about him sank to an unheard murmur. [...] He lifted his head and he could see through all the steel and concrete and humanity above him. He could see the beacon set in space to lure men outwards. He could see it shining down – the naked sun. ”

— Isaac Asimov, *The Naked Sun*